A geophysical and hydrological investigation of palæochannels in Northern New South Wales

Christopher P. Vanags

BS (Geology) – The University of Georgia, USA

MSc (Agronomy) – The University of Georgia, USA

A thesis submitted

in fulfillment of the requirements

for the degree of

Doctor of Philosophy

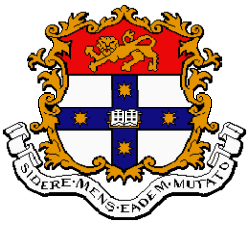

Faculty of Agriculture, Food and Natural Resources

The University of Sydney

New South Wales

Australia

MMVII

CERTIFICATE OF ORIGINALITY

The text of this thesis contains no material which has been accepted as part of the requirement of any other degree or diploma in any university, or any material published, unless due reference is made to that material.

Christopher P. Vanags

Abstract

Palæochannels are common features in much of the irrigated landscape of the Murray Darling Basin. Exensive research has been carried out on palæochannels in the Namoi and Murrumbidgee River Basins and has indicated that these features are associated with irrigation water loss due to their sandier textures. While these features have been identified as potential sources of deep drainage, little is known about the pathways and movement of water after infiltration and how changes in soil properties and sedimentary layering govern this movement. This is particularly the case in the Gwydir River Basin, where palæochannels are less understood due to the expensive and invasive nature of direct physical measurement and the extreme variability of hydraulic properties in these structues. Previous research in this region has been aimed at identifying the characteristics of these structures through ancillary data, such as electromagnetic induction, but has generally been limited to one or two dimensions.

This study uses traditional measurements to identify the geomorphological and hydrological characteristics of a palæochannel in the Gwydir River Basin, where palæochannels are thought to affect water-use efficiency on farms relying on surface irrigation techniques. To improve on the information gained from a limited number of direct observations, the conceptual model is further refined through the use of geophysical information. Depth information was derived from the electromagnetic induction data by inverting bulk electrical conductivity readings from various combinations of electromagnetic measurements and using a regularisation process to stabilise the solution of the inverse problem. Four different inversion algorithms and three conceptually-different scaling relationships are subsequently used to derive saturated conductivity fields based on data from pedotransfer functions.

To test the utilitity of the geophyhsical data, two interpolation procedures are used to distribute this information in three dimensions. Three-dimensional ordinary kriging was used to interpolate the limited soil measurements, and the scaling factor-derived saturated conductivity predictions. A more sophisticated method, regression kriging, incorporates the electrical conductivity data into the interpolation of the direct observations, providing the maximum amount of information.

This study finds that the palæochannel is morphologically-different from those previously described in this area. This channel contains coarse-textured bedload sediment of variable thickness along the length of the channel. A thin, but hydrologically-significant clay layer separates the coarse sediments from the unconfined aquifer below. The hydrological measurements indicate that significant pulses of water are being channelled through the structures from a neighbouring irrigation channel. The fate of this water remains unknown, but it is likely contributing to groundwater recharge in the underlying unconfined aquifer.

The electromagnetic induction measurements delineated the palæochannel, but the vertical predictions were highly dependent on the inversion method. Regularisation of the inversion process was a necessary step, as the unregularised profiles were significantly affected by instrument noise. This was attributed to the use of several different instruments to construct the conductivity profile. Furthermore, the relationship between the predicted EC and the various soil properties depended on the regularisation order. While 0^{th} order Tikhonov regularisation provided the best fit to forward-modelled EC_a, clay and saturated hydraulic conductivity predictions from the pedotransfer functions, 2^{nd} order Tikhonov regularisation was most strongly correlated with EC_e. In cases where a significant relationship existed between EC and saturated conductivity, the scaling factors approach provided more support for the palæochannel presence than was obtained using measured properties. This will likely translate to more realistic input for future groundwater model parameters. However, the relationship between saturated hydraulic conductivity and electrical conductivity, as a function of the inversion algorithm and the scaling factor multiplication procedure, needs to be improved before this information can be incorporated into a realistic groundwater model of the surrounding area.

Acknowledgements

I am truly grateful for the fact that I have had the opportunity to travel half-way across the world to study a well-supported and interesting scientific topic. I recognise that I am in this position because of many fine individuals. My wife, Loren, left her family and gave up her career back in the U.S. to support me in my academic pursuits. Loren has always taken care of the important things, and this work is dedicated to her.

Were it not for the unwavering support of my parents, Sandy and Pete, and my brother Scott, I likely would not have ever attended a university, far less receive an advanced degree. Two of my high school teachers, Kim Whimpey and Sean Page, so strongly believed in me that they convinced me to believe in myself. The same goes for my supervisor, Dr. Willem Vervoort. He has encouraged me to push beyond my comfort zone and reach what I thought were unobtainable goals. I think that his mentorship has not only made me a better scientist, but a better person as well. I hope that he continues to educate and inspire students as much as he has educated and inspired me over the last three and a half years.

I would like to thank the Faculty of Agriculture, particularly Dr. Edith Lees, for supporting my IPRS scholarship and for helping me and my family adapt to Sydney. I am grateful to my associate supervisor, Professor Alex McBratney, for continually encouraging me and others to explore and appreciate the world around us. Drs. Budiman Minasny, Damien Field, Stephen Cattle, John Triantafilis, and Bryce Kelly treated me as one of their students and were always helpful and responsive to my numerous questions. I'd like to give a special thanks to my good friends, Sam Buchanan, Mick Rose, and Angus Crossan for always having the time for a whinge and a beer. My two other friends in the hydrology group, Floris van Ogtrop and Claire Glendenning were also always there to give me a hand or lend me an ear.

Many people helped collect these data, usually in adverse conditions. I am indebted to Dianna Bennett and heaps of volunteers including Nicholas Crinquant, Cathy Viguier, Fred Henry, Guillaurie Mary, Michael Jones, Robert Dittman, Soraya Cave, Loren Vanags, Scott Vanags, Annekaee Vervoort, and Sebastian, Anna and Annette Vervoort. I would also like to recognise Tim Richards, Harvey Gaynor and the staff at Auscott Midkin for allowing me to trample their paddocks and teaching

me about life in rural New South Wales. It is due to their progressive thinking in farm management that this study proceeded as smoothly as it did. Funding for this project and my candidature has been graciously provided through the Cotton CRC, The University of Sydney, and the Australian Department of Education Science and Training. Without this support, none of this research would have been possible.

Table of Contents

List of Figures

List of Tables

List of symbols and abbreviations

Greek symbols

Symbol	Description	Dimension
δ	instrument skin depth	L
ζ	coupling efficiency	-
ε_o	permittivity of free space	$F\ L^{-2}$
θ_v	volumetric moisture content	$L^3\ L^{-3}$
θ_g	gravimetric moisture content	$M\ M^{-1}$
λ	smoothing operator	-
λ	scaling factor multiplier	-
μ_o	magnetic permeability of free space	$F\ L^{-2}$
σ	apparent electrical conductivity	$F\ L^{-1}$
σ	standard deviation	-
φ^V	instrument response in vertical coil configuration	-
φ^H	instrument response in vertical coil configuration	-
ψ	soil moisture potential	L
ω	instrument frequency	T^{-1}

Roman alphabet

Symbol	Description	Dimension
A	cross-sectional area	L^2
b	aquifer thickness	L
C	speed of light	$L\ T^{-1}$
C_i	chloride concentration in applied water	$M\ L^{-3}$
$\bar{C}$	mean depth-weighted chloride at saturation	$M\ L^{-3}$
CV	coefficient of variation	-
C_z	chloride concentration in soil	$M\ L^{-3}$
ET	evapotranspiration	L
f	instrument frequency	T^{-1}
G_{RX}	directional gain of radar receiver	-
G_{TX}	directional gain of radar transmitter	-
h	moisture potential	L
h	potential	L
h	instrument height off the ground	L
H_p	primary component of the magnetic field	$F\ L^{-1}$
$\partial H / \partial z$	hydraulic gradient	$L\ T^{-1}$
H_s	secondary component of the magnetic field	$F\ L^{-1}$
I	irrigation water application rate	$L\ T^{-3}$
I	irrigation	L
K	saturated hydraulic conductivity	$L\ T^{-1}$
K_s	hydraulic conductivity	$L\ T^{-1}$
K	dielectric constant	-
K_{ref}	reference saturated conductivity value	$L\ T^{-1}$
l	collum length	L
l	distance	L
l	channel meander wavelength	L
L_e	length of well screen interval	L
m	mean of logistic formula	-
n	node	-
P	precipitation	L
q	specific discharge	$L\ T^{-1}$
Q	discharge	$L^3\ T^{-1}$
$q_{1.58}$	bank-full discharge	L^3
R	recharge	$L\ T^{-1}$
R	reflected energy	$F\ L^{-2}$
r	radius of well casing	L
R	runoff	L
ΔS	change in storage	L
s	EM coil spacing	L
s	slope of logistic formula	-
SP	radar system performance	-
Ss	specific storage	$L\ L^{-1}$
T	transmissivity	$L\ T^{-1}$
t	thickness of predicted layer	L
t	time	T
t_{37}	time for well to recover to 37% of the initial change in head	T

Symbol	Description	Dimension
V	velocity	$L\ T^{-1}$
w	channel width	L
z	gravimetric potential	L
z	depth	L

Abbreviations

Abbreviation	Description
CMP	common midpoint radar survey method
DD	deep drainage
EC	electrical conductivity
$EC_{1:5}$	electrical conductivity from a 1:5 soil:deionized water slurry
EC_a	apparent electrical conductivity
EC_e	electrical conductivity from a saturated extract
EM	electromagnetic
GPR	ground-penetrating radar
K_{sat}	saturated hydraulic conductivity
PC	palæochannel
ptf	pedotransfer function
RDP	relative dielectric permittivity
RMSE	root mean squared error
TDR	time domain reflectrometry
TL	thermoluminescence

Chapter 1

General Introduction

1 Introduction

In the cotton-growing regions of the Northern Murray-Darling Basin, agricultural practices are mostly constrained to the flood-plains of existing streams. Soils in these areas are predominantly composed of heavy clays of alluvial and æolian origin (Page et al., 1991; Cattle et al., 2002; Young et al., 2002). Near the floodplains, relict streams and palæochannels commonly occur as linear inclusions of coarse-textured material (sand to clayey sand) underlying heavy clays (Page et al., 1996; Triantafilis et al., 2002). In 1968, a detailed soil survey by Stannard and Kelly identified palæochannels as likely source of deep drainage in the Gwydir River Catchment, based on the coarser-textured topsoil above the structures. Studies have since shown that these types of structures pose risks ranging from excessive deep drainage (Triantafilis et al., 2003a), water-logging (Dwivedi and Sreenivas, 2002; Smith and Maheshwari, 2002) and offsite movement of agrochemicals (Yoder et al., 2001). However, the soil overlying palæochannels is still being utilised to grow crops such as cotton where their presence is either unknown or is simply ignored.

Many of the problems associated with managing palæochannels in an agricultural setting is due to the application of irrigation water. More than 90% of cotton grown in Australia relies on irrigation to supplement the country's limited and unpredictable precipitation. Most of this water is applied using furrow irrigation techniques, which hinge on a proper understanding of the soil infiltration characteristics to ensure crop productivity and limit deep drainage (Smedema, 1984; Hodgson et al., 1990).

Studies of irrigated Vertosols have shown that soil water pathways vary considerably under different moisture regimes (Willis et al., 1997). Under drier conditions, soil moisture flux is dominated by bypass flow; once wet, the soil swells and seals off further water infiltration (Smedema, 1984; Timms et al., 2001). Where coarser materials and kaolinitic clays are found as inclusions in the landscape, micropore-dominated flux is thought to occur, regardless of moisture content (Larsson and Jarvis, 1999). When infiltrating water encounters coarse-textured materials at depth, it may preferentially flow into the channel under saturated conditions, or around the channel under unsaturated conditions due to the low potential in the coarse

sands (Hendrickx et al., 2003). If infiltrating water enters the palæochannel, it is assumed that the channel will carry the water down gradient after it reaches saturated conditions (Fetter, 2001). Due to variable connectedness to present water courses, a nearby watercourse may or may not receive this water in the process (Sophocleous, 1991; Rogers et al., 2002). Given this variability in water dynamics, it is imperative to understand where these inclusions of sand occur in the environment and how they are affecting the water dynamics in the vadose zone. The first part of the research component in this thesis is dedicated to understanding the properties of these structures and how they relate to the surrounding landscape.

Palæochannels have traditionally been described by directly observing them, through soil coring and aerial photography (Schumm, 1968; Pels, 1973; Stannard and Kelly, 1977; Page and Nanson, 1996). Geophysical methods have been used to rapidly (and non-invasively) detect the extent of palæochannels (Salama et al., 1994a; Godwin and Miller, 2003). Furthermore, empirical relationships have been developed to transform geophysical information into soil property information. Relationships have been developed to describe clay content (Doolittle et al., 1994; Sudduth et al., 2005; Triantafilis and Lesch, 2005), water content (Sheets and Hendrickx, 1995), salinity (Rhoades and Corwin, 1981; Lesch et al., 1995b; Triantafilis et al., 2000) and hydraulic conductivity (Vervoort and Annen, 2006). To date, most of these (and other) studies have been limited to two dimensions due to the nature of EM measurements.

Of the properties previously mentioned, saturated hydraulic conductivity is the most variable and has the largest impact on the prediction of soil and groundwater flow associated with soil and geologic heterogeneity (Buchter et al., 1991; Bird et al., 1996; Gee et al., 2005). The prediction of this property through the use of ancillary (geophysical) data is far from being well-understood. But, considering the amount of information to be gained from using non-invasive methods to predict saturated conductivity, there is great interest in obtaining this type of information for future investigations, particularly where soil property measurements are limited.

This thesis aims to describe the hydraulic properties and the associated water fluxes in the upper ten metres of the regolith associated with the palæochannel system. By relating this information to questions raised in previous studies, a more comprehensive conceptual model of water flow through palæochannels in northern New South Wales can be obtained. Specifically, this thesis aims to:

- describe the morphology of the palæochannel system in comparison to other systems in Northern New South Wales
- measure deep drainage and lateral flow associated with the palæochannel under irrigation
- explore non-invasive methods for detecting palæochannels, specifically ground-penetrating radar and electromagnetic induction
- use the geophysical information to predict the distribution of soil hydraulic properties in three-dimensions

In regards to these aims, the thesis explores the following hypotheses relating to palæochannel presence under irrigated agriculture:

H1: Palæochannels are areas of both lateral and vertical preferential flow

H2: A combination of geophysical and direct soil property measurements is needed to describe the hydrologic properties of these features in three dimensions.

Chapter 2

Review of Literature

2 Review of Literature

2.1 Introduction

The term "palæochannel" is used to describe stream or river beds which have been abandoned and subsequently filled with transported sediments. Generally these features have no surface expression, meaning that in the landscape there is no visible difference in elevation. Palæochannels of various sizes occur in much of the Australian landscape, usually in close proximity of presently flowing streams. Palæochannels containing coarse-textured sediments may play an important role in the movement of shallow groundwater and have the potential to adversely affect water-use efficiency in irrigated landscapes (Mailhol et al., 1999; Triantafilis et al., 2003a; Triantafilis et al., 2004). Despite this potential, there has been little effort to quantify the impact these structures have on water movement in the vadose zone over a period of time.

This review has three broad objectives. Firstly, it provides background information on the broader study area and research findings at similar sites around Australia. Included in this section are details of the geology, soils, and climate of the region, as well as human settlement patterns and the resulting impacts on the environment. From this point, the focus narrows to palæochannels and the impact they may have on the vadose zone and irrigation management. A general overview of palæochannels around Australia, including their formation, morphology, and methods used to identify their age, sediment characteristics, and palaeodischarge is provided. Additionally, the possible effects of palæochannels on groundwater and surface water quality are described.

Given these effects, it is important to find and characterise these structures in three dimensions. This leads to the second objective of this chapter, which is to review different methodologies for imaging subsurface structures and predicting groundwater flow. In this section, hydrological and geophysical theory is discussed, with an emphasis placed on methodologies most commonly used in similar studies.

The section on hydrologic modelling presents common techniques for estimating infiltration and recharge, an important topic when considering interaction between surface and subsurface water. Following this, theories of saturated and unsaturated flow are discussed, as they are the foundation of many groundwater models. The section concludes by presenting several case studies from groundwater modelling investigations around Australia, providing a general overview of the strengths and weaknesses of some commonly-used groundwater models

In the section on geophysics, several methods used for imaging shallow sediments are examined. Here, emphasis is placed on electromagnetic methods which operate in the frequency domain (electromagnetic induction) and time domain (ground-penetrating radar). Because frequency domain instruments present special problems in signal processing, a subsection is dedicated to describing several methods to invert geophysical data to construct conductivity profiles from depth-weighted measurements.

This chapter aims to show how this research ties in to existing scientific knowledge by highlighting gaps in the understanding of ways which palæochannels can be detected and their impacts predicted in semi-arid environments such as the Murray-Darling Basin.

2.2 The Murray-Darling Basin

The Murray-Darling Basin is Australia's largest river system. It encompasses a large portion of southeastern Australia, including the majority of New South Wales and parts of Queensland, Victoria and South Australia. The Murray and Darling Rivers both originate in the Great Dividing Range, and subsequently receive flow from 18 major tributaries to finally converge approximately 300 km from the point of final discharge in Lake Alexandrina, 3 780 km from the headwaters (Figure 2.1). In total, the Murray-Darling Basin drains one-seventh of continental Australia.

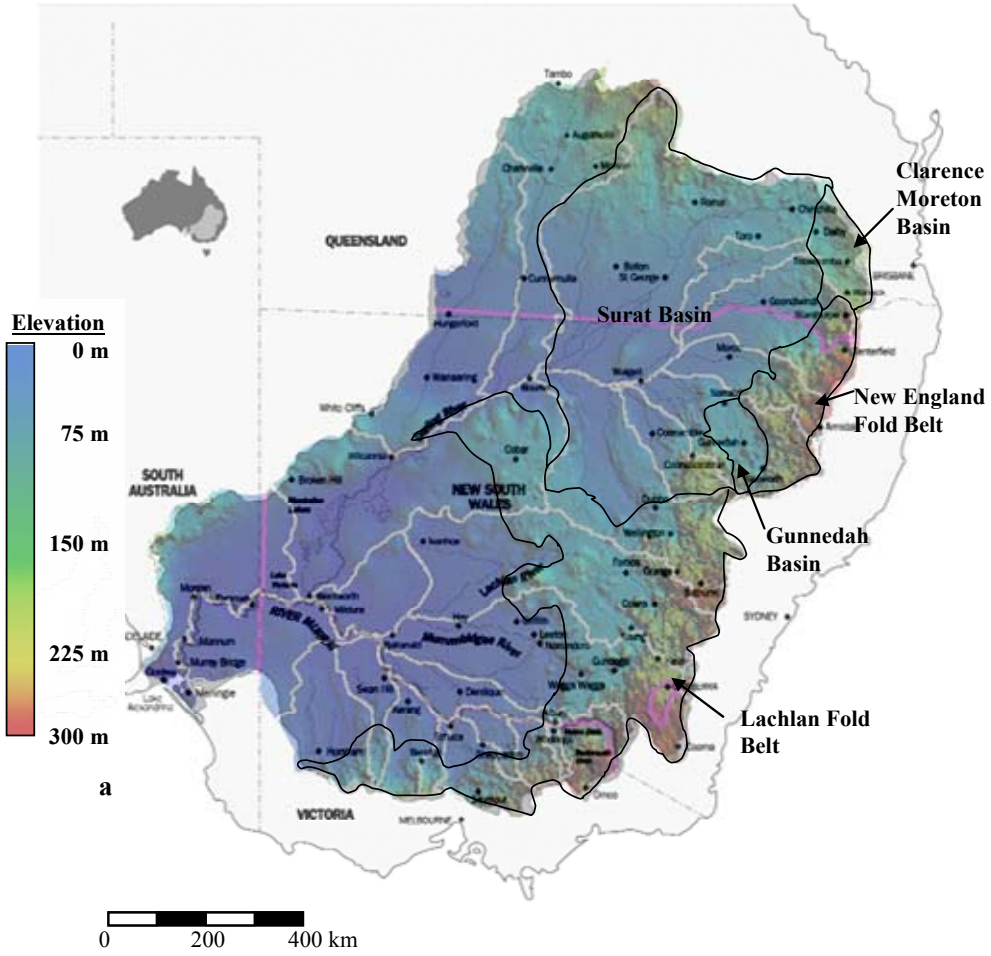

Figure 2.1. Outlined major tectonic units (black), catchment boundaries (white), state boundaries (purple) and relief of the Murray-Darling Basin. From (Kingham, 1998; MDBC, 1999).

Although the basin spans over 1 000 000 km^2, the mean annual discharge of the river is only 12 200 GL, approximately 1/20 of the average discharge of basins with similar catchment sizes and lengths worldwide . This is because the majority of rivers in the catchment are classified as "losing reaches", where variably-connected aquifers are recharged through ephemeral flow events (Braaten and Gates, 2003). In addition, evaporation rates are very high relative to precipitation (Table 2-1), also limiting the amount of runoff. In losing streams, base flow is negligible and waters typically increase in soluble salts as they flow away from their source (Winter, 1999). This flow system has resulted from, and contributes to, several unique environmental factors, such as the geology, soils and climate of the region.

2.2.1 Climate

Climate in the Murray-Darling Basin is classified as semi-arid to arid with the majority of the rainfall falling on the eastern edge, coinciding with the Great Dividing Range (Australian Bureau of Meteorology, 2002). Further inland, precipitation decreases by an order of magnitude over 500 km (Figure 2.2). The potential evaporation rates increase westward from the Great Dividing Range and can equal four times that of precipitation. Parallelling this trend is the rainfall variability, which also increases significantly westward. For example, in several towns located at (or near) the Gwydir and Darling Rivers, the reduction in rainfall away from the coast is accompanied by monotonic increases in rainfall variability, average minimum and maximum temperatures and evapotranspiration rates (Table 2-1, bolded in Figure 2.2).

On an annual basis, much of the Australian continental weather patterns are driven by the Southern Oscillation – commonly associated with the global phenomenon of El Niño. This means that rainfall patterns throughout most of Australia are inversely linked with sea surface temperatures around the Pacific and Indian Oceans, where higher sea surface temperatures correspond to lower than average precipitation in Southeast Australia (Pittock, 1975). The relationship is strongest from September through November (McBride and Nicholls, 1983) but continues throughout the year. The relationship with the Southern Oscillation has a significant impact on the natural discharge of the Murray and Darling Rivers, mainly due to winter rainfalls (Simpson et al., 1993; Chiew et al., 1998). These climatic patterns result in long droughts followed by occasional heavy rains, and subsequent flooding. Given the low hydraulic gradient in much of the basin (Figure 2.1), it is not uncommon for fields and towns to remain flooded for weeks during major storm events (Robertson et al., 2001). Although long-term forecasts are still prohibitively uncertain, seasonal rainfall prediction may be made several months in advance based on sea surface temperatures (Chiew et al., 1998).

Table 2-1. Geographical and climatological information for six towns located near the Gwydir and Darling Rivers (Figure 2.2), showing decreases in annual precipitation and air temperature with distance downstream (which are inversely related to precipitation variability and evapotranspiration).

			Temperature#		Precipitation#			
Town	Distance downstream	Elev.	Max	Min	Total	Variability##	Events	ET#
	km	m	—— °C ——		mm		days	mm
Uralla	0	970	19.6	6.3	804	0.50	100	1580
Bingarra	129	299	26.1	10.0	744	0.66	73	1800
Moree	233	206	26.0	12.3	586	0.72	78	2200
Walgett	436	132	26.9	12.5	475	0.87	55	2150
Bourke	655	106	27.6	12.9	355	1.18	47	2350

#Annual average
##Variability = (90p-10p)/50p

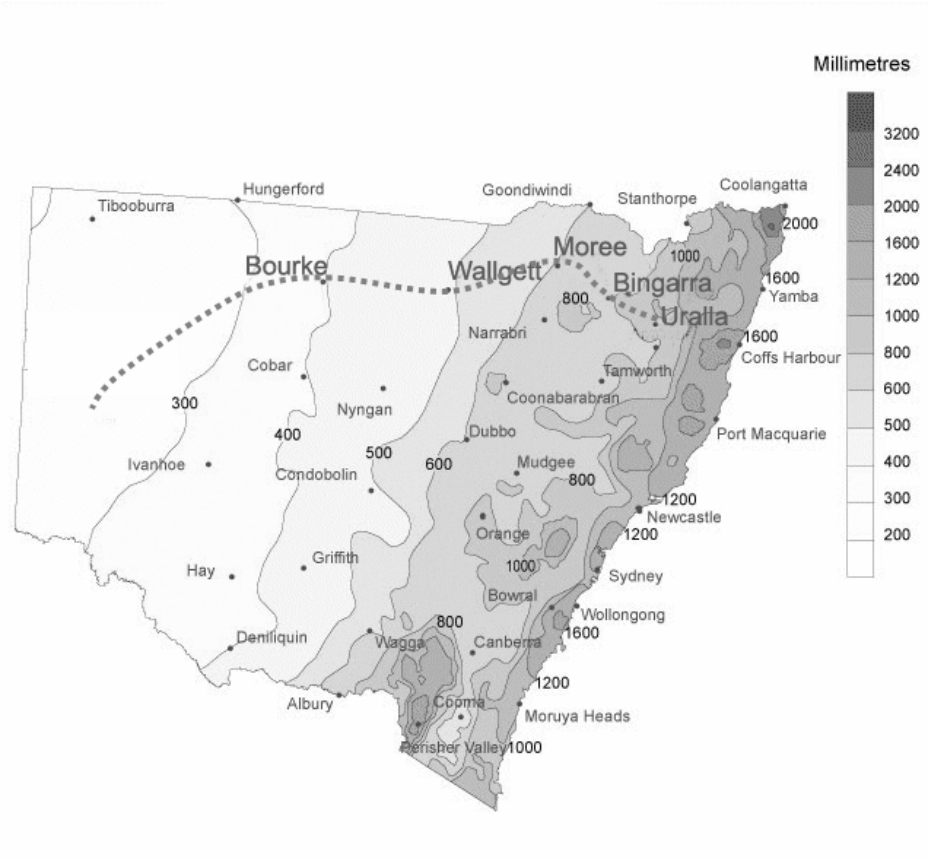

Figure 2.2. Isohyet contours for New South Wales based on a 30 year data set. Precipitation steadily decreases westward and inland. Dotted line shows path for climate data from five towns along the Gwydir and Darling Rivers (Table 2-1). From the Australian Bureau of Meteorology (www.bom.gov.au).

2.2.2 Geology

The northern portion of the Murray-Darling basin consists mostly of sediment deposits derived from three main sources: the New England and Lachlan Fold Belts, the Surat Basin, and the Gunnedah Basin. The Murray-Darling Basin is bounded by metamorphic and crystalline rocks of the Lachlan and New England Fold Belts to the east and southeast (Figure 2.1). The Lachlan Fold belt, once a series of deep and shallow marine sediments punctuated by basaltic volcanoes, was accreted onto the active margin of Gondwanaland during the middle to late Palaeozoic adding an extra 700 km of metamorphic and igneous material to the eastern edge of Australia (Gray et al., 1997; Foster and Gray, 2000). The resulting felsic rocks (enriched in silica, aluminium, and potassium) are mostly comprised of high temperature, low-pressure metamorphosed sediments (green schist facies) and extensive granite batholiths, punctuated with mafic material (enriched in magnesium, iron, calcium and sodium) from the relict volcanoes (Gray et al., 1997; King et al., 1997; Kingham, 1998; Fergusson, 2003).

Off the coast of Gondwanaland, the New England Fold Belt underwent a similar orogeny, but with a more complex array of sediments due to the presence of felsic forarc volcanoes (Fergusson, 1984). These sediments were accreted onto Australia during subduction in the late Carboniferous Period (Leitch, 1975; Holcombe et al., 1997). The metamorphosed sediments are more resistant to weathering and are generally more felsic, but are chemically similar to those sediments from the Lachlan Fold Belt.

Overlying these fold belts are the Surat and Gunnedah basins. These basins both contain transgressive sequences of marine and non-marine sediments which contain economical petroleum and coal reserves (Kingham, 1998; Glen, 2000). The sandstones, mudstones, and conglomerates of the Gunnedah Basin were deposited from the Permian into the Triassic Periods. During the Tertiary, these sediments were intruded by a series of basaltic volcanoes.

Similar to the Gunnedah, the Surat Basin contains marine and continental clastic material, ranging from coarse terrestrial sandstones to marine siltstones. Much of this material was deposited between the Jurassic and the Cretaceous Periods, and

has since weathered to produce a range of coarse- and fine-textured acidic sediments (Glen, 2000). This series was also punctuated by the mafic Tertiary volcanos. Through alluvial activity, the weathered products of these volcanoes produced a veneer of fine-grained alkaline soils in much of the basin (Stannard and Kelly, 1968; Stannard and Kelly, 1977; Kingham, 1998; Young et al., 2002). The wide range in physical and chemical properties of transported and in-situ sediments have given the Northern Murray-Darling Basin a variety of soil types which can vary over short distances (Figure 2.1).

2.2.3 Soils

Many of the soil types found in the northern part of the Murray-Darling Basin have characteristic mineralogy and horizonation due to dramatic shifts in the underlying geology and sediments deposited over time. Three of these soils, Vertosols, Kandosols, and Sodosols, dominate much of the landscape and have distinctive contrasts in their chemical and physical properties.

The majority of the soils found in the alluvial flats of the basin are Vertosols. These soils resulted from fluvial and æolian transport of sediments from the Lachlan and New England Fold Belts and the basaltic intrusions in the Gunnedah Basin (Stannard and Kelly, 1977; Young et al., 2002). They are relatively young in age (less than 100 000 years) and are associated with the vast flood plains of the Darling River and its tributaries. Vertosols contain appreciable amounts of smectitic clays which swell with hydration, are high in basic cations (Ca^{2+}, Mg^{2+}, K^{+}), and have a high cation exchange capacity (40 – 80 $cmol^{+}$ kg^{-1}) (Stannard and Kelly, 1968). Subsequently, they are nutrient-rich and have high water holding capacity and, hence, are ideally suited for agriculture (Stannard and Kelly, 1968; Stannard and Kelly, 1977).

Commonly associated with Vertosols are palæochannels, where rivers which once cut through the alluvium have since dried up or changed course. The coarse-textured sediments associated with palæochannels contrast the surrounding Vertosols and are can sometimes be recognised as lighter-coloured linear features. In much of the Northern Murray-Darling Basin, the clay mineralogy within the palæochannels is dominated by Kaolinite and Illite and, hence, has a lower cation exchange and water-holding capacity and does not exhibit the same swelling behaviour as Vertosols

(Stannard and Kelly, 1968; Stannard and Kelly, 1977; Triantafilis et al., 2002). This is often reflected in dramatic contrasts in natural vegetation around the features (Stannard and Kelly, 1968; Stannard and Kelly, 1977) and crop yield (Bishop and McBratney, 2001).

Kandosols are widely distributed around the basin and are derived from sediments transported from the Lachlan and New England Fold Belts. Similar to Vertosols, Kandosols show very little signs of clay or oxide illuvation, mostly due to their young age (Daniells et al., 2002). Unlike the Vertosols, however, Kandosols are much more acidic and have less clay (usually less than 15 – 20%, compared to 40 – 70% for Vertosols) (Isbell, 1996). Similar to the palæochannels, the clay mineralogy is dominated by Kaolinite and Illite and they have little cation exchange and water holding capacity.

Sodosols are commonly found where the parent material contains appreciable amounts of sodium. Australia is renowned for these soils, mainly because of its arid climate, and has more hectares of Sodosols than all other countries combined (Levy et al., 2005). These soils are neutral to alkaline and have been derived from the underlying sediments of the Surat Basin. Sodosols have a strongly-developed clay-rich subsoil and have a high exchangeable sodium percentage (Isbell, 1996). These soils pose special problems to agricultural management because they disperse due to the repulsion of monovalent-saturated clay particles (Pons et al., 2000). Dispersion severely limits the soil hydraulic conductivity and often results in a limited crop root length (Bird et al., 1996; Levy et al., 2005). Also, topsoil crusting occurs when dispersed clays are displaced by the impact of rainfall or irrigation water, filling in soil pores and severely limiting infiltration (Daniells et al., 2002; Foley and Silburn, 2002). Some methods to ameliorate these soils include lime and gypsum applications (Khosla et al., 1979; Kowalik et al., 1979; Wild et al., 1992), and tillage (Wild et al., 1992; Levy et al., 2005).

2.2.4 Land-use patterns

Land-use patterns in the basin have been dramatically altered since European settlers traversed the Great Diving Range to find suitable land for grazing and cropping. Early settlers cleared large areas of forests to make way for European-style

agriculture. Today, the land-use distribution west of the Great Dividing Range is dominated by grazing and dryland agriculture.

The clearing of native vegetation has had lasting impacts on Australia's ecosystem, and has likely caused large-scale salinity outbreaks in an estimated 300 000 ha of land in the Murray-Darling Basin alone (White, 2000). The use of traditional European tillage techniques and grazing of introduced sheep and cattle has further damaged the soil structure in otherwise fertile lands (Proffitt et al., 1995b; Proffitt et al., 1995a; da Silva et al., 2003). Fortunately, Australian farmers have adapted with non-traditional farming methods such as reduced tillage (Lawrence et al., 1994), precision management (Triantafilis et al., 2001b; Whelan and McBratney, 2001; Stewart et al., 2002) and on-farm water recycling (Goyne and McIntyre, 2003). In some areas, these methods have slowed or reversed declining trends of soil health, surface water, and groundwater contamination.

The Australian economy relies heavily on introduced crops and livestock (ABS, 2005). Of the 467 million hectares currently used for agricultural practices, 430 million hectares are currently utilized to graze livestock, mostly consisting of cattle and sheep (ABS, 2005). Over 80% of the 22 million used for cropping is used to grow cereals, with the majority of this land dedicated to dryland cropping of wheat (Australian Natural Resource Atlas, NHT, 2001). Irrigated agricultural products occupy approximately 0.4% of the area used for cropping. However, these commodities have major impacts in terms of their economic value and environmental impacts (Suarez, 1989; van Schilfgaarde, 1994; MDBC, 1999; ABS, 2005).

2.2.5 Irrigated agriculture

Irrigated crops and pastures in Australia generate an estimated $7 billion in pre-processed farming revenues. Given that irrigated agriculture utilises 0.4% of land dedicated for agricultural activities, it follows that irrigation is a major component of the agricultural part of Australia's gross domestic product. The Murray-Darling basin contributes 41% of the total agricultural production in Australia and contains 71% of the land dedicated to irrigated agriculture, the majority of which are pasture crops.

Second to pasture crops, cereals and cotton each occupy 16% of the area dedicated to irrigated agriculture (ABS, 2005). As one of the most economical, but resource-intensive crops, cotton accounted for $1.3 billion of the $16.2 billion of the

gross value of agricultural products produced in 1994 (ABS, 2005), accounting for 3.5% to 8.3% of the total value of agricultural goods produced between 1994 and 2004. In Australia, nearly all of the cotton is grown on the alluvial floodplains of tributaries of the Murray and Darling Rivers (Figure 2.3), and is spread throughout the Namoi, Gwydir, McIntyre, Macquarie, and Murrumbidgee valleys with isolated patches in the Darling Downs, Bourke and Emerald Regions (Figure 2.3). The distribution pattern is dictated by the need for irrigation water, requiring the farm to be within 5 km of a managed waterway (Stannard and Kelly, 1968; Lincare, 2005).

Rice is another major irrigated crop in Australia, generating $409 million worth of exports. Produced from only 148 000 ha of land, rice is one of the most profitable grains grown in Australia (ABS, 2005; RCRC, 2006). Rice growing is constrained to the southern portion of the Murray-Darling Basin, mainly in the Lachlan and Murrumbidgee Regions, due to the cooler temperatures and the suitability for the soils to support flood irrigation methods (Figure 2.3).

2.2.6 Irrigation Management

Irrigation management in Australia is constrained by the semi-arid climate, extreme rainfall variability (Figure 2.2, Table 2-1) and the steady increase in the size of farms over the past few decades (ABS, 2005). In the late 1980's open market water trading was introduced in Australia in the form of transferable water entitlements. The trading scheme was adopted with the hope of maximising water-use efficiency by shifting the perception of water from a "right" to a "commodity". Although this change initially had unwanted side affects as non-users sold their entitlements to users (increasing the total amount of water used state-wide), the wide-spread adoption of water trading has indicated a paradigm shift in the traditionally conservative mentality of Australian farmers (Crase et al., 2004).

Figure 2.3. Major cotton and rice-growing regions around Australia. From (CRCD, 2005; RCRC, 2006).

In New South Wales, 4.5% of establishments traded water to secure extra supplies (Lincare, 2005). Using current government-constrained open market pricing, the cost of water for irrigating an average 400 ha cotton farm was only $17 151 (ABS, 2005; Lincare, 2005; www.statewater.com.au, 2006). Without government price regulation, which is likely to be phased out over the next five years, this price will increase to $48 258 (www.statewater.com.au, 2006). Considering that many cotton farms in NSW exceed 1000 ha and use approximately 7.0 Ml ha^{-1}, it seems likely that price increases such as these will significantly affect the mentality of the Australian irrigator.

Although irrigation managers generally strive to maximise their water-use efficiency, it is not uncommon for them to make sacrifices in order to meet short term productivity goals. This management scheme mainly results from Australia's extreme variability in precipitation (Table 2-1) and the strict control over water distribution by

government agencies on a seasonal basis. By choosing efficient methods for irrigating crops, irrigators reduce the risks associated with these fluctuations, but this usually comes at the expense of increased initial capital and energy requirements.

In 2003-2004, 98% of Australian irrigators used a combination of surface water, sprinkler and drip irrigation for distributing water to their crops. Although the majority of land in Australia is irrigated using surface methods, drip and sprinkler methods have been increasingly implemented over the last few decades (Lincare, 2005). The adoption of sprinkler and drip irrigation methods has steadily increased since World War II (Walker and Skogerboe, 1987; Dasberg and Or, 1999) as a result of a world-wide shortage of suitable irrigation water and smaller profit margins in agriculture (Letey et al., 1990; Ross et al., 1990; Smith, 1998).

2.2.6.1 Surface irrigation

Surface irrigation methods are the most widespread method used in Australia. In New South Wales, surface irrigation techniques supplied water to 75% of the irrigated land during the season of 2003-2004 (Lincare, 2005). The dominance is due to the large areal extent of Vertosols and the associated cotton and rice cropping across the state (Section 2.2.4). The most commonly-used surface irrigation methods in Australia are flood and furrow irrigation, which are employed to irrigate farms with suitable soils and a sufficient water distribution system.

Flood irrigation is mainly associated with rice and pastures in the southern portion of the Murray-Darling Basin. As the name implies, flood irrigation works by flooding a field with pulses of water. Typically, water is channelled to the paddock via earthen netrowks, and is siphoned out onto the field. As water infiltrates into the soil, the effective hydraulic conductivity is decreased, leading to variably-saturated overland flow as the flood wave advances (Green, 1991). Earthen embankments are positioned around the paddock to ensure that the water stays on the field. Once the flood wave travels over the entire paddock, the excess water either remains ponded for a period of time (in the case of rice) or is channelled through a tail drain and returned to the water storage.

Due to variability in soil hydraulic conductivity and microtopography, this method does not distribute water uniformly, and performs especially poorly in non-graded fields (Green, 1982; Green and Middlemas, 1985). Furthermore, preferential

flow pathways can dominate infiltration patterns in certain soil types (such as dried-out heavy clays), resulting in increased water loss and reduced crop yield due to water logging (Yasuda et al., 2001; Kim et al., 2004). The average amount of water required to irrigate rice crops using this technology in 2003-2004 was 12.4 Ml ha^{-1} (down from 14.7 Ml ha^{-1} the previous year) making rice the most water-intensive crop grown in Australia (Lincare, 2005).

Research in flood irrigation technology aims to improve water-use efficiency and maintain the system's simplicity. Grading and laser levelling have been shown to greatly enhance water-use efficiency, by homogenising the soil surface and ensuring the correct slope and aspect of the paddock (Green and Middlemas, 1985; Kim et al., 2004). The technique also redistributes smaller soil particles, filling in soil pores, effectively lowering the saturated hydraulic conductivity and reducing the risk of preferential flow and deep drainage. Tillage is also known to have a similar effect, particularly in terms of reducing preferential flow (Yasuda et al., 2001).

Furrow irrigation systems are similar to flood irrigation, but channel water through shallow trenches across the paddock. Crops are typically planted in the mounded soil separating the furrows, which serves to reduce the rooting depth and limit the affects of water logging. The trenches are cut at a precise slope which depends on the infiltration characteristics of the soil. As water is channelled into the furrows, it infiltrates as the flood wave progresses (Figure 2.4) similar to flood irrigation. Ideally, all of the water applied will have infiltrated uniformly down the furrow, but tail drains are placed at the ends to channel water off of the paddock and back into storage (Hodgson et al., 1990; Esfandiari and Maheshwari, 2001; Smith et al., 2005).

Although this method improves on the water distribution of flood irrigation, there are still significant problems with the systems. Waterlogging commonly occurs at the distal portions of the furrows due to excess water accumulation (Smith and Maheshwari, 2002). These areas are also prone to deep drainage and water loss through evaporation (Hodgson et al., 1990; Wichelns, 1999). Because of the surges required to ensure an even distribution of water, soil particles can be transported and deposited in soil pores, essentially clogging the soil surface and limiting infiltration at the distal ends of the furrows (Al-Qinna and Abu-Awwad, 1998). This means that furrow irrigation techniques, although economically beneficial, can be resource

intensive. In some extreme cases, these systems lose up to 75% of water allocated for irritation due to evaporation, deep drainage, and lateral flow (Borrell et al., 1997; Smith et al., 2005).

2.2.6.2 Sprinkler irrigation

Although surface irrigation methods are the most widespread (covering the largest area), sprinkler methods are the most commonly used by irrigators. Sprinkler irrigation is possibly the most versatile irrigation technology and offers the most control of application rates and irrigation timing (Ross et al., 1990). It is used to irrigate row crops, pastures, vegetables, orchards and grapes on various soil types in Australia (Lincare, 2005). Because the application rate can be controlled by altering the water pressure and sprinkler aperture, these methods are commonly used to irrigate lighter textured and gently undulating soils (Ross et al., 1990; DeBoer and Chu, 2001).

Sprinklers come in many forms, but the technology is based on the distribution of small droplets of water to simulate rainfall. Sprinkler irrigation techniques mostly differ in their capacity to distribute water to the field. The sprinkler network can be fixed, where sprinkler heads remain in a set position and rotate to distribute water, or they can be mounted on a movable distribution system. Simple, fixed systems can effectively distribute water to smaller parcels of land and are commonly linked to high pressure pumps to maximise water distribution. These systems have been used in orchards and vineyards in Australia (Lincare, 2005) but for large scale row crop agriculture, these systems are cost-prohibitive (Ross et al., 1990).

Large farms commonly employ movable sprinkler systems to reduce the effects of wind on the uniformity of water distribution. Two of the most common methods on larger farms are linear movement and centre-pivot systems (Ross et al., 1990; Goyne and McIntyre, 2003). Both systems use large laterals, which travel above the crop canopy. The linear system travels parallel to the beds, and can be set on tracks or moved using motorised wheels. Sprinkler heads dangle from hoses connected to these laterals in order to effectively distribute water to the plant by minimising spray drift.

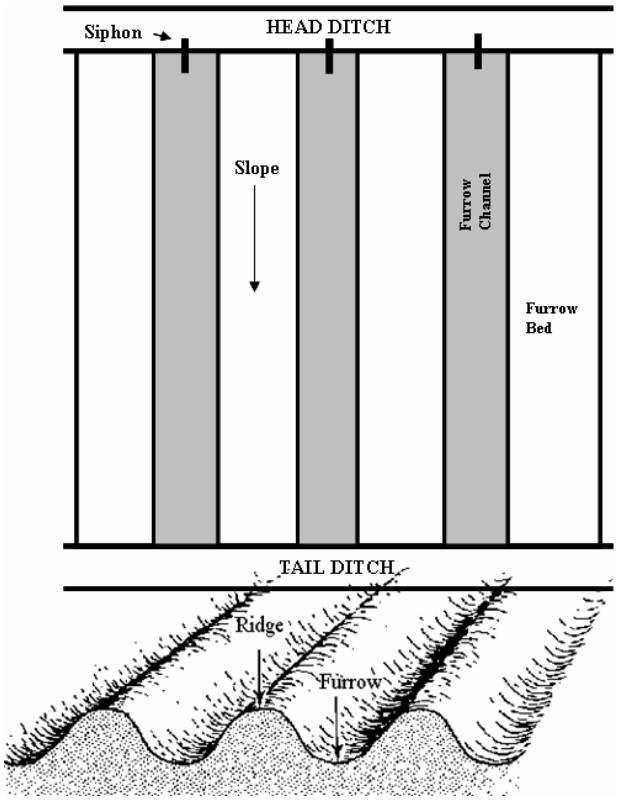

Figure 2.4. Typical layout for irrigated paddocks under furrow irrigation. Water leaves the head ditch, travels along the furrow channels and returns through the tail ditch. From Esfandiari and Maheshwari, 1997.

Centre-pivot irrigation works similarly to moving laterals, but with one stationary point, where water enters the lateral. The main difference between the methods is the water pressure distribution. Because the outside of the lateral travels faster than the inside, water must be applied at a faster rate in order to apply the same amount of water. For this reason, the application is best suited for soils with higher infiltration rates (Foley and Raine, 2001).

The main benefit of sprinkler irrigation is that it provides the irrigator with the maximum amount of control over the distribution of water to the crop. By changing the irrigation rate, frequency and uniformity, it is possible to completely eliminate water-related stress on high-value crops, resulting in increase yields (Al-Jamal et al., 2001; NHT, 2005). Sprinklers can also significantly improve water-use efficiency and nearly eliminate the risk of water logging, deep drainage, and runoff. Studies have shown a 19 – 42% savings of water-use when compared to surface irrigation on

neighbouring paddocks (NHT, 2005). Properly calibrated, these systems are able to operate at 100% water-use efficiency, outperforming both surface and drip methods (Al-Jamal et al., 2001; NHT, 2005). By incorporating fertilizers and herbicides into the water supply (termed "fertigation"), the farmer also saves on spraying cost and increases the effectiveness of the nutrient, herbicide, and insecticide applied (Pinto and Da Costa, 1999; Vieira and Sumner, 1999; Vieira Junior et al., 2000).

The most significant barrier with sprinkler technology is the initial cost and required maintance. In 1991, the cost of installing a high pressure travelling system was \$2 700 ha^{-1}, as compared to \$800 ha^{-1} for a surface system (Ross et al., 1990). There are also added costs of diesel to run the water pumps (however, this is often beset by the diesel saved in fertilizer and herbicide spraying) and the large crews needed to set up the distribution lines during an irrigation event (NHT, 2005). Sprinkler irrigation also requires a clean water supply, or a filtration mechanism to keep sprinkler heads from clogging with sediment. Also, foliar application of water is much more likely to spread disease than surface or subsurface distribution (Gray and Guthrie, 1977; Vieira Junior et al., 2000).

Where centre pivots are used, changes must be made in the layout of farms, requiring specialised equipment for field operations. It has been suggested that these systems are ideally suited for farming near watercourses, where coarser-textured soils exist, and floodplain geometry can be easily incorporated (Ross et al., 1990).

2.2.6.3 Drip irrigation

"Only when water is severely limited, highly priced and when its distribution is tightly controlled by a central agency, is the high degree of control of water application offered by drip irrigation of real economic advantage". – (Dasberg and Or, 1999, p.4)

This statement exemplifies the true motives behind the adoption of advanced irrigation techniques. In New South Wales, only four percent of irrigators employ drip (sometimes referred to as "trickle") irrigation to supply water to their crops. Although this number appears small, the amount has increased significantly in the last decade (Lincare, 2005). This trend has been attributed to a steady decline in the amount of irrigation water allocated to farmers in the Murray-Darling Basin (Crase et al., 2004) and the subsequent increase in water prices. From the farmer's perspective,

these trends are predicted to worsen over the next five years due to continued drought and the inevitable withdraw of government subsidies on traded water (Crase et al., 2000; Raine et al., 2000; www.statewater.com.au, 2006). Although Dasberg and Or were speaking in general terms, it appears that an Australian case study would provide a reasonable amount of support for their statement.

Drip lines became commercially available during the "plastic revolution" following World War II. However, it wasn't until the last couple of decades that technological advances in plastics enabled irrigators to use them to irrigate large plots and row crops (Dasberg and Or, 1999; Raine et al., 2000). In Australia, they are still mainly used to irrigate high-value horticultural crops in greenhouses, but their adoption has increased in the last five years for broad acre crops such as cotton (Lincare, 2005).

Drip systems are comprised of laterals made of plastic tubes or tapes with variably-spaced emitters designed to distribute a fine trickle of water directly to the soil surface or subsurface. Irrigators can continuously supply small amounts of water to the plants, ensuring a high moisture potential in the soil, and minimal water loss. Traditionally, the laterals were buried, but recent advances in drip tape technology allow farmers to lay tapes on the soil surface during irrigation events and remove them for field operations (Dasberg and Or, 1999).

Although expensive, drip irrigation provides many benefits over the other common irrigation techniques. Because the irrigator is able to continuously supply water to the soil, the moisture potential can be matched to the crops evaporative demands, completely eliminating water stress on the crop (Dasberg and Or, 1999). For this reason, the method may significantly improve crop yields in many different environments, even with the use of saline water and deficit irrigation techniques (Cuevas et al., 1984; Mateos et al., 1991b; Mateos et al., 1991a; Dasberg and Or, 1999; Raine et al., 2000).

Water-use efficiency in drip irrigation systems is very high, when compared to other systems. Application efficiencies above 90% have been reported, nearly eliminating the risk of deep drainage (Ayars et al., 1999; Raine et al., 2000). Because emitters are below or at the soil surface, irrigation scheduling is not contingent upon

wind speed, unlike sprinkler systems. Also, fertigation techniques are possible using these systems, similar to the sprinkler methods.

Similar to sprinkler systems, the most negative aspect of drip irrigation is the capital required to purchase, operate and maintain the system. In 1995, Dhuyvetter and others estimated the initial cost of a system to be \$1 942 ha^{-1} (cited in Dasberg and Or (1999)). Apart from it being the most expensive initially, running costs are also quite expensive. Batty (1975) reported that the energy required to operate drip irrigation systems, although less than sprinkler systems, was 10 times more than surface irrigation methods. In several Australian cotton trials, the high cost of buying and running the equipment significantly outweighed the potential yield increases (Constable and Hodgson, 1990; Raine et al., 2000).

Because the systems are located at or below the soil surface, problems with emitter clogging can significantly increase the amount of energy required to maintain the system and lead to uneven water distribution (Amali et al., 1997; Dasberg and Or, 1999; Raine et al., 2000). Clogging can also occur due to impurities in the irrigation water, such as salts or sediment (Dasberg and Or, 1999).

Technological advances in drip irrigation aim to improve the efficiency and reduce the likelihood of clogging. Significant reductions in water-use can be made by doubling the lateral spacing on some crops, with little sacrifice in crop yield (Cuevas et al., 1984; Mateos et al., 1991b; Raine et al., 2000; Al-Jamal et al., 2001). But, this can have significant adverse affects on crop performance where the application is non-uniform making these methods site-specific (Amali et al., 1997; Ayars et al., 1999). The most effective technique to prevent clogging is by incorporating an in-line filtration system. These systems have become automated in order to reduce the management required to maintain proper filtration (i.e. periodical back-flushing), although the water savings inherit in the system are quickly dissipated by using these methods (Ross et al., 1990). By incorporating herbicides in buried systems, or using treflane-impregnated emitters, the irrigator can reduce the likelihood of root impregnation in the system.

2.3 Palæochannels

Palæochannels[1] are abandoned streams and rivers which have subsequently filled with sediments of æolian and alluvial origin. Palæochannels extend through every part of Australia, including the Great Barrier Reef (Fielding et al., 2003), the Gibson Desert (Beard, 2002) and even around Uluru (Ayers Rock) (English, 1999). Shallow palæochannels are often found near present water courses (often within the floodplains). Deeper ones, however, are commonly linked with palæodrainages which may not have any connection with current water courses (Figure 2.5). At times, the occurrence of palæochannels is marked by contrasts in vegetation or soil colour. More commonly, the characteristic properties have only subtle effects on the landscape, making their detection difficult.

Although they are subtle in appearance, palæochannels record dramatic changes in the environment. Rivers respond to environmental stresses by incising their channel bottom or increasing their width and sinuosity (Schumm, 1985). River channels are therefore constantly being reworked and are sometimes abandoned in response to tectonic activity, sediment supply, or climate change. To illustrate how this may happen at various spatial and temporal scales, several scenarios for channel abandonment have been suggested:

- Geologic uplift at a plate boundary increases the channel gradient, leading to channel incision and decreasing sinuosity over the course of tens of millions of years (Beard, 2002).
- Small changes in the tilt of the Earth's axis create climatic fluctuations, driving the cyclic meandering of a major river, depositing a 1 100 m

[1] Palæochannels are known throughout the world as "relict channels", "ancient streams" and "prior streams". Each of these terms implies specific qualities such as age, size, sinuosity, amount of surface expression and connectedness to present streams (Butler, 1950, Schumm, 1968, Page and Nanson, 1996). However, as the Latin-derived definition only translates to "ancient stream", this thesis lumps all of these terms together for the sake of simplicity and readability.

thick succession of palæochannel sediments over several hundred thousand years (Olsen, 1990).

- The end of an ice age prompts a global sea level rise, decreases a stream's base level, which increases sinuosity over the course of thousands of years (Page and Nanson, 1996).
- A regional drought is punctuated by several large storm events. Overbank conditions result in the incision of the flood plain and the rerouting of the stream during the course of a season (Nanson and Young, 1981).

The scenarios show how a wide range of environmental processes over various temporal scales can alter rivers and result in the ubiquitous and variable nature of palæochannels world-wide. As it would be difficult to cover the entire range of attributes which palæochannels may encompass, this review will contrast two of the most extensively studied regions in Australia, those associated with the Yilgarn Craton in Western Australia, and the Murray-Darling Basin (Figure 2.5). This review will particularly concentrate on palæochannels found in the Riverine Plain and the Namoi and Gwydir Valleys in the Murray-Darling Basin, because of their importance to agriculture and their proximity to the field site used in this study.

Palæochannels are a valuable source of historical climatic information. The morphology and sediment composition reflect the palæoenvironment at the time of deposition. Clues may also be found from associated phytoliths or pollen of the ancient vegetation (Macphail and Stone, 2004), layers of æolian sediment deposited during dry periods (Page et al., 2001; Cattle et al., 2002) or anabranches created during geologic upheaval (Holbrook and Schumm, 1999). Palæochannels may also contain remnants of the palæoenvironment in the form of economically-beneficial material such as gold (Johnson and McQueen, 2001), uranium (Morgan, 1993; Anand and Paine, 2002) or groundwater (Hou et al., 1999; Young et al., 2002). However, palæochannels may also have a negative impact on the environment, harbouring saline groundwater (Salama et al., 1994b) and increasing the risk of deep drainage (Triantafilis et al., 2003a; Triantafilis et al., 2004).

Initial studies of palæochannels in Western Australia found that the structures contained economical mineral deposits in vast quantities. In some instances, up to

30% of the economically-beneficial deposits come from palæochannels (Anand and Paine, 2002), providing Australia with the worlds largest supply of uranium, silver, nickel, lead and zinc (McKay et al., 2000) and significant deposits of gold (Morgan, 1993; Johnson and McQueen, 2001).

Although early studies were principally aimed at mineral identification, it was soon discovered that palæochannels could serve as a groundwater conduit. The coarse-textured nature of the channel fills and the close proximity to the land surface make palæochannels well-suited for groundwater extraction (Rogers et al., 2002). Morgan (1993) suggested that the economic potential of groundwater outweighed those of mineral extraction in parts of Western Australia. Palæochannels near the Namoi River in Northern New South Wales also contain good quality water which is used for irrigation purposes (Young et al., 2002). However, those in the Murrumbidgee River District contain high quantities of dissolved solids, which could increase the threat of salinity in the area (Lavitt, 1999; Rogers et al., 2002; Timms and Acworth, 2002). The quantity and quality of extractable groundwater and minerals is a product of many different processes which incised and filled the channel. Because we currently lack the knowledge to predict their presence and impacts due to the complexity of their formation, detailed investigations of their characteristics are warranted.

2.3.1 Palæochannel characteristics and identification

Palæochannels and their associated levies generally coincide with a gently undulating topography; however, this is usually not visible to the untrained observer. Because most palæochannels lack surface expression and are sometimes buried far below the surface, it is difficult to determine their areal extent and sediment characteristics using traditional soil survey techniques. In fact, much of what we know about palæochannels has resulted from studying their impacts on the environments *ex post-facto* (Salama et al., 1993b; Clarke et al., 2002; Knight et al., 2002). To understand more about these structures, researchers have used many different methods to accurately, and efficiently determine important characteristics such as the time of deposition, their areal extent, and other channel characteristics which might affect their impacts on the environment, or point to their formational pathways.

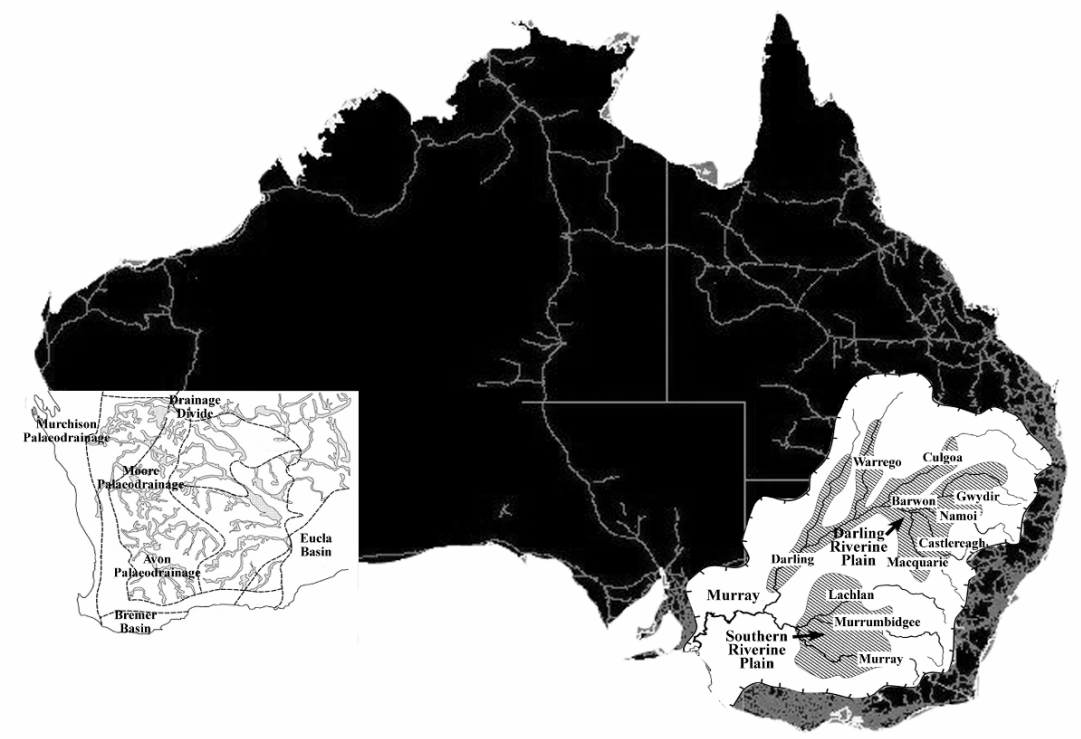

Figure 2.5. Detailed mapping efforts of palæochannels in the Yilgarn Craton in Western Australia and the Murrumbidgee, Namoi, and Gwydir Basins in Southeastern Australia. Current water courses (shown in grey) show a better correlation with the shallow palaeochannels in the Murray Dar ling Basin than the deeper ones in the Yilgarn Craton. Adapted from (Anand and Paine, 2002; Young et al., 2002).

2.3.1.1 Palæochannel age and chronology

In Australia, palæochannels have formed during a variety of geologic episodes, from Jurassic tectonic uplift in the west (Morgan, 1993; Johnson and McQueen, 2001; Beard, 2002) to Quaternary climatic oscillations in the southeast (Page and Nanson, 1996; White, 2000; Page et al., 2001; Young et al., 2002). Age estimates have improved with technological advances, and have increased our understanding of the history of palæochannel formation in Australia. For example, Page et al. (1996) improved on Pels' (1970) radio carbon dates, to include an additional active phase in the chronology of palæochannels in the Murrumbidgee district. Using thermoluminescence (TL), the authors showed that palaeochannels in this region were active during a series of four climactic oscillations occurring 105 to 80 ka ago, 55 to 35 ka ago, 35 to 25 ka ago, and 20 to 13 ka ago (Page et al., 1996).

Until recently, it was thought that palæochannels in the Northern Murray-Darling Basin were analogous to those in the southern part of the basin. However, Young et al (2002) challenged this belief, providing evidence that the oldest palæochannels in the north were only active during the most recent of Page et al.'s (1996) reported phases of activity.

Over the past few decades, geomorphologists and archaeologists have increasingly employed TL dating techniques to determine when a mineral grain was last exposed to sunlight or high temperature (Roberts et al., 1990; Robertson et al., 1991; Nanson et al., 1993; Nott et al., 2002; Young et al., 2002). Because minerals are inherently radioactive, sediment deposits are constantly storing and emitting free electrons. The bombarded minerals store the free electrons in their mineral structure. This occurs at a relatively constant rate, termed the *annual radiation dose*, which depends on the mineralogy of a sediment deposit.

Upon exposure to sunlight or fire, a sample is "bleached" as the free electrons are released. The stored electrons can therefore be used to determine the time of burial by artificially bleaching the sample with incremental heating and recording the luminescence. A plot of this luminescence versus temperature is called a *growth curve*, where the area beneath the peak represents the *palaeodose*, or amount of stored electrons. The palaeodose is correlated to the time of deposition by determining the annual radiation dose and applying the equation:

$$\text{age (years)} = \frac{\text{palaeodose (Grays)}}{\text{annual radiation dose (Grays year}^{-1}\text{)}} \qquad (2.1)$$

Depending on the amount of solar radiation and mineralogy, a sample may be bleached after only a day of exposure; however, it can take up to a week of full exposure to completely bleach a sample (Robertson et al., 1991; Prescott and Robertson, 1997). An incompletely-bleached sample can result in an over-prediction of the time of deposition due to an excess of stored electrons (Wray et al., 2001).

Although TL improves on the 30 ka range of carbon dating, and does not require a sample of uncontaminated carbon, there are some drawbacks to the technique. The uncertainty in the dates is typically one standard deviation, and not all sediments are ideally suited for TL dating. Because the method requires complete bleaching in the natural environment, sediment size is an important factor (Prescott

and Robertson, 1997; Young et al., 2002). Whereas finer materials are easily bleached, because they can remain suspended in streams for much longer periods of time, coarse fluvial sediments often produce less-reliable age estimates as they typically travel on stream bottoms. Because minerals can only store a finite amount of free electrons, the age limit for this method is determined by the saturation point of the mineral. Saturation typically occurs after 150 ka of burial (Prescott and Robertson, 1997), depending on the sample mineralogy and the annual radiation dose from the surrounding sediments (Roberts et al., 1990; Robertson et al., 1991; Banerjee et al., 2002).

2.3.1.2 Palæochannel morphology

The size and shape of palæochannels varies considerably and depends on the stream order, sediment supply, and the palæoclimate when deposition occurred. The larger palæochannels of Western Australia have been noted to extend to 90 m in depth and are several kilometres wide (Figure 2.5). These palæochannels are of low sinuosity, and once contained annual discharges similar to those of the Amazon river (Salama et al., 1994b; Johnson and McQueen, 2001; Anand and Paine, 2002). Palæochannels found in the Murray-Darling Basin vary considerably in size, shape, and discharge. The Namoi palæochannels are known for their high palæodischarges, as indicated by their wide, straight channels which extend tens of metres below the surface (Stannard and Kelly, 1977; Page and Nanson, 1996; Young et al., 2002). In contrast, palæochannels are much smaller in the Murrumbidgee catchment to the south, and the Gwydir catchment to the north. They are buried only a few metres below the surface, have channel widths of tens of metres and have more sinuous channel patterns (Stannard and Kelly, 1968; Stannard and Kelly, 1977; Page and Nanson, 1996; Young et al., 2002).

Because larger palæochannels are generally of high economic importance, sophisticated methods of investigation, such as aerial photography and Landsat imagery, were used for their detection (Morgan, 1993; Salama et al., 1994a; Johnson and McQueen, 2001; Fielding et al., 2003). These methods target topsoil and vegetative properties which contrast palæochannels form the surrounding sediments.

Remote sensing is an important tool for supplementing costly sampling strategies to identify channel characteristics. Aerial photography is perhaps the most intuitive method for characterising geologic structures, and has been the most commonly used remote sensing method for decades (Godwin and Miller, 2003). Aerial photography does not require specialized equipment and the resolution is limited only by the camera's optical resolution, the film format and sensitivity, and the height of the flight path (Curran, 1985; Fensham and Fairfax, 2002). Aerial photographs have successfully been used to map palæochannels throughout Australia based on differences in topsoil colour and the type and vigour of vegetation (Figure 2.6) (Stannard and Kelly, 1968; Beard, 2002; Godwin and Miller, 2003; Metternicht and Zinck, 2003).

For larger scale investigations, satellite imagery has been a useful and cost-effective method for identifying surficial changes which can be detected in the visible and infrared spectrum. The currently operative satellite, Landsat 7, incorporates sensors which detect visible, infrared, and thermal properties at 30, 30, and 60 m resolutions, respectively.

Landsat has proven to be an effective tool in identifying palaeochannels throughout Australia. Bands outside the visible spectrum have been used to determine changes in soil moisture associated with palæochannels (English, 1999; Dwivedi and Sreenivas, 2002). Using data from the visible spectrum, Dwivedi and Sreenivas (2002) and Salama et al. (1994a) mapped vegetation shifts associated with the structures. Additionally, sensors have been used in tandem to highlight buried palæochannel properties which had previously been unperceivable using aerial photography (Young et al., 2002).

a

b

Figure 2.6. Aerial photographs demonstrating (a) the changes in topsoil colour above a series of small-scale shallow palæochannels located in an agricultural setting in the Gwydir River Basin New South Wales, and (b) natural vegetation differences above a larger sinuous palæochannel on the floodplain of the Thurra River in Victoria (White, 2000).

Measurements of channel dimensions can be used to estimate the discharge of current and prior streams. For example, Dury's (1976) equation suggests that the prior discharge occurring at a 1.58 year flood recurrence (equal to 1 year on the

partial-duration series) of a prior stream can be estimated from the channel width and wavelength of the meander:

$$q_{1.58} = (l / 32.36)^{1.81} \quad (2.2)$$

$$q_{1.58} = (w / 2.99)^{1.81} \quad (2.3)$$

where:
$q_{1.58}$ = bank-full discharge (1.58 year recurrence) (m s^{-1})
l = wavelength of channel (m)
w = width of channel (m)

Based on this, several studies have estimated discharge of current and prior streams using aerial photographs and Landsat imagery (Nanson and Young, 1981; Wang and Xie, 2000; Young et al., 2002) and have delineated palæoenvironments where measurements of bedload sediments are highly variable or costly to sample (Kale, 1990; Young et al., 2002). Although discharge prediction models can vary by as much as 20% (i.e. Dury (1976) vs. Schumm and Khan (1972)), this uncertainty is small when compared to the differences in discharge between palæochannels in different regions of New South Wales (Young et al., 2002).

There are clear differences in palæochannel characteristics and hydrologic relationships in the Namoi and Murrumbidgee basins. Unlike the Murrumbidgee, the Namoi River has moved progressively away from its Tertiary channel (Young et al., 2002). The river avulsed the adjacent fine-grained alluvium, depositing coarser-grained bedload in its place. This coarse deposit, termed the Narrabri Formation continually expanded during this process. Although the river is still connected to the underlying Narrabri Formation, recharge to the deeper Gunnedah Formation is much less than was once thought (Williams et al., 1989; Ife and Skelt, 2004). The disconnection meant that the extracted water, a main source of irrigation water in the region was older and more limited than expected (Williams et al., 1989; Young et al., 2002). Also, because some of the structures in the Narrabri Formation harbour salinity, over-extracting water from the Gunnedah would potentially draw saline water from the overlying formation and degrade the water quality (Merrick et al., 1986; Lavitt, 1999; Ife and Skelt, 2004).

In contrast, the Murrumbidgee district presents a simpler scenario. Palæochannels are known to harbour salinity in these areas due to the high amounts of

original salts (Butler, 1950). These channels are more disconnected from the present water course, and have a thinner veneer of fine-textured sediments (Page and Nanson, 1996; Rogers et al., 2002; Young et al., 2002). Therefore, they are directly connected to the surface and are more likely to be recharged during irrigation and flood events (Willis and Black, 1996; Willis et al., 1997) carrying salts to the surface. Palæochannels in this area are used to control soil salinity by pumping the saline groundwater water out of the channels and lowering the water table in the surrounding areas (Rogers et al., 2002).

2.3.1.3 Channel fill: bedload and æolian deposits

Once regular stream flow ceases, channels typically fill with sediment which may or may not be representative of the old flow regime in the channel. In some cases, bedload is directly deposited and covered with a veneer of fine sediment such as loess (Young et al., 2002). Æolian material is commonly deposited in channels during drier periods, and can be reworked through alluvial and æolian forces (Page and Nanson, 1996; Cattle et al., 2002; Timms and Acworth, 2002; Young et al., 2002). Palæochannels typically contain multiple sequences of sediments of varying texture class and mineralogy (Page et al., 1996; Salama, 1997; Taylor and Brewer, 2001; Taylor et al., 2003) and often contain erosional disconformities associated with channel deposition (Paine et al., 2002), making them difficult to generalise.

In the Northern Murray-Darling Basin, palæochannel sediments are coarser than the surrounding soil and range from gravely sands to fine sands. It is common to find fine-textured beds, termed "stringers" inside the coarse deposits (Stannard and Kelly, 1968). Stringers may contain sediments in the silt to fine clay size fraction, ranging from a few millimetres to several centimetres in thickness. Depending on the stream energy, sediment supply, and the frequency of the depositional events, channels may fine or coarsen upwards (Wood et al., 1988; Morgan, 1993; Jones et al., 1995). Upward fining often results from the narrowing of the channel zone at the distal end of each stream (Butler, 1950; Tooth, 2000). Additionally, palæochannels have a characteristic deposit of coarse-textured material (typically fine sand sized) on what would have been the leeward side of the palæoriver resulting from æolian transport (Butler, 1950; Stannard and Kelly, 1977; Page et al., 1996). These complex patterns made it difficult to study palæochannels and extensive drilling is often

required to determine the chronology and morphology of these systems (Figure 2.7) (Butler, 1950; Pels, 1964; Stannard and Kelly, 1968; Stannard and Kelly, 1977).

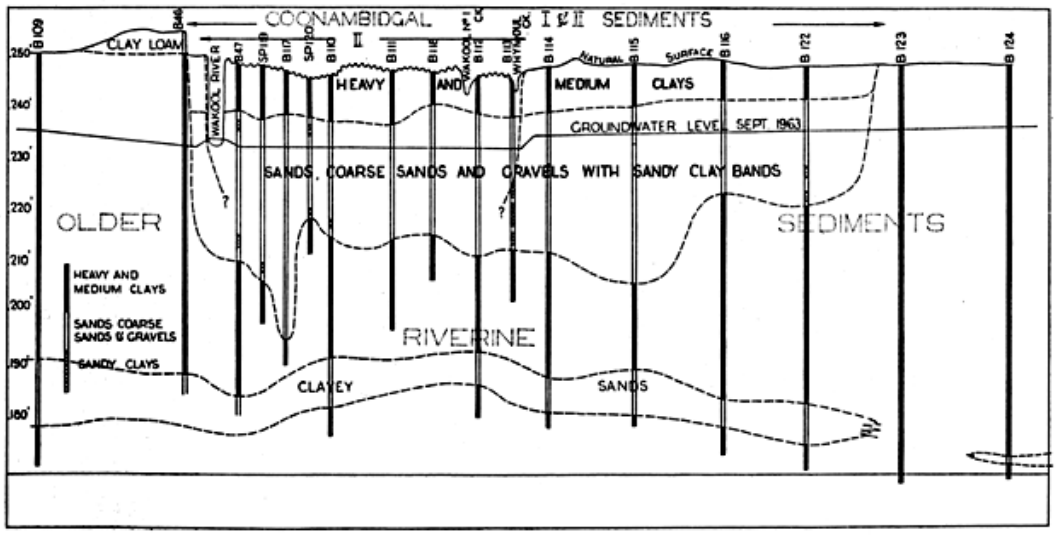

Figure 2.7. Cross-section of a large palæochannel complex in the Murray Darling Basin derived from extensive deep drilling techniques (Pels, 1964).

2.3.2 Problems associated with palæochannel presence in an agricultural setting

Salinity and salinisation of soil and water are some of the main problems facing agriculture in New South Wales. The NSW State Salinity Strategy predicts that losses due to large-scale salinisation from rising water tables will amount to three to four billion dollars by 2050 (NSWDLWC, 2000). Irrigation-induced salinisation has affected an estimated 300 000 ha of land in the Murray-Darling Basin, with roughly twice that number being in danger (MDBC, 1999).

Soil salinisation results from several different processes, but is currently described in terms primary and secondary components. Primary salinity refers to naturally-occurring salts in the landscape. Australia contains significant amounts of primary salinity in the form of deposited salts stored in the soil profile and regolith (Salama et al., 1994b; MDBC, 1999; Clarke et al., 2002). In Australia, salts are derived from many natural sources including the influx of airborne sea salts as particulate aerosols (Simpson and Herczeg, 1994; Herczeg et al., 2001); weathering of

Na-plagioclase and other Na-containing minerals (Salama et al., 1999); and evaporation of semi-saline precipitation (Salama et al., 1999; Herczeg et al., 2001). These salts often precipitate in the soil surface during evaporation, or can reach the soil surface in natural saline seeps occurring at slope breaks, or where geologic structures or palæochannels divert groundwater flow to the soil surface (Salama et al., 1993b).

The term *secondary salinity* typically refers to anthropogenic sources of soil and river salinisation. Secondary salinisation is occurring throughout most of Australia in response to the initial clearing of deep-rooted, salt-tolerant vegetation like the native *Eucalyptus* more than 150 years ago (Herczeg et al., 2001; Clarke et al., 2002; Peck and Hatton, 2003). Because interception rates and extinction depths were severely reduced, groundwater recharge was intensified. As groundwater levels rose, natural salts were carried to the soil surface, resulting in widespread land degradation (NSWDLWC, 2000).

In irrigated areas, soil salinisation is intensified through the application of additional water which, in some cases, exceeds the annual precipitation four times over (BOM, 2002; Lincare, 2005). This excess water can raise water tables, potentially bringing salts to the soil surface (Punthakey et al., 1994) or can evaporate and leave impurities behind (Hillel, 1998).

It is difficult to generalise the effects that irrigation has had on soil salinity due to the various sources from which groundwater and surface water is extracted for irrigation purposes in the Northern Murray-Darling Basin. Irrigation water in the Northern Murray-Darling Basin ranges from 200 – 2000 μS cm^{-1} in groundwater sources and 200 – 700 μS cm^{-1} in surface water sources (Stannard and Kelly, 1968; Williams et al., 1989; Ahmed, 2001; NSWDLWC, 2002; Mawhinney, 2005). When irrigation water contains appreciable amounts of salts (including those applied as fertilizer), evaporative enrichment can lead to salinisation over the course of a single growing season (Hulugalle, 2004). Where sodium is the dominant cation, sodicity can have serious deleterious affects on soil structure, causing soil crusting through dispersion of clay particles (Hillel, 1998). Although cotton is a relatively salt-tolerant plant, salt accumulation in the soil profile can significantly affect growth at 5000 μS cm^{-1} (Maas and Hoffman, 1977). In these conditions, irrigators are recommended to over-irrigate by as much as 20% of the required amount of water (Hulugalle, 2004).

Using higher-quality water, the amount needed to leach the enriched salts (leaching fraction) is much lower and is typically accounted for by normal amounts of deep drainage.

Butler (1950) reported that palæochannels in the Murrumbidgee district once contained appreciable amounts of primary salinity, which has been leached away in some areas. He envisioned a causal relationship between palæochannel presence and soil types, primary salinity, and leaching potential in the surrounding region based on the occurrence of sandy deposits within the heavy clay alluvial plains. A decrease in primary salinity with distance from prior streams is coupled with an increase in leaching potential due to the coarse grained sediment (Figure 2.8) (Butler, 1950). This lead to the conclusion that these structures pose a risk to soil salinisation throughout much of the Southern Murray-Darling Basin (Talsma and Van Der Lelij, 1976; Willis and Black, 1996; Triantafilis et al., 2004).

The Northern Murray-Darling Basin contains significantly fewer deposits of original salinity in the regolith (Stannard and Kelly, 1968; Stannard and Kelly, 1977). Although slaking has been reported in several palæochannel deposits (Young et al., 2002), they typically contain lower levels of dissolved salts when compared to the surrounding clay landscape (Stannard and Kelly, 1968; Stannard and Kelly, 1977; Lavitt, 1999; Triantafilis et al., 2002). In this case, the main salinity threat in this region is due to irrigation-induced secondary salinisation where excessive rates of deep drainage could lead to a rise of a semi-saline unconfined aquifer (Triantafilis et al., 2002; Triantafilis et al., 2003a) which has been enriched in salts through evaporation. Until now, irrigators in the Northern Murray-Darling Basin have escaped major instances of salinisation due to the significant depth to the water table, and the periodic flooding and subsequent leaching of the topsoil (Stannard and Kelly, 1968; Young et al., 2002). However, this has also resulted in the increased salinisation of the Murray and Darling Rivers, and it is projected that future problems are likely (Talsma, 1981; MDBC, 1999; Triantafilis et al., 2001c; Triantafilis et al., 2003b).

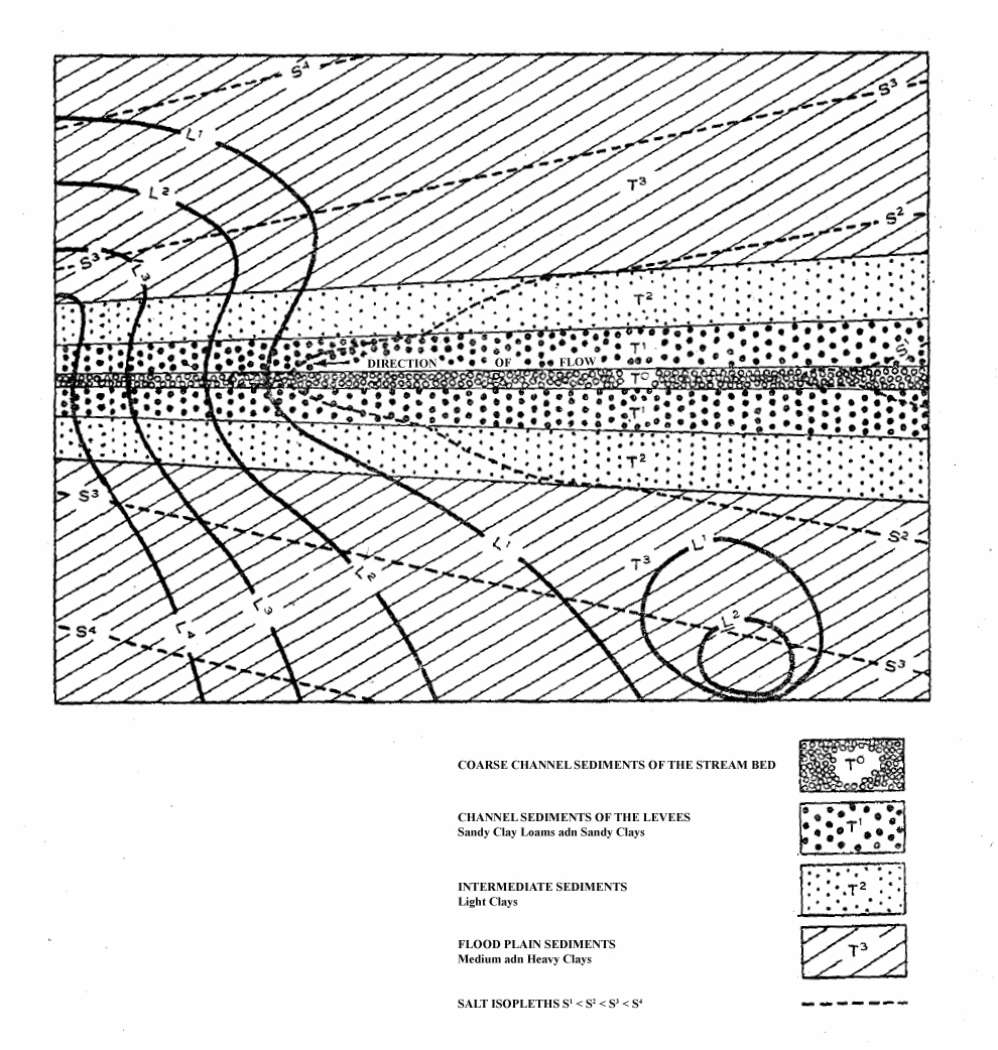

Figure 2.8 Butler's (1950) simplified schematic showing the relationship between prior streams and the (T) texture, (S) salt content, and (L) leaching potential of the surrounding environment. In general, the original salt content and leaching potential increase with distance from the channel and towards the distal ends of the channel. From Butler, 1950

Salinity control hinges on a proper understanding of the landscape hydrology. Since palæochannels are scattered through the landscape, and are difficult to identify and predict, irrigation planning in the Northern Murray-Darling Basin has generally ignored them in their design (Figure 2.3, Figure 2.5). However, local knowledge from irrigators suggests that paddocks containing palæochannels use appreciably more water during irrigation events. Water infiltrates at a much higher rate through surface soils overlying palæochannels because of their coarser texture and lack of swelling

clays (Bird et al., 1996; Willis and Black, 1996; Willis et al., 1997; Huckel, 2001; Rogers et al., 2002; Triantafilis et al., 2003a; Triantafilis et al., 2004).

Because of the differences in infiltration characteristics between contrasting adjacent soils (such as palæochannels located in heavy clays), deep drainage predictions in these landscapes have been tenuous at best. Several studies have attempted to measure deep drainage through traditional hydrological investigations involving costly and invasive monitoring networks (Heng et al., 2001; Petheram et al., 2002).

Palæochannels are thought to have an intimate relationship with groundwater (Salama et al., 1993b; Salama and Hawkes, 1993; Young et al., 2002) and surface water (Sophocleous, 1991) and should, therefore, affect the transport of subsurface solutes and contaminants (Subrahmanyam and Yadaiah, 2000; Clarke et al., 2002). However, groundwater flow through these systems is not as straightforward as conceptualised. Even in the same landscape, palæochannels can either serve as a groundwater conduit (due to their lighter texture) or remain completely dry, depending on surface sealing and connectivity to currently flowing streams (Sophocleous, 1991; Salama et al., 1993b; Huckel, 2001; Triantafilis et al., 2001b; Rogers et al., 2002; Young et al., 2002). This suggests that developing new strategies to predict deep drainage and groundwater flow in irrigated areas which contain palæochannels can have significant positive impacts on the environment and the management of irrigation water.

2.4 Estimating deep drainage and groundwater flow in an agricultural setting

Many of Australia's natural resource issues, particularly deep drainage and soil salinisation are thought to originate from variability in soil and groundwater characteristics and human-induced changes to these systems (Sections 2.2.3, 2.3.2). Deep drainage is commonly defined as "water which moves past the root zone". It occurs naturally during flooding events when rainfall and runon exceed evapotranspiration rates. However, in the Murray-Darling Basin and much of Australia, deep drainage rates have increased through the introduction of dryland and irrigated agriculture. Agriculture has contributed to these problems in two ways; first from the clearing of deep-rooted perennial vegetation and replacement by annuals,

and later from the over-application of irrigation water (Allison and Hughes, 1983; Al-Jamal et al., 2001; Silburn and Montgomery, 2001; Ringrose-Voase et al., 2003; Tolmie et al., 2004)

The quantity and quality of groundwater is highly variable throughout the Murray-Darling Basin and has likewise been affected by agricultural practices (Rogers et al., 2002; Peck and Hatton, 2003). Groundwater has a dichotomous nature in the Murray-Darling Basin, existing as a beneficial source of irrigation water in some areas, and a vector for salts and chemicals in others (Pels, 1973; Timms and Acworth, 2002; Young et al., 2002). Because of the basin's semi-arid climate, recharge and discharge zones are highly variable both temporally and spatially, making prediction and management difficult at times (Cook et al., 1989a; Timms et al., 2001; Doble et al., 2004; Weaver et al., 2005).

Most agricultural practices in Northern New South Wales utilise the region's productive Vertosols (Section 2.2.4), because of their ideal chemical and physical properties. These soils also have a high water-holding capacity and, because of their swelling characteristics, should limit deep drainage. However, these soils can leak considerable amounts of water past the root zone, potentially leading to groundwater rise and subsequent secondary salinisation (Willis et al., 1997; Silburn and Montgomery, 2001; Vervoort et al., 2003; Triantafilis et al., 2004; Vervoort et al., 2004; Weaver et al., 2005).

The measurement of deep drainage in semi-arid regions can be an expensive and difficult process, due to the spatial and temporal variability of recharge events and the difficulty to "observe" the phenomenon (Scanlon et al., 2002; Walker et al., 2002; Hendrickx et al., 2003). Deep drainage estimates can be made by directly measuring water volumes, but indirect methods have been developed to circumvent the high cost and invasive nature of direct measurements. Where more accurate measurements can be made with direct measurement, landscape-scale predictions must then be made from very few measurements due to the high cost. Conversely, indirect measurements allow for more observations, with each measurement having a higher degree of uncertainty. Methods such as chloride mass balance, Darcian flux, and water balance approaches have been used with mixed success in the Murray-Darling Basin (Willis and Black, 1996; Willis et al., 1997; Silburn and Montgomery, 2001; Tolmie et al., 2004; Weaver et al., 2005). In most cases, research has revealed

highly variable deep drainage estimates, mostly due to geologic and climactic variability, but also because of the nature of the methods (Table 2-2).

While some studies found negligible amounts of deep drainage, others showed that as much as 30% of applied water leaked past the root zone. In some cases, the same technique used on the same site gave large discrepancies in the amount of predicted deep drainage (Silburn and Montgomery, 2001). Deep drainage estimates based on the chloride mass balance, water balance, and Darcian flux gave estimates of 236, 214, and 67 mm, respectively on the same field over a season of cropping (Willis et al., 1997). Similarly, variation in recharge estimates in Australia correlates more strongly to the method of detection, than the soil type (Petheram et al., 2002).

Table 2-2. Estimates of deep drainage on heavy shrink/swell clay Vertosols in Northern New South Wales. Adapted from Silburn and Montgomery (2001) and Humphreys (2003).

Location	Irrigation	Precip.		Deep drainage			Reference
	method	— mm —		method	mm	LF%	
Dubbo, NSW	furrow	491		Cl^-	17		Willis and Black, 1996
					16		
					18		
				WT rise	37		
Macalister, Qld.	furrow	327	478	lysimeter	182	23	Moss et al. 1999
		343	667		162	16	
		487	579		152	14	
	drip	478	478		305	32	
		142	667		95	12	
Merah N., NSW	furrow			Cl^-	98		Weaver et al, 2002
					76		
					19		
Moree, NSW	furrow	397	161	water balance	158	28	Silburn and Montgomery, 2001
		176	0		3	2	
Mullah, NSW	furrow	378#	328	water balance	236	33	Willis et al, 1997
				Cl^-	214	30	
				Darcy's law	67	9	
Narrabri, NSW	furrow	154#	550	Darcy's law	nil	nil	Cull et al, 1981
		247#	550				
		302#	550				
		132#	502				
		298#	502				
		277#	502				
		389#	502				
		443#	502				

2.4.1 Chloride mass balance

The chloride mass balance approach has been used extensively in the Murray-Darling Basin to predict deep drainage from the distribution of chloride ions in the soil profile (Rose et al., 1979; Slavich and Yang, 1990; Willis et al., 1997; Weaver et al., 2005). This method is well-suited for investigation in arid and semi-arid climates and is cost effective and relatively accurate, making it one of the favoured methods used in Australia (Allison et al., 1994; Walker et al., 2002). Chloride makes an ideal tracer because, unlike positively charged cations which are attracted to negatively charged clay mineral surfaces, chloride is repulsed from clay minerals. Termed a conservative ion, chloride doesn't sorb to clay minerals and does not form insoluble complexes with most cations due its very small charge density. Therefore, chloride anions move freely in the soil solution, and can be used as a naturally-occurring tracer to calculate the flux or age of water in the soil profile (Rose et al., 1979; Allison and Hughes, 1983; Scanlon, 2000).

The mass balance method is based on the assumption that infiltrating water will leach chloride from the soil profile. For example, the amount of chloride entering and leaving the root zone can be calculated by sampling the soil at various depths and measuring the solute, relative to the water applied. Under steady-state conditions (where the mass of chloride input equals the amount output) deep drainage (DD) at a depth (z) is equal to the ratio of the concentration of chloride in the water applied (C_i) to that in the soil above (C_z) multiplied by the rate of water application (I), shown as:

$$DD_z = I\left(\frac{C_i}{\overline{C}_z}\right) \tag{2.4}$$

The chloride mass balance has been used successfully to show how changes in land-use over many years have impacted deep drainage (Allison and Hughes, 1983; Allison et al., 1990; Tolmie et al., 2004). Considering the changes in the Australian landscape over the last century and the variability in farming practices, soil types, and irrigation water quality, it is hardly surprising that there are contradicting opinions on whether steady-state conditions can exist in agricultural landscapes. For example, contrary to other studies (Slavich, 1990; Thorburn et al., 1990; Tolmie et al., 2004), Willis et al. (1997) and Weaver et al. (2005) suggested that steady-state conditions

can prevail in irrigated landscapes with high clay contents over a season. However all authors recognised that partially-irrigated and non-irrigated agricultural fields generally can not reach steady-state conditions in this short time span. In fact, both processes can occur simultaneously in different zones in the soil profile (Willis and Black, 1996).

To calculate a transient flux, the change in chloride flux over time needs to be accounted for (Rose et al., 1979):

$$DD = C_z(IC_i - z\bar{\theta}_s \frac{d\bar{C}}{dt}) \quad (2.5)$$

Where:

DD = deep drainage
z = depth
$\bar{\theta}_s$ = mean depth-weighted volumetric water content at field capacity (avove z)
$\bar{C}$ = mean depth-weighted soil water chloride concentration at saturation (above z)
t = time
I = rate of water application
C_i = chloride concentration of irrigation water
C_z = chloride concentration of soil water at field saturation (at depth z)

Using a transient model, changes in deep drainage resulting from events (such as planting or irrigation) can be quantified simply by sampling the same location before and after an event (Slavich and Yang, 1990). The model provides a more realistic approximation for most field conditions, but still works under the assumption of 1-dimensional piston flow and does not allow for long term estimates, such as historical accumulation of salts in the soil profile (Scanlon, 2000).

Due to the high amount of shrink-swell clays in Vertosols, preferential flow and anion exclusion can significantly affect deep drainage predictions using the chloride mass balance (Slavich and Petterson, 1993a; Allison et al., 1994; Scanlon, 2000). The rate that ions move in the soil solution is complicated by the velocity dependence of the dispersion coefficient of ions, and the velocity gradient created by the attractive forces on clay mineral surfaces (Bond et al., 1982; Smiles and Gardiner, 1982). While the dispersion coefficient is mostly independent of the types of ions in solution, the velocity gradient increases the movement of chloride (and other anions)

due their exclusion from the diffuse double layer (Bond et al., 1982; Smiles and Gardiner, 1982; Saarenketo, 1998). This is mainly a function of the cation exchange capacity and the total exchangeable cations in the soil solution (Bond et al., 1982; Bond and Phillips, 1990; Slavich and Petterson, 1993a). In fine-textured samples, Slavich and Petterson (1993a) showed that anion exclusion created a 11 to 14% difference in deep drainage predictions when compared to those which did not account for anion exclusion.

Preferential flow has a large impact on the solute flux in the vadose zone, particularly in well-structured or swelling soils (Iqbal and Krothe, 1995; Vervoort et al., 1999; Yasuda et al., 2001; Petheram et al., 2002). Also termed "bypass flow" or "macropore flow", the process occurs when large pores or cracks in the soil are responsible for channelling water through the soil profile. Soil chemistry is difficult to predict in these circumstances due to kinetic restrictions on chemical reactions, and exclusion of soil water in micropores (Bouma and Wosten, 1979). Preferential flow results in a lower chloride flux through the profile than is predicted using the steady-state and transient models. This is because water flowing through macropores is not in equilibrium with the soil water, limiting ion dispersion in the soil water (Thorburn and Rose, 1990; Chen and Wagenet, 1992). Although macropores commonly occupy less than 5% of the total porosity of soils (Beven and Germann, 1982), they channel appreciable amounts of water through the soil profile; in some cases constituting 60% of water in cracking clays (Bouma and Wosten, 1979; Thorburn and Rose, 1990).

2.4.2 Water Balance

Water balance approaches are best suited for field- and landscape-scale predictions of deep drainage on a large time step. This is because the spatial and temporal variability of measurements become prohibitively uncertain at smaller scales (Hendrickx et al., 2003). Similar to the salt balance, a water balance is an accounting procedure whereby all or some of the sources and sinks of water are quantified, with the objective of finding one or more unmeasured parameters. Due to the complex nature of landscape hydrology and groundwater flow, one or more variables are typically inferred. In the case of an irrigated paddock, we could assume that the major source of water is from irrigation and precipitation. This means that deep drainage can be inferred:

$$DD = P + I - (ET + R + \Delta S) \tag{2.6}$$

where:
P = precipitation (L)
I = irrigation (L)
ET = evapotranspiration (L)
R = runoff (L)
DD = deep drainage (L)
ΔS = change in storage (L)

In this simplified model, the system inputs, precipitation (P) and irrigation (I) and runoff (R) are easily measured. In a controlled setting, such as a levelled field, R can be measured, or has been estimated as 0.2 x P (Baumhardt et al., 1993; Willis et al., 1997). The change in soil moisture is typically measured using TDR, neutron probe, or capacitance probes at the beginning and end of the experiment (Sophocleous and Perry, 1984; Jarvis and Leeds-Harrison, 1990; Scanlon, 1994; Willis et al., 1997; Greco, 2002; Charlesworth, 2005).

In arid and semi-arid landscapes, uncertainties in ET and precipitation measurements can far outweigh the magnitude of the deep drainage prediction (Kennett-Smith et al., 1994; Hendrickx et al., 2003). Evapotranspiration is generally estimated using a combination of pan evaporation, relative humidity and wind speed (Talsma and Van Der Lelij, 1976), crop factors (Kennett-Smith et al., 1994), and empirical relationships (Sarma et al., 1980). Preferential flow has also been shown to significantly affect water balance calculations (Jarvis and Leeds-Harrison, 1990), especially in semi-arid regions (Greacen and Hignett, 1984). Still, several authors have found that these predictions agree well with those using chloride mass balance in both steady-state and transient conditions (Willis et al., 1997; Walker et al., 2002).

2.4.3 Darcian Flux and lysimetry

Unsaturated water flux can be quantified at points in the landscape through the use of tensiometers coupled with measured (or predicted) moisture-retention curves. The method requires an analytical solution to the Buckingham-Darcy unsaturated flow equation (Buckingham, 1907):

$$q = -K(h)\frac{\partial H}{\partial z} \tag{2.7}$$

Where:

q = specific discharge (L/T)

$K(h)$ = hydraulic conductivity (as a function of moisture potential) (L/T)

$\frac{\partial H}{\partial z}$ = hydraulic gradient (L/L),

where $H = h + z$

h = moisture potential

z = gravitational potential

Integrated over a specific amount of time t, the formula becomes:

$$DD = \int_0^t K(h)\left(\frac{dh}{dz} + 1\right)dt \tag{2.8}$$

where the total amount of water (DD) can be calculated between two points located beneath the zero flux plain (where water is assumed to only travel downwards).

This method commonly draws criticism from the fact that the unsaturated hydraulic conductivity curves are difficult to establish and can be quite variable at low moisture potential (Allison et al., 1994; Walker and Zhang, 2002). Although soil moisture content is routinely measured, soil water potential is difficult to obtain because of the maintenance required for most tensiometers. And, because soil hydraulic conductivity measurements can vary by as much as three orders of magnitude on the same soil type (Bird et al., 1996; Hutchinson and Bond, 2001; Walker et al., 2002; Gee et al., 2005), point measurements need to be taken at the site of the tensiometers.

When compared to chloride mass balance and the water balance approach, Willis et al. (1997) found this method gave highly uncertain estimates of deep drainage; noting that they used saturated hydraulic conductivity estimates in lieu of the unsaturated functions and placed the tensiometers above and below the zero flux plane. Advances in tensiometry have made measurements of the soil water potential gradient much more practical, with precision and accuracy comparing favourably to mercury tensiometers (van Grinsven et al., 1988; Hutchinson and Bond, 2001). By automating the instruments, individual drainage events can be logged. These instruments are particularly useful for semi-arid regions, where the sporadic recharge flux has traditionally been difficult to capture (Allison et al., 1994).

An alternative approach to the Darcian flux calculation is to directly capture and measure draining soil water through the use of lysimeters. Considered "possibly the best-documented measurement technique for comparing deep drainage under different land-uses" (Walker et al., 2002), a lysimeter is simply a containment vessel for soil and plants which is placed in the ground to simulate natural conditions. They range in size from several centimetres (Grimmond et al., 1992; O'Connell et al., 2003) to several metres in diameter and can be tens of metres deep (Gee et al., 1994). The entire vessel can be weighed (termed a *weighing lysimeter)* using a pressure transducer to determine changes in soil water storage. Typically, there is also a mechanism for collecting samples of soil water, either through a membrane, or a porous cup placed under suction (similar to the tensiometer). In all cases, lysimeters are costly and require a significant amount of time to perform maintenance and sample collection (Allison et al., 1994; Walker et al., 2002). This then limits their utility in upscaling to larger spatial scales because of the resulting small sample size (Allison et al., 1994; Fetter, 2001). However, they have been extremely valuable for measuring soil water and serve as a benchmark for other measurement methods (Walker and Zhang, 2002).

2.4.4 Modelling groundwater and recharge

Many different types of groundwater models have been created to visualise and understand the complex process of groundwater flow through porous media. Our understanding of the process has been aided through the use of different types of models, which Fetter (2001) classifies as: scaling, analogue, and mathematical.

Scaled physical models, or "sandbox models", range from one-dimensional experiments with homogeneous, packed columns (Darcy, 1856) to 2- and 3-dimensional sandbox models (Silliman et al., 1987; Barth et al., 2001; Sternberg, 2004) which attempt to accurately mimic water flow and dispersion in a controlled environment. These are often effective tools for visualising flow in heterogeneous and homogenous media (Hills, 1971; Barth et al., 2001), but run the risk of being over-simplified or inaccurate representations of the larger-scale landscapes (Hill et al., 1998; Fetter, 2001).

Analogue models utilise processes which are similar to groundwater and may be more aptly observable and/or malleable. An example of this is the viscous fluid

model developed by H.S. Hele-Shaw (Hele-Shaw, 1898) where two closely-spaced parallel plates and a viscous liquid mimic the adhesive properties of sediments in an aquifer. This type of model has been used in conjunction with a sandbox model to model groundwater mounds below leaky irrigation channels (Youngs, 1977).

A second type of analogue model is based on the flow of electrons through a series of resistors and capacitors, where the resistors represent the hydraulic conductivity and the capacitors represent the storativity of the aquifer. The voltage drop (or hydraulic head difference) can be measured at any location in the model using a simple multi-metre. These predecessors to current computer-based "numerical" models have been largely phased out due to their expensive and cumbersome nature, as a change in one or more parameters can only be accomplished by physically rebuilding the model. However, they are still being used for medical research (Lee et al., 2004). Mathematical models use the basic principles of fluid dynamics to solve a set of physically-based differential equations. These are broadly based on the conservation of mass and energy.

2.4.4.1 Groundwater flow equations

Darcy first characterised the basic components of saturated flow in his experiments with water columns, concluding that the two main components of force acting on a body of water are the elevation potential (z) (governed by the gravitational force of the earth acting on the mass of water) and the pressure (p) from the overlying column of water acting on the observed volume of water. In the simplest case, Darcy showed that 1-dimensional flow through a porous medium can be expressed as:

$$\frac{Q}{A} = -K\frac{\Delta h}{\Delta l} \tag{2.9}$$

Where:
Q = discharge (L^3/T)
K = hydraulic conductivity (L/T)
A = cross-sectional area (L^2)
Δh = change in potential (L) : $h = z + p$
Δl = column length (L)

In the case of one-dimensional steady-state flow in a homogeneous confined aquifer, this equation can be solved analytically, provided four of any of the five parameters can be measured to solve for the missing value. On a field scale, these

parameters can be estimated using hydrological techniques, such as piezometers, combined with information of the underlying geology through bore holes and geologic maps. Analytical solutions to these problems can be quickly solved using a hand calculator, and provide continuous estimates along the column length.

In three dimensions, the groundwater flow equation is a 3rd-order partial differential equation relating the continuous change in potential h over time t to the product of specific storage S_s and the hydraulic conductivity K and the three-dimensional potential distribution (Bear and Verruijt, 1987p 63-64):

$$S_s \cdot \frac{\partial h}{\partial t} = K\left(\frac{\partial h}{\partial x} + \frac{\partial h}{\partial y} + \frac{\partial h}{\partial z}\right) \tag{2.10}$$

This is a combination of the mass balance

$$S_s \cdot \frac{\partial h}{\partial t} = q_x + q_y + q_z \tag{2.11}$$

and the flux components for each direction

$$q_x = K\frac{\partial h}{\partial x}, q_y = K\frac{\partial h}{\partial y}, q_z = K\frac{\partial h}{\partial z} \tag{2.12}$$

However, in a heterogeneous anisotropic medium, the potential and conductivity functions also vary in three dimensions

$$S_s \cdot \frac{\partial h}{\partial t} = \frac{\partial}{\partial_x}(K_{xx}\frac{\partial h}{\partial x}) + \frac{\partial}{\partial_y}(K_{yy}\frac{\partial h}{\partial y}) + \frac{\partial}{\partial_z}(K_{zz}\frac{\partial h}{\partial z}) \tag{2.13}$$

Under homogeneous, isotropic, steady-state conditions, $\left(\frac{\partial h}{\partial t} = 0\right)$ the equation reduces to:

$$\frac{\partial^2 h}{\partial x^2} + \frac{\partial^2 h}{\partial y^2} + \frac{\partial^2 h}{\partial z^2} = 0 \tag{2.14}$$

This is known as the Laplace equation, which can be solved analytically, given certain constraints. The Laplace equation (like any differential equation) can also be discretised into nodes of equal heads. The process of discretisation approximates the continuous nature of groundwater flow using finite cells by making potential in one cell equal to the average of the potentials of the neighbouring cells. In the case of

one-dimensional, steady-state flow, only two values need to be considered; those of the adjacent cells. Therefore, the potential values at nodes (n_1, $n_{2,}$, . . n_4) become:

$$n_1 = \frac{(h_1 + h_2)}{2}, n_2 = \frac{(h_2 + h_3)}{2}, n_3 = \frac{(h_3 + h_4)}{2}, n_4 = \frac{(h_4 + h_5)}{2} \quad (2.15)$$

The solutions to these become more complex with added recharge R between nodes n, at distance l (as shown above).

$$n_1 = \frac{Rl_1^2}{2T} + \frac{(h_1 + h_2)}{2} \quad (2.16)$$

Where:
R = recharge (L/T)
T = transmissivity (L/T)
and:
$T = K \times b$
where:
b = aquifer thickness (L)
(Transmissivity is described as "the amount of water that can be transmitted horizontally through a unit width by the full saturated thickness of an aquifer under a hydraulic gradient of 1" (Fetter, 2001, p. 100))

2.4.4.2 Numerical Models

Several groundwater modelling packages have been developed to achieve the goal of accurately approximating the groundwater flow equations in one- (Dawes et al., 1997), two- (Healy and Ronan, 1996), and three-dimensions (McDonald and Harbaugh, 1988). Each of these models is governed by certain constraints and boundary conditions, such as saturated versus unsaturated flow in transient or steady-state conditions. A review and quantitative comparison of several two-dimensional models is provided by McCord and Goodrich (1994) and three-dimensional models by Middlemis et al (2001).

Groundwater modelling packages are not only the interface used to specify input parameters and retrieve output, but are also responsible for the combination of many ancillary equations or the coupling of existing models. This is done to simulate other processes which can affect the basic groundwater flow equations such as stream-aquifer interaction (Osman and Bruen, 2002) and recharge (Facchi et al., 1994). Although many commercially-available models exist in the private and public

domain, some are better at predicting the various aspects of groundwater flow. While some codes can model more complex groundwater interactions, they usually require more input data to perform the operation, and can increase the overall uncertainty of the model (Massmann and Hagley, 1995; Middlemis et al., 2001).

In a groundwater model appraisal conducted for the Murray-Darling Basin Commission, Middlemis et al. (2001) compared nine commercially-available three-dimensional groundwater models, selecting the USGS-developed code MODFLOW (McDonald and Harbaugh, 1988) as the most appropriate model for most three-dimensional applications. The reasons for this choice were based on: the wide range of verified prior case studies, the modular construction of the package (whereby new modules can easily be incorporated into the package), the public availably of the code (increasing the likely-hood of scrutiny through peer review and model verification), and the relatively-inexpensive price.

2.4.4.3 MODFLOW case studies from around Australia

MODFLOW is a quasi-three dimensional finite difference code (McDonald and Harbaugh, 1988) which has been considered the industry standard for saturated flow modelling for over ten years (Anderson, 1995; Armstrong and Narayan, 1998; Middlemis et al., 2001). Several studies in Australia have used the code to solve complex problems, such as the remediation of rising groundwater in response to land-use changes (Salama et al., 1993a), the effects and likelihood of salinity outbreaks due to irrigation (Doble et al., 2004), groundwater resource management (Khan et al., 2002; Khan et al., 2004) and historical flux rates of naturally-occurring tracers (Harrington et al., 1999).

Using a 3-dimensional MODFLOW model on a first order catchment in Western Australia, Salama et al. (1993a) identified a strong connection between the underlying confined aquifer and the rising water table. The model was then used to evaluate various intervention scenarios to aide in remediation efforts.

Doble et al. (2004) compared the effectiveness of two- and three-dimensional models in explaining the occurrence of salinity outbreaks near an irrigated area on the Murray River. The three-dimensional model (MODFLOW) was much better able to predict salinity outbreaks than a two-dimensional model. However, detailed

topographic information was needed to counter some of the assumptions in MODFLOW's evapotranspiration package.

To improve on two past models of the Murrumbidgee Irrigation Area (Prathapar et al., 1994; Punthakey et al., 1994), Khan el al. (2002; 2004) used 2 809 available bore logs from previous studies to construct a 6 700 km^2 regional MODFLOW model. The conceptual model included four aquifers (the top one being unconfined), the Murrumbidgee River and tributaries, and a massive complex of irrigation canals from 4 117 farms spanning a total length of 795 km over the area (as compared to 255 km for the river and creeks).

Measured piezometric data were highly correlated to those predicted by the model (R^2 = 0.99) with only a small discrepancy in the water balance (0.01%). Sensitivity analysis showed that the model was most sensitive to horizontal hydraulic conductivity and specific yield, where changes in these parameters resulted in slight increases in groundwater levels in both the confined and unconfined aquifers. Overall, the model showed a decrease in groundwater levels based on current practices. Using several possible future scenarios, the authors demonstrated that a 50% decrease in irrigated agriculture would lower groundwater levels by one metre and increase groundwater salinity by 1 000 $\mu S\ cm^{-1}$.

Williams et al (1989) aimed to identify the effects that groundwater withdraw (mainly by the cotton industry) was having on the Namoi Catchment water balance. The study incorporated radio carbon data reported by Calf (1978), to improve the river recharge estimates of an existing MODFLOW model previously used by Merrick et al. (1987). The coarsely-gridded two layer model covered a 3 737 km^2 area using 598 nodes (2.5 km^2 each) to represent the Narrabri, Gunnedah, and Coobaroo Formations. The calibration process suggested that river recharge rates varied downstream from 500 $m^3\ day^{-1}$ to nil over the 165 km span. The recharge information from the steady-state model was used with data from 200 bores to calibrate a transient model based on several flood events occurring over a 12 year period. After successful calibration, the authors concluded that over-extraction of water from the lower aquifer had caused a gradient reversal. Where minimal recharge was occurring from the rivers, leakage from an overlying aquifer of dubious water quality was occurring (in some cases contributing 30% of the water pumped from the

deeper aquifer). This finding was confirmed by wells in the study area, which showed the steady increase in electrical conductivity of the deeper groundwater.

On a much larger temporal scale, Harrington et al.(1999) coupled MODFLOW with a compartmental mixing model (CMC) to predict changes in solute flux due to sea level transgression and regressions over a period of 27 000 years in South Australia. With the intent of modelling the flux of ^{14}C into a confined aquifer (which was directly connected with sea water) the model was calibrated based on known concentrations of the solute from the confined aquifer. Groundwater flux into the confined aquifer (from the overlying unconfined aquifer) was estimated using MODFLOW. This information was then used for the CMC model to predict the solute flux, based on the conservation of mass. These estimates were then used to recalibrate the MODFLOW model to obtain reasonable estimates of flux which agreed with observations (Figure 2.9). The model coupling proved to be a useful way to inversely predict input parameters such as hydraulic conductivity.

Although the MODFLOW package has had considerable success in a wide variety of applications in the Australian landscape, the model requires a large amount of measured or predicted input data to predict groundwater flow in complex systems (Zhang et al., 1997; Harrington et al., 1999; Doble et al., 2004; Khan et al., 2004). In simple groundwater flow systems, good results have been found using much simpler models, in some cases outperforming the more complex models. Holland et al. (2004) found that floodplain discharge estimates using a one-dimensional analytical model compared favourably ($R^2 = 0.998$) with the MODFLOW model developed to predict the same parameters targeted by Doble et al. (2004).

The utility and appropriateness of numerical and analytical models have also been tested on two sites in Amsterdam (Olsthoorn, 1999) revealing that a well-developed analytical model can outperform complex numerical models in some instances (Massmann and Hagley, 1995). These observations point to the importance of developing a sound and parsimonious conceptual model, whereby (1) complexity is only added where it is necessary to describe the system in terms of the model objectives and (2) the model adheres to the assumptions embedded in the groundwater flow equation used by the modelling code (Middlemis et al., 2001).

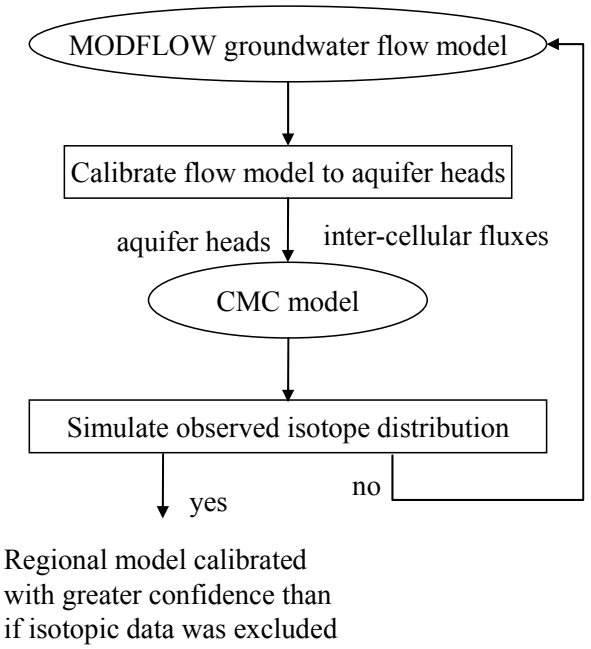

Figure 2.9. The modelling concept used by Harrington et al. (1999) whereby flux output from a 27 000 yr MODFLOW simulation was used to predict the isotopic distribution in a regional aquifer through the use of a compartmental mixing cell (CMC) model.

2.5 Geophysical characterisation of subsurface properties

The study of geophysics complements that of groundwater modelling in many ways. Both fields of study attempt to measure things that are relatively unobservable. A great deal of research is therefore aimed at correlating measured properties to perceivable ones using a combination of empirical and physically-based relationships.

By indirectly looking at the flow of electrons, electromagnetic pulses, and compressional waves through the earth, we are able to suggest something about the way other things (such as water) will flow through the subsurface. The analogy proves useful mostly because the mathematical representation of both processes is strikingly similar. Darcy's law translates exactly to Ohm's when the conductivity of a direct current translates to the proportionality constant K - both constants serve to limit the flow of water or electrons driven by the potential generated from changes in pressure or voltage.

Because of this relationship and the cost-effectiveness of supplementing traditional surveys with geophysical data, geophysical instruments have proven to be

a very useful tool in hydrology. Geophysical surveys have improved conceptual models by refining coarsely spaced bore holes (Gish et al., 2002; Triantafilis et al., 2003a), identified areas of recharge and discharge (Cook et al., 1989b; Salama et al., 1994b; Triantafilis et al., 2004), and provided point- to field-scale estimates of soil moisture (Chan and Knight, 1999; Huisman et al., 2001; Grote et al., 2003), water flux (Lambot et al., 2004), and salinity (Triantafilis et al., 2000).

2.5.1 Electromagnetic induction surveys

Electromagnetic induction instruments have successfully been used to delineate landscape features from the shallow subsoil to deep regolith on a wide variety of scales and environments (Corwin and Lesch, 2005a). Electromagnetic induction is the process whereby a low frequency (10 – 17 000 Hz) alternating current is used to induce an electromagnetic wave which travels into the ground. Because the soil is (relatively) electrically conductive it generates secondary "eddy" currents which radiate away from the primary electromagnetic (EM) field. The amplitude of the secondary EM waves are proportional to the conductivity of the earth, and is 90° out of phase (quadrature phase) of the original current applied (Figure 2.10). A receiving coil on the instrument measures the in-phase and quadrature phases of the primary and secondary electromagnetic fields. The instrument is calibrated so that the amplitude of the quadrature phase is proportional to the electrical conductivity of the soil, which is termed the apparent electrical conductivity (EC_a). The in-phase component of the EM wave is proportional to the magnetic suscepability of the medium which is strongly affected by metal and rarely varies in the natural environment (McNeill, 1983).

The instrument gives a single reading at a location, corresponding to the *bulk conductivity* of the underlying media integrated over the depth of the EM wave penetration. The contributing factors to the bulk conductivity include the soil solution chemistry, the water content, clay mineralogy, and magnetic susceptibility of the mineral phase (McNeill, 1980a). Like many geophysical investigations, the complexity of this relationship is not straight forward. Although several studies have aimed at elucidating the various components of electrical conductivity (Rhoades et al., 1976; Bottraud and Rhoades, 1985; Rhoades et al., 1989b; Friedman, 2005) site-specific empirical relationships are more traditionally used to predict the variation of

properties over the survey area (Cook et al., 1989b; Lesch et al., 1992; Triantafilis et al., 2000; Triantafilis and Lesch, 2005; Vervoort and Annen, 2006).

The commonly-used Geonics instruments (EM 38, EM 31, EM 34) derive the electrical conductivity EC_a from electromagnetic induction measurements, using a linear relationship:

$$EC_a = \frac{4}{\varpi \mu_0 s^2}\left(\frac{H_s}{H_p}\right) \tag{2.17}$$

where the instrument is calibrated to the ratio of the secondary (H_s) to primary (H_p) magnetic fields, under the assumptions that the instrument frequency ω, magnetic permeability of free space μ_0, and coil spacing s, are held constant. This is based on the low induction number principle, where the ratio of the skin depth δ (the depth that the signal is attenuated to 1 e^{-1}) to the coil spacing is much less than 1.

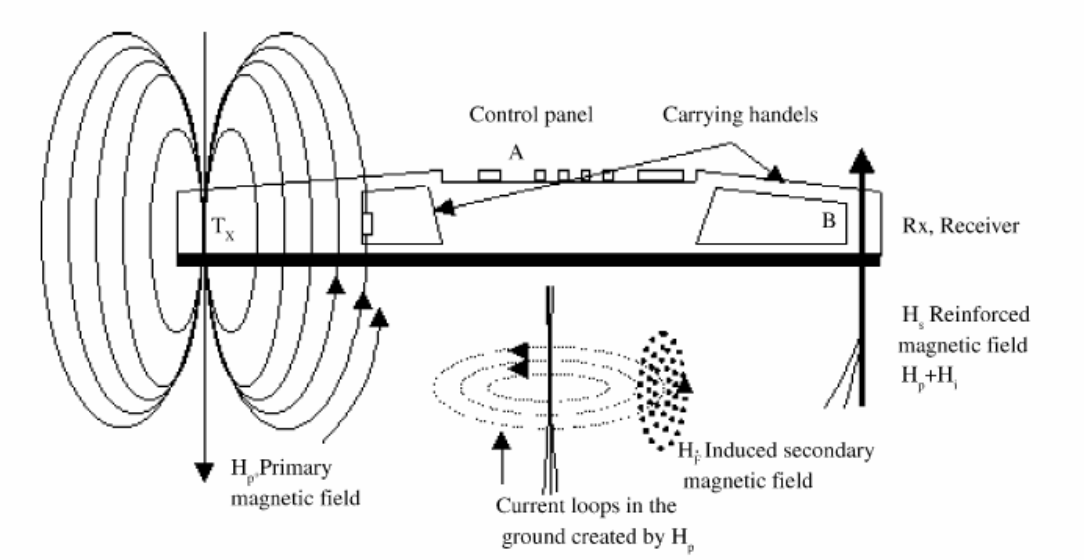

Figure 2.10. General schematic of the Geonics EM38 electromagnetic induction conductivity metre. A transmitter coil (T_x) emits an electromagnetic pulse which, in the presence of a conductive medium, generates secondary eddy currents measured by a receiver coil (R_x). In this schematic, the measured eddy currents are exactly 90° out of phase from the primary magnetic field (pointing out of the page) and are generated half way between the receiving and transmitting coils. From Lesch et al. (2005).

An advantage of this method compared to other geophysical survey methods (ie. seismic and direct current resistivity) is the independence of ground contact and

the linearity of the instrument sensitivity. This not only speeds up surveys, allowing for more observations, but also allows for repeated measurements without ground disturbance. Electromagnetic induction has been used for a variety of purposes including salinity modelling (Cameron et al., 1981; Lesch et al., 1992; Rhoades, 1993; Lesch et al., 1995a) identifying contaminant transport in soils and shallow aquifers (Yoder et al., 2001) measuring soil water content (Sheets and Hendrickx, 1995) and characterising subsoil physical properties such as clay content, depth to clay, and saturated conductivity (Doolittle et al., 1994; Stroh et al., 2001; Doolittle et al., 2002; Triantafilis and Lesch, 2005; Vervoort and Annen, 2006). Several studies in Australia have also identified palæochannels using EM (Williams and Hoey, 1987; Huckel, 2001; Rogers et al., 2002; Vervoort and Annen, 2006).

Apart from being a relatively expensive technology, electromagnetic induction also has several physically-based disadvantages. Instruments must be calibrated daily and are known to drift due to changes in ambient conditions such as soil and air temperature, humidity and solar activity. These effects can combine to affect conductivity readings by as much as 3 mS m^{-1} h^{-1} (Sudduth et al., 2001). Because the instruments require an electrically-conducive body for the generation of eddy currents, the instruments are best suited for conductive environments (McNeill, 1980b). Also, unlike time-domain electromagnetic methods, the depth of investigation is only constrained by the geometry of the coil separation. When the low induction number principle is invalidated, the skin depth, ς is related to the magnetic permeability of the soil μ_o (assumed to be that of free space = 1.25 x 10^{-6} Henry m^{-1}), the conductivity σ of the medium, and the angular frequency of the instrument $2\pi f$, where:

$$\delta = \sqrt{\frac{2}{2\pi f \sigma \mu_0}} \tag{2.18}$$

This can result in effectively stretching the response curve to include material below the theoretical depth of penetration stated by the manufacturer[2]. Hendrickx et al. (2002) suggested that the stretching of the instrument response occurs at conductivities above the linear range of detection and can be accounted for by using a non-linear response model.

This more computationally-expensive non-linear model can be used to predict the output above the 100 mS m^{-1} threshold (Ward and Hohmann, 1987; Hendrickx et al., 2002). Unlike linear models, which assume the depth of penetration is limited by the coil geometry, the non-linear models calculate the response curve based on Maxwell's equation, which predicts the flow of an electromagnetic current through a homogeneous half space. Ward and Hohmann (1987) presented a model specifically for electromagnetic induction, where the skin depth and induction number of the first layer are used as scaling factors. Comparing the two models using height-adjusted EM 38 data over various soil types, Hendickx et al. (2002), showed that the linear model was sufficient in predicting electrical conductivities under 500 mS m^{-1}. However, the non-linear model outperformed the linear one in all cases above this range.

Because EM instruments only report the underlying bulk conductivity, surveys have traditionally been constrained to two dimensions, where survey depth is held constant. Numerous studies in electromagnetic induction have recently focused on determining electrical conductivity profiles by directly manipulating the equipment or changing the survey design. Some common techniques to determine conductivity variation with depth are to increase the coil separation (only available in a few models), change the height of the instrument, or change the dipole configuration

[2] It should be noted that the terms *skin depth*, *(effective) depth of penetration* and *depth of investigation* are often used interchangeably ;in the literature. While the term *skin depth* refers to a specific constant (e^{-1}, or 37%) attenuation, the other terms incorporate instrument-specific notation. For example, the depth of penetration may be many skin depths using magnetotelluric methods techniques, but is less than one with FEM techniques (due to instrument noise) (Spies, 1989). Throughout this thesis, the term *depth of penetration* refers to 2/3 of the initial response (1.5x the coil separation with vertical dipole, 0.75x the coil separation in horizontal dipole), according to the cumulative depth responses provided by the instrument manufacturer (McNeill, 1980).

(direction that the EM wave travels from the coil) (Corwin and Rhoades, 1982; Williams and Baker, 1982; McNeill, 1985; Williams and Hoey, 1987; McNeill, 1991; Cook and Walker, 1992a; Borchers et al., 1997; Rogers et al., 2002; Triantafilis et al., 2003b; Vervoort and Annen, 2006).

A greater penetration depth can be achieved (theoretically, it is 0.75 times the coil separation in vertical configuration and 1.5 times the coil separation in the horizontal configuration (McNeill, 1980b) by moving the coils apart., With most currently available instruments, the frequency of the alternating current must match the coil separation (McNeill, 1996) under the low induction number principle (McNeill, 1980b). As a result, multiple instruments are sometimes required to perform these surveys (Triantafilis et al., 2002; Vervoort and Annen, 2006). By changing the dipole configuration (controlling the orientation of the EM dipole), the waves can penetrate deeper into the substrate (using a vertical configuration) or be more sensitive to shallow depths (with a horizontal configuration). The two coil configurations have a corresponding depth response function, which is used to weight the received signal to predict the contributions of electrical conductivity with depth (Figure 2.11)(Corwin and Rhoades, 1982; Cook and Walker, 1992b; Triantafilis et al., 2003a). Because the instruments linearly respond to changes in height above ground (ie. a 1 m shift upwards corresponds to a 1 m shift in depth of exploration), the instruments can also be lifted off the ground to vary the depth of penetration (Cook and Walker, 1992a; Sheets and Hendrickx, 1995; Borchers et al., 1997; Hendrickx et al., 2002).

By changing all or any of these configurations, it becomes possible to identify changes in the electrical conductivity of the profile. The process of deciphering finite layers of varying thickness and conductivity is not straight-forward, and an infinite number of solutions exist to explain the measured property (Aster et al., 2005). The process of choosing which solution most closely represents that of reality is termed *inversion*.

2.5.1.1 Inversion of electromagnetic induction data to derive conductivity profiles.

Two methods for inverting electromagnetic induction conductivity data from the hand-held Geonics instruments are a linear inversion model by McNeill (1980)

and the regularisation of this method by using Tikhonov regularisation (Borchers et al., 1997).

For example, one way to predict the conductivity profile is by changing the coil configuration. While the ratio of the primary to secondary magnetic fields (Equation 2.17) holds true regardless of the instrument orientation, the instrument sensitivity is affected by the ground conductivity in two different manners. When the coils are held in the vertical position the instrument response, ϕ, to ground conductivity as a function of depth z is given as:

$$\phi^{V}(z) = \frac{4z}{(4z^2+1)^{\frac{3}{2}}} \tag{2.19}$$

whereas in the horizontal position the response is given as:

$$\phi^{H}(z) = 2 - \frac{4z}{(4z^2+1)^{\frac{1}{2}}} \tag{2.20}$$

The two measurements can be made at the same location to derive conductivity data from two heights, which are weighted towards the various responses.

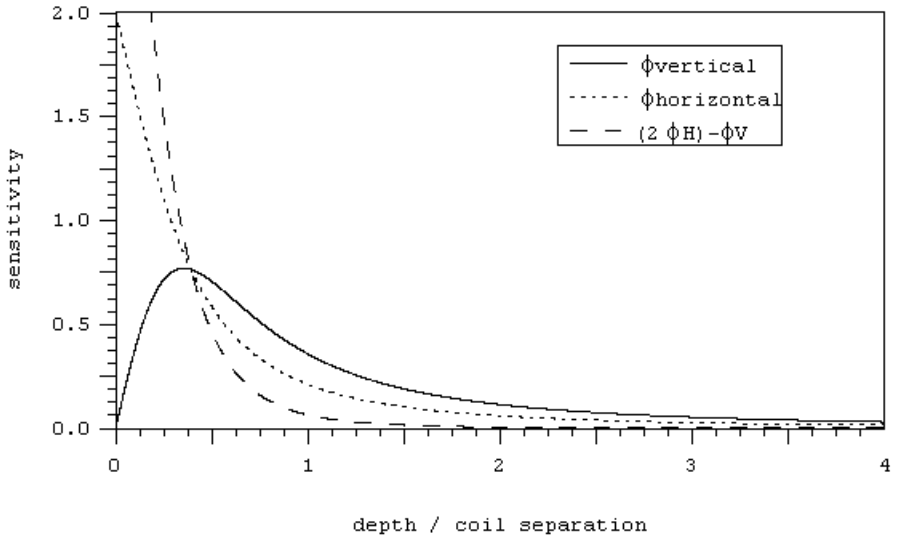

Figure 2.11. Relative response of the Geonics EM conductivity meters in the vertical and horizontal dipole configurations with depth, and a linear combination of the two readings commonly-used to maximise sensitivity in the shallow surface. Axes are normalised to the coil separation of the instruments.

Based on the linear relationship discussed previously, variations in the instrument height linearly shift these response curves with the height raised. Because of this, a conductivity profile can be reconstructed using the two configurations at varying heights. Borchers (1997) sums up these responses into two distinct linear equations:

$$ECa^{V}(h) = \int_{0}^{\infty} \phi^{V}(z+h)\sigma(z)dz \tag{2.21}$$

$$ECa^{H}(h) = \int_{0}^{\infty} \phi^{H}(z+h)\sigma(z)dz \tag{2.22}$$

The combination of this set of linear equations, each defined for a number of measurements at various heights, designates a forward linear model where the apparent conductivity is determined by: the actual electrical conductivity of the soil σ, the instrument height h, and the instrument response curve φ as a function of the instrument height and depth of penetration. To solve for σ, however, the problem is inverse, where a number of solutions exist to explain the output.

By nature, the solution is both ill-defined and non-unique, or that any number of solutions could exist to explain the change in conductivity with depth, given a limited number of observation points. By discretising the function where the number of observations is greater than the number of desired layers, the problem becomes even-determined and a unique solution is achievable.

For example, to predict the electrical conductivity of the soil at several depths (i), described by a column matrix σ, where: $\sigma = [\sigma_1, \sigma_2 \ldots \sigma_i]$ from a number of measurements (j) $d = [EC_{a1}, EC_{a2} \ldots EC_{ai}]$) made in the vertical coil configuration, a series of linear equations exists based on Equation 2.21 in the form $d = K\sigma+\varepsilon$, where the K matrix, with dimensions i x j is the predicted instrument responses at varying heights. This can be used to find an exact solution by solving for d where:

$$\begin{bmatrix} EC_{a1}^{V} \\ EC_{a2}^{V} \\ \dots \\ EC_{aj}^{V} \end{bmatrix} = \begin{bmatrix} \sigma_1^V \\ \sigma_2^V \\ \dots \\ \sigma_j^V \end{bmatrix} \bullet \begin{bmatrix} \int_0^{z_1} \phi^V(z+h_1)dz & \int_{z_1}^{z_2} \phi^V(z+h_1)dz & \dots & \int_{z_j}^{\infty} \phi^V(z+h_1)dz \\ \int_0^{z_1} \phi^V(z+h_2)dz & \int_{z_1}^{z_2} \phi^V(z+h_2)dz & \dots & \int_{z_j}^{\infty} \phi^V(z+h_2)dz \\ \dots & \dots & \dots & \dots \\ \int_0^{z_1} \phi^V(z+h_j)dz & \int_{z_1}^{z_2} \phi^V(z+h_j)dz & \dots & \int_{z_j}^{\infty} \phi^V(z+h_j)dz \end{bmatrix} + \begin{bmatrix} \varepsilon_1 \\ \varepsilon_2 \\ \dots \\ \varepsilon_j \end{bmatrix} \quad (2.23)$$

Mathematically, a unique solution exists to the problem, which would be the intersection of *i* lines defined by the instrument height and response functions (McNeill, 1980b). Due to the instrument limitations described earlier, or any instrument for that matter, it is nearly impossible to find a unique solution to this system of equations due to the random error in the prediction. However, a solution can be approximated by minimising the errors associated with the solution shown as:

$$\min \left\| K\sigma - d \right\|^2 \quad (2.24)$$

This procedure outlined by Borchers et al. (1997), provides a unique solution to the ill-defined problem. However, there are several limitations to the layered-earth model. Intuitively, the method is unrepresentative of the natural, continuously-changing conductivity profiles commonly found in the topsoil, unlike distinct geologic units (McBratney et al., 2000). Mathematically, the solution becomes more ill conditioned as the number of discrete layers increases. This increases the model sensitivity to small perturbations in measurements (due to random noise) can produce significant errors in the predicted response (Borchers et al., 1997; Hendrickx et al., 2002). Given that individual measurements from the EM 38 have a 10% uncertainty at 0.2 dS m^{-1} (Geonics, 1998) it is not uncommon for the model to generate unrealistic soil profiles (Hendrickx et al., 2002; Deidda et al., 2003).

One way to condition the response is through Tikhonov regularisation. The minimisation is conditioned by modifying the least squares problem to include an error term, which is shown as:

$$\min \left\| K\sigma - d \right\|^2 + \lambda^2 \left\| L\sigma \right\|^2 \quad (2.25)$$

In this case, the derivative operator L can be used to smooth the response in terms of the size, shape, or curvature etc. of the predicted response using the K^{th} derivatives, respectively. These are subsequently termed K^{th} order Tikhonov regularisation.

These operators constrain the problem and ensure a stable solution. An optimal value of λ can be found through the use of L-curve criterion, which simultaneously minimises the error and smoothness functions (Aster et al., 2005).

One problem with this method is the subjectivity in choosing the regularisation order. Borchers et al (1997) suggested that 2nd order regularisation provided the best fit for continuously changing profiles. However, McBratney et al (2000) explored the use of each derivative operator for reconstructing soil profile information from EM, and found that *a priori* information was necessary to select the appropriate regularisation order. Henrickx et al (2002) and Vervoort and Annen (2006) both found that 2nd order regularisation provided reasonable estimates in shallow and deep conductivity profile reconstruction.

Several studies have focused on the use of other linear techniques, mostly because of their simplicity. Rhoades and Corwin (1981) first used the EM 38 at various heights to derive the conductivity profiles of several types saline soils. They established a site-specific approach where EC_a readings at various heights were correlated to those obtained from a salinity probe. This method was later extended to a physically-based "established coefficients" approach which was less site-specific, but also less accurate (Corwin and Rhoades, 1982). Slavich (1990) compared these two methods using measured and synthetic data, concluding that the former method provided a much better fit to the measured EC_a profiles. Cook and Walker (1992a) derived conductivity profiles from linear combinations of measurements by minimising the response surrounding the desired depth of interest. These were best fit when *a priori* information was available (i.e. increasing or decreasing conductivity with depth). Using data from a range on non- to highly-conductive environments, Hendrickx et al. (2002) compared the commonly accepted linear models to more sophisticated non-linear models. The authors found that the linear models performed as well as the nonlinear models in sediments where the electrical conductivity was less than 500 mS m^{-1}, but the models substantially diverged above this range. Over the entire range both modelling techniques averaged 20 to 50% error from the conductivity determined by a conductivity probe. For this reason, there is still a considerable opportunity to improve on these models.

2.5.2 Ground-penetrating radar

Ground-penetrating radar operates by emitting electromagnetic waves into the earth generated by an alternating current flowing through a coil of wire, as used in EM surveys. Similar to EM, ground-penetrating radar induces electromagnetic waves into the ground. However the two methods differ in that radar uses high frequency waves (10MHz – 3GHz) from an amplified power source. These waves are sampled on a time referenced basis, so that waveforms of individual reflected waves can be seen. Scans are stacked next to one another as the machine passes over the ground to produce time-referenced profiles (Figure 2.12).

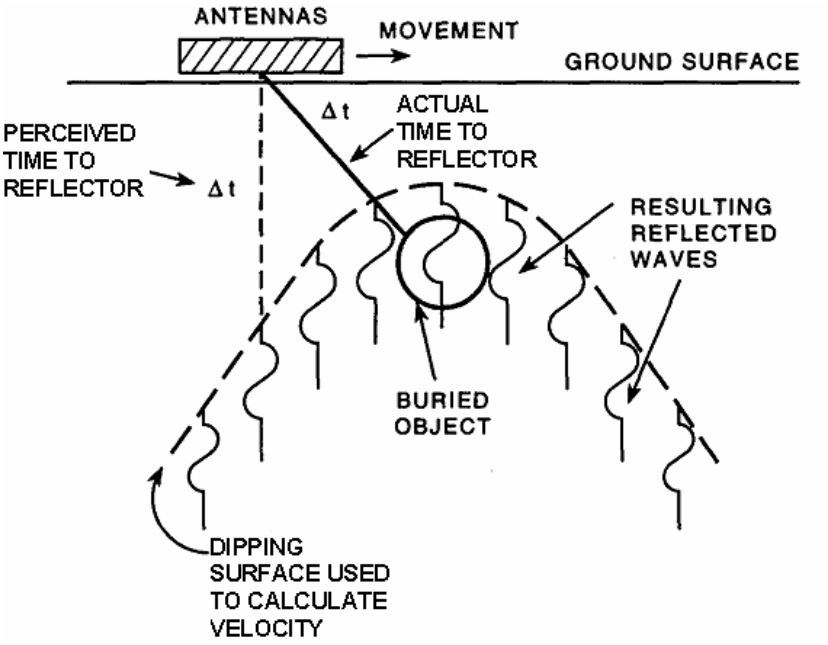

Figure 2.12. Schematic of ground-penetrating radar profile showing hyperbolic reflection of electromagnetic pulses from a point source reflector. From Conyers and Goodman, 1997.

Ground-penetrating radar has proven to be particularly useful in soil science reducing the average cost of a soil survey by 70% and increasing human productivity per hour by 210% (Doolittle, 1987). The method generates a continuous data set along a transect, which can tie into a grid system for micro-variability studies involving high resolution subsurface imaging (Collins and Doolittle, 1987; Davis and Annan, 1989; Butnor et al., 2001) and broader-scaled investigations (Asmussen et al.,

1986; Doolittle and Collins, 1998). Like many other geophysical instruments, radar works best in certain environments, particularly where there is minimal signal loss due to attenuation, and a strong reflector exists. Authors have attempted to detail the site specificity of this instrument, but much work still needs to be performed in soils with varying electrical properties (Doolittle and Collins, 1995).

In areas where signal penetration is acceptable and spreading loss minimal, ground-penetrating radar has successfully been used to map the stratigraphy of shallow fluvial and æolian deposits (Asprion and Aigner, 1999; Vandenberghe and van Overmeeren, 1999; Bailey et al., 2001). These GPR profiles have revealed the complex geometry of river systems by correlating with outcrop information (Table 2-3).

Table 2-3 Ground-penetrating radar signatures from various fluvial deposits in the Netherlands. From Vandenberghe and vanOvermeeren, 1999.

	Braided river		Meandering river		Transitional
	channel	floodplain	channel	floodplain	
Reflection configuration	prograded or trough-shaped; diffractions	Sub-horiz to hummocky and undulating	trough-shaped with subhorizontal fill	oblique (low angle)	cross-bedded in small troughs overlying more continuous undulating
Continuity of reflections	low-moderate	low	moderate	low	low
Reflection amplitude	low	low	moderate	low	low
Geometry of facies unit	channel	wavy	channel	cross-layered sets	small trough overlying wavy patterns

Because each pulse is time-referenced, an understanding of the velocity of EM wave propagation is required to describe the thickness and nature of the material through which they travel. The relationship is complex and is defined by the real and imaginary components of the dielectric constant where:

$$K = K' + i\left[K'' + \frac{\sigma_{dc}}{2\pi f \varepsilon_o}\right] \tag{2.26}$$

The real component *K'* primarily controls the velocity of the EM wave and is often referred to as the *relative dielectric permittivity*. The imaginary part of the dielectric describes signal loss. Signal attenuation is dictated by the loss associated with the frequency-dependant relaxation of water, K'', and the electrical properties of the sediments, which are represented by a ratio of the direct current resistivity σ_{dc} to the angular frequency of the instrument, $2\pi f$, and the permittivity of free space ε_o.

The speed that electromagnetic waves move through the ground, termed the *relative dielectric permittivity,* shown above as K of the material beneath at a velocity, *V* such that:

$$V = \frac{C}{\sqrt{K'}} \tag{2.27}$$

where:

K' = relative dielectric permittivity (RDP) of the material through which the radar energy passes (see dielectric properties of sediments)
C = speed of light (3 x 10^8 m/s)
V = velocity of the radar energy as it passes through a material (m ns^{-1})

The potential amount of signal reflected back to the receiver, *R,* is governed by the contrast in *K* of two adjacent layers, where K_1 overlies K_2 such that:

$$R = \frac{\sqrt{K_1} - \sqrt{K_2}}{\sqrt{K_1} + \sqrt{K_2}} \tag{2.28}$$

The maximum depth of penetration (defined as the maximum depth to which a target can be resolved) is defined by the radar equation. Noon et al. (1998) separate the radar equation into two components, where the instrument properties are defined on the left-hand side of the formula and the material properties on the right hand side of the formula:

$$G_{Tx} G_{Rx} \xi_{Tx} \xi_{Rx} SP = \left[\frac{e^{(-4\alpha R_{\max})\lambda\sigma_T}}{(4\pi)^3 R_{\max}^4} \right]^{-1} \tag{2.29}$$

The directional gains of the radar transmitter, G_{Tx}, and receiver, G_{Rz}, are controls on the amplification of the signal generated and received as they vary with time. These are set by the user prior to data acquisition. The coupling efficiency of the transmitter and receiver, ζ_{Tx} and ζ_{Rx} respectively, are determined by the antennae construction. The System Performance, *SP*, is "the ratio of mean transmitted power to

the minimum detectable signal" (Noon et al., 1998). One method of increasing the signal/noise ratio by "stacking" waveforms, where small amplitude, high frequency "noise" is removed through simulated destructive interference of two waveforms (Davis and Annan, 1989).

The right-hand side of Equation 2.28 encompasses the properties of the medium and geometry of the radar wave relative to the target of interest. This includes the wavelength λ of the radar wave, the radar cross-section of the target σ_T and the absorption loss factor ($e^{-4\alpha R_{\max}}$), which incorporates the signal attenuation α and the maximum depth of penetration R_{max}. In a low-loss medium, Davis and Annen (1989) approximate α as being directly related to the electrical conductivity σ, where:

$$\alpha = \frac{1.69 \times 10^3 \sigma}{(K')^{1/2}} \tag{2.30}$$

This relationship and coupled with Equation 2.29 demonstrates that signal attenuation is strongly related to electrical conductivity and that a stronger current is required to image a target in electrically-conductive media. The properties responsible for attenuating the radar signal are those that accentuate EM surveys (Section 2.51).

The dielectric behaviour of sediments has been studied in controlled setting through the development of time domain reflectometry (TDR). Time domain reflectometry works on the same principals as GPR, but under constraints placed on the EM wave through the use of wave-guides, where the distance that that the EM wave travels is held constant, and the time that it takes for it to flow through the wave guides is recorded and used to predict the volumetric moisture content of the medium (Topp et al., 1980).

2.5.2.1 Dielectric properties of sediments

Dielectric properties in sediments vary widely, and are a function of the water content and ionic strength, clay mineral content, bulk mineralogy, and magnetic susceptibility (Hallikainen et al., 1985; Jacobsen and Schjonning, 1993). In short, the relative dielectric permittivity (RDP) of a material is determined by its ability to store and subsequently transmit electromagnetic waves. As the EM wave travels through the medium, polar ions are aligned to the direction of the EM wave, which are responsible for slowing the wave (Figure 2.13). Water content, particle size,

elemental composition, bulk density, and temperature all influence this relationship (Dobson et al., 1985; Chan and Knight, 2001). In general, as the material contains more polarisable substances (such as water), the electromagnetic wave is attenuated and accordingly slowed. Because the signal returned is time-referenced, it is important to correct for the velocity of the waves to determine the depth and thickness of the underlying layers.

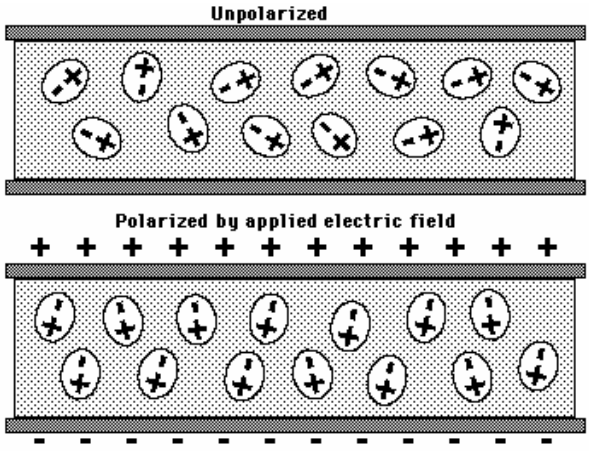

Figure 2.13. Polarization of water molecules in response to applied electric field. This effect shows the work required for an electromagnetic wave to travel through a polarisable medium. From Topp et al, 1980.

Values for RDPs are derived in laboratories to minimize spatial variability. The RDP is a universal standard unit, defined as the ratio of a material's electrical permittivity to the electrical permittivity of a vacuum (= 1). Values for RDPs in different materials have been published extensively (Davis and Annan, 1986; Saarenketo, 1998; Chan and Knight, 1999). A sharp decrease in velocity (calculated using Equation 2.26) occurs in drier sediments due to differences in the RDP of geologic materials (Figure 2.14).

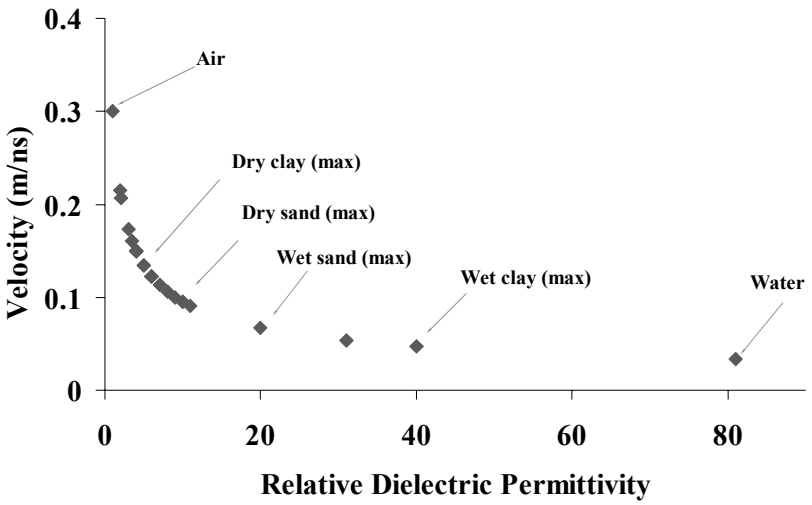

Figure 2.14. Relative dielectric permittivity of various sediments in relation to the velocity of the electromagnetic wave. From Chan and Knight, 1999; Conyers and Goodman, 1997; Davis and Annen, 1989.

Typically, ground-penetrating radar surveys use published values to determine the RDP for a specific site. Most surveys simply plug in a number for the RDP and use this to calculate the depth to a certain reflector. There are two problems with the published values. First, because of spatial soil variability, RDPs may change over the transect distance, giving false depths with each change in dielectric properties. Secondly, most published values do not account for the precise volumetric water content, the ionic strength of the solution, or the bulk density of the soil.

Changes in the dielectric permittivity down the profile can contribute significant amounts of error when determining depth to reflections. There are a few ways to circumvent the problems associated with published RDP values. A common seismic imaging procedure, common midpoint stacking (CMP) has been adopted to take a "vertical sounding" of the media (Davis and Annan, 1989). By increasing the distances between antenna and receiver incrementally, wave velocities are calculated by the increase in time over the distance that they travel (Figure 2.15). This method gives a high-resolution "snapshot" of the subsurface, resembling seismic reflection profiles. It has been used to determine layer thickness, electromagnetic wave velocity through each reflection-generating layers as well as water content and solute concentrations in underlying media (Boll et al., 1996; Reppert et al., 2000; Nakashima et al., 2001).

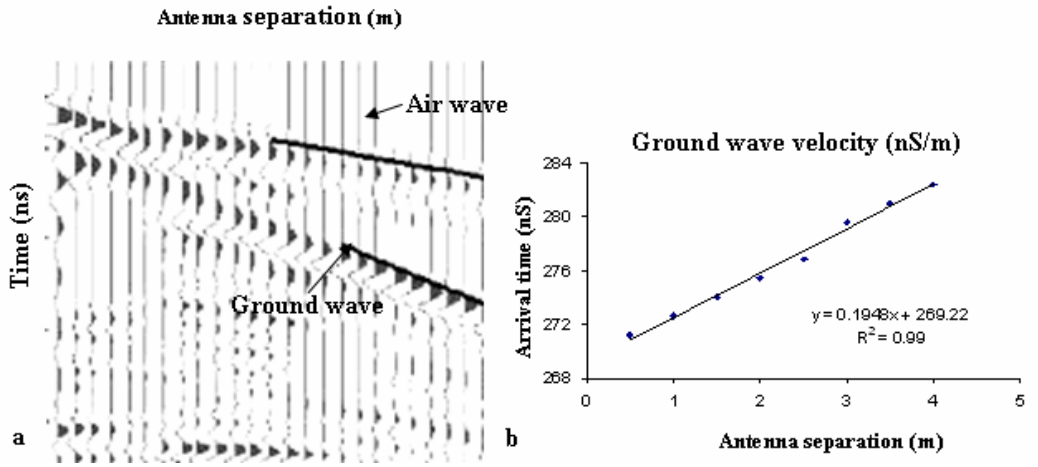

Figure 2.15. Radar gram of a common midpoint survey, where the transmitter and receiver are incrementally separated (a). A plot of the second arrivals (b) shows the calculation of the ground wave travel time.

2.6 Bridging the gap between geophysical and hydrological data

There is considerable interest in using data from high resolution geophysical data to supplement sparsely-sampled hydraulic data. The obvious reason for this is that geophysical surveys are much cheaper and less invasive and, hence, can be used to acquire more information about subsurface properties than can be obtained from coring alone. Presently, information from a few bore holes is used to describe the highly variable spatial distribution of hydraulic properties (Chen et al., 1999; Ritter et al., 2003; Schwartz et al., 2003; Severino et al., 2003). Although advances in geostatistics over the years have helped to improve prediction resolution, there is still considerable uncertainty in groundwater models based on the unknown spatial variability of hydraulic properties.

A physically-based relationship exists between the flow of electrons, electromagnetic and compression waves, and water molecules through the subsurface (Sections 2.4.4,). In all cases, flow is limited by a proportionality constant which is related to the soil properties. Transformation of geophysical to hydrological data has been performed using three different scale- and support-dependant techniques which include: the delineation of hydraulically-important features (i.e. aquifers), the use of

geophysical data to improve geostatistical predictions or stochastic simulations of borehole measurements, or the direct transfer of geophysical data to hydraulic properties using empirical or physically-based relationships. The nature of the support (i.e. resolution) provided in direct relation to the overall contribution to flow processes from a hypothetical contaminant plume is shown graphically in Figure 2.16.

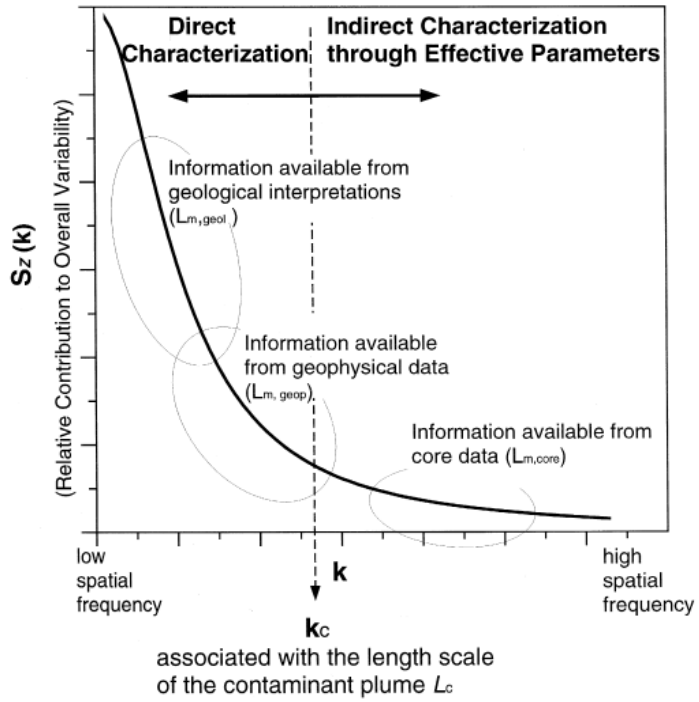

Figure 2.16. A graphic representation of the spectral density information (Sz(k)) relating the survey resolution to the variability of an aquifer system, in relation to the utility of the data collected. In this example the lower wave number information is useful for direct characterisation of the site, where as the higher frequency information is more useful for determining the effective parameters. From Hubbard and Rubin (2000).

2.6.1 Geophysical delineation of hydraulically-important features

Commonly, geophysical methods are used to characterise large-scale hydraulic properties by delineating hydraulically-important geologic facies, such as aquifers and aquicludes. Where two bodies have distinctly different physical properties, geophysical surveys can provide considerable support to geologic maps and borehole information. For this, bore-hole geophysical measurements such as down-hole EM (Timms and Acworth, 2002), gamma-gamma (Crestana and Manoel

Pedro Vaz, 1998), and radar (Binley et al., 2002; Rucker and Ferre, 2004) have been used to identify the vertical distribution of aquifer properties in the vicinity of monitoring bores. To delineate the thickness and horizontal extent of aquifers, seismic reflection and ground-penetrating radar are commonly used because they detect changes in the acoustic or dielectric permittivity of the bodies, which affects wave which affects wave velocity (Day et al., 1992; Cardimona et al., 1998; van Overmeeren, 1998; Asprion and Aigner, 1999; Fielding et al., 2003). Similarly, direct current resistivity and electromagnetic induction are useful to track changes in electrical conductivity, which affects the attenuation of the current or wave (Williams and Hoey, 1987; Tabbagh et al., 2000; Triantafilis et al., 2003b; Shei et al., 2006). Although these methods provide valuable geologic information, they are of limited use for hydrologic modelling purposes because they assume aquifer homogeneity.

2.6.2 Landscape-scale distribution of hydraulic properties

Geostatistics have provided valuable insight to the spatial distribution of hydraulic properties, based on information from limited boreholes. The most commonly-used technique is kriging. The power of kriging (over classical statistical interpolation techniques, i.e. linear or nearest-neighbour) is that it assumes that the variability of a property is spatially-dependant and is weighted accordingly. Several geostatistical methods, such as co-kriging, regression kriging and kriging with external drift, have been adopted to include ancillary information to describe the spatial structure (Odeh et al., 1999). These models use more densely-sampled surveys such as seismic, resistivity, and electromagnetic induction to coerce the interpolation of measured soil properties to more accurately reproduce estimates (Hubbard et al., 1996; Hubbard and Rubin, 2000; Troisi et al., 2000; Gloaguen et al., 2001; Vervoort and Annen, 2006).

Similarly, where the variability of soil hydraulic properties is thought to exist within a certain range (based on direct measurements), the theoretical distribution of soil properties can be predicted using geophysical surveys. The spatial correlation structures obtained from surveys are subsequently used to generate stochastic hydraulic conductivity fields for modelling purposes (Copty et al., 1993; Hubbard and Rubin, 2000). Although individual points are deemed “unknowable”, the uncertainty

of measurements and predications is quantifiable, and can be carried throughout the modelling process to generate confidence limits on predictions.

2.6.3 Direct correlation between geophysical data and hydraulic properties

The most recent advances in this field are based on the direct correlation of measured hydraulic properties with geophysical data. Because of uncertainty in the distribution of hydrologically-relevant variables, this has mainly been accomplished through empirical relationships, where measured hydraulic properties are correlated to geophysical measurements using regression models (Topp et al., 1980; Rubin et al., 1992; Copty et al., 1993; Vervoort and Annen, 2006). These types of relationships can also be incorporated into correlation structure models (Section 2.6.2) through Bayesian updating (Copty et al., 1993; Hubbard and Rubin, 2000) or can directly provide estimates of model uncertainty (Binley and Beven, 2003). Although these methods show considerable promise, they are currently limited by uncertainty in the relationship between geophysical and hydrological properties, and the support scale that each provides (Hubbard and Rubin, 2000).

Hubbard et al (1997) determined the hydraulic properties of a highly-fractured aquifer using down hole ground-penetrating radar. The authors identified preferential flow paths by looking at the change in moisture content over time, using Topp's empirical relationship (Topp et al., 1980), relating moisture content to the dielectric permittivity (which was calculated from the EM wave velocity). The relative differences in moisture content were related to the hydraulic permittivity and highly variable regions were determined to be preferential flow pathways.

Copty et al (1993) used seismic tomography to improve on the spatial correlation structure from measured permeability and pressure data. Utilising Bayesian theory the authors updated an initial (prior) probability distribution function with more finely-resolved seismic data through semi-empirical relationships between the two data. Generating numerous synthetic data sets, the authors concluded that, even with highly corrupted (noisy) geophysical data, the incorporation of the seismic information always improved the model predictions.

Binley and Beven (2003) identified the pitfalls of a similar approach, which was termed the "landscape space to model space mapping approach", in unsaturated

media. Using multiple downhole radar and resistivity surveys over a two year period, the authors were unable to improve on model estimates, mostly due to scale-dependant variations in hydraulic properties relative to the support given by the geophysical data (even when repeated over time), and the limited variation in moisture content over the observation window. However, the geophysical data were useful for determining model uncertainty through Monte-Carlo simulation.

De Lima and Niwas (2000) combined the information from direct resistivity and induced polarisation measurements to determine the hydraulic properties of a shaly sandstone aquifer. Using pre-defined semi-empirical relationships (based on Darcy's and Archie's Laws), the authors showed how the two electrical pathways (i.e. conduction through pore water, and conduction through adsorbed water) combined to limit the flow of electrons from an induced potential. The use of the combined surveys enabled the authors to distinguish the differences in the two conductivities. Although this greatly improved estimates from hydraulic conductivity measurements from boreholes, the model was constrained by dozens of assumptions due to the physically-based model. It was, therefore, specific to the bimodal aquifer which consisted of separate sand and clay facies.

In a numerical study of a bimodal aquifer, Hubbard et al (1999) evaluated the utility of down-hole seismic reflection and ground-penetrating radar to improve estimates of the spatial correlation structure from measured hydraulic data from a limited number of bores. Using previously-derived petrophysical relationships (Rubin et al., 1992), the authors showed that the incorporation of either geophysical method significantly improved coarse-scale heterogeneity estimates (i.e. between geologic facies), but that both geophysical methods failed to capture the small scale heterogeneity (i.e. within geologic facies).

Vervoort and Annen (2006) used electromagnetic induction to directly predict soil hydraulic conductivity, which was thought to vary due to the presence of a palæochannel. The authors explored various EM inversion techniques to use as a trend surface for regression and trend kriging, where multiple linear regression was used to correlate EM data to pedotransfer-derived hydraulic conductivity data. The addition of EM data significantly improved the prediction of soil hydraulic properties, when compared to ordinary kriging of measured soil properties.

These studies all show that these relationships (although complex) could potentially provide the most useful information to hydrologists, as they incorporate several scales of support. However, they are currently relatively uncertain and prone to non-uniqueness and site-specificity. To date, most of the experiments in this field of study follow from petrophysical relationships developed in the oil industry which relate seismic and radar wave velocity to hydraulic properties. The use of electrical conductivity measurements is therefore hampered by the lack of previously developed-relationships. However, EM wave attenuation strongly relates to hydraulic properties, and in clay-rich or highly-conductive environments, can overcome the shortcomings of radar wave attenuation and the non-uniqueness of seismic information.

2.7 Concluding remarks

The Murray-Darling Basin is a unique and productive part of the Australian landscape. The increase in agricultural activity, particularly irrigated agriculture, has greatly benefited the Australian economy. However, this economic benefit has come at the expense of the environment where problems such as soil salinisation, water loss, and contamination of water courses pose serious threats to the sustainability of the industry. Agriculturalists have started to recognise that these problems exist due to soil and climactic variability, and have been slowly adapting irrigation practices to accommodate these problems.

One of the main issues affecting water-use efficiency in the Northern Murray-Darling Basin is the presence of palæochannels in the landscape. It has recently been recognised that palæochannels can play a large part in the hydrological function of a soil, especially under irrigation. Although the impacts of palæochannels on the environment have been reported, there still is scant information on the causality between their presence and their impacts. Of particular concern is figuring out where the water goes once it enters the channels.

Groundwater models are an effective and efficient way to look at groundwater flow in many types of environments. By characterising the structures in detail we can start to develop sound conceptual models of the structures in relation to shallow groundwater flow. By observing trends in groundwater responses to environmental stimuli, we can effectively predict how future stimuli will affect this response.

However, a model is only as good as the input data and it has been shown that these types of environments contain significant variability in subsoil hydraulic properties (one of the most sensitive parameters in groundwater models). So it is important to know how the hydraulic properties of the subsurface are distributed across the landscape.

Geophysical investigation is an ideal complement to groundwater modelling because it provides the modeller with much more information than can be obtained by a limited amount of soil cores. Electromagnetic induction has proved to be a versatile and informative geophysical tool in the agricultural industry, particularly in semi-arid regions which are prone to be electrically conductive. This being said, there is still a great deal to learn about the ways that we can use these instruments to predict differences in hydraulic properties with depth.

Combining geophysics with groundwater modelling will enable modelling of the palæochannel system in detail. This is because the geophysical investigation will allow "filling in" of the subsurface information. Although electromagnetic induction has been shown to outperform most other geophysical methods in highly conductive environments, there are issues with translating the geophysical information to hydrologically-relevant information (i.e. groundwater model parameters) due to a paucity of published models relating the parameters. This study will endeavour to foster the link between geophysics and hydrology by developing these relationships in hopes of providing a valuable tool for water resource management in highly conductive environments.

Chapter 3

Methods used to characterise the field site and install monitoring equipment

3 Methods used to characterise the field site and install monitoring equipment

The purpose of this chapter is to describe the methods that were used in the study. Following a general site description, three sections discuss the methodologies including the hydrological methods to characterise water flow on the site, pedological methods to characterise soils on the site, and geophysical methods to image the geologic properties. These methods will be referred to throughout the thesis.

3.1 General Site Description

The field study site is located in northern New South Wales on an irrigated cotton farm positioned on the floodplain of the Gwydir River (Figure 3.1). The study site is located at latitude 29.33397° S, longitude 149.7738° E (6751816.77 Northing, 769350.02 Easting) and is located approximately 20 km north of the town of Moree, NSW. The study site consists of approximately 25 ha of cropped and uncropped land, including the northern half of an irrigated cotton paddock and an additional five ha of land on the floodplain of Carroll Creek, which forms the northeast boundary of the site (Figure 3.2).

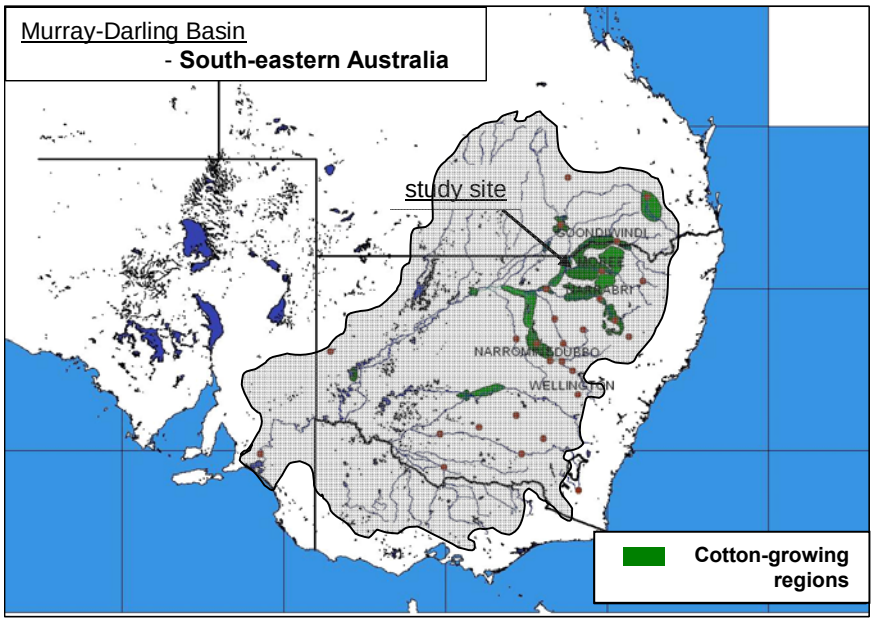

Figure 3.1. Map of the Murray-Darling Basin indicating the study area in respect to the major cotton-producing regions located on the flood-plains of the Darling River and tributaries in Northern New South Wales.

The majority of the 70 000 ha farm is under a cotton-wheat rotation which is irrigated using furrow irrigation methods. Several paddocks on this farm have shown irregularities in irrigation efficiency which have been linked to the presence of coarse-textured palæochannels throughout the farm (Huckel, 2001; Triantafilis et al., 2003a; Vervoort and Annen, 2006). Anecdotal evidence of their impact in the particular study site suggests that waterlogging and abnormal crop yield is correlated with areas of lighter coloured soil (Figure 3.2).

The soils at the site are mostly black Vertosols, with uniform (smectitic) clay contents down several metres. These aeolian and alluvial sediments were derived from the nearby basaltic Nandewar Range (Stannard and Kelly, 1968; Young et al., 2002). Annually, the site averages 585 mm of summer-dominated rainfall which occurs on 78 days of the year. The amount of potential evapotranspiration greatly exceeds rainfall and ranges from 9.7 mm day^{-1} in December to 2.3 mm day^{-1} in July.

Figure 3.2. Aerial photograph showing a portion of Auscott's "Midkin South" cotton farm. Circles indicate the areas near the field site where extensive water logging has been found. The study site is outlined. This aerial photo was taken during seed emergence and shows the disrupted emergence occurring in linear patches of bare soil above the palæochannels (pers. com Tim Richards, Auscott Farm Manager, May 2006).

3.2 Hydrological methods for monitoring water flux through the palæochannel system

3.2.1 Installation of groundwater monitoring equipment

Although costly and time-consuming, direct measurements of infiltrating water and local groundwater levels are a fundamental part of understanding the landscape hydrology. This study uses piezometers and drainage metres to monitor water flow on the site. In order to accommodate field operations and to provide for a more realistic study, all of the monitoring equipment was buried below the maximum depth of field operations (60 cm) and linked to junction boxes which were buried at the same level. These were coupled to data loggers, external power supplies, and solar panels on removable boxes above ground (Figure 3.3). These boxes also allowed the piezometers to equilibrate with atmospheric pressure when installed.

3.2.1.1 Drainage meter specifications and installation

Soil drainage meters (also termed "tube tensiometers") can be used to measure the soil water potential at various depths (Hutchinson and Bond, 2001). The instruments are similar to traditional tensiometers, where a sensing tip is in direct contact with the soil and the amount of pressure that the soil exerts on the tip is proportional to the moisture potential. The advantage of tube tensiometers is that they can be buried and that they are able to dry out without having to be manually rewetted (Hutchinson and Bond, 2001).

By measuring the difference in soil moisture potential at two points (ψ), the Darcy-Buckingham Law can be used to calculate water flux (q) between two points by knowing the distance between the points (z) and the hydraulic conductivity of the medium ($K(\psi)$) where:

$$q = K(\psi)(\partial\psi / \partial z - 1) \qquad (3.1)$$

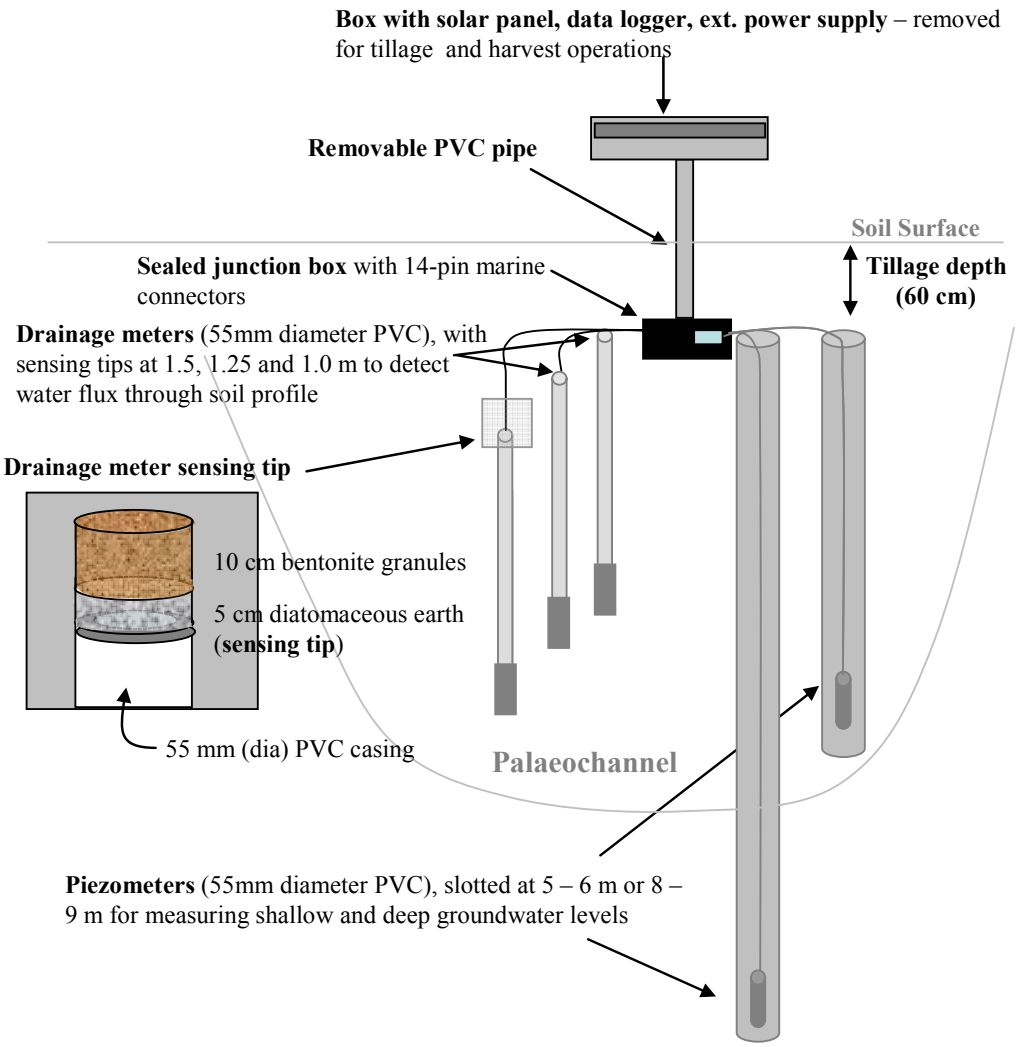

Figure 3.3. Unscaled diagram of monitoring equipment used to track the movement of water through below the root zone (drainage metres) and into and through the proposed palæochannel (piezometers). This setup was replicated in three places along the channel and two places outside the channel to identify flow along the channel.

Of these variables, soil water potential is the most transient and difficult to measure. To measure potential, the tube tensiometer uses a sensing tip which is composed of diatomaceous earth. The sensing tip is in hydraulic contact with the surrounding soil and located directly above a smaller column of the same material which is encased in a 22 mm diameter PVC tube. A bentonite plug is packed on top of the diatomaceous earth sensing tip to ensure that deep percolation, resulting from the disturbed earth above the sensing tip, does not affect the soil water potential. As soil moisture increases, tension decreases and water enters the column increasing the pressure at the bottom of the tube. A pressure transducer below the column measures the pressure change and sends the information to the data logger above ground. Silicon tubing is used to vent entrapped air from the column.

After preliminary testing of the instruments, several adjustments were needed to accommodate the heavy clays at the field site. The three major concerns with the initial design were: the purity of the sensing tip, the instrument orientation and height, and the exposure of wires and ventilation tubes to sharp materials in the sidewalls during installation. Hutchinson and Bond (2001) suggested drilling a second, larger hole for the sensing tip. However, during the preliminary testing it was found that, while drilling the second hole, a significant amount of soil fell into the first hole. Although the material was packed down into the hole beneath the instrument, this created problems with pre-determining the instrument height. When the hole was drilled after instrument installation, the sensing tip was fouled by soil during hole collapse. To circumvent these problems, the tube tensiometers were encased in a 55 mm PVC sleeve and fitted with a collar which had four holes for the wires and tubing to pass through at the top. Both the sleeve and the collar were sealed with silicon to ensure that moisture would not pass through the holes and into the space between the tube and the casing. Because of the collar, the sensing tip could be created directly on top of the instrument, rather than drilling the second hole above the instrument. The advantage of this is the need for only one drilling procedure, which would avoid all three problems previously described.

In September, 2004, 15 tube tensiometers were installed on the field site. Three instruments were nested at five locations, co-located with deeper piezometers (Figure 3.4). The instruments were separated (vertically) by approximately 25 cm to record the potential at three separate points. Four sites were chosen in the paddock

consisting of two nested tensiometers above the palæochannel, two outside the palæochannel, and one in the natural vegetation area above the palæochannel. A truck-mounted drill rig using a 55 cm auger was used to drill the holes to 3, 2.75, and 2.5 m in order to place the bottom of the sensing tips at 1.5, 1.25, and 1 m below the soil surface, respectively. Each hole was separated horizontally by approximately 50 cm. This was estimated to be the minimum separation distance without the hole collapsing from drilling adjacent holes. During the drilling process, samples were taken from the auger at 50 cm intervals and sealed in aluminium weighing tins for analysis of gravimetric water content. In order to expedite the drilling process, PVC lengths with fitted collars were temporarily placed in non-instrumented holes to keep them from collapsing.

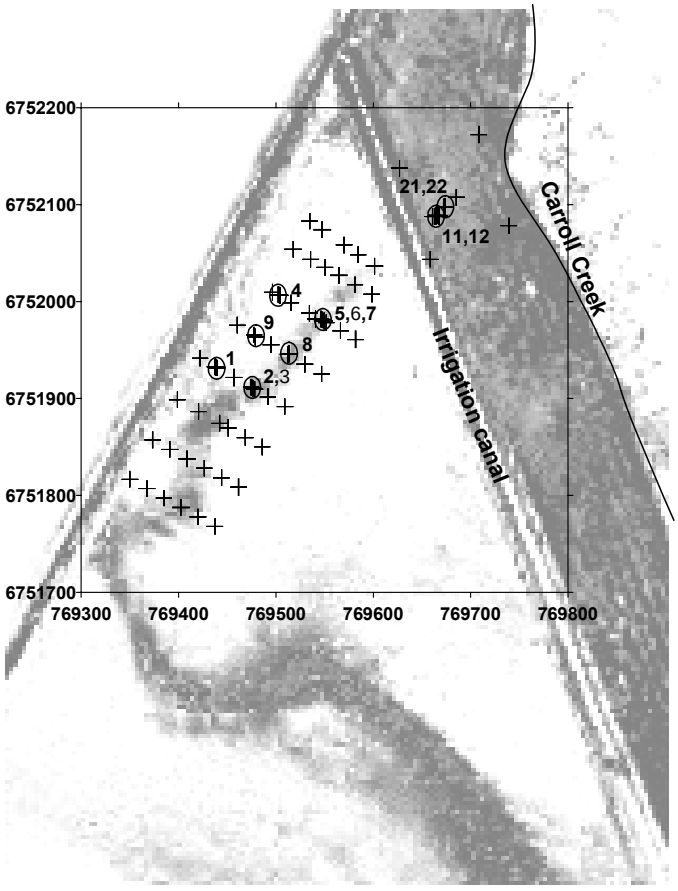

Figure 3.4. Sampling and piezometer locations shown on red-band enhanced aerial photograph. Sampling locations are marked with crosses and deep cores with circles. Cores and piezometers are numbered, including the 6 m piezometers (3,6,12,22), 9 m piezometers (1,2,4,5), 20 m piezometers (11,21) and 9 m cores used only for ground-truthing (7,8,9). The north-east corner of the paddock is bordered by an irrigation canal. The tree-lined bank of Carroll Creek is shown in the north-east corner of the photograph.

The tube tensiometers were packed with moist diatomaceous earth at the study site. Water was added to the diatomaceous earth in the field and allowed to equilibrate inside sealed bags for two hours prior to packing the instruments. The packing method described by Hutchinson and Bond (2001) was used where small amounts were placed in the tube and gently packed using a wooden broom handle.

Once packed, instruments were lowered into the holes by grasping the bundle of wires and drainage tubes connected to the instruments. When instruments were impeded by the wall surface, they were forced down to the bottom of the hole by gently tapping a length of PVC tubing placed over the instrument. Bentonite granules were poured around the tube until the tip of the instrument was reached. Then, the same mix of diatomaceous earth was added and gently packed, to create a 5 cm-thick sensing tip on top of the tube which was in contact with the surrounding soil. An additional 10 cm of bentonite was added to the hole and the soil replaced and packed on top. After the nest of three instruments was in place, a small trench was dug between the instruments to connect the wires and tubes to the junction box located approximately 50 cm from the closest instrument (Figure 3.3).

3.2.1.2 Piezometer installation

Piezometers are used to measure the pressure head of groundwater in confined or unconfined aquifers (Section 2.3.3). They are simple in design, consisting primarily of a length of PVC tubing with a screened interval at the depth of interest. Piezometers need to be in direct contact with the atmosphere in order for water to flow into them from the surrounding aquifer which is also under the influence of atmospheric and lithostatic pressure (Fetter, 2001).

In May 2004, six piezometers were installed at the field site to quantify the water flux through and around the palæochannel (Figure 3.4). Two piezometers were placed outside the channel, two inside the channel and two beneath the palæochannel (nested with the ones inside the channel) (Figure 3.3). The piezometers were made of 60 mm Class 12 PVC lengths joined with PVC glue. The bottom of each piezometer contained a one metre length of slotted PVC to serve as a screen.

Holes inside the palæochannel were first drilled to nine metres using a 95 mm diameter auger in tandem with a split spoon-corer (for sampling). The cores from the first hole were used to determine the depth to the channel bottom for the subsequent

hole, which terminates at the channel bottom (indicated by a thick layer of reduced clay at all locations). Folling the drilling the three metre PVC lengths were joined with the one metre length of screen and the piezometer was lowered into the hole using a crane. Gravel was then poured around the PVC length to the top of the screen. This was then topped with several metres of bentonite granules. The excess soil was then packed into the hole. A pit (1 m diameter) was dug around the top of the piezometre to a depth of approximately one metre below the soil surface to encase the piezometer head. Approximately 0.4 m^3 of concrete was poured into each hole and allowed to dry for several days.

Several weeks after drilling, the six piezometers located in the paddock were fitted with submersible pressure transducers (WL1000W, Hydrological Services Pty Ltd, Sydney, Australia) to record water heights in the piezometers. Wires from the transducer and a separate four mm (diameter) silicon tube were pulled through a small hole in the top of the well and were then wrapped around the pipe and taped down to ensure that the transducer remained stationary. A PVC cap was then placed over the piezometer and along with the hole in the piezometer, was sealed with silicon. The wires were joined with those from the tube tensiometers into a 14-pin parallel connector located inside a sealed junction box. This connector was then joined to the upper box (which housed the data logger, solar panel and external power supply) through a sealed PVC pipe (Figure 3.3). The 14-pin connector was later replaced with a single marine connector, due to corrosion. The data logger was programmed to record the raw levels every 15 minutes using a one second scan time.

In November 2004, four additional piezometers were installed in the area of natural vegetation inside and below the palæochannel. Two piezometers were nested at 6 and 20 m below the surface at two locations (Figure 3.4). The 100 mm-diameter holes were drilled with a rotary drill using an organic polymer to lubricate the bit. The 95 mm Class 18 threaded PVC lengths were joined with a three metre section of screen followed by a one metre length of solid PVC used as a sump. The piezometer heads were cemented into the ground and encased with a steel housing.

3.3 Soil physical and chemical properties

3.3.1 Coring methods

During the course of two years, soil samples were collected to characterise the topsoil and deeper sediments inside and outside the paddock on four separate occasions. In July 2003, eight 100 metre-long transects were surveyed on the paddock. The eight transects were separated by 50 m and were offset so that they bisected the palæochannel (as identified from the aerial photograph) (Figure 3.4). On each transect, samples were taken at 20 m intervals. A tractor-mounted pneumatic push probe was used to extract 56 cores from the topsoil extending to 1.5 metres below the soil surface. Following extraction, each core was laid out on a sampling dish (plastic gutter) and was described in terms of: texture (by hand), colour at field moisture content (using a Munsell chart), horizon boundary (if present), and amount, size, and type of nodules present. Following field description, several cores were subsampled and placed into sealed aluminium sampling tins to determine gravimetric water content in the lab. The rest of the samples were bulked in 0.5 m increments and placed in plastic bags for future analysis.

In December 2003, transects were surveyed in a similar fashion, parallelling the irrigation canal and bisecting the palæochannel in the area of natural vegetation (Figure 3.4). Samples were taken at the beginning, end and midpoints of one transect and the beginning and ends of two transects using a hand auger. The augered cores were described as before, subsampled and bagged by horizon.

In May 2004, several samples were collected during the installation of the groundwater monitoring equipment. A drill rig equipped with a 95 mm auger and a dynamic penetrometer (Figure 3.5) was used to drill the holes for the piezometers. The components were used in tandem to auger the holes to the desired depth of investigation, perform a standard penetration test to 15 cm and then extract the cores. The standard penetration test, commonly used in civil engineering to predict penetration strength (related to bulk density, mineralogy, liquefaction potential) (Aboumatar and Goble, 1997) was performed by counting the number of times it takes a 40 kg weight to drive a special split-spoon core 15 cm downward. After the first core was extracted, two additional tests were performed totalling 45 cm of intact cores per metre. Inside the paddock, six holes were drilled to a depth of nine metres

using this method with samples taken every metre. Samples were removed from the split-spoon casing and described in terms of colour, visible inclusions, and boundary characteristics. Cores were subsampled every 15 cm and placed in airtight weighing tins. The rest of the soil was placed in sealed bags and tightly packed to maintain the core integrity. Four additional holes were drilled (using only the auger) to install the piezometers inside the palæochannel occurring approximately five to six metres below the surface. The drill cuttings were recorded in terms of boundary (approximate), colour, and hand-determined texture. Samples were also taken from Well 7 (Figure 3.4) in one metre increments and placed in plastic bags for laboratory analysis.

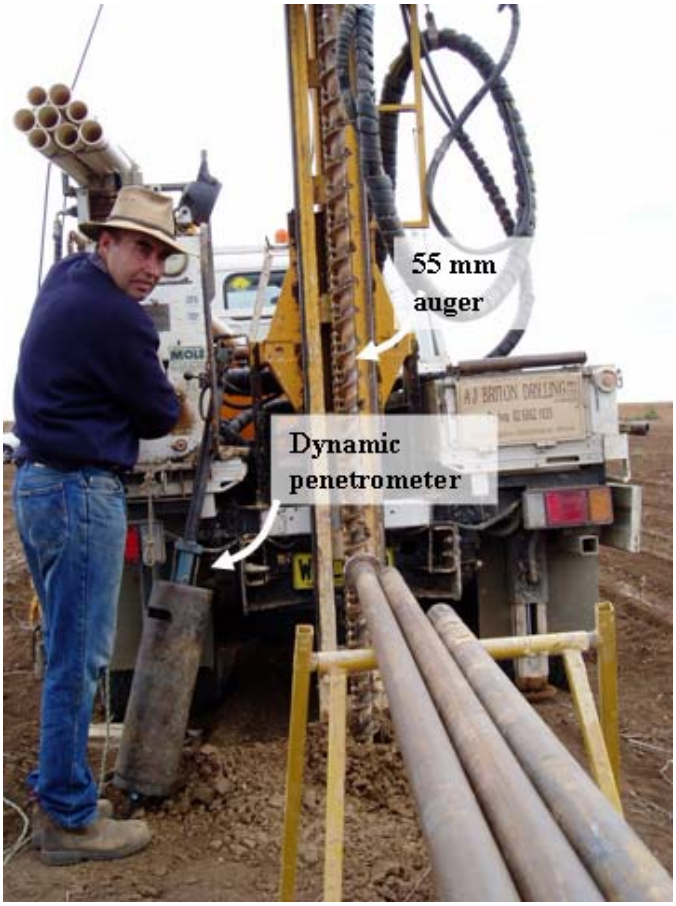

Figure 3.5. The drill rig set up for deep coring. Shown are the 55 mm auger, which was used to drill holes, and the 40 kg weight from the dynamic penetrometer which was used to drive extensions (shown in the foreground) linked to a split spoon corer (not shown) to extract samples.

The last sampling event took place outside the paddock in November 2004. A drill rig equipped with a 100 mm rotary drill was used to drill two holes to six metres and two holes to 20 m. Samples were taken in 50 cm increments as they were brought to the surface with the organic polymer (used to lubricate the drill bit). After drying in the sun to degrade the organic polymer, samples were placed in burlap bags and transported to the laboratory for analysis.

3.3.2 Sample preparation and analysis

Soil samples (excluding those from the 100 mm holes) were transported to the lab and allowed to dry over the course of two weeks. The dimensions of the split-spoon cores were measured at field moisture content using digital callipers and were subsequently dried at 105°C and weighed to estimate the bulk density and gravimetric water content following from McBratney et al. (2000).

Once dried, samples were placed in a tumbling soil grinder and sieved to 2 mm. Particles greater than 2 mm were weighed and recorded as a percentage of the overall dry sample weight (typically 2 – 3 kg). The particle size distribution for each soil sample was determined using the pipette method (Gee and Bauder, 1986) following the International Society of Soil Science classification of clay (< 2 μm), silt (2 - 20 μm), fine sand (20 - 200 μm) and coarse sand (200 - 2000 μm) fractions from a 50 g air-dried sample. The air-dried moisture content of the samples was determined by placing them in the oven at 105°C and recording the change in weight (Gardner, 1965).

Mineralogical analysis of the samples was carried out using binocular microscopy and X-Ray diffraction techniques. Sediments were first examined under microscope prior to particle size analysis to identify bulk mineralogy, oxide coatings, and approximate grain sorting. Following separation and dispersion, sediments were re-examined to identify sand grains which were stripped of their oxide coatings. The mineralogy of the sand fraction was estimated from the colour, luster, and cleavage planes of the sediments (Klein and Cornelius, 1993, pps. 613-646). This method was also used to estimate the amount of sorting and rounding of the sediments to determine the likely sources of deposition and transport (Prothero and Schwab, 1996). X-ray diffraction was also carried out on the bulk samples to qualitatively identify differences in mineralogy between 5 samples using CuKα radiation at 2 - 70° 2θ

following from Whittig and Allardice (1986). The samples used for XRD analysis consisted of two topsoil samples located in the area of natural vegetation, two samples from inside the palæochannel and one outside the palæochannel at 3.0 – 4.0 m, and two samples from below the palæochannel and one at the same depth outside of the palæochannel from 7.0 – 8.3 m.

The electrical conductivity ($EC_{1:5}$) and pH of each sample was determined using a 1:5 soil to water suspension (Rayment and Higginson, 1992). Both measurements were made from the same suspension using calibrated electrodes. A pH electrode was calibrated using three buffers at pH 4, 7, and 10 and the EC using a 1014 μS standard sample of KCl (Rhoades, 1996). The soluble chloride was extracted using a different 1:5 soil to water suspension. After centrifuging the sample at 20000 rpm's for 20 minutes to settle the soil colloids (Diamond, 2001), the sample was decanted. The extract was then mixed with mercuric thiocyanate and analysed colourmetrically using a FOSS FIAstar 5000 flow injection analyser (ESS Method 140.4).

3.3.3 Hydraulic property prediction using pedotransfer functions

Bouma, (1989) defined pedotransfer functions as "translating data we have into what we need". Several programs have utilized robust data sets containing easy to measure soil physical properties (sand, silt, clay etc.) and difficult to measure soil hydraulic properties (K_{sat}, and $K(\theta)$, $\theta(\psi)$ curves) to develop relationships between the properties for prediction purposes. These programs are generally termed *pedotransfer functions* because they allow the user to transform their measured data into desirable hydraulic properties.

Prediction models have used multiple linear regression, non-linear regression, and artificial neural networks to develop relationships between the measured and predicted properties. Neural networks, which are based on our concept of the human central nervous system, have been shown to outperform prediction techniques based on multiple linear regression analysis (Schaap et al., 1998; Koekkoek and Booltink, 1999; Minasny and McBratney, 2003), and extended nonlinear regression (Minasny et al., 1999) without the use of pre-determined relationships; however, predictions can vary with every model run. Using a bootstrap method (Breiman, 1996), where multiple runs are performed using resampled data, confidence intervals are placed on

the predictions, providing realistic constraints to the predictions. While trying to predict continuous Ksat fields using geophysical and soil property data, Vervoort and Annen (2006) suggested that the main uncertainty in the resulting field originated from the use of pedotransfer functions.

The particle size and bulk density data were used to predict saturated conductivity values and water retention curves using 5-parameters in the Neurotheta model (Minasny and McBratney, 2003). Inputs consisted of coarse sand, fine sand, silt, clay and bulk density. Because Neurotheta uses a training set from Australian soils, it is skewed towards fine-textured soils (Minasny, pers. comm., May, 2006). To compare the differences with another popular pedotransfer function, the input data was also run through Rosetta, a program which also uses artificial neural networks, but has a larger data base (1 306 samples, as compared with 412) and has a larger proportaion of coarser-textured samples found in the US and Europe (Figure 3.6). Unlike, Neurotheta, which differentiates between fine and coarse sand, Rosetta only incorporates a 4-parameter model, based on the three basic particle size criteria and bulk density data.

3.3.4 Direct measurement of hydraulic properties: Slug tests and groundwater recession

Slug and pump tests can be used to directly measure aquifer transmissivity (hydraulic conductivity x aquifer thickness) or specific yield (hydraulic conductivity x water level). In aquifers with high yields, pump tests are commonly performed, whereas slug tests are more commonly used in slower-responding aquifers (Fetter, 2001, p. 190). Slug tests are performed by adding a known amount of water to a well and recording the fall in head over time.

In December 2004, slug tests were performed on each piezometer using approximately two litres of water for the slug. In the non-instrumented piezometers (11,12,21,22) the fall in head was recorded using a "wolf whistle" connected to a measuring tape. Measurements were taken at one minute intervals for the first ten minutes and then at 10 minute intervals once the fall in the head tapered off. In the instrumented piezometers, the pressure transducers were used to measure the fall in head at one minute intervals for the duration of the test.

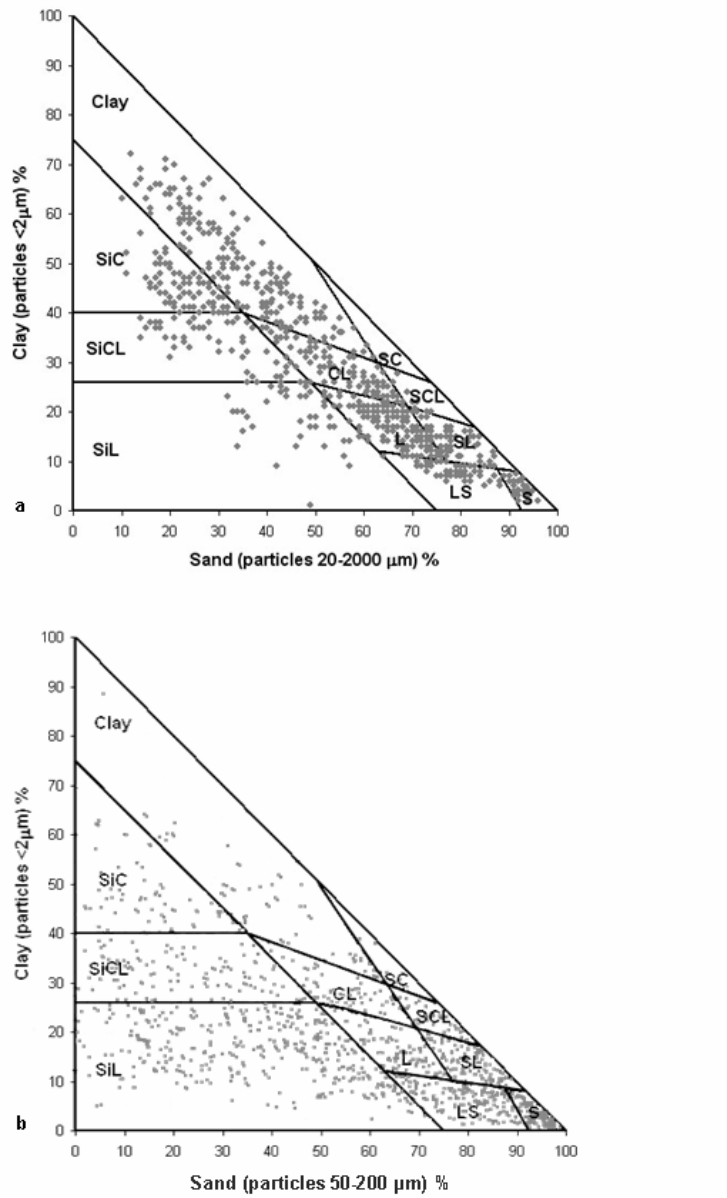

Figure 3.6. Training data used for the pedotransfer functions Neurotheta (a) and Rosetta (b). Although the two databases used different classification for silt size and textural class denomination, the graphs clearly show the relative distributions, where the Neurotheta contains more samples with high clay contents, and fewer sandy samples.

The Hvorslev method (Hvorslev, 1951) was chosen to interpret slug test results. The method is based on the assumptions that piezometers are placed in unconfined aquifers where the length of the well is significantly more than the radius. Additionally it is assumed that the water table fully penetrates the well screen. These

conditions were met in six of the ten piezometers at the time the test was performed. The model estimates the hydraulic conductivity K based on the equation as outlined by Fetter (2001, p.194):

$$K = \frac{r^2 \ln(L_e / R)}{2 L_e t_{37}} \tag{3.2}$$

Where:

K – hydraulic conductivity (L/T)
R – radius of the well casing (L)
L_e – length of the screened interval (L)
t_{37} – time for the well to recover to 37% of its initial changed state (T)

In addition to the slug tests, long term groundwater levels were used to estimate the saturated hydraulic conductivity. This method assumes that water pulses into the system are instantaneous and immediately start to recess at the peak. The Hsorslev test is then used to solve for the recession leg, assuming that the difference between the minimum and maximum points represents the slug (or pulse of water). The benefit of this method is that several measurements can be made over the course of the year to compensate for uncertainty in the hydraulic properties and the moisture contents of the deposit measured.

3.4 Electromagnetic measurements of the soil and regolith

Ground-penetrating radar and electromagnetic induction are two geophysical methods used by earth scientists to predict changes in subsurface hydraulic properties (Hubbard and Rubin, 2000; Vervoort and Annen, 2006). Both instruments utilise electromagnetic waves, which are recorded in the time- and frequency domains, respectively. The two instruments compliment each other, due to the nature of the dielectric properties of sediments. This is evident from the complex nature of the dielectric permittivity as a function of the angular frequency (Equation 2.26), where the imaginary component is directly proportional to the electrical conductivity σ of the medium

$$K''(\omega) = \frac{\sigma}{\varepsilon_o \omega} \tag{3.3}$$

where the permittivity of free space (ε_o) = 8.85 x 10^{-12} F m^{-1}

The result is a dimensionless number, relating the electrical conductivity of the medium to the normalised capacitance of free space where the frequency and voltage of the EM wave are taken into account. Using electromagnetic induction, the electrical conductivity can be rapidly measured across the area of interest.

The real component of the dielectric permittivity is determined by the storage and subsequent release of the electromagnetic wave, which affects the speed the wave travels through the earth. This property is mostly controlled by the water content of the soil (due to the polarisation of water molecules) and varies from 1 in air to 81 in water (Section 2.5.2). While time domain reflectrometry has traditionally been used to measure this property in a controlled setting (Topp et al., 1980), ground-penetrating radar can be used to measure water content using a common-midpoint survey design (Huisman et al., 2002). The combination of these instruments can effectively describe the dielectric properties of the sediment in terms of the speed that the waves travel through the earth, and the attenuation of the waves in relation to the electrical conductivity. This, in turn relates to many desirable soil properties, which are associated with the potential movement of water through the subsurface (clay content, porosity) and the effects that this movement has had on the soil (electrical conductivity, chloride content).

3.4.1 Hand held EM survey

Apart from the deep cores drilled outside the paddock, each sampling campaign corresponded with an EM survey to measure the apparent electrical conductivity EC_a of the soil. A datum was inserted on the edge of the paddock to calibrate the instruments at the start of each day of survey, as outlined in the instrument documentation. Wooden stakes were used to mark transects in furrows located between designated wheel tracks, which were approximately 50 m apart. In total, eight of these transects were surveys and numbered from 1 (on the southern most area) to 8 (on the northern most area). Each transect measured 100 m and was pegged at either end (Figure 3.7). Each sampling point was then resurveyed using a NavMan GPS (Compaq) unit.

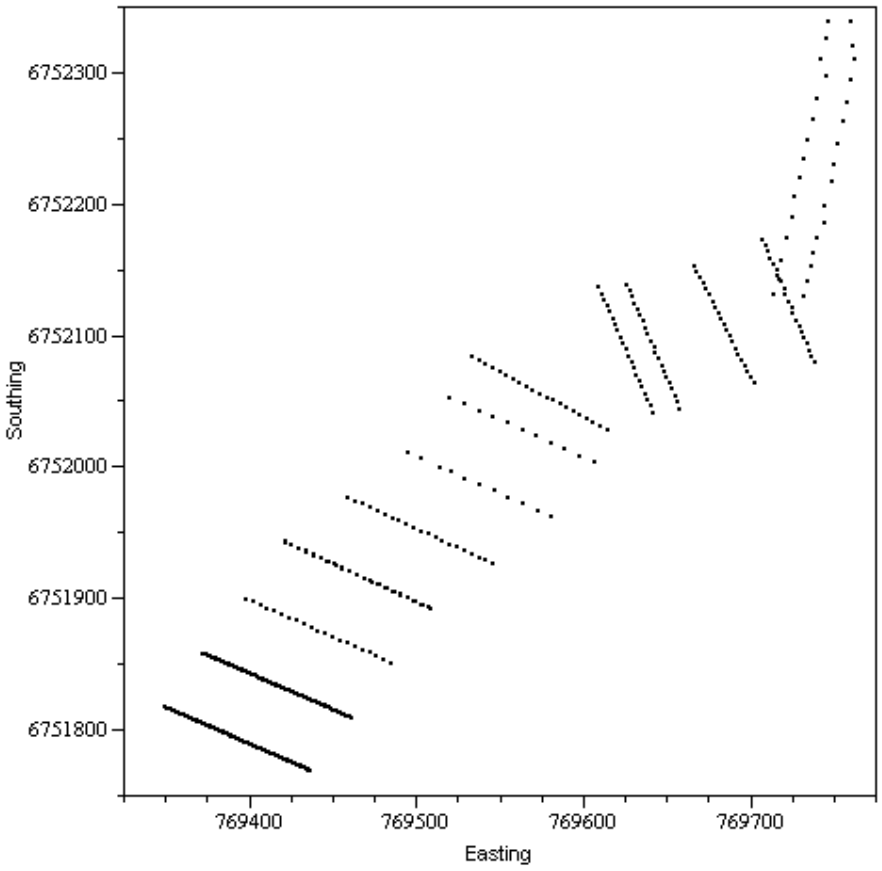

Figure 3.7. Locations sampled using the hand-held EM instruments during the 5 surveys. The paddock outline is shown in bold. Carroll Creek is shown as bold dotted line to the East.

Apparent electrical conductivity readings were taken at various spacings and heights in the study area. The three instruments used for this were the EM 38, EM 31, and EM 34 all manufactured by Geonics Ltd, Ontario Canada. The EM 38 is a frequency-domain ground conductivity meter which consists of two coils (one transmitter and one receiver) separated by one metre (Figure 3.8). An alternating current pulses through the transmitter coil at 14.6 kHz, inducing a magnetic field normal to the plane of the coil, in accordance with Faraday's law of electromagnetic induction. In the presence of a conductive body (such as soil) the primary magnetic field will induce eddy currents perpendicular to those generated by the transmitter. These eddy currents induce a secondary magnetic field of a magnitude proportional to the ground conductivity, which is measured by the receiver coil. The instrument is calibrated so that the ratio of the primary to the secondary electromagnetic fields in

the quadrature phase (90° out of phase) is equal to the conductivity of the ground beneath

$$\left(\frac{Hs}{Hp}\right)_Q = \frac{i\omega\mu_o\sigma s^2}{4} \tag{3.4}$$

Where:
Hs – secondary magnetic field in quadrature phase
Hp – primary magnetic field in quadrature phase
i- $\sqrt{-1}$
μ_o – magnetic permeability of free space (4π E-7 Wb$*$ $A^{-1}*$ m^{-1})
ω – instrument frequency (Hz)
s- coil spacing (m)

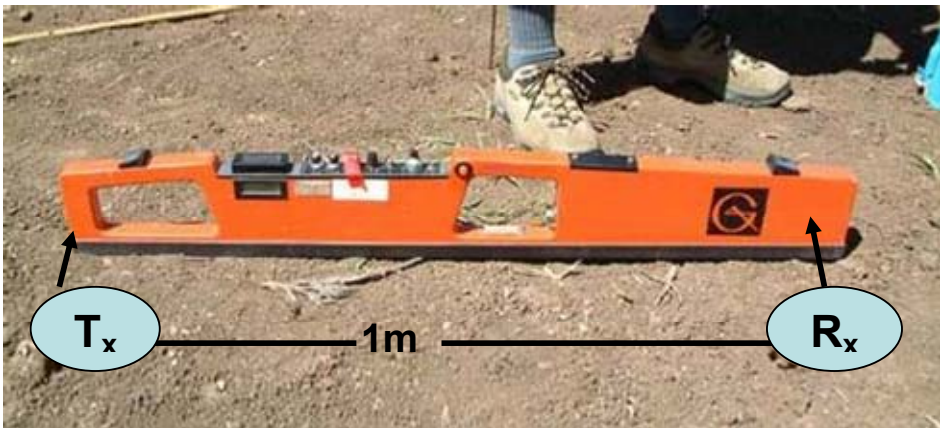

Figure 3.8. The Geonics EM 38 shown in the vertical mode of operation (dipoles are oriented vertically).

The instrument can be held with the dipoles in the vertical coplanar or horizontal coplanar orientation with respect to the ground surface. The change in dipole configuration results the instrument being more sensitive to deeper or shallower soil properties, respectively. According to the manufacturer, the depth of penetration (herein defined as the point representing 70% of the cumulative depth response, as defined by the sensitivity function or 1.5x the coil separation in the vertical dipole orientation or 0.75x the coil separation in the horizontal coil orientation) is 1.5 and 0.75 m for the vertical and horizontal dipole configurations, respectively when placed on the ground surface (Table 3-1). The peak of the sensitivity function (Figure 2.11) is the maximum value of the sensitivity function, which is above the soil surface when the instrument is held at any height above the

soil in the horizontal dipole configuration, and above 1.5 m in the vertical dipole configuration of the EM 31.

Table 3-1. Relationship between dipole orientation, coil spacing, shift in height and theoretical depth of investigation and peak sensitivity for different EM instruments used for this study. Negative values represent distance above soil surface. (McNeill, 1980b).

Instrument	Dipole orientation	Coil spacing	Instrument height	Depth of investigation	Peak sensitivity (depth)
		m			
EM 38	Vertical	1.00	0.0	1.50	0.40
EM 38	Horizontal	1.00	0.0	0.75	0.00
EM 31	Vertical	3.67	0.0	6.00	1.47
EM 31	Horizontal	3.67	0.0	3.00	0.00
EM 31	Vertical	3.67	1.0	5.00	0.10
EM 31	Horizontal	3.67	1.0	2.00	-1.00
EM 31	Vertical	3.67	1.5	4.50	-0.03
EM 31	Horizontal	3.67	1.5	1.50	-1.50
EM 34	Horizontal	10.00	0.0	7.50	0.00
EM 34	Horizontal	20.00	0.0	15.00	0.00

The EM 31 operates on the same principals as the EM 38 but at a lower frequency (9.8 kHz) and a longer coil separation of 3.6 m (Figure 3.9). According to the manufacturer, the depth of penetration is six metres in the vertical orientation and three metres in the horizontal orientation when laid on the ground surface. It has been shown that varying the height of electromagnetic instruments enables the user to change the depth of investigation, at a 1:1 ratio, giving the user the ability to construct conductivity profiles of the subsurface (Corwin and Rhoades, 1990; Cook and Walker, 1992a; Borchers et al., 1997). For this reason, measurements were taken with the EM 31 at 0, 1, and 1.5 m above the soil surface in both the horizontal and vertical coplanar coil configurations.

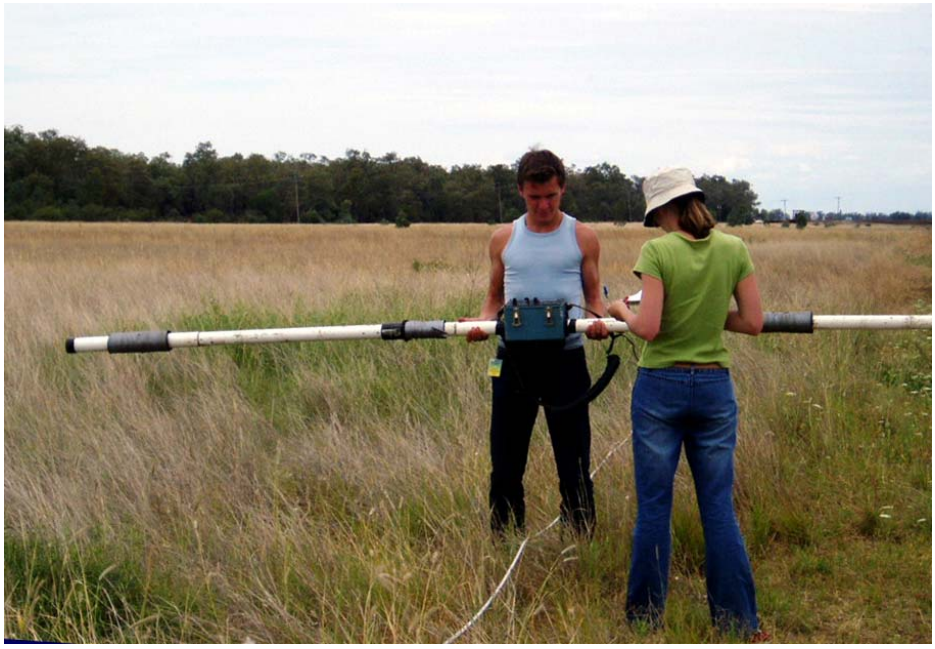

Figure 3.9. The Geonics EM 31 at 1 m above ground with dipoles vertically oriented during the survey the area of natural vegetation outside the paddock. The trees along the banks of Carroll Creek can be seen in the background.

Unlike the EM 38 and EM 31, the EM 34 uses coils which are connected to the power source via insulated cables and may be moved apart to increase the depth of penetration at specific spacings. The EM 34 operates at 6.4 kHz, 1.6 kHz or 0.4 kHz using coil spacings of 10, 20 and 40 m respectively. The instrument also has the ability to perform surveys in horizontal coplanar and vertical coaxial coil orientations; however, only the horizontal coplanar orientation at 10 and 20 m spacings were chosen due to the instrument's sensitivity to coil misalignment in the vertical orientation and the relatively shallow depth of interest. The sampled volume of the EM 34 (as well as the other EM instruments) is estimated as an isosceles triangle with base at the surface (Figure 3.10). Because the separation distance is great relative to the surveyed area, the point where the transmitter was located was referred to as the sampled location. This is slightly different than the other two instruments, where the centre of the instrument was located above the sampled location.

Figure 3.10. The Geonics EM 34 held in the horizontal coaxial dipole configuration, during the initial survey of the paddock. Shown below is a diagram of the instrument sampling depth of as a function of the separation distance (not to scale).

Six months after the initial survey a "control" plot was surveyed outside the irrigated paddock. This was intended to extend the image of the palæochannel for subsequent coring and monitoring of infiltration characteristics and to explore the differences in natural vegetation versus a managed plot of land. Transects were surveyed to straddle the palæochannel, assuming that it continued on the same trajectory as inside the paddock. Three transects in total were surveyed and a separate survey was performed using only the EM 31 at 1 m above ground. The 100 metre-long transects were surveyed using the NavMan GPS, with wooden pegs placed at end points. EM readings were taken every five metres using the same configurations as in the paddock (Table 3-1). Additionally, transects were surveyed inside the irrigation channel and along the edge of the natural vegetation closest to Carroll Creek (Figure 3.7).

3.4.2 Quad-bike mounted EM survey

Six months after the survey outside the irrigated paddock, the field site was resurveyed using a quad-bike-mounted EM 31. The quad-bike was equipped with an EM 31 mounted onto the back of the bike using a height-adjustable non-conductive stabiliser made of PVC tubing. The instrument was separated from the conductive bike by approximately 1.5 m (figure 3.11). Because the separation distance is much less than the skin depth of the instrument, it is expected that the conductivity of the bike will affect the conductivity readings of the instrument. Under the assumption that the bike's conductivity is a constant, the conductivity contribution from the bike was subtracted from the readings. This correction was performed by separating the instrument from the quad bike and taking several measurements at a location outside the study area.

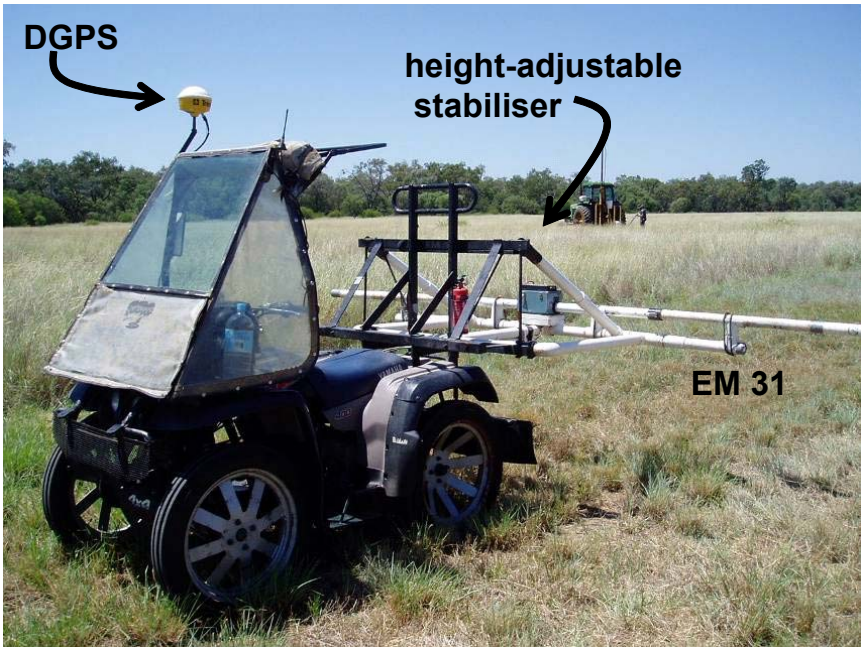

Figure 3.11. Quad-bike-mounted EM 31 used to survey the entire study area. The EM instrument (mounted with coil dipoles vertically-oriented) was linked to a differential GPS and a data logger for taking apparent electrical conductivity readings.

The bike travelled at 5 – 10 km hr^{-1} with EC readings recorded every five seconds giving a sampling interval of 6.5 – 13.5 m. The speed differed according to the terrain, resulting in a closer sampling interval for the outside area because the bike travelled slower to stabilise the instrument. A differential GPS unit was used to trace the path of the bike and record the elevation. In total, 2700 data points were recorded. To account for temporal variation in the EM readings due to changes in moisture content and ambient conditions from previous surveys and to calibrate the instruments to the original paddock survey, one transect from the paddock was resurveyed using all of the coil configurations used previously with the EM 31.

3.4.3 Ground-penetrating radar survey

Ground-penetrating radar is often used to identify contrasting soil properties, and is particularly informative when contrasts in volumetric water content exist in the profile. Several methods have been adapted to explore these properties with depth by controlling the separation distance between the transmitter and receiver coils (Greaves et al., 1996; Reppert et al., 2000). Common-midpoint surveys are analogous to seismic reflection surveys, where an increase in coil separation translates to a longer arrival time. The ratio of this increase directly translates to the velocity of the wave in the soil, which is directly related to the soil water content. In contrast, by maintaining the coil separation and traversing the field, the common-offset configuration results in time-referenced traces of reflected electromagnetic waves at various locations. The individual traces are combined to form a three-dimensional image of contrasts in the relative dielectric permittivity with time, which is related to depth using an assumed or measured dielectric constant. In this study, we used the two surveys to provide accurate representations of the contrasting subsurface properties, by using the velocity data derived from the common-midpoint survey to help predict the depth of reflection from the time-referenced traces in the common-offset survey.

3.4.3.1 Velocity sounding (common-midpoint)

During the first survey in July 2003, a Mala Geosciences ground-penetrating radar with 100 MHz and 50 MHz antennae was used to survey the transects previously described (Section 3.4.1). Velocity soundings were conducted at the start and midpoints of each transect to determine the velocity of the electromagnetic waves using both the 100 MHz and 50 MHz antennae. Whereas the lower frequency

antenna theoretically provided better penetration depth, the higher frequency should detect smaller discontinuities in the subsoil. During the velocity sounding survey, the antennae were separated by 25 cm increments to the maximum distance of 4.5 m. Sixteen soundings were carried out at each spacing and were subsequently stacked in order to reduce the signal-to-noise ratio (Nakashima et al., 2001). The images were processed using *Groundvision*, a software package from MALA Geosciences. Several filters and signal amplification procedures were used reveal reflections in the data. The fist of these was a high pass filter used to remove the low-frequency, high amplitude air waves, which commonly overwhelm traces where small reflections are thought to exist. Secondly, automatic gain control was used to boost the amplitude of reflections at depth which were weakened due to signal attenuation. Finally, filters to remove background direct current noise were used to reduce the high frequency noise, which was amplified due to the automatic gain control.

3.4.3.2 Velocity profiling (common-offset)

Following the velocity sounding, transects were surveyed using a common offset configuration, where a one metre separation was used for the 100 MHz antennae and two metres for 50 MHz antennae (Figure 3.12). Surveys were carried out using a "hip-chain" device where a string is pulled from a spool whose angular velocity is calibrated to distance prior to the start of the survey. The sampling interval was set to send pulses at 5 or 30 cm along each transect using the 100 and 50 MHz antennae, respectively. Each trace was composed of 16 stackedsoundings which were sampled 512 times over a 1 160 nS window. Several transects were re-surveyed using a much slower process where 64 scans were stacked to produce a single scan. The same signal processing techniques were used as the common-midpoint survey data.

Figure 3.12. Self-contained ground-penetrating radar survey using the 50 MHz antennae in the common-offset orientation (two metre separation). The antennae were held at a constant height above the ground by attaching them to the backpack, which also held the harness-mounted laptop computer. The computer was used to adjust the survey parameters and view the raw data during collection.

Chapter 4

Measured and inferred physical and chemical properties of the field site

4 Measured and inferred physical and chemical properties of the field site

4.1 Soil and regolith characteristics

Soil physical and chemical attributes form the backbone of many hydrological investigations. Some soil properties can predict the pathways of flow (Kennett-Smith et al., 1994; van Overmeeren, 1994; Sophocleous and Perkins, 2000), others indicate the effect of water flow (such as the migration and enrichment of solutes in the soil profile) (Johnston, 1987; Allison et al., 1990; Slavich and Yang, 1990; Willis et al., 1997; Joshi and Maule, 2000; Scanlon, 2000). In this study, the soil data are used to quantitatively verify the geophysical model results, thereby increasing the "uniqueness" of the geophysical measurements (Doolittle et al., 1994; Hubbard and Rubin, 2000). The soil properties additionally help define the conceptual model for future groundwater modelling (Middlemis et al., 2001) and provide hydraulic property inputs through the use of pedotransfer functions (Schaap and Leij, 1998; Wosten et al., 2001; Minasny et al., 2004).

In this chapter, the term *palæochannel* is used for the area in the field in which the presence of such a feature was hypothesised from the aerial photograph. *Topsoil* is used as a term to refer to the top 1.5 m of the regolith, and properties are reported as the mean of all measurements within this increment, unless otherwise stated.

4.1.1 Pedology and stratigraphy

Because the study site has been managed for furrow irrigation, much of the upper 0.5 m of the soil was likely mixed during laser levelling. Despite this disturbance, the soil and deep cores revealed a complex stratigraphy in most areas of the study site. Two selected profile descriptions are given in (Table 4-1), with a complete list of profile descriptions in Appendix 4.2. Stratigraphic layers have been lumped based on the chemical and physical analysis of 0.5 m increment cores coupled with field observations. The numerous layers indicate that the soil has developed on a highly variable alluvial system resulting in the presence of both geomorphic and pedogenic features (Table 4-1, Figure 4.1).

Table 4-1. Profile descriptions for two deep cores outside the palæochannel (Well 1) and inside the palæochannel (Well 2). Because samples were analysed at 0.5 m intervals, EC and pH measurements are averaged over the thickness of the identified horizon. A complete list of profile descriptions can be found in Appendix 4.2.

	Depth	Description	$EC_{1:5}$	pH
	m		$\mu S\ cm^{-1}$	
Well 1	0.0 - 0.3	very dark grayish brown (10YR 3/2) **clay**	446	8.6
	0.3 - 3.0	dark grayish brown (10YR 4/2) **clay** with common $CaCO_3$ nodules	363	8.6
	3.0 - 5.0	yellowish brown (10YR 5/4) **clay** with $CaCO_3$ nodules and coarse Mn nodules	438	8.5
	5.0 - 6.3	light brownish gray (10YR 6/2) **clay**	337	8.3
	6.3 - 9.0	light yellowish brown (10YR 6/4) **clay loam** with common coarse subangular gravel	209	8.1
	9.0 - 9.3	strong brown (7.5 YR 5/6) **sandy loam** with common coarse subangular **gravel**	165	7.6
Well 2	0.0 - 1.0	dark brown (7.5YR 3/4) **clay**	225	8.3
	1.0 - 2.0	dark yellowish brown (10YR 4/4) **clay loam**	245	8.6
	2.0 - 4.2	dark yellowish brown (10YR 4/6) **loam** with common thin **gravel lenses** at 3.3m and grading to coarse sand at 4.0 m	123	8.0
	4.2 - 6.2	dark brown (7.5 YR 4/4) **loamy coarse sand** to **sandy loam,** common, thick **coarse sand stringers,** few thin **clay lenses** increasing with depth	84	7.8
	6.2 - 7.0	grey (2.5Y 6/1) **clay loam** with common **coarse gravel**	81	7.2
	7.0 - 8.0	light brownish gray (2.5Y 6/2) **clay** with common browish yellow (10YR 6/6) inclusions and common **fine gravel**	89	6.8
	8.0 - 8.3	pale brown (10YR 6/3) **clay loam** with common **coarse gravel**	114	6.7
	8.3 - 9.3	strong brown (7.5YR 5/8) **sandy loam** with common medium to coarse angular **gravel**	71	7.0

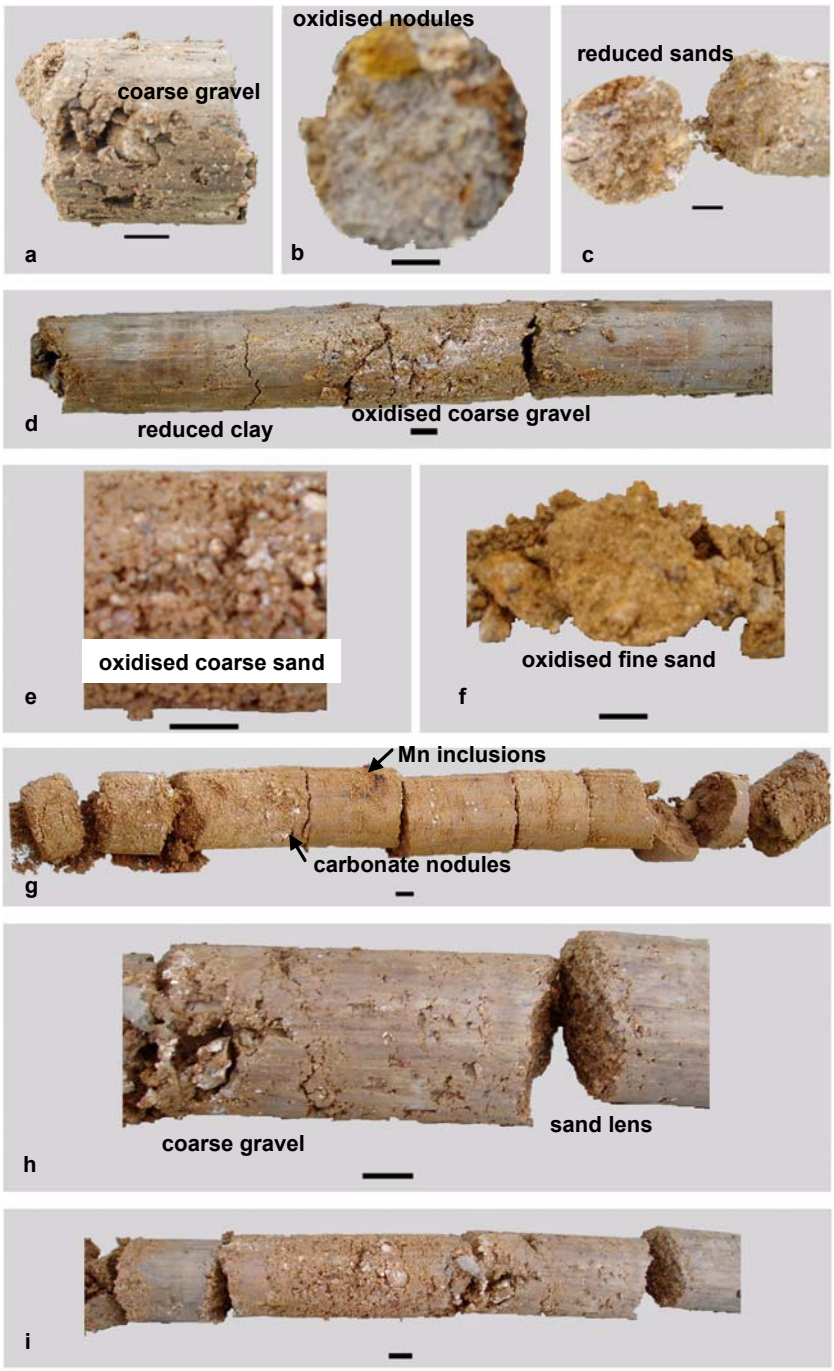

Figure 4.1. Subsections of cores from Well 2 (inside the palæochannel). Beneath the channel (a,b,c,d) a reduced layer of clay exists, which contains several deposits of coarse angular gravel and nodules of oxidised material. The top of the palæochannel (e,f,g) shows highly-oxidised fine and coarse sand with manganese inclusions and small carbonate nodules. The thick gravel deposit below the clay (h,i) contains significant amounts of sub-angular to sub-rounded gravel, similar in appearance to the thick deposit of gravel found below.

Geomorphic features occur throughout the palæochannel deposit in the form of gravel pockets, sand stringers, and clay lenses (Figure 4.1). The deposits vary in thickness from one to five cm (fine-textured bands less than one cm were termed "lamellae"). In general, the sand stringers and clay lenses are well-sorted, unlike the bulk of the palæochannel deposit which is highly mixed. The exception is the coarse sand and gravel deposit in Well 2, between 2 and 4.2 m, which is relatively well-sorted (Table 4-1). In general, soil textures inside and below the palæochannel range from sandy loam to gravely coarse sandy clay, while outside the palæochannel, textures are predominantly clay (Appendix 4.2). Also evident is a much higher EC and higher pH in the soil samples outside the palæochannel and above 2 m (Table 4-1).

Although the topsoil overlying the palæochannels contains appreciably less clay, many fine-scale variations exist throughout the channel due to the channel stratigraphy (such as the inclusion of clay lenses and sand stringers) (Figure 4.1, Table 4-2). In the main deposit, clay content ranges from 0.06 to 0.39 g g^{-1} and increases along the length of the palæochannel deposit from Well 2 (with an average of 0.23 g g^{-1}) towards Carroll Creek in Well 12 (0.34 g g^{-1}). The most dramatic change occurs in the 50 m stretch between Well 8 (0.25 g g^{-1}) and Well 5 (0.31 g g^{-1}).

Compared to the surrounding heavy clays, there is significantly less clay inside the palæochannel ($p < 0.001$) (Table 4-2, Figure 4.2), and significantly more fine and coarse sand ($p < 0.001$). However, there is no significant difference in the silt sized fraction ($p = 0.192$). Under magnification, the coarse sands found in the base of the palæochannel appeared subrounded to subangular. Through x-ray diffraction (Appendix 4.3) and by examining the cleavage planes of the minerals, it appears that these sands are mostly comprised of quartz and plagioclase feldspars, with minor inclusions of opaque minerals and orthoclase feldspar (less than 5%).

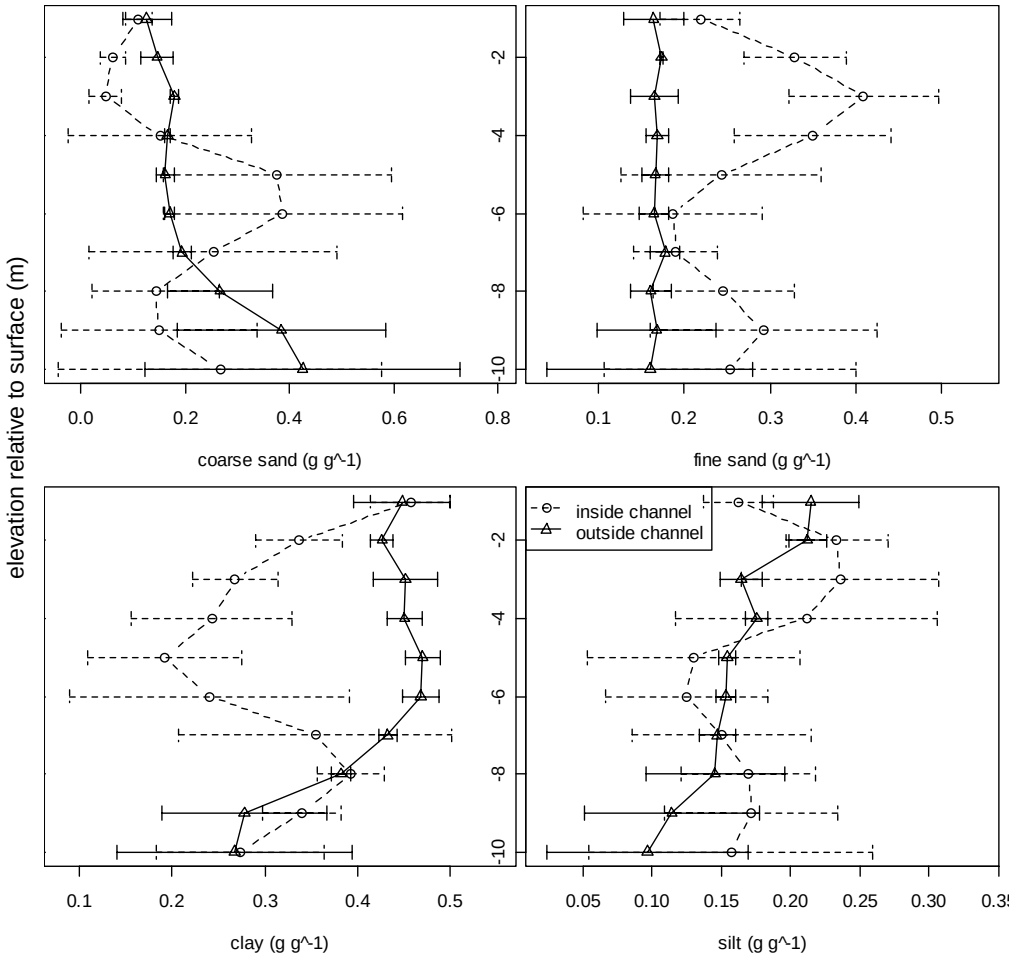

Figure 4.2. Coarse sand, fine sand, clay and silt distribution with depth. Error bars indicate one standard deviation from the mean value of all points inside or outside of the palæochannel.

A one to two metre-thick deposit of fine sand conformably overlies the coarse sand in the channel and also extends several metres to either side (Figure 4.3). The shape of the sand grains varies from subangular to angular. Inside and above the palæochannel, the fine sand component is coated with iron oxides, unlike the grains found outside the palæochannel, which appear to be relatively free of these coatings.

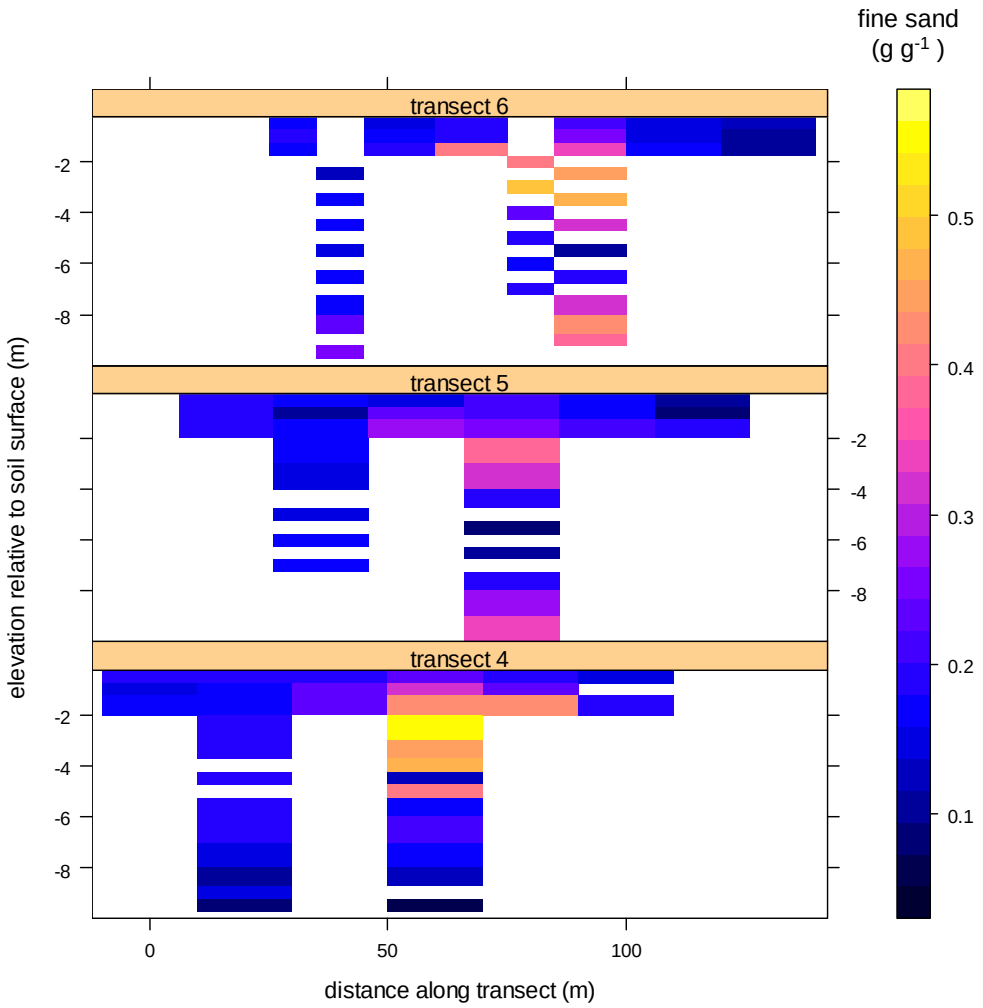

Figure 4.3. Fine sand content along Transects 4, 5, and 6. Deep cores inside the palæochannel (50 – 80 metres along the transects) show a two metre-thick deposit of mostly fine sand. This layer extends away from the channel and is likely part of an associated levee deposit.

Gravel deposits sporadically appear below six metres in most wells, and are well-mixed with the surrounding matrix. Well-sorted gravel appears in the main palæochannel deposit and also decreases in frequency to the northeast. A coarse gravel deposit underlies much of the site approximately nine metres below the surface (Figure 4.1, Table 4-1). This gravel is thought to form the top of the Narrabri formation, an unconfined aquifer which extends through much of the Gwydir and Namoi Valleys (Young et al., 2002; Vervoort and Annen, 2006). The 20 m cores taken outside the paddock show that this deposit is about seven metres thick and rests on top of heavy clays. Similar to the palæochannel deposits, the Narrabri Formation

consists of medium to coarse subangular to subrounded gravel which is capped by a (fining upwards) mixture of fine and coarse sands.

Pedogenic features appear throughout the profiles and are mostly comprised of calcium (and possibly sodium) carbonates and, to a lesser extent, gypsum nodules. These features are assumed to be pedogenic, due to their dull white colour and crumbly texture (van Grinsven et al., 1988). In most profiles, the nodules appear below one metre and do not appear to be correlated with the presence of the palæochannel.

A reduced clay layer exists beneath the palæochannel, which contains coarse gravel (Figure 4.1a) and oxidised nodules (Figure 4.1b). A similar deposit occurs in several wells outside of the channel at five to six metres (i.e. Well 1 (Table 4-1)), but the deposit is not as reduced and lacks the oxidised nodules found below the channel. Similar to most sands found outside the palæochannel, the fine sand found in this deposit lacks iron oxide coatings.

Although the upper 0.5 m of the topsoil has been significantly disturbed during laser levelling, the topsoils found in this site would likely be classified as Black Vertosols or Red Vertosols (above the palæochannel) under natural conditions. The soil appears to be self mulching, with moderate to firm subangular blocky structure throughout the solum. Shrink-swell characteristics are also evident with large cracks developing in the dried profile (including the soil above the palæochannel).

The average topsoil clay content ranges from 0.27 to 0.58 g g^{-1} and is significantly lower above the palæochannel (Figure 4.4, Table 4-2). The same trend is found in the silt fraction of the particle size distribution. Both size fractions are inversely related to fine sand, however, there is no significant difference in the coarse sand fraction at any depth (Table 4-2). It was assumed that the area nearest the stream would contain coarser-textured topsoil sediments (due to sediment transport during overbank conditions), however there is no significant difference in the amount of clay or sand content inside and outside of the paddock (Table 4-2).

Table 4-2. Mean and standard deviations of the particle size distribution data. Statistical comparisons made between properties within separated rows, where * p < 0.05, **p < 0.01, ***p < 0.001, using the one-tailed t-test.

			Clay		Silt		F.Sand		C.Sand	
			ave	std	ave	std	ave	std	ave	std
			g g^{-1}							
Inside Paddock	Regolith	Inside PC	0.23***	0.14	0.14	0.01	0.28	0.14	0.28	0.04
		Outside PC	0.41	0.09	0.15	0.01	0.17***	0.04	0.23	0.04
	Topsoil	Inside PC	0.41***	0.07	0.17***	0.06	0.29	0.07	0.10	0.04
		Outside PC	0.47	0.06	0.21	0.06	0.20***	0.06	0.09	0.04
		Total	0.45	0.06	0.19*	0.03	0.21	0.07	0.09	0.04
Outside Paddock	Topsoil	Total	0.46	0.06	0.21	0.04	0.23	0.07	0.08	0.03

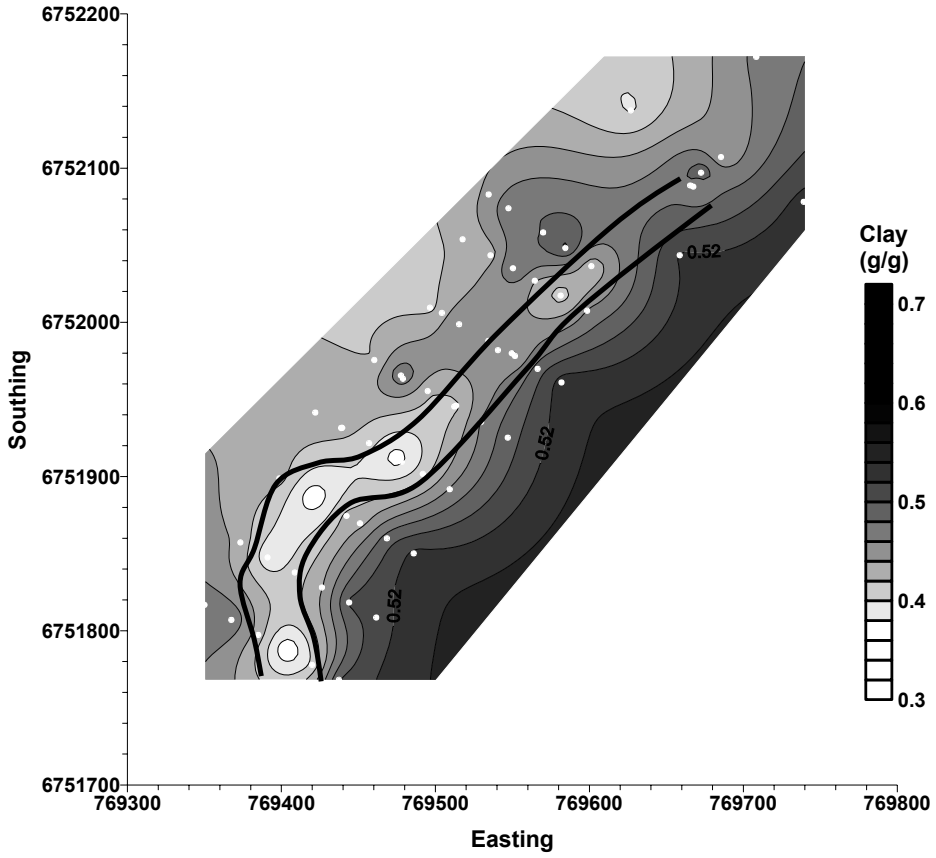

Figure 4.4. Average clay content for topsoil samples (< 1.5 m). Sampled locations denoted with diamonds. Clay contents within the channel (outlined in white) were significantly less than outside the channel (p < 0.001).

4.1.2 Bulk density measurements and predictions

Throughout the regolith, the bulk density ranges from 1.09 to 1.72 g cm^3. The mean of the palæochannel deposit, 1.48 g cm^{-3}, is similar (but significantly less than) measurements made outside the palæochannel which average 1.54 g cm^{-3}. However, the majority of the coarse sand deposits in the palæochannel have bulk densities ranging from 1.10 to 1.51 g cm^{-3}.

Because of the various sampling techniques, bulk density could not be estimated for the topsoil sediments and the 20 m core samples. Therefore, the 42 bulk density measurements from the split spoon cores were used as a training set to predict bulk density from the clay, silt, fine sand, coarse sand, and gravel from the other 206 samples. An artificial neural network was developed to do this using JMP 5.1 (SAS Institute, 2003). The model consisted of four hidden units to describe the five parameters following Minasny and McBratney (2002). The iterative model used a convergence criterion of 0.0001 within a maximum of 100 iterations an overfit penalty of 0.001. The number of nodes was chosen to allow for model convergence and provide the best prediction (as denoted by the minimum root mean squared error from the residuals).

The bulk density measurements made from the split-spoon cores are consistent with the coarseness of material, showing significant correlations with clay and sand (r^2 = 0.30, 0.26). When compared to measured values the model provides a good fit for bulk density, with an r^2 value of 0.92 ranging from 0.7 g cm^{-3} in the coarse gravel deposits to 1.9 g cm^{-3} in the heavy clay samples (Figure 4.5). The plotted residuals have a mean of zero and appear normally distributed (Figure 4.5). Like the measured bulk density, the predicted bulk density is significantly lower inside the palæochannel, as would be expected from the coarse-textured material in the channel (Figure 4.6). These predictions will enable the use of a 5 parameter model for our saturated conductivity predictions using pedotransfer functions, following the SINFERS approach (McBratney et al., 2002).

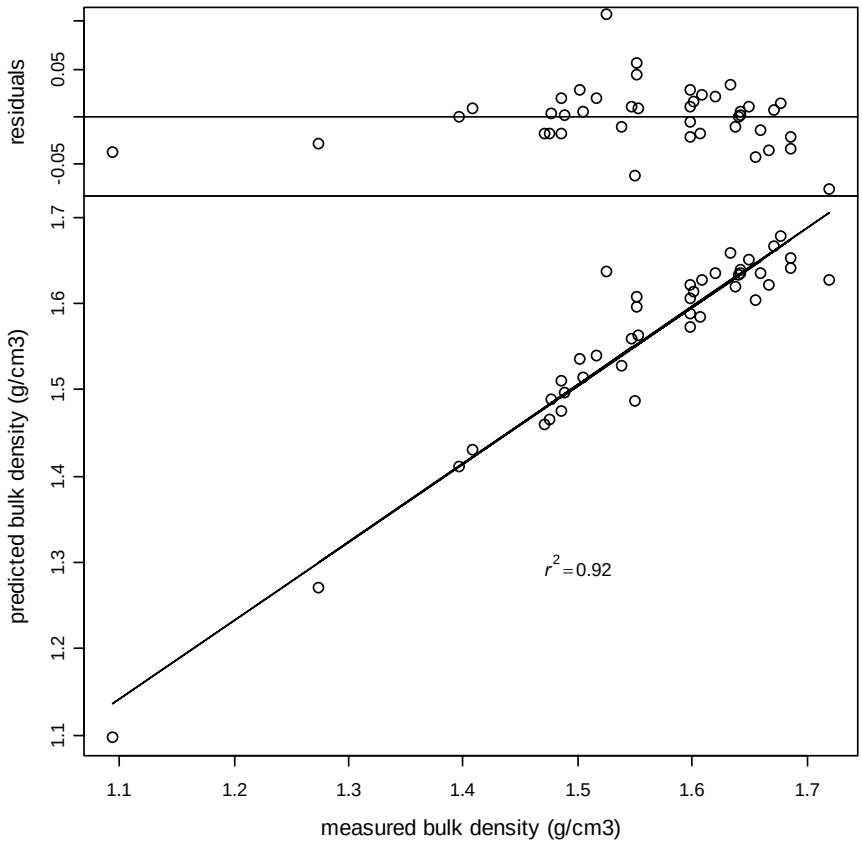

Figure 4.5. Bulk density measurements plotted against those predicted from artificial neural networks based on clay, silt, fine sand, coarse sand and gravel content. The plot shows a strong correlation with the measured properties ($r^2 = 0.92$, n = 42, $\alpha = 0.95$, $p < 0.001$) with intercept and slope not significantly different from 0 and 1. Above, the residuals (measured – predicted) are plotted showing the mean (0) with points symmetrically scattered about the 0 line indicating a lack of systematic error in the model.

4.1.3 $EC_{1:5}$ in deionised water

To compare the $EC_{1:5}$ measurements to previous studies and to provide a better comparison to the EM data, $EC_{1:5}$ in water was converted to EC_e using a model developed by Slavich and Petterson (1993b) for rapid salinity assessment of Australian soils. Their empirical model, which was based on a least squares multiple linear regression of EC_e, $EC_{1:5}$, and saturation percentage θ_{SP} appears in the form:

$$EC_e = \left(2.46 + \frac{3.03}{\theta_{SP}} \right) EC_{1:5} \qquad (4.1)$$

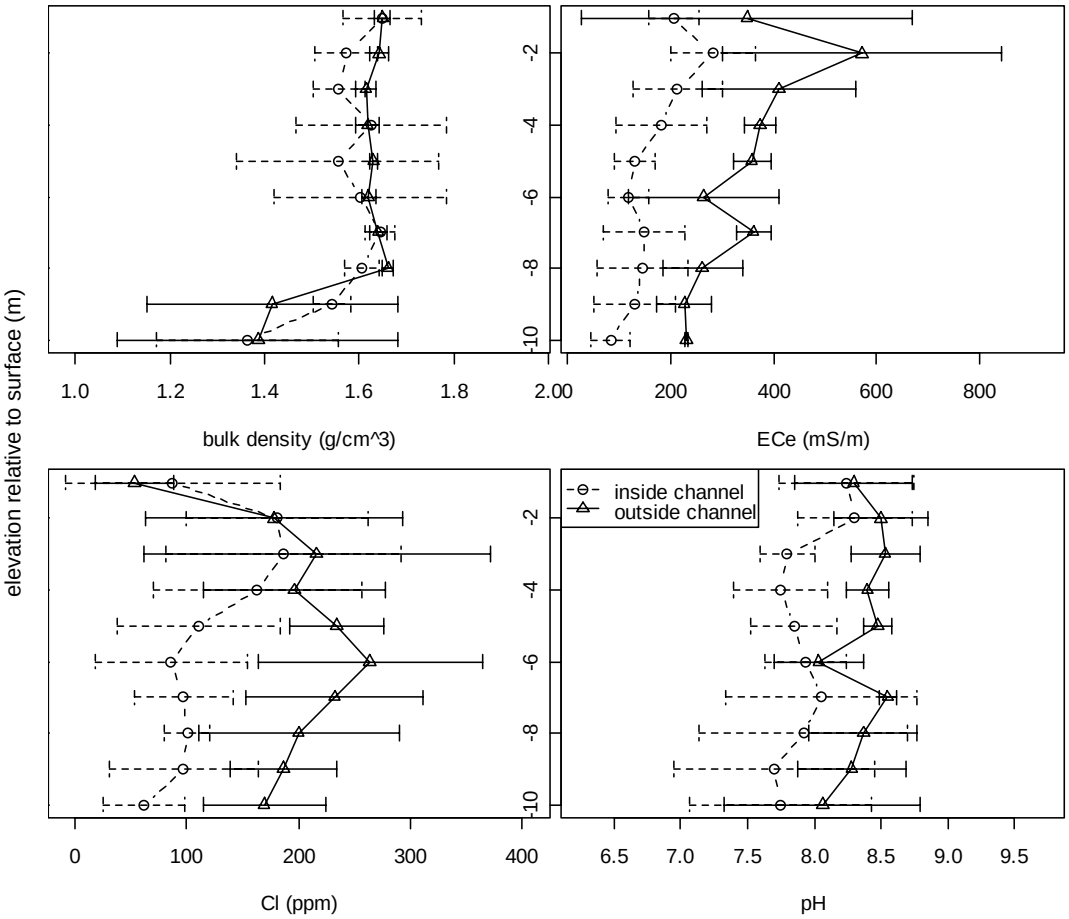

Figure 4.6. Average bulk density, electrical conductivity (EC_e), chloride content, and pH of samples inside and outside the palæochannel. Error bars represent 1 standard deviation from the mean. The mean measurements are significantly lower in the channel from a two tailed pair-wise student t-test (assuming unequal variances, with $p < 0.001$).

The model uses Northcote's (1979) table of soil texture classes to categorize groups of soil based on their texture grade, and hence their saturation percentage. (Northcote, 1979). The majority of the error in the model is due to the conversion from soil texture to saturation percentage (Slavich and Petterson, 1993b). This makes the model diverge in coarser-textured sediments, so care should be taken when considering the palæochannel sediments.

The field samples show clear changes in electrical conductivity across the topsoil and with depth. The topsoil samples above the palæochannel are significantly less conductive than the rest of the topsoil samples (Figure 4.6, Table 4-3). There is also a general increase in the topsoil electrical conductivity to the northwest (down slope) of the palæochannel. For example, all of the highest 14 values of EC_e occur in the topsoil down slope of the palæochannel. Compared to the area of natural vegetation, the topsoil samples inside the paddock are significantly more conductive than those outside ($p < 0.001$) (Table 4-3). In the deep cores, the sediments inside the channel were significantly less conductive than those outside the channels (Table 4-3).

Table 4-3. Electrical conductivity (EC_e), chloride and pH for selected portions of the field site. Statistical comparisons made between properties within separated rows, where * p < 0.05, **p < 0.01, ***p < 0.001, using the one-tailed t-test.

			EC_e		Cl		pH	
			ave	std	ave	std	ave	std
			— mS m^{-1} —		—— ppm ——			
Inside Paddock	Regolith	Inside PC	164.0***	85.8	117.0***	88.7	7.75***	0.06
		Outside PC	316.8	99.3	215.0	78.7	8.40	0.07
	Topsoil	Inside PC	212.4**	110.3	73.4	101.7	8.25***	0.44
		Outside PC	289.6	175.6	80.6	66.7	8.43	0.36
		Total	276.2	71.1	79.4	73.5	8.40	0.38
Outside Paddock	Topsoil	Total	116.4***	168.4	91.3	74.7	8.28	0.63

4.1.4 Chloride

The topsoil chloride content is the most variable soil property on the site having the highest coefficient of variation (91). The coefficient of variation is calculated as:

$$CV(\%) = \frac{\sigma}{\bar{x}} \times 100 \qquad (4.2)$$

where: σ = standard deviation
and $\bar{x}$ = sample mean.

Unlike other soil properties, the chloride content is not significantly different in the topsoil overlying the palæochannel compared to the rest of the paddock ($p = 0.532$) or inside versus outside the paddock ($p = 0.529$) (Table 4-3, Figure 4.6). However, there appears to be a general trend associated with the palæochannel, where topsoil chloride content increases on the tail drain side of the field (Figure 4.7). In the deep cores, there is significantly less chloride inside the palæochannel, compared to outside the channel (Figure 4.6, Table 4-3).

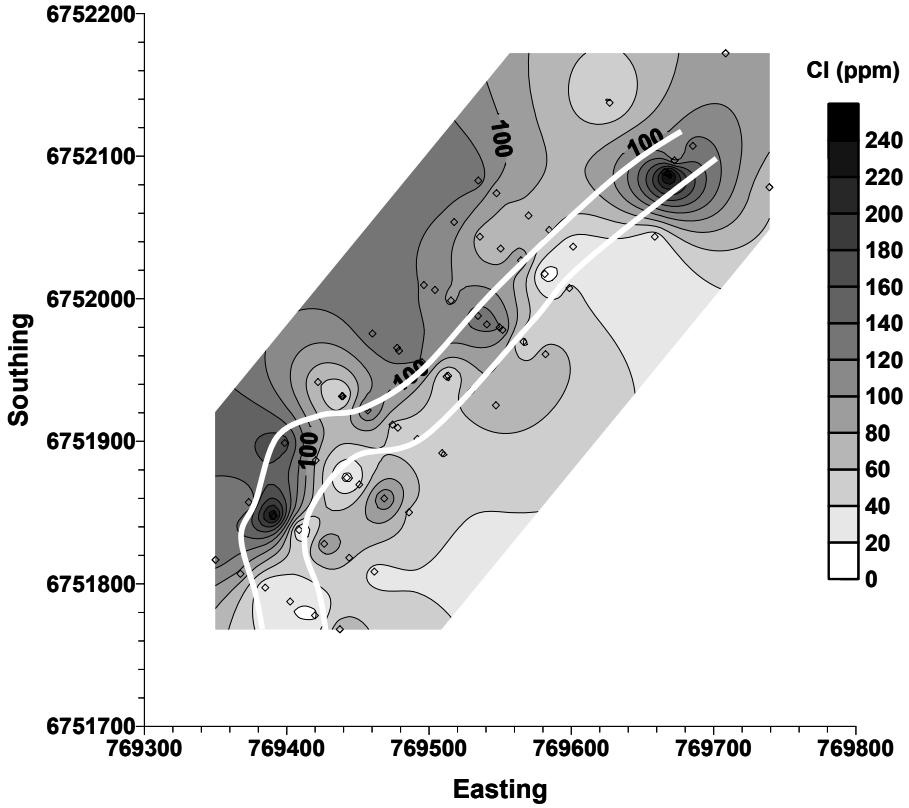

Figure 4.7. Topsoil chloride content associated with the palæochannel (outlined in white). Although there is no significant difference associated with the structure, there is a general increase in chloride content north-east of the structure, which also coincides with the direction of irrigation water flow.

4.1.5 Soil and regolith pH

The topsoil pH ranges from 7.2 to 9.2, with significantly lower values associated with the soil overlying and within the palæochannel (Table 4-3). There is

no significant difference between the sediments inside and outside the paddock. Several values are above the solubility product of calcium carbonate (8.4), which could indicate the presence of sodium bicarbonate due to excess sodium in the profile. The majority of these high pH readings occur from 1 to 1.5 m below the soil surface, coinciding with the presence of calcium carbonate nodules.

4.1.6 Hydraulic property predictions using two different pedotransfer functions

The pedotransfer function software packages Neurotheta and Rosetta both estimate saturated conductivity (K_{sat}) from particle size distribution and bulk density using artificial neural networks. As such, small differences in model predictions occur with each model simulation. Both software packages report the average, $\bar{x}$, and standard deviation, σ, of the results for 50 simulations for each predicted point. The standard deviation is reported in terms of the log of the saturated hydraulic conductivity, shown as:

$$\sigma = \sqrt{\frac{1}{N}(\log 10(x_i) - \log 10(\bar{x})} \tag{4.3}$$

Both models gave reasonable mean predictions of K_{sat} and predicted significantly higher K_{sat} inside the channel compared to outside the channel ($p < 0.001$) (Figure 4.8). Predicted K_{sat} range from 2.7 to 670 cm day^{-1} for the Neurotheta model and from 2.0 to 430 cm day^{-1} in Rosetta. Comparing the inputs from the measured soil properties (Figure 4.9) to those used for the training data in each model (Figure 3.6), it appears that the data more closely resemble the training data used for the Neurotheta program. However, the Rosetta model produced estimates which were closer to the mean within each prediction (Table 4-4), which is likely due to the larger training set used for Rosetta. Both of these models will be compared with the majority of the output in later models, with emphasis placed on the Neurotheta model which was developed using data from soils in Australia.

Table 4-4. Model predictions from Neurotheta and Rosetta pedotransfer function software packages. Column one compares the average CV from the model predictions between the models which are significantly less in Rosetta (p = 0.002).

	Individual predictions	Field		Inside PC	Outside PC
Method	Mean CV	CV	Mean logKsat		
					cm day-1
Neurotheta	33.4a	53.0	1.02	1.31a	0.83b
Rosetta	28.2b	66.3	0.87	1.18a	0.67b

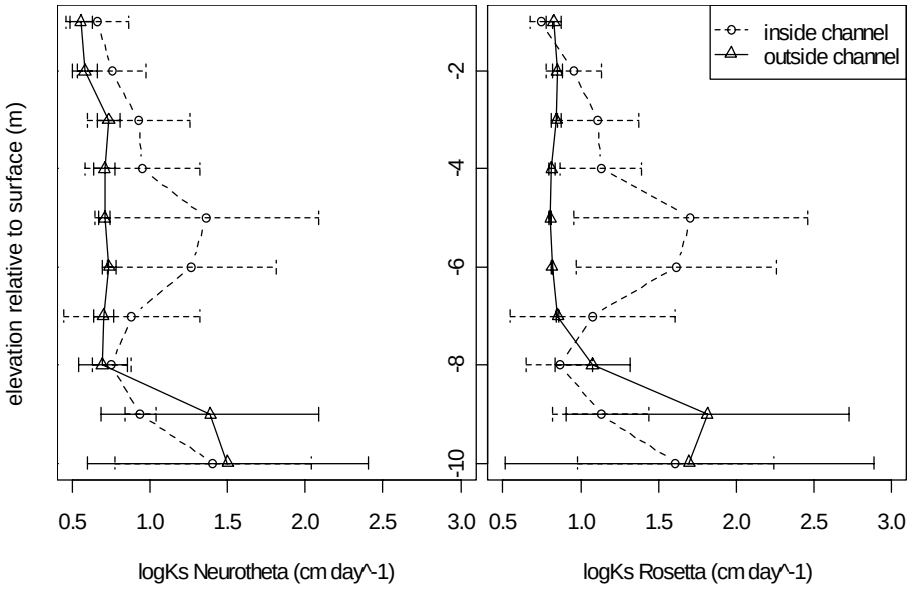

Figure 4.8. Comparison of K_{sat} distribution with depth in the wells inside and outside the palæochannel using both pedotransfer function programs, Neurotheta and Rosetta. Means from the wells are plotted with error bars representing one standard deviation from the mean.

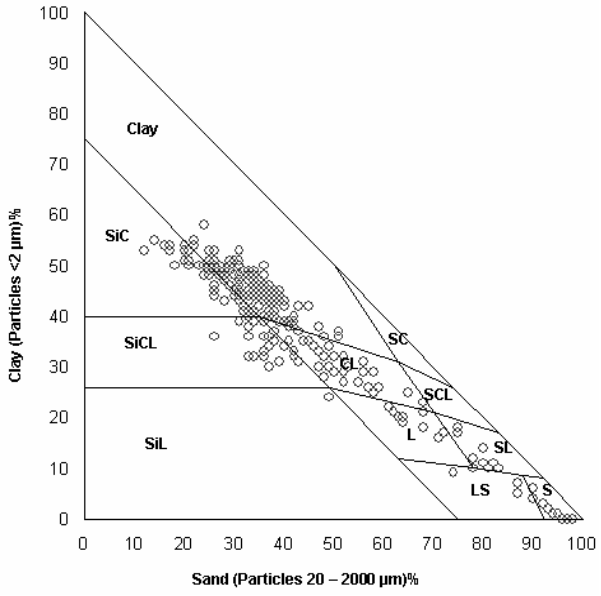

Figure 4.9. Particle size distribution from all samples plotted on the textural triangle. Figure 3.6 provides a comparison to the data sets for both Neurotheta and Rosetta.

4.1.6.1 Sample clustering

Due to the complex stratigraphy within the palaeochannel, demarcations of stratigraphic layers were not straight-forward in many cases (Table 4.1). Given the large differences in soil physical properties over the study site, it was hypothesised that the presence of the palæochannel and associated deposits would dictate the spatial structure of the soil physical properties. Clustering the samples based on particle size distribution data should objectively reflect the visual palæochannel pattern observed in the aerial photographs. Such clusters can later be used for assigning hydrological properties for modelling purposes and for determining various soil management zones (Triantafilis et al., 2001d). Because of the number of samples and their spatial outlay, the data were partitioned based on the K-means of clay, silt, fine sand, coarse sand, and gravel.

The program FuzME was used to perform the classification using hard classes (using a fuzzy exponent of 1) (Boydell and McBratney, 2002). In order to circumvent biases based on sample ordering, the program initially generates random classes of the data based on soil properties. The chosen number of clusters was based on the local

minimisation of Wilks' Λ, a property which relates the differences within classes to the differences between classes (Wilks, 1932).

The value Λ varies from 0 to 1, with 0 suggesting class means differ (and the attributes differentiate the classes more), and 1 suggesting all class means are the same. A plot of Wilks Λ with the number of classes indicated that there were 4 distinct classes, producing a local minimum of 0.21. However, because one of the classes only contained one sample, three clusters were chosen, generating a similar Wilkes Λ of 0.26. Physically, this agrees with observations made by Stannard and Kelly (1977) who noted the presence of three distinct depositional units in the upper ten metres of the regolith, which were the background soil, the palæochannel, and the associated levee deposits from the palæochannel.

The data clusters clearly revealed the arrangement of the sediment deposits. A visual representation of the clusters in relation to the palæochannel sediments (Figure 4.10, Figure 4.1) indicates that cluster 3 is biased towards the heavy clay background soil, cluster 2 contains mostly coarse sand and gravel deposits associated with the bottom of the palæochannel and the lower Narrabri Formation (which is only reached in 2 of the 6 wells) and cluster 1 is dominated by fine sand, and occurs throughout most of the palæochannel deposit, as well as on either side of the banks (Table 4-5).

Table 4-5. Soil cluster means, derived from K-means clustering of particle size analysis. In general, cluster 1 is dominated by gravel, cluster 2 by fine sand, and cluster 3 by clay content. In this study, cluster 3 is considered the background soil.

Cluster	Count	Clay	Silt	Gravel	F.sand	C.sand
				$g\ g^{-1}$		
1	56	0.32	0.20	0.35	0.09	0.00
2	28	0.10	0.05	0.09	0.70	0.35
3	156	0.46	0.20	0.19	0.11	0.00

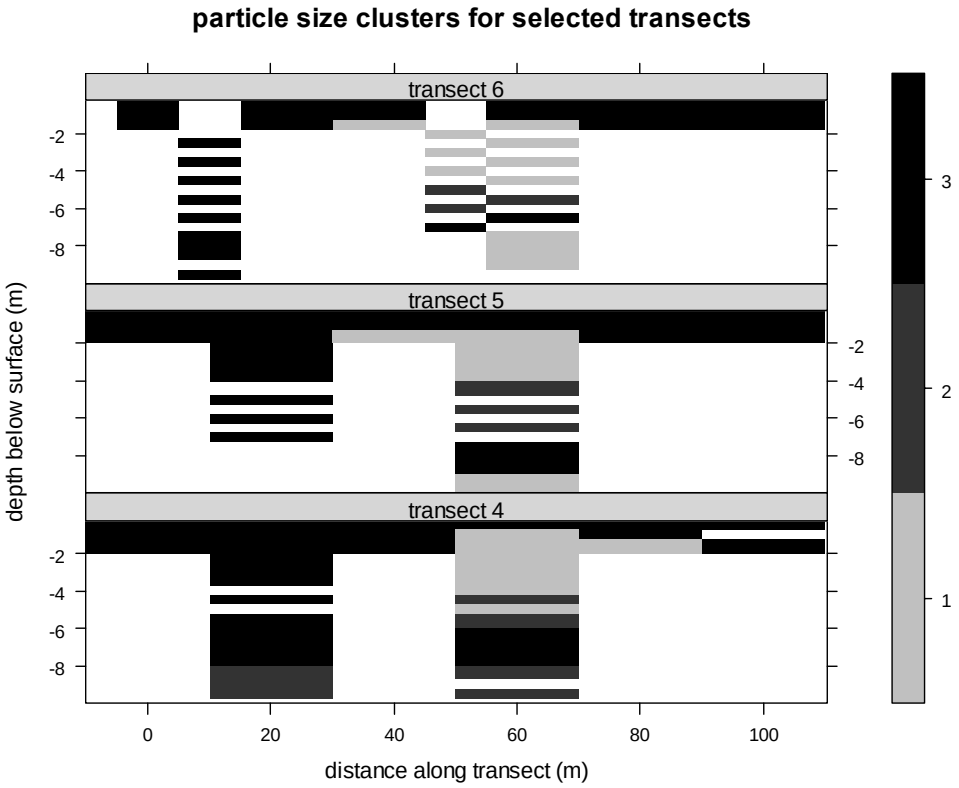

Figure 4.10. Particle size clusters shown for three transects inside the paddock. Cluster 3 corresponds to heavy clays, cluster 2 is coarse sands with gravels, and cluster 1 is fine sands. The figure shows the distinct delineation of the palæochannel sediments, which encompass clusters 2 (for the bedload sediments) and cluster 1 for the fine sand deposited on top (and possible levees on both sides of the channel).

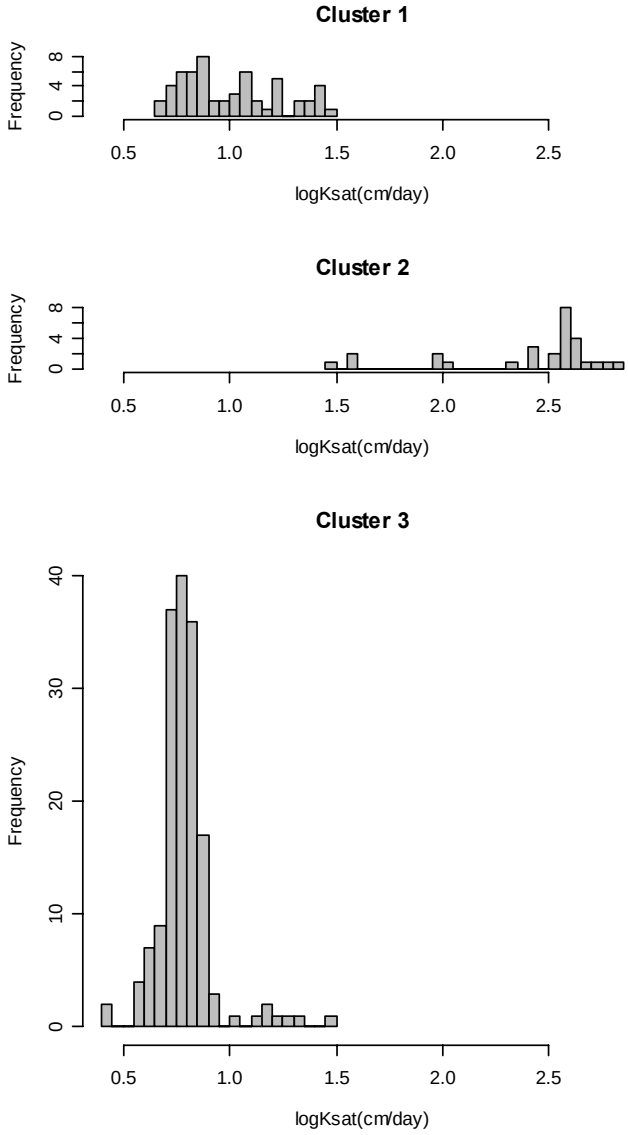

Figure 4.11. K_{sat} distributions for clusters generated by particle size analysis. Cluster 1 is mostly comprised of fine sands and occupies the area on top and to the sides of the palæochannel, and the top of the Narrabri Formation. Cluster 2 is the palæochannel bedload sediments and the bulk of the Narrabri formation, and is heavily left-skewed. Cluster 3, is the spatially-dominant class because it encompasses the surrounding heavy clays and is also right skewed.

Cluster 3 is the spatially-dominant cluster, which will hereafter be referred to as the "background soil". This cluster has a mean K_{sat} (derived from Neurotheta, and defined as $10^{mean(\log(Ksat))}$) of 6.5 cm day^{-1} and is normally distributed about the range of 2.6 to 31.1 cm day^{-1} (Figure 4.11). Cluster 2 is a left skewed distribution, which has a mean of 326.0 cm day^{-1} and ranges from 31.2 to 698.7 cm day^{-1}. Cluster 1 is also normally distributed about the mean (11.6 cm day^{-1}) and ranges from 4.5 to 28.9 cm day^{-1}. These clusters will later be used for determining the reference K_{sat} for the entire soil, and for each of the separate deposits, to determine the distribution of this property around the study site.

4.2 Soil and groundwater measurements

Topsoil moisture measurements were made at various times of the year with each EM survey. During the first survey (July 2003) measurements were made across Transect 5 after a 3.2 mm rainstorm the previous day. The measurements show a general decrease in volumetric moisture down the soil profile (Figure 4.12). During this period, the topsoil overlying the palæochannel deposits was significantly drier ($p = 0.02$) than the topsoil in the rest of Transect 5. During the quadbike EM survey in December, 2003 average topsoil moisture content inside the paddock (0.24 g g^{-1}) was higher than outside the paddock (0.15 g g^{-1}). Finally, topsoil measurements taken in September 2004 revealed a much lower soil moisture content inside the palæochannel (0.15 g g^{-1}) compared to the rest of the paddock (0.19 g g^{-1}). During this time, the average moisture content outside the paddock (0.16 g g^{-1}) was also significantly less than inside the paddock (0.19 g g^{-1}).

Measurements from the deeper profiles were taken in May, 2005. The results show a significant variation in subsoil moisture content, associated with the various deposits, with the palæochannel sediments being significantly drier than the surrounding clay ($p = 0.01$). Unlike others studies performed nearby (Vervoort and Annen, 2006), there was no indication of perched water within or above the palæochannel deposit during any of the soil coring inside the paddock.

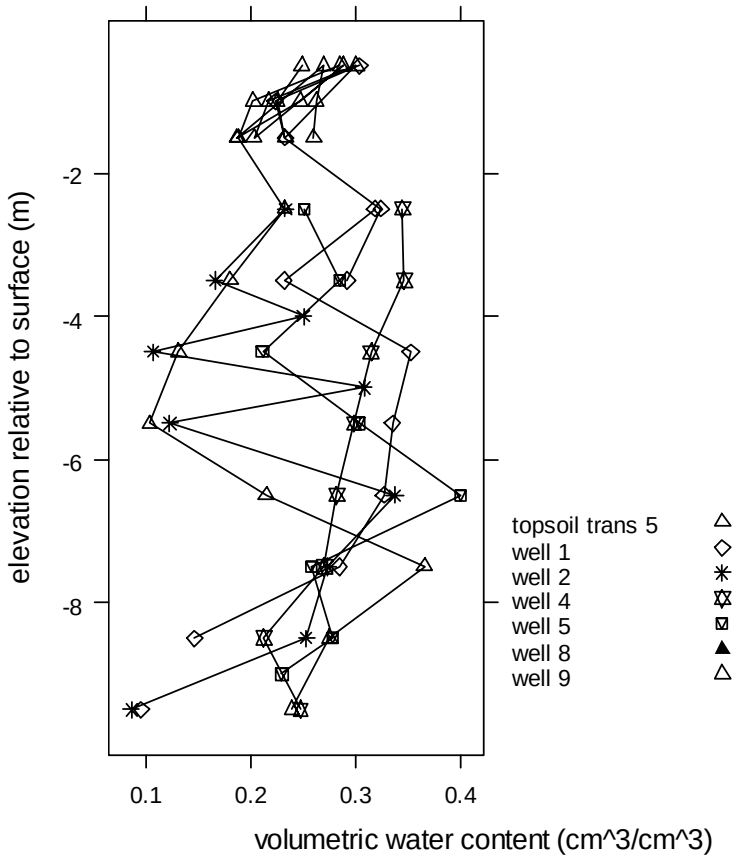

Figure 4.12. Volumetric soil water content from sampled sites at different times. Topsoil samples were taken during the first survey, and those below were sampled at the same time of the year, 2 years later.

Water table monitoring inside and below the palæochannel indicated that perched water tables were forming in both deposits and were associated with irrigation events. Several periods of missing and corrupted data existed throughout the monitoring period. The gaps in the data and the noise resulted from several different sources:

- During field operations, boxes had to be removed from the junction boxes. On several occations, the boxes were removed for extended periods due to delays in field operations, which were often difficult to predict due to climatic influence and the remoteness of the location. This was rectified by making the boxes asier to remove, so that field personal could remove

the boxes before operations. But, because of the requirement to reprogram the data logger, a researcher is still required to visit the site to reinstall the equipment.

- Instruments malfunctioned when several flooding events resulted in the junction boxes filling with water and sediment. This resulted in shorting the connection and corroding the connectors. This was rectified by replacing the original copper-alloy connectors with water-tight 14-pin gold-plated marine connectors.
- The high frequency sampling (15 minute interval) of raw data (rather than averaged) resulted in noisy, high resolution data. While this data was could have been filtered using a moving average, there was unnecessary resolution in the data. The sampling interval was subsequently shorted to 1 hour intervals for the piezometers.

Do to these circumstances only Wells 2, 3, and 4 gave a relatively clear picture of the local hydrology (Figure 4.13) and the flood events were not recorded on any of the instruments. Wells 5 and 6 produced similar results over a shorter period of time (Figure 4.14). During the measured period, 13 responses were recorded by the pressure transducers located within and below the palæochannel (Figure 4.13). The hydrological response to the events was almost immediate, with large pulses of water raising the water table up to 1.5 m over a few hours. The water table recession was different between wells, which is attributed to the K_{sat} of the surrounding sediments. For example, in the palæochannel deposit, water levels quickly fell over the course of a couple hours. However, below the channel the water table fell much slower, taking several days to reach the level prior to the event. Outside the palæochannel, there were two major responses to irrigation events (Figure 4.13). The recession from the first pulse appears to be similar to the well below the palæochannel (Figure 4.13).

Slug tests were performed on each of the wells using a 10 litre slug of water. Due to the low water table in several of the wells, only the data from Well 5 and Well 6 could be used to predict the subsurface K_{sat}, using the Hvorslev method (Hvorslev, 1951), which assumes the well fully penetrates the groundwater table. Using this method, the K_{sat} in the palæochannel deposit was estimated at 4.98 cm day^{-1} (Well 6)

while the sediment below had a much lower hydraulic conductivity of 0.55 cm day^{-1} (Well 5) (Table 4-6).

Table 4-6. Comparisons of various methods for estimating the saturated hydraulic conductivity for the six piezometers in the paddock. The pedotransfer function methods predict significantly higher K_{sat} values than the other measurements, although in some cases only one measurement was possible.

Method		Well 1	2	3	4	5	6
		K_{sat} (cm day^{-1})					
slug test	10 l slug	0.4				0.6	5.0
	GW recession		0.1	4.3	0.1	0.2	0.5
ptf	NT	97.7	38.0	123.0	6.8	11.0	22.4
	Rosetta	24.0	12.1	91.2	4.9	8.5	12.8

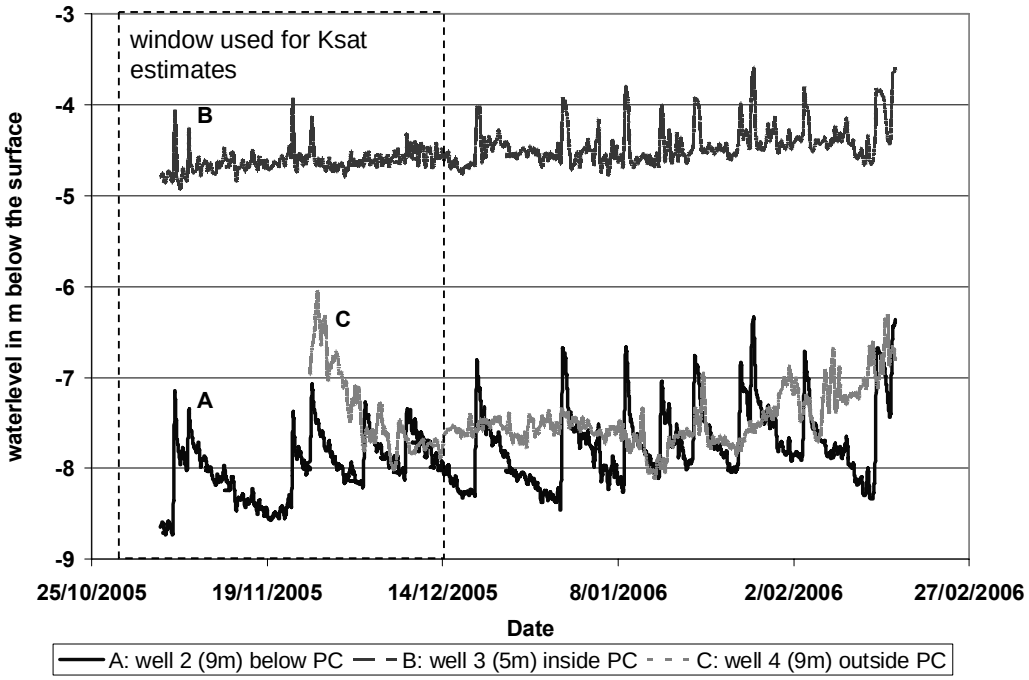

Figure 4.13. Groundwater data for Wells 2(A), 3(B), and 4(C). Over the course of the irrigation season, the water table rose 14 times in Wells 2 and 3.

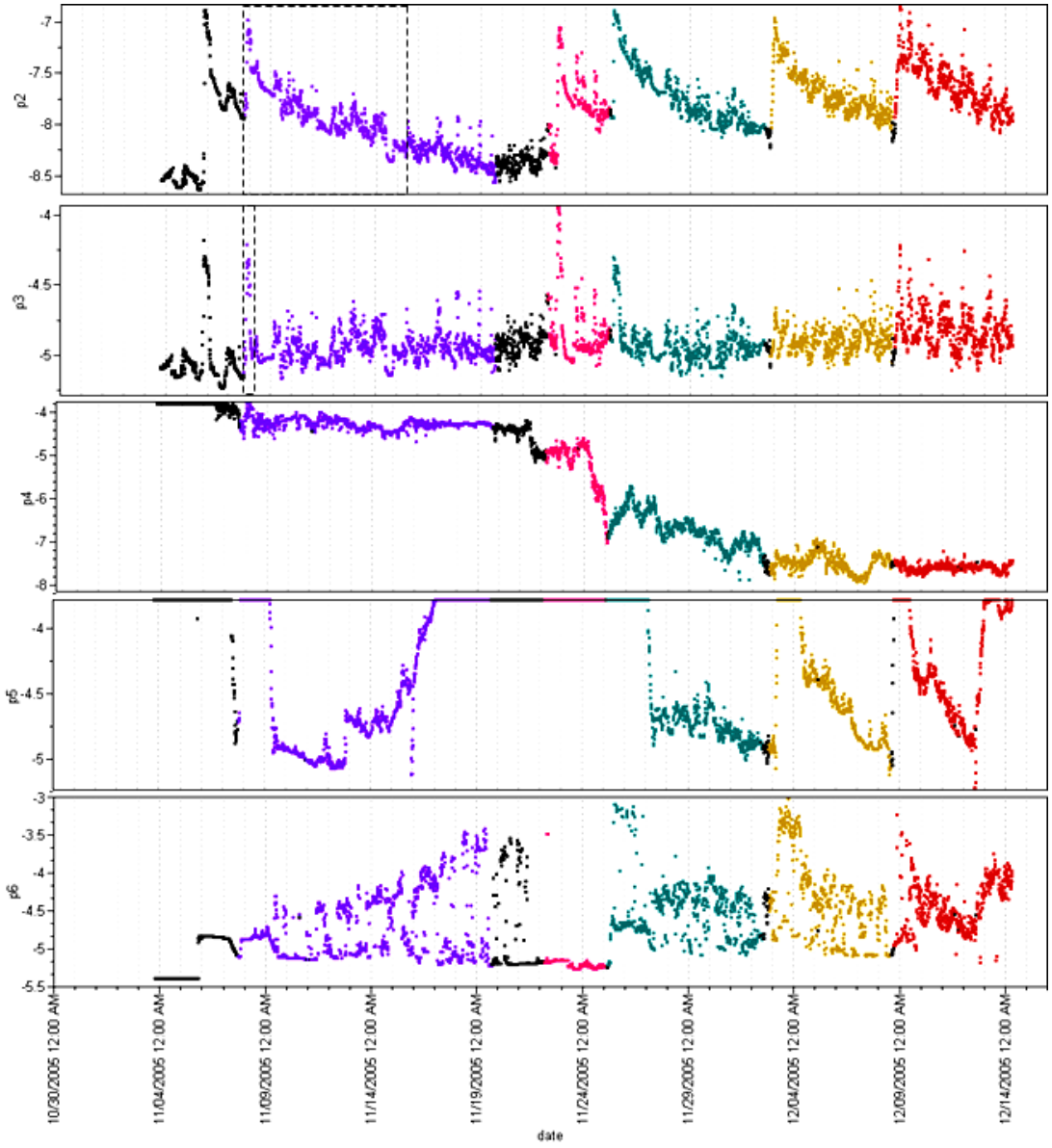

Figure 4.14. Raw groundwater data for six piezometers inside the paddock over the course of a month. Irrigation events are coloured, showing the immediate groundwater response during most of the events. Shaded areas in Well 2 and 3 (p2 and p3) indicate data used for recession curves (Figure 4.15). Well 5 (p5), fluctuated past the five metre range of the pressure transducer and was truncated. Levels are reported as elevation relative to soil surface.

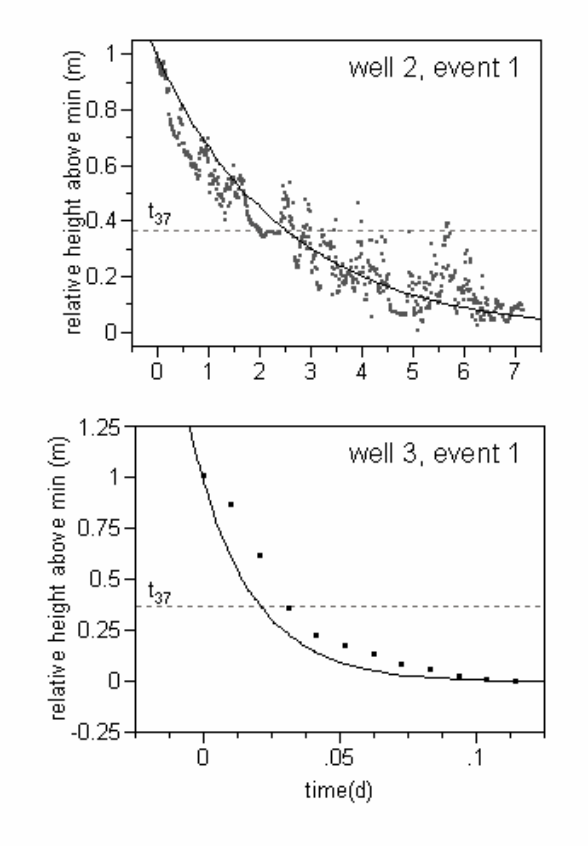

Figure 4.15. Recession curves from two piezometers during event 1 (data range in Figure 4.14) which was used to estimate the saturated hydraulic conductivity from long term monitoring using the Hvorslev slug test approach, which is based on the time it takes the well to return to 37% of the initial level. This is identified using a log linear fit of the data, which is constrained to an intercept of 0.

The recession leg of the groundwater hydrographs (Figure 4.14) was also used to estimate K_{sat} of the surrounding sediment (Figure 4.15). This was based on the assumption that the recharge from the irrigation water pulse occurred nearly instantaneously and did not contribute to the water table after the initial pulse. From these measurements the average estimated hydraulic conductivity of the sediments below the palæochannel was 0.09 cm day^{-1} with a coefficient of variation of 55 from the six events used for the prediction (Table 4-7). The piezometers located outside the palæochannel predicted a similar K_{sat} of 0.04 cm day^{-1}, but only one event was available to make this prediction. Inside the palæochannel a much higher saturated conductivity of 4.34 cm day^{-1} was predicted. This prediction varied from 3.67 to 7.42 cm day^{-1} from the four events used, with a CV of 23. Throughout the irrigation

season, the water table slowly rose by approximately 0.25 m month^{-1} in the deep wells below and outside the palæochannel (Figure 4.13). This was not the case inside the palæochannel, where the periodic water table rises receded within 24 hours.

Table 4-7. Derived saturated hydraulic conductivity values for available piezometers using the water table recession method. Similar to the pedotransfer functions, several orders of magnitude exist between the palæochannel and underlying sediments, however the predictions are much smaller than those based on the model predictions.

Location	Event							
Well	1	2	3	4	5	6	ave.	stdev
	K_{sat} (cm day^{-1})							
2	0.67	0.04	0.16	0.06	0.07	0.06	0.09	0.05
3	7.42	5.51	5.00	3.67			4.34	0.94
4			0.04				0.04	
5					0.15	0.18	0.17	0.02
6					0.55		0.55	

4.3 Geophysical investigation

Ground penetrating radar and frequency-domain electromagnetic induction were used to predict the distribution of soil properties across the study area. Both instruments use electromagnetic waves to predict the electromagnetic velocity and electrical conductivity of the soil with depth, which relate to soil physical properties such as particle size distribution, bulk density, and water content (Section 2.5.1, 2.5.2).

4.3.1 Electromagnetic induction surveys

The surveys of the area included several types of electromagnetic induction instruments. Hand-held instruments were useful for determining the changes in electrical conductivity with depth by changing the height of the instrument, while the survey area was extended and the resolution increased by using a quad-bike mounted unit.

4.3.1.1 Hand-held EM survey

The hand-held instruments delineated the palæochannel on all transects inside the paddock. The distribution of apparent electrical conductivity values for all of the hand-held surveys show three clusters of electrical conductivity for mostof the configurations (Figure 4.16). This likely reflects the soil property clusters described earlier (Section 4.1.6.1). Overall, the EM 31 in the vertical dipole configuration gave the highest reading, followed by the same instrument in the horizontal configuration. This is consistent with Figure 4.5 which shows a maximum electrical conductivity (from $EC_{1:5}$ measurements) around 3 metres below the surface. The instrument depth response functions (Equations 2.19, 2.20) coupled with the depth of penetration using the various dipole configurations (Table 3-1) shows that the maximum sensitivity for the instruments occurs at this depth. The EM 31 held above the soil surface gave the lowest EC_a readings, due to the amount of non-conductive air between the instrument and the soil surface (Figure 4.16).

A localised low in electrical conductivity occurs above the palæochannel in most of the transects apart from Transect 8 (Figure 4.17). The higher sample density in Transects 1 and 2 (1 m spacing for EM 38 and 5 m spacing for EM 31) improved the resolution of the image of the palæochannel. However, compared to Transect 7 (which was taken at ten metre spacing and did not include EM 38 measurements), it appears that the improvement was not that substantial.

In Transect 6, the contrast between the palæochannel and the surrounding sediments is not as distinct as in the other transects (Figure 4.17), although the mean (95.0 mS m^{-1}) falls within the confidence limits of the entire paddock (95.6 +/- 1.4 mS m^{-1}). Cores taken along Transect 6 (Wells 4, 5, 6, and 7) indicate that the palæochannel deposit contained much more clay than in Well 3 (0.31 versus 0.23 g g^{-1}). It is likely that this would reduce water flow through the channel due to a reduced saturated conductivity and this is shown in the groundwater recession curves, which predict a much higher K_{sat} in Well 3 than in Well 6 (Table 4-6).

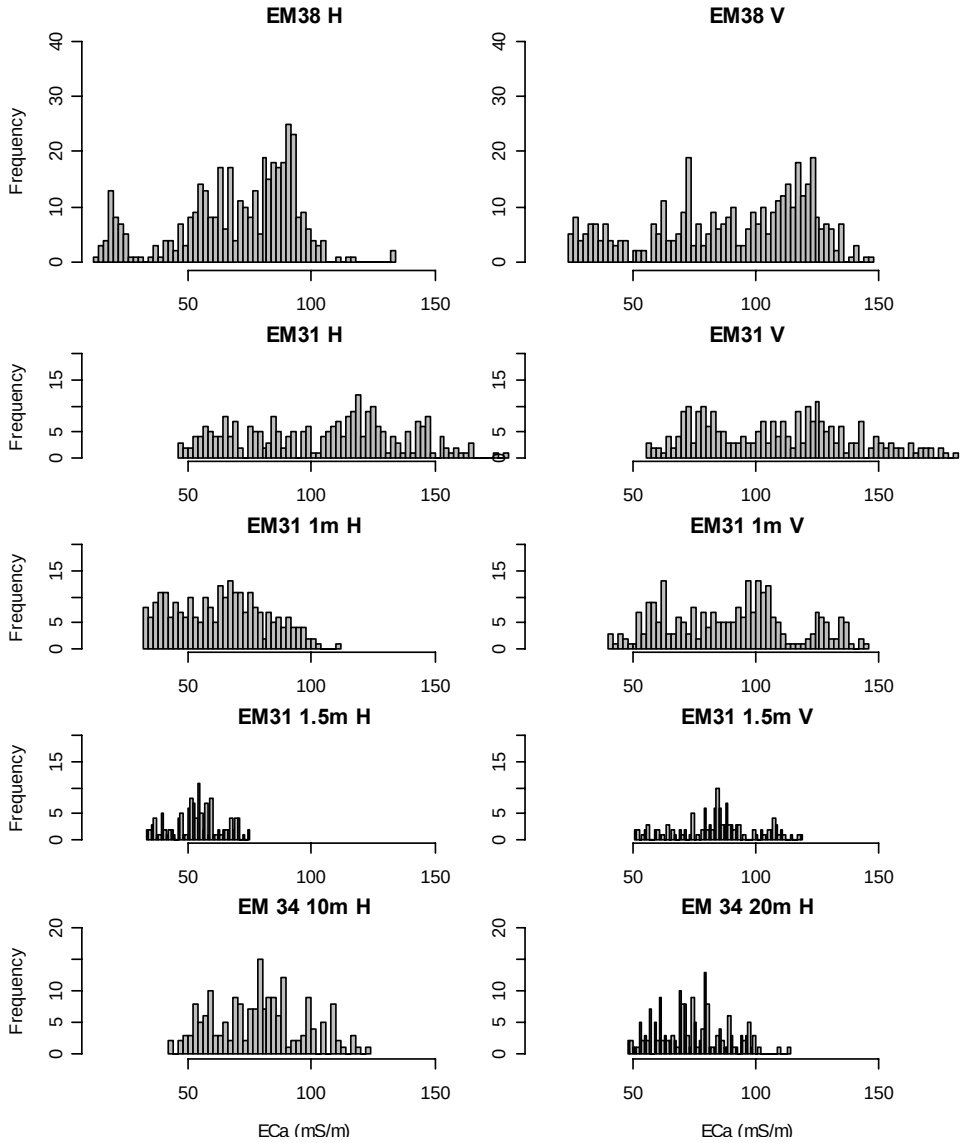

Figure 4.16. Histograms of EM data from all of the hand-held instruments. The majority of the plots show a trimodal distribution in conductivity values, similar to the soil property clusters discussed earlier in the chapter.

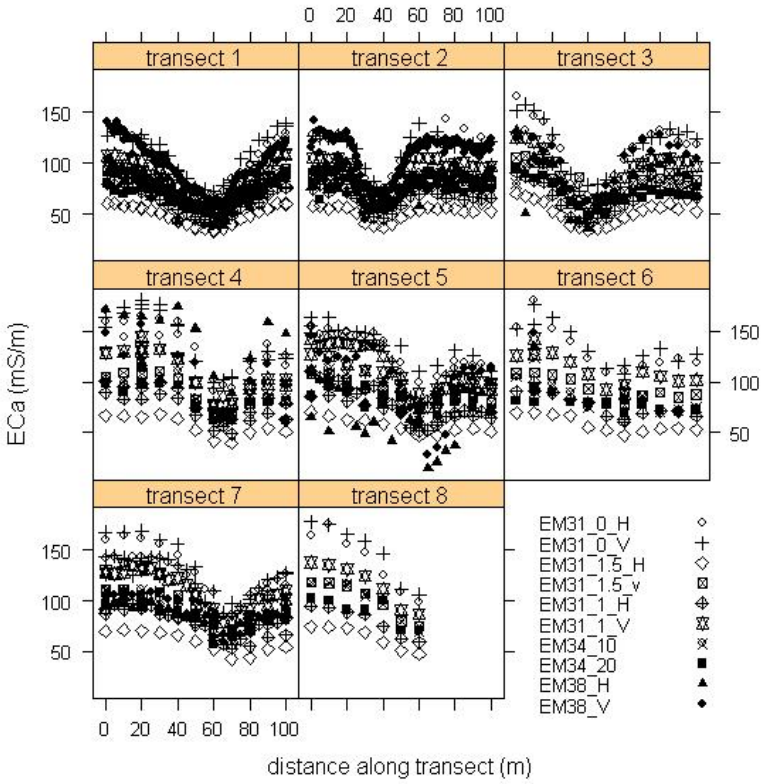

Figure 4.17. EM transects from inside the paddock showing all available instrument and dipole configurations over all the sampling intervals. Apart from Transect 8 (which did not entirely cross the channel) all transects clearly delineate the palæochannel feature.

In the area of natural vegetation, the apparent electrical conductivity (EC_a) was significantly lower than inside the paddock ($p < 0.001$) (Figure 4.18) with conductivities ranging from 13 to 134 mS cm^{-1}, and a mean conductivity of 61 mS cm^{-1} compared to a range of 15 to 180 and a mean of 90 mS cm^{-1}. This is also reflected in the laboratory EC_e measurements (Table 4-2).

Although there were anecdotal indications that the palæochannel extended into the natural vegetation area (such as isolated patches of greener vegetation), it was not clear from the aerial photographs whether the channel continued on the same trajectory as in the field (Figure 3.3). The three EM transects located in this area did not show the same large fluctuations as inside the paddock (Figure 4.18). For this reason, it was difficult to determine if the palæochannel was underneath (although the palæochannel presence was confirmed during deep drilling). The only exception is

the small decline in EC_a in line with the palæochannel trajectory using the EM 31 in the vertical dipole configuration (Figure 4.18, Transect 11). Interestingly, Transect 9 shows a localised high in EC_a, associated with the palaeochannel. This was also associated with localised vigorous plant growth. Coupled with the groundwater data, this points to the likelihood that the palæochannel was responsible for transporting water from the nearby irrigation channel, increasing subsurface soil moisture, and resulting in high readings in Transect 9.

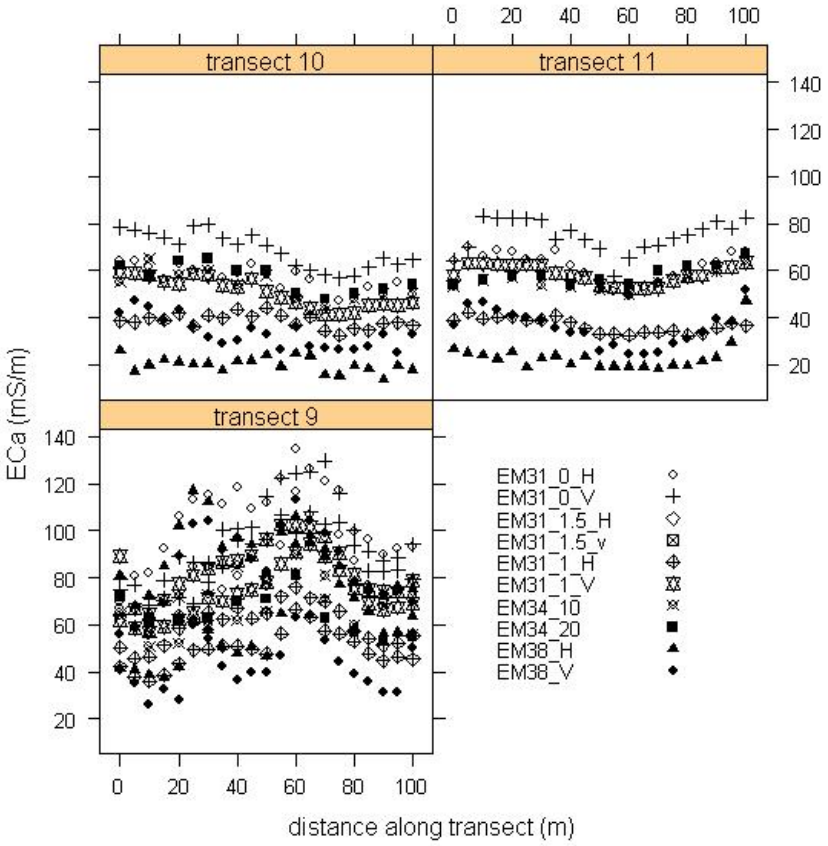

Figure 4.18. Transects from the area of natural vegetation. In general, the palæochannel was not well defined by most of the EM instruments, apart from the EM 31 in the vertical dipole configuration.

4.3.1.1.1 Transient responses

During the two years of this study, five EM surveys were conducted (Table 4-8). Several transects were repeatedly measured to determine if a transformation was needed to incorporate new data to the existing grid, and to identify whether the timing of an EM survey would significantly affect model predictions, as EM measurements are used quantitatively. The first expedition was separated into two surveys (1 and 2) to identify the effects of a single 3.2 mm rainstorm (Table 4-8). Although soil moisture was not measured during Survey 1, there was a significant fluctuation in the instrument response between the surveys (Figure 4.19, Table 4-9). However, contrary to the predicted rise in EC_a following the event, the shallow measuring instruments all recorded a decrease in electrical conductivity, while the deeper-penetrating instruments did not respond to this event (Figure 4.19).

Table 4-8. Rain and evapotranspiration measurements for the days leading up to the sampling date. Volumetric soil moisture (θ_v) is the average gravimetrically determined topsoil measurement multiplied by the average predicted bulk density.

		7 days		5 days		3 days		1 day		
Date	Survey	P	ET	P	ET	P	ET	P	ET	θ_v
		mm								cm^3/cm^3
8/7/03	1	15.8	14.0	0.0	10.0	0.0	6.2	0.0	1.4	-
9/7/03	2	3.6	13.8	3.2	10.0	3.2	5.8	3.2	2.2	0.24
2/12/03	3	0.0	75.2	0.0	53.2	0.0	32.4	0.0	11.2	0.37
24/5/04	4	0.2	28.4	0.0	19.0	0.0	10.2	0.0	3.6	0.25
11/7/05	5	5.4	17.0	5.4	12.8	5.4	8.4	0.0	3.2	0.21

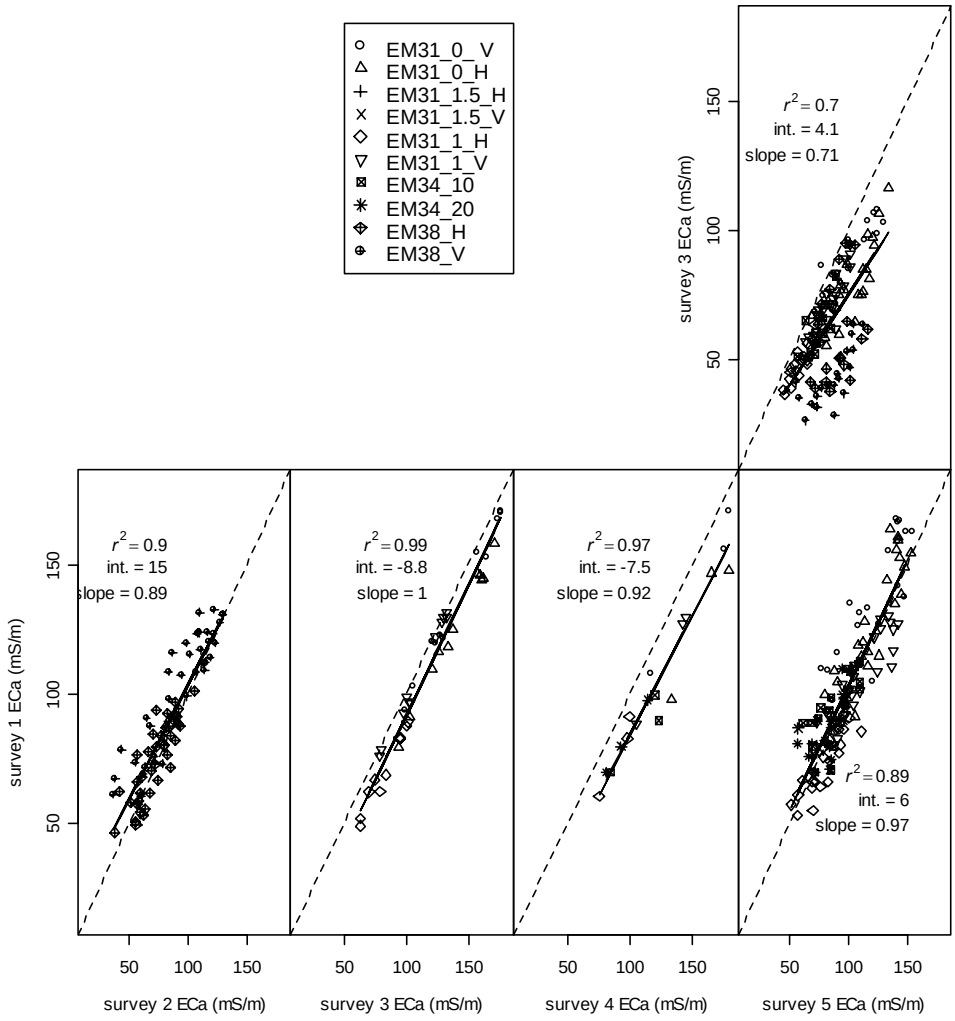

Figure 4.19. Bivariate plots of repeated measurements from different surveys. The largest difference was in the area of natural vegetation, which was surveyed only during Survey 3 and Survey 5. The three other repeated surveys were highly correlated, with significant differences only in the y intercepts which ranged from -7.5 to 15 mS m^{-1}.

The slope of the regression between the two surveys was not significantly different from 1, and the linear shift only correlated to 6.6 mS m^{-1}. Sudduth et al. (2001) found that diurnal temperature fluctuations can increase apparent electrical conductivity readings by as much as 3 mS m^{-1} hr^{-1}. Given that the decrease in EC_a is less than 10 mS m^{-1}, it is likely that this may have been due to a decrease in soil and air temperature following the storm.

Table 4-9. Mean EC_a from EM surveys inside and outside the paddock using all points in the survey. Statistical comparisons made by row using Tukey-Kramer t-test, α = 0.05.

Location	Survey				
	1	2	3	4	5
	mean EC_a (mS m^{-1})				
Inside paddock	90.5a	83.1b	121.8c	108.7cd	98.6d
Outside Paddock	---	---	53.5a	---	85.8b

In general, the instrument depth of penetration was related to the variability in the measurements over the survey period (Table 4-10). The highest variability occurred with the horizontal configurations of the EM 38 and EM 31 and the shallower reading for the EM 34. This is because the response curve of the horizontal configuration emphasises the shallower depths (Figure 2.13). This trend indicates a greater fluctuation in soil moisture in the surface than in the deeper profile, where it is expected to remain relatively constant.

Table 4-10. Instrument configurations in relation to the coefficient of variation in measurements from all surveys. In general, the horizontal reading from each instrument had fluctuated more during the repeated surveys. In the case of the EM 34, the shallower penetrating dipole configuration (10 m spacing) was more sensitive to changes.

Instrument	EM38				EM31				EM34	
Diople config.	V	H	V	H	V	H	V	H	H	H
Height (m)	0				1		1.5		0	
Coil separation (m)	1		3.6						10	20
Penetration (m)	1.5	0.8	6.0	3.0	5.0	2.0	4.5	1.5	7.5	15.0
CV	25.3	37.6	27.7	30.4	28.2	29.3	18.8	19.1	22.9	18.6

Similar results were found in all of the other surveys inside the paddock, with a maximum difference of 7.8 mS m^{-1} between Survey 1 and Survey 3 (using only the matched points). This was likely due to the change in average volumetric water content from 0.24 to 0.37 cm^3 cm^{-3} at the respective surveys. The significant change in slope of the linear regression between the surveys may have been due to instrument calibration differences in Survey 3, or changes in the conductivity profiles in the soils.

Given that Survey 3 was performed in the winter, it is possible that these changes are due to differences in air or soil temperature (Sudduth et al., 2001) or difference in the moisture content at depth in response to seasonal fluctuations in the water table (Sheets and Hendrickx, 1995).

4.3.1.2 Quad-bike EM survey

The quad bike survey provided a high resolution map of the apparent electrical conductivity across the entire field site. Inside the paddock, the quad-bike mounted EM 31 clearly delineated the palæochannel (Figure 4.20). Like the hand-held EM surveys, the method was not as effective outside the paddock, and did not delineate the palæochannel.

The quadbike survey results had similar trends to those collected with the hand-held instrument (in the vertical dipole orientation at 1 m height), but at a significantly higher apparent electrical conductivity (26 mS m^{-1} from the linear regression) ($p < 0.001$) (Figure 4.21). This could have been due to interference from the quadbike, where the instrument mounts did not adequately separate the instrument from the machine. While a correction factor was included to account for such interference, these results indicate that this correction is possibly not accurate, or that other factors were interfering with the instrument, such as heat from the exhaust. The distribution of predictions was also different, in that the hand-held instrument predicted three separate clusters in the EM data, while the quad-bike mounted survey appeared to produce a bimodal distribution of results.

4.3.2 Ground-penetrating Radar

Because the signal is time-referenced, ground-penetrating radar is commonly used to predict the depth to layers which have contrasting dielectric properties. In the case of the palæochannel, the dielectric contrasts between the coarse sands (K = 5 - 20) and the heavy clays beneath (K = 7 - 40) should generate strong reflections (eq. 2.27). However, the 50 and 100 MHz antennae were significantly attenuated in all surveys on in the paddock. After a series of filters and signal amplification techniques were applied to the radargram (Section 3.4.3), some reflections and ground waves were resolvable.

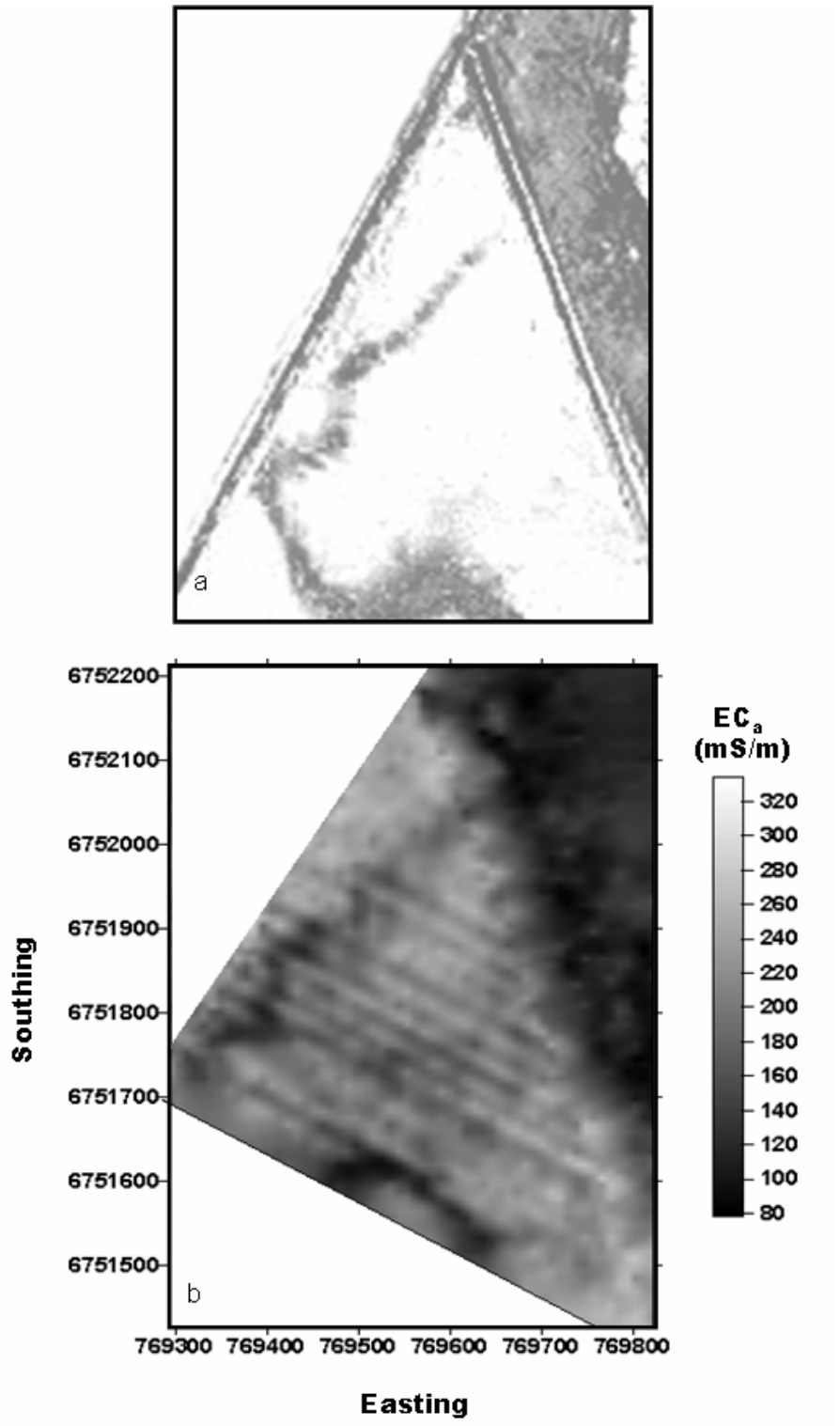

Figure 4.20. Enhanced aerial photograph (a) and predicted EC_a (b) across the field site from the quad bike survey. The palæochannel is clearly shown in both data sets at the northwest side of the paddock running parallel to the edge and to the south winding through the middle.

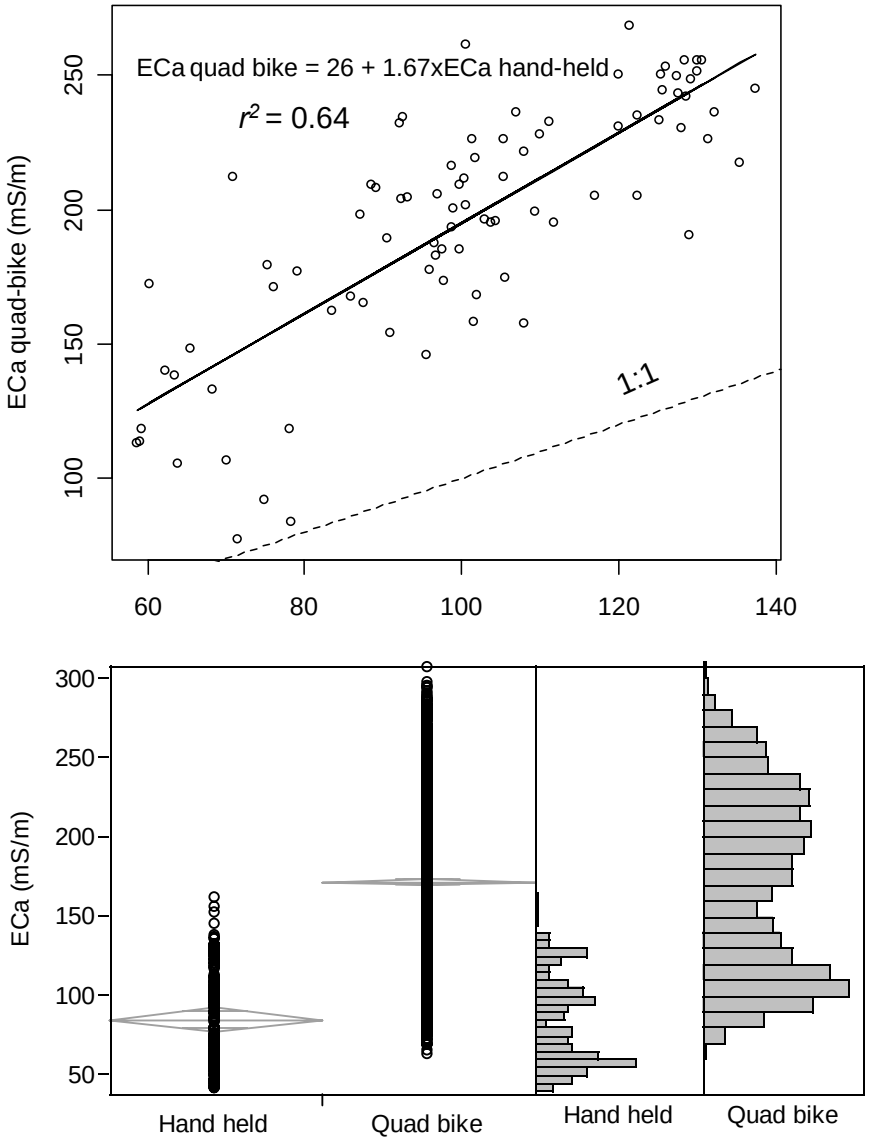

Figure 4.21. Comparison between the hand-held and quad-bike mounted EM 31 measurements. The means diamond plots below show the mean and 5 to 95% confidence limits for the two data sets.

4.3.2.1 Common midpoint measurements

A common midpoint measurement survey was performed on several sites across the study site to provide a preliminary estimate of the dielectric permittivity and to predict the volumetric moisture content of the soil in the upper two metres. Of the three common midpoint sounding surveys performed across the study area, only the ground waves at the start of Transect 4 were visually identified after filtering (Section 3.43). After visually picking the ground waves, the velocity of the topsoil was calculated by fitting a line through the highest amplitude of the first arrival just beneath the air wave (Figure 4.22). Using this technique, the topsoil velocity was estimated to be 0.85 m ns^{-1}, corresponding to a dielectric permittivity of 15.2 (Equation 2.27). Using Topp's equation (Topp et al., 1980) to relate the EM velocity to the soil moisture content, this translates to an average soil moisture content of 0.25 cm cm^{-3} of water. This was very similar to the average measurement of 0.24 cm cm^{-3} determined gravimetrically at the same time (Table 4-8).

The ground waves from the common offset profile also provided a direct determination of the skin depth, which was calculated from the change in amplitude of the ground waves with distance. It was found that the signal quickly deteriorated with separation distance, and at 1.2 metres was reduced to e^{-1} of the original amplitude. Traditionally, the skin depth is calculated from the formula relating the instrument frequency f (Hz), the electrical conductivity of the soil σ (S m^{-1}), and the permittivity of the soil, μ_o (assumed to be that of free space = 1.25 x 10^{-6} Henry m^{-1}) (Equation 2.18).

Using an average electrical conductivity of 200 mS m^{-1}, this translates to a skin depth of 0.16 m. The measured skin depth does not correspond to that from the formula until the soil conductivity reaches 2 mS m^{-1}, which is an unrealistic value for this site. Typically, this calculation is performed to determine the suitability for radar at a specific site (Goodman, 1994). In this case, the two predictions differ significantly and this could be attributed to the magnetic permeability of the soil, nearby metal objects, or instrument-specific attenuation.

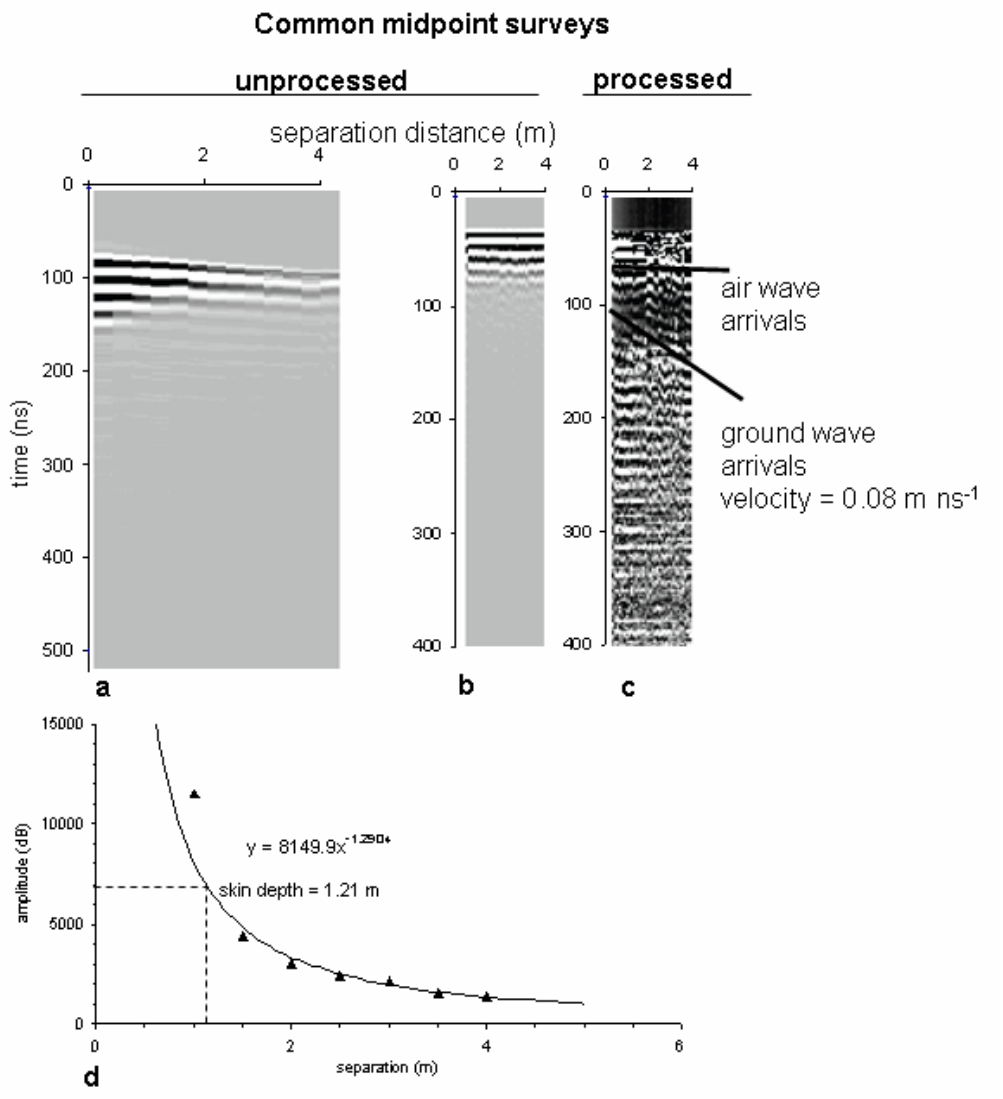

Figure 4.22. Two unprocessed profiles from common-midpoint surveys (a,b), and (c) a processed version which was used to pick the ground waves to estimate the dielectric constant of the subsurface. Using the unprocessed data (a), the signal attenuation was plotted with separation distance (d) showing the skin depth of the 50MHz antennae to be 1.21 m in the heavy clay sediments.

4.3.2.2 Common offset measurements

Similar to the common midpoint surveys, the common offset profiles generally provided little information due to the attenuation of the electromagnetic waves in the heavy clays. Using the 50 MHz antennae with background and DC removal filters, reflections from the palæochannel bottom are apparent, but very weakly defined (Figure 4.23). Only the survey spanning Transect 6 produces

reflections which were clean enough to be visually identified. As the reflector dips to the left (towards the assumed bottom of the palæochannel) it becomes more difficult to distinguish.

Considering the likely changes in the dielectric constant with depth (due to water content, bulk density, and mineralogy) an estimate of the bulk dielectric permittivity was based on the depth to the palæochannel reflector from direct observation (Well 5). At the point where the well intersects the palæochannel (5.5 m), the reflection occurs at 110 ns. This correlates to a dielectric permittivity of 10.4, which would reflect the observed sandier material in the palæochannel at depth (Figure 2.15).

4.4 Conceptual model of the palæochannel site

Although the link between the palæochannel found in this study and those described by Stannard and Kelly is still unclear, the structures all appear to strongly affect the hydrology of the surrounding area. The groundwater observations suggest that a significant source of excess water exists, which is directly connected to the palæochannel (Figure 4.13). Initially, it was hypothesised that this source of water was Carroll Creek, which was located nearby and appeared to be directy connected to the palæochannel. This would have resulted in significant pulses of water which would likely correspond to the height of the creek. Given that Carroll Creek is used to transport irrigation water to the entire farm, it remains full for several days at a time, while water is transferred to the storage dams. If this creek was the sole source of water in the palæochannel, the perched water in the palæochannel would remain for several days at at time, corresponding to the entire irrigation season.

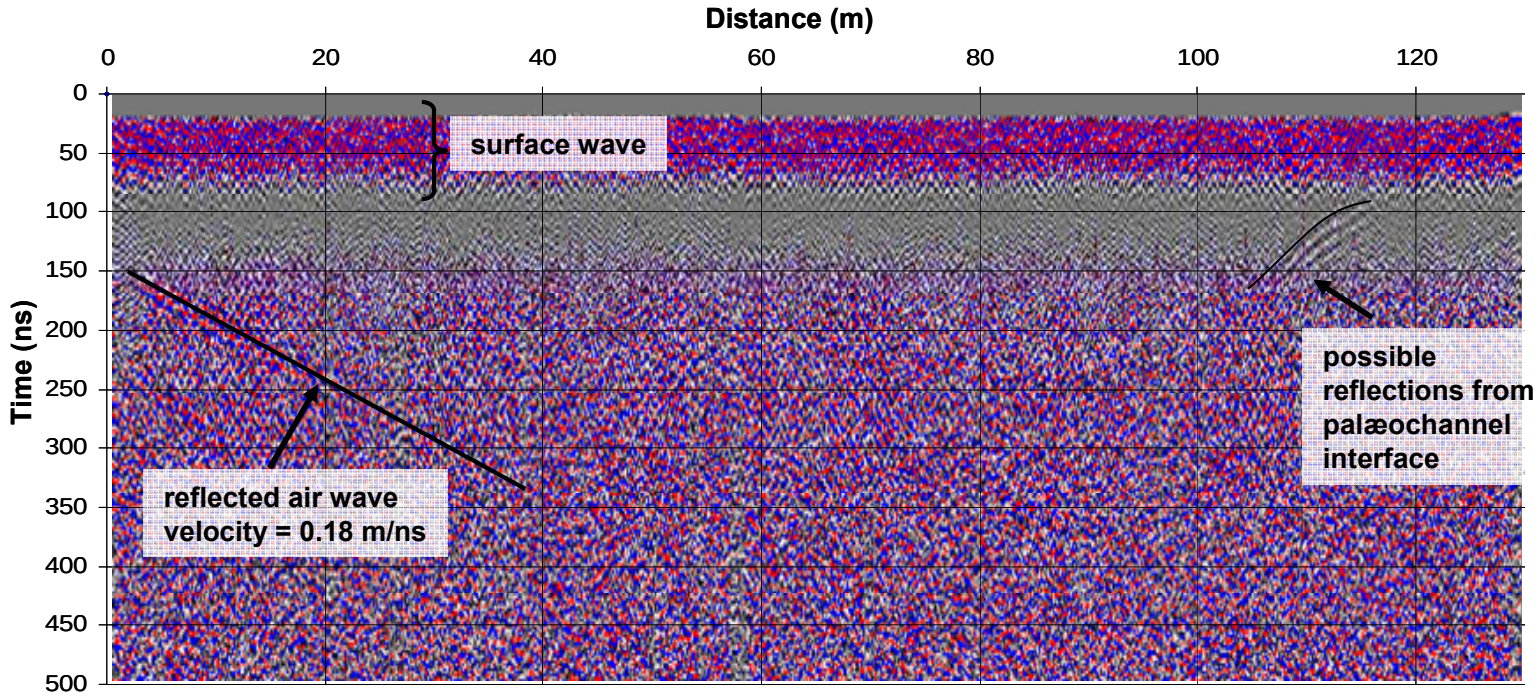

Figure 4.23. Radar profile using common offset survey method using a 50 MHz antenna with a 2 m offset. The radargram was processed using *MALA Groundvision* and were filtered by subtracting the mean trace (60 trace average), removing DC interference, and automatic gain control (which boost the signal with depth). The unstructured noise throughout most of the profile is due to signal attenuation in the heavy clay soils. Reflections from the palæochannel occur at 90 to 120 m along the transect (60 to 90 m in the EM transects) and are outlined and annotated.

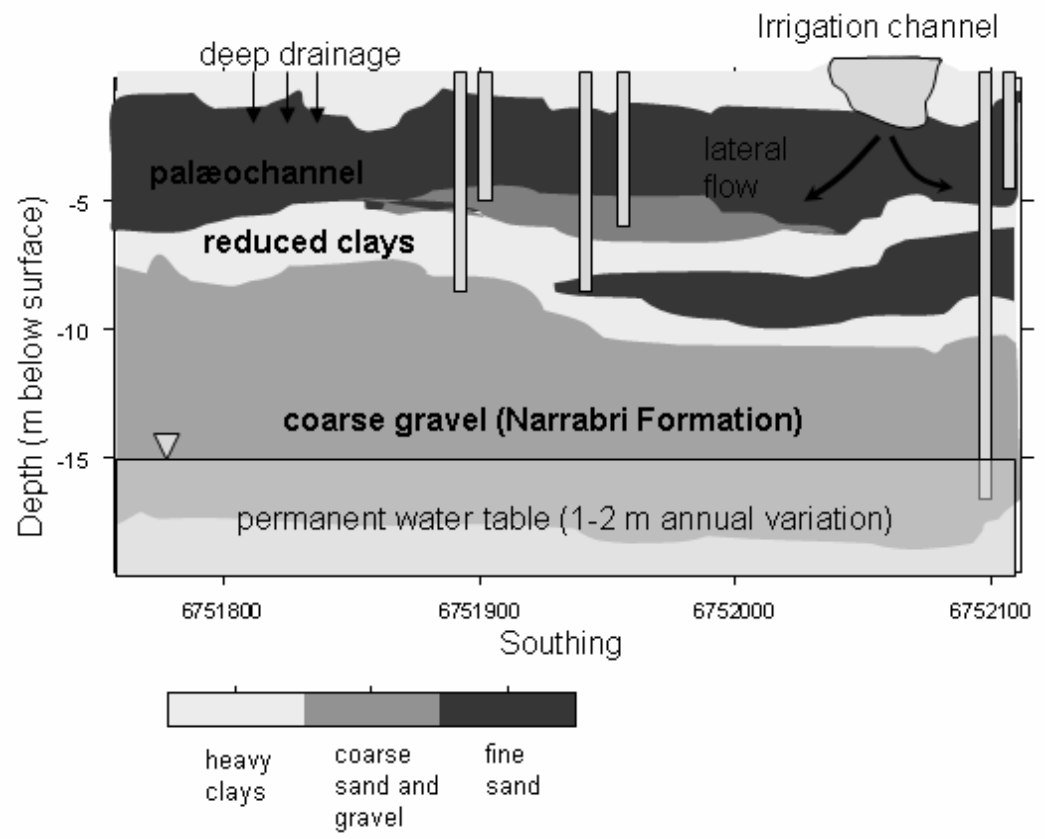

Figure 4.24. Conceptual model of longitudinal water flow through the palæochannel, based on the clustered soil physical properties, EM data and the measured groundwater responses to irrigation events. Indicated are the location of the deep cores, the irrigation channel and the approximate location of the groundwater table in the Narrabri Formation.

The other potential source of water in the palæochannel is a nearby irrigation canal. Given the flashy hydrograph of the perched water in the palæochannel, the timing relative to irrigation events near the study site, and the fact that the irrigation canal regularly transports in excess of two metres of water, it seems likely that water is being transported to the palæochannel from this feature. Once the water enters the channel it has the chance to move rapidly through the subsurface in the palæochannel conduit. Because there is only a relatively thin layer of clay separating the palæochannel bottom from the underlying Narrabri Formation, it appears that excess water is recharging this formation (Figure 4.24). This type of groundwater flow is thought to exist in palæochannels in the Murrumbidgee Irrigation District, where palæochannels are being targeted to reduce recharge into the underlying aquifers

(Rogers et al., 2002). Given the limited data set, this model of groundwater flow on this site is still somewhat speculative, but is certainly worth investigating. Long term monitoring will be useful in determining if this excess water will have an impact on the water table in this formation.

4.5 General discussion of results

This study used two different sampling strategies to determine the soil and regolith properties. Topsoil cores were sampled on a regular grid using a 20 × 48 m spacing, where the grid width was determined from the palæochannel presence in the aerial photograph. Because of the high cost and invasive nature of the deep cores, ancillary data was used to determine their placement. This method is used to derive the most information about the soil property of interest (e.g. the palæochannel) from a limited number of measurements, and is similar to more sophisticated models which incorporate the ancillary data to derive the spatial structure of a soil property (McBratney et al., 1981; Odeh et al., 1990). Although this type of sampling strategy provides a good deal of information about the palæochannel properties, it is highly biased towards the anomaly. In this case, half of the deep core samples were from inside the palæochannel. Considering that the palæochannel occupies less than 5% of the paddock, and about 30% of the measured transects, the reported overall mean of any of the soil properties has little relevance for the soils in the paddock.

The hypothesised palæochannel (as identified by aerial photograph) was identified through soil coring and more clearly defined using the geophysical methods. According to the aerial photograph and the EM data, the palæochannel on this site is approximately 30 m wide. Through the deep coring the bottom of the palæochannel appears to occur between five and six metres below the soil surface, disconformably overlying heavy clays of variable thickness which are located above the Narrabri Formation. The palæochannel varies in thickness from around three to four metres. From this information it appears that the palæochannel banks have a minimum slope of 11% from the bottom (assuming the channel itself has no width). Considering a simple two-layer conductivity model (ie. McNeill, 1980), where the bulk conductivity is related to the thickness of two constrained layers of varying conductivities, the EM data could be qualitatively used to describe the depth to the palæochannel to improve on the prediction. From Figure 4.17, it appears that the

banks of the palæochannel are asymmetrical, where the western bank appears to slope at a steeper angle.

Compared to the surrounding clays, which were derived from a nearby basaltic formation (Stannard and Kelly, 1968; Stannard and Kelly, 1977; Triantafilis et al., 2003a), the palæochannel sediments appear to have been derived from a felsic formation. This can be seen by the dominance of well-sorted quartz and plagioclase feldspars in the sand fraction and the presence of kaolinitic clays in nearby palæochannels (Triantafilis et al., 2003a). It is also reflected in the significantly lower pH of the sediments inside the palæochannel, although this difference has likely been dampened due to the diffusion of bicarbonates into the channel over time through leaching. Given the similarities in the sediment composition to other studies (Stannard and Kelly, 1968; Stannard and Kelly, 1977; Young et al., 2002; Triantafilis et al., 2003a) it is possible that the source of the palæochannel sediments are the Pilliga Sandstone Formation, which is comprised of the mineral suite found in the palæochannel, (along with muscovite) and crops out nearby. Ideally, the source of the material in the palæochannel could be derived using other techniques such as single-grain XRD, to compare mineral impurities to those of the suggested parent material, or simply a more complete mineralogical analysis of the sediments.

The coarse fraction found in the palæochannel was likely deposited while the channel was still active. The size of the coarse fraction indicates that the prior stream had a substantial carrying capacity, when compared with active streams in the region, which have similar dimensions but mostly carry suspended sediments (Fried, 1993). The fining of the channel sediments likely coincides with the termination of stream flow due to a limited carrying capacity, while the fine sand flanking the channel would be a relict levee deposit indicating overbank conditions (Stannard and Kelly, 1968; Stannard and Kelly, 1977). The angular shape of the fine sand fraction towards the top of the palæochannel deposit suggests a significant amount of æolian input. This occurrence been noted throughout the Namoi region during arid conditions related to the last glacial maximum (Ward et al., 1999; Cattle et al., 2002; Young et al., 2002). Coinciding with drier conditions was a possible shift in the sediment supply at the onset of the last glacial maximum, which could explain the anomalously high sinuosity related to the observed bedload (Fried, 1993).

Stannard and Kelly (1977) described two types of palæochannels in the nearby Namoi Region which have traditionally been thought analogous to this region. The main palæochannel structures described are much larger than the ones found near the study area, having channel dimensions of 150 metres wide by 8 metres deep. These structures were also less sinuous and had embankments of only 4 - 5°. However, the channels have similar geomorphic and redoximorphic features including the oxidised sediments inside the channel, the reduced sediments below the channel, and the levee deposit on either side. They were also filled with felsic bedload, derived from the nearby Pillaga Sandstone. The other palæochannels, termed "terminal branches", were described as being up to 30 m wide, but only a few metres deep, and having weakly defined banks which slope around 7°. These features are also much more clay rich and are composed of brown sandy loam to sandy clay loam texture covered with a thick veneer of clay (Stannard and Kelly, 1977). This type of feature may have been present at a nearby site (Triantafilis et al., 2003a), however, it is unlikely that this feature is similar to the one found on this site.

Many of the soil chemical properties reflected the presence of the palæochannel. The exception to this is the presence of carbonates and gypsum nodules which were found throughout the study area and were not associated with the palæochannel presence. Given the felsic nature of the palæochannel, this could suggest the transport of solutes into the palæochannel sediments. The lower electrical conductivity in the palæochannel deposits is likely due to the decrease in clay content inside and above the channel (Figure 4.2). However, unlike the clay content, the property shows a much smoother vertical transition typical of solute breakthrough curves (Figure 4.6) (Rhoades et al., 1989b). It is likely that the relationship between EC_a and clay was compounded due to low cation exchange capacity of the sandier sediments, and the kaolinitic clays found within the palæochannel (Triantafilis et al., 2003a).

Chloride is commonly used as a naturally-occurring environmental tracer (Allison and Hughes, 1983; Scanlon et al., 2002) and, in the absence of chloride-bearing (halide) deposits, it is mainly sourced from rain and irrigation water. This means that qualitative comparisons between profiles can also contain a good deal of information about the hydrology of the sites. From previous studies outlining the effects of palæochannels on deep drainage (Huckel, 2001; Triantafilis et al., 2003a;

Vervoort and Annen, 2006), it was expected that the chloride content would have been significantly lower inside the palæochannel because a greater proportion of water would infiltrate into the palæochannel through the coarser-textured surface sediments. However, the results from the soil chloride measurements suggest that preferential flow is not taking place in the coarser-textured sediments associated with the palæochannel. This is contrary to the results found by Triantafilis et al. (2003a) on a nearby field where the lower EC_a above a palæochannel was related to the lower clay content and presence of 1:1 versus 2:1 clay minerals which was associated with the preferential leaching of soluble ions.

There are two possible explanations for this. The first is that there were not enough measurements to describe the extreme variability of the soil property. This is substantiated by the high coefficient of variation and the weak semivariogram of the chloride data compared to other soil properties. The extremely variable nature of the property could be explained by anion exclusion, where preferential flow through desiccation cracks, rather than micropores, would lead to the heterogeneous leaching of the ion (i.e. Thorburn and Rose, 1990; Weaver et al., 2005).

Another possible explanation for the difference can be found in the general trend of the topsoil chloride data. Over the study area, the soil chloride content is generally lower to the east of the palæochannel and increasing to the west of the channel (Figure 4.7). This corresponds to the direction of irrigation water flow, and could indicate that a greater proportion of irrigation water is being lost upslope of the palæochannel and is therefore unable to leach soils down slope. Bcause this area is located near the tail ditch, water could be ponded for longer periods evaporate and enrich the soil with salts.

It is assumed that the majority of chloride on the study site is derived through the evaporative enrichment of salts from precipitation and irrigation water. However, in the Southern Murray Darling Basin, relict chloride has been found in the regolith, which was likely deposited via æolian dust and sea level encroachment (Simpson and Herczeg, 1994; Timms and Acworth, 2002). Considering the fine sands atop the palæochannel occur at the same depth as the maximum chloride content, it is possible that primary salinity exists in this deposit though the æolian deposition (Page et al., 2001; Cattle et al., 2002). Where this material directly overlies the palæochannel, the fine sand would be continuously leached given a steady supply of irrigation water.

However, where the fine sand resides atop clay, vertical leaching would be minimal. This would lead to a localised salinity bulge associated with the palæochannel levee deposits and would explain the localised highs occurring just down slope of the palæochannel, where fine sand deposits occur. This is exemplified in Transects 2,3,5 and 6, and is particularly obvious in the wells outside the paddock (Figure 4.7) where there is no additional irrigation input. However, because the cores only penetrate to 1.5 m this data set does not provide enough information to support this hypothesis.

The palæochannel was clearly identified by changes in most of the measured soil properties from both the deep and shallow cores. The most hydrologically-relavent of these properties was the dramatic increase in fine and coarse sand associated with the structure, which was also found in a nearby site containing a palæochannel (Vervoort and Annen, 2006).

This study used all available sources of information to predict saturated conductivity. Because of this, there is a discrepancy in the scale of the predicted K_{sat}. Whereas in situ measurements such as slug tests were used to measure the K_{sat} of several cubic metres surrounding the well, those from the pedotransfer functions predict K_{sat} at the core scale. This makes it difficult to compare measurements. As a result, the various techniques used to estimate the saturated conductivity of sediments in this study gave much different predictions.

Although a single slug test was performed on only three wells, the analysis of groundwater recession in these wells gave similar, repeatable estimates from each irrigation event. However, the slug test analysis is based on the time it takes for the water to return to the initial level (prior to the slug), making the determination of the start and finish of these events somewhat subjective. For example, the end of the event did not occur for most of the wells in the fine-textured sediments because of the slow recession times relative to the onset of irrigation events. Therefore, only part of the recession curve was analysed in some events. The assumption that the pulse of water is instantaneous and does not contribute to the recession was based on the coarse-textured wells, which clearly show this relationship (Figure 4.14). However, this assumption is likely invalid in the fine-textured wells due to the slow hydraulic conductivity.

Estimates of K_{sat} from the Murrumbidgee Irrigation district, which contains a similar formation (upper and lower Shepparton Formation) average between 52 to 157 cm day^{-1}, respectively (Khan et al., 2002). These formations were later estaimated to be 320 cm day^{-1}, contrasting the extremely slow shrink-swell clays which were estimated to be 9.0 x 10^{-4} cm day^{-1} (Khan et al., 2004). Compared to these estimates, the slug test results appear to underpredict the saturated conductivity in the palæochannel sediments and overpredict the K_{sat} of the regolith clays.

Through the use of pedotransfer functions, many more K_{sat} predictions were made at distances far from the deep soil cores. Both of the pedotransfer function packages predicted similar K_{sat} for the palæochannel and surrounding sediments. These predictions agreed well with predictions from Vervoort and Annen (2006), who used a similar method nearby. Compared to the in situ measurements however, these estimates were several orders of magnitude greater than those measured.

The difference between the observations is likely due to two factors. First, there is a difference due to the scale of the measurements. Because the prediction is based on a smaller sample it will be inherently more variable. The two pedotransfer functions predicted average topsoil saturated conductivities of 6.46 cm day^{-1} (Neurotheta), and 4.57 cm day^{-1} (Rosetta) over the site. Comparing these estimates to those previously measured on similar soils gives an indication of the difficulty in estimating this parameter. Estimates have included 842.2 cm day^{-1} (topsoil) and 15.2 cm day^{-1} (subsoil) in the Gwydir River Basin (Vervoort et al., 2003), 257.2 cm day^{-1} in the Northern Murray Darling Basin (Vervoort and Cattle, 2003) and 0.58 cm day^{-1} (topsoil) 0.40 cm day^{-1} (subsoil) in similar soils in the Macquarie Valley (Bird et al., 1996).

A major difference in these predictions is likely due to the overburden pressure in the regolith. The sediments, particularly the clays, are likely compacted due to overlying six to nine metres of soil. Therefore, they would likely have much lower hydraulic conductivities than what would be measured in topsoil samples. Furthermore, once these samples are transported to atmospheric conditions they would immediately swell. This is likely a much different scenario than the topsoil cores used to supply the the majority of the Neurotheta and Rosetta training set.

The utility of the geophysical instruments in this environment was based on a combination of the soil physical and chemical properties associated with the structure. Whist the EM clearly identified the palæochannel in the paddock, due to the associated reduction in EC_a, the high electrical conductivity in the majority of the paddock dissipated the radar waves. Similar results have been found comparing the two technologies for mapping soil discontinuities in semi arid landscapes (Stroh et al., 2001). In this case, the radar attenuation was likely due to the high cation exchange capacity of the 2:1 clays (Saarenketo, 1998). For this reason, ground-penetrating radar is not a viable option for mapping the morphology of palæochannels in this type of environment.

The efficacy of the EM instruments in the natural vegetation was also very limited. Only one of the EM instruments detected the palæochannel presence in the area of natural vegetation, apart from the localised high near the irrigation channel (Figure 4.18). In this instance, the relatively wet sands were more conductive than the surrounding dry clay, suggesting a strong subsoil moisture influence. This was reflected in the temporal variation of EC_a between surveys in the area of natural vegetation which had the largest difference in slope and intercept between matched points (Figure 4.18). The considerably lower electrical conductivity could have been a product of salt accumulation in the paddock due to the application of impure irrigation water at a rate which was not sufficient to leach the salts from the profile (Shaw and Thorburn, 1985).

Relative to changes in the electrical conductivity in the area of natural vegetation, the EM was relatively insensitive to changes in soil moisture inside the paddock which was relatively moist throughout the year (Table 4-8, Figure 4.19). This points to the likelihood of a minimum moisture threshold moisture content for the instruments, which is based on the conduction pathways for the EM waves in this type of environment (Rhoades et al., 1989b; Saarenketo, 1998). This phenomina was also replicated nearby, where the EM 31 was unable to image a known palæochannel in a very dry area during the site selection for a reservoir (Tim Richards, Auscott Ltd. farm manager, pers. comm), and in poor spatial correlation between EM 38 measurements (Brus et al., 1992). Therefore it appears that the EM instruments are best suited when there is sufficient soil moisture to enhance the differences in

apparent electrical conductivity, a techniques which is commonly used with ground-penetrating radar surveys (Davis and Annan, 1989).

Appendix 4.1 – Topsoil descriptions

Transect	Distance along transect	Depth	Colour class and description
	m	cm	
1	0	0-65	black (10YR 3/1) **silty loam**
		65-150	grey (10YR 4/2) **silty clay loam**
	20	0-33	black (10YR 3/2) **clay loam**
		33-100	red (7.5YR 3/3) **clay loam**
		100-150	red (10YR 4/4) **clay loam** with black (10YR 3/2) mottles
	40	0-16	black (10YR 3/2) **clay loam**
		16-77	red (7.5YR 4/4) **clay loam**
		77-150	red (10YR 4/4) **silty clay loam**
	60	0-53	black (10YR 3/2) **clay**
		53-86	red (7.5YR 5/4) **clay**
		86-150	red (10YR 5/4) **clay**
	80	0-52	black (10YR 3/1) **clay loam**
		52-90	grey (10YR 4/2) **clay**
		90-150	red (10YR 5/4) **clay**
	100	0-70	black (2.5YR 3/1) **silty loam**
		70-110	red (10YR 3/3) **clay loam**
		110-150	grey (10YR 4/2) **silty loam**
2	0	0-19	black (10YR 3/2) **clay loam**
		19-81	red (10YR 4/3) **silty clay loam**
		81-150	red (10YR 4/4) **clay loam** with black (10yr 3/2) mottles
	20	0-65	black (7.5YR 3/2) **clay loam**
		65-150	red (7.5YR 4/4) **silty clay loam**
	40	0-19	black (7.5YR 3/2) **clay loam**
		19-95	red (5YR 3/3) **clay loam**
		95-150	red (7.5YR 4/6) **silty clay** with red (5YR 5/6) mottles
	60	0-20	black (7.5YR 3/1) **clay loam**
		20-85	black (7.5YR 3/2) **clay loam**
		85-150	red (10YR 4/4) **clay**
	80	0-60	black (10YR 3/1) **loam**
		60-150	red (10YR 4/3) **silty loam**

Transect	Distance along transect	Depth	Colour class and description
	m	cm	
2	100	0-85	black (10YR 3/1) **silty loam**
		85-150	grey (10YR 4/2) **silty loam**
3	0	0-36	black (7.5YR 3/2) **clay loam**
		36-87	red (10YR 4/3) **clay**
		87-150	red (7.5YR 4/4) **clay**
	20	0-18	red (7.5YR 3/3) **clay** with (10YR 3/1) mottles
		18-60	red (7.5YR 3/4) **clay**
		60-150	red (10YR 4/6) **clay**
	40	0-18	black (10YR 3/2) **clay**
		18-80	red (7.5YR 3/4) **clay**
		80-150	red (10YR 4/4) **clay**
	60	0-31	red (10YR 3/3) **clay loam**
		31-100	red (7.5YR 3/3) **clay loam**
		100-150	red (10YR 4/4) **silty clay loam**
	80	0-65	black (10YR 3/1) **loam**
		65-150	red (10YR 3/3) **silty clay loam**
	100	0-90	black (2.5YR 3/1) **silty loam**
		90-150	grey (10YR 4/1) **silty loam**
4	0	0-40	black (10YR 3/2) **clay loam**
		40-150	grey (10YR 4/2) **silty clay loam** with (5YR 4/3) mottles
	20	0-28	black (10YR 3/2) **clay loam**
		28-118	grey (10YR 4/2) **clay loam**
		118-150	red (7.5YR 4/4) **clay loam**
	40	0-11	black (10YR 3/2) **clay loam**
		11-88	red (10YR 4/3) **clay loam**
		88-150	red (10YR 4/4) **silty clay loam**
	60	0-7	black (7.5YR 2.5/2) **clay loam**
		7-50	red (7.5YR 3/4) **clay loam**
		50-95	red (7.5YR 4/4) **clay**
		95-150	red (10YR 4/4) **clay**
4	80	0-15	black (10YR 3/2) **clay loam**
		15-83	red (7.5YR 3/3) **clay loam**
		83-150	red (10YR 4/4) **clay**

Transect	Distance along transect	Depth	Colour class and description
	m	cm	
	100	0-67	black (2.5YR 2.5/1) **silty clay loam**
		67-150	red (10YR 3/3) **silty loam**
5	0	0-80	black (10YR 2/2) **silty clay loam**
		80-150	red (10YR 4/3) **clay loam** with (10YR 3/1) mottles
	20	0-29	black (7.5YR 3/2) **clay loam**
		29-100	grey (10YR 4/2) **silty loam**
		100-150	grey (10YR 4/2) **silty clay loam** with (5YR 4/4) mottles
	40	0-50	black (7.5YR 2.5/1) **clay loam**
		50-100	red (10YR 4/3) **silty clay loam**
		100-150	red (10YR 4/4) **silty clay loam**
	60	0-13	black (7.5YR 2.5/2) **clay loam**
		13-100	red (7.5YR 4/3) **clay**
		100-150	red (10YR 4/4) **silty clay loam**
	80	0-45	black (10YR 3/2) **clay loam**
		45-150	red (10YR 4/3) **clay loam**
	100	0-95	black (10YR 3/1) **silty loam**
		95-150	grey (10YR 4/1) **silty clay loam** with (10YR 3/1) mottles
6	0	0-34	black (10YR 2/2) **clay loam**
		34-150	red (10YR 3/3) **clay loam**
	20	0-45	black (7.5YR 2.5/1) **loam**
		45-105	red (10YR 3/3) **clay loam**
		105-150	red (7.5YR 4/3) **silty clay loam** with (7.5YR 3/1) mottles
	40	0-68	black (10YR 2/1) **loam**
		68-110	black (10YR 3/2) **clay loam**
		110-150	red (10YR 4/4) **clay**
6			
	60	0-44	red (7.5YR 2.5/3) **clay loam**
		44-100	black (7.5YR 3/2) **clay loam**
		100-150	red (7.5YR 4/4) **clay**
	80	0-80	black (7.5YR 3/1) **loam**
		80-150	grey (10YR 4/2) **silty loam**

Transect	Distance along transect	Depth	Colour class and description
	m	cm	
	100	0-90	grey (10YR 4/1) **silty loam**
		90-150	grey (7.5YR 4/1) **silty loam** with (10YR 4/2) mottles
7	0	0-25	black (7.5YR 3/1) **clay loam**
		25-120	red (10YR 3/3) **silty clay loam**
		120-150	red (10YR 4/3) **clay loam** with (7.5YR 4/3) mottles
	20	0-32	black (7.5YR 2.5/1) **clay loam**
		32-100	black (7.5YR 3/2) **silty clay loam**
		100-150	black (5YR 2.5/1) **silty clay loam** red (7.5YR 3/3) mottles
	40	0-47	black (5YR 2.5/1) **silty clay loam**
		47-130	black (7.5YR 3/2) **loam**
		130-150	black (10YR 3/2) **silty clay loam** with (5YR 4/3) mottles
	60	0-57	black (7.5YR 2.5/1) **loam**
		57-100	black (7.5YR 3/2) **silty clay loam**
		100-150	red (7.5YR 3/3) **silty clay loam**
	80	0-25	black (7.5YR 2.5/2) **clay loam**
		25-100	red (7.5YR 3/3) **clay**
		100-150	red (10YR 4/4) **clay**
	100	0-70	black (5YR 2.5/1) **clay loam**
		70-130	black (7.5YR 2.5/2) **clay loam**
		130-150	red (7.5YR 4/4) **clay**
8	0	0-33	black (5YR 3/1) **clay loam**
		33-130	black (7.5YR 3/2) **clay loam**
		130-150	grey (7.5YR 4/2) **clay loam** with (5YR 4/4) mottles
	20	0-60	black (10YR 3/1) **clay loam**
8		60-110	red (10YR 4/3) **clay loam**
		110-150	red (10YR 4/3) **clay loam** with (5YR 4/3) mottles
	40	0-60	black (7.5YR 3/1) **clay loam**
		60-120	black (5YR 3/1) **silty loam**
		120-150	red (7.5YR 4/3) **silty loam** with (5YR 4/4) mottles

Transect	Distance along transect	Depth	Colour class and description
	m	cm	
	60	0-80	black (10YR 3/2) **clay loam**
		80-150	red (10YR 4/4) **clay loam**
	80	0-33	black (10YR 3/2) **clay loam**
		33-110	red (7.5YR 4/4) **clay**
		110-150	red (7.5YR 4/4) **clay**
9	0	0-15	red (10YR 3/3) **clay**
		15-40	red (5YR 4/4) **clay**
		40-60	red (7.5YR 4/6) **clay**
		60-75	red (10YR 5/6) **clay**
		75-150	red (10YR 5/6) **clay**
	100	0-75	grey (10YR 4/2) **loam**
		75-85	red (10YR 4/4) **loam**
		85-100	red (10YR 4/4) **loam**
10	50	0-50	grey (10YR 5/2) **clay loam**
		50-80	red (10YR 4/3) **clay loam**
		80-95	red (10YR 3/4) **clay loam**
		95-100	red (10YR 3/4) **clay**
11	0	0-75	black (2.5YR 3/2) **clay loam**
		75-80	black (10YR 3/2) **clay loam**
		80-100	red (10YR 4.4) **clay loam**
	100	0-80	black (10YR 3/2) **silty loam**
		80-100	brown (2.5YR 4/3) **silty loam** with (10YR 3/2) mottles

Appendix 4.2 – Deep core descriptions

	Depth	Description
	m	
Well 1	0.0 - 0.3	very dark greyish brown (10YR 3/2) **clay**
	0.3 - 3.0	dark greyish brown (10YR 4/2) **clay** with common CaCO3 nodules
	3.0 - 5.0	yellowish brown (10YR 5/4) **clay** with CaCO3 nodules and coarse Mn nodules
	5.0 - 7.3	light brownish grey (10YR 6/2) **clay**
	7.3 - 9.0	light yellowish brown (10YR 6/4) **clay loam** with common coarse subangular gravel
	9.0 - 9.3	strong brown (7.5 YR 5/6) **sandy loam** with common coarse subangular **gravel**
Well 2	0.0 - 1.0	dark brown (7.5YR 3/4) **clay**
	1.0 - 2.0	dark yellowish brown (10YR 4/4) **clay loam**
	2.0 - 4.2	dark yellowish brown (10YR 4/6) **loam** with common thin **gravel lenses** at 3.3m and grading to coarse sand at 4.0 m
	4.2 - 6.2	dark brown (7.5 YR 4/4) **loamy coarse sand** to **sandy loam,** common, thick **coarse sand stringers,** few thin **clay lenes** increasing with depth
	6.2 - 7.0	grey (2.5Y 6/1) **clay loam** with common **gravel** inclusions
	7.0 - 8.0	light brownish grey (2.5Y 6/2) **clay** with common browish yellow (10YR 6/6) inclusions and common **fine gravel**
	8.0 - 8.3	pale brown (10YR 6/3) **clay loam** with common **coarse gravel**
	8.3 - 9.3	strong brown (7.5YR 5/8) **sandy loam** with common medium to coarse angular **gravel**

	Depth m	Description
Well 4	0 - 0.34	very dark brown (10YR 2/2) **clay**
	0.34 - 1.5	dark brown (10YR 3/3) **clay** with CaCO3 nodules
	2.0 - 2.45	dark greyish brown (10YR 4/2) **clay**
	3.00 - 5.45	pale brown (10YR 6/3) **clay** with very dark greyish brown (10YR 3/2) inclusions and few med FeOOH nodules
	6.0 - 6.45	greyish brown (10YR 5/2) **clay**
	7.0 - 8.3	yellowish brown (10YR 5/4) **clay** with few medium grey (10YR 5/1) mottles, many fine CaCO3 nodules and few med qtz clasts
	9.0 - 9.3	yellowish brown (10YR 5/6) **clay loam**
Well 5	0 - 1.0	very dark brown (7.5YR 2.5/3) **clay**
	1.0 - 1.5	dark brown (7.5YR 4/4) **clay loam**
	2.0 - 4.45	dark yellowish brown (10YR 4/4) **clay loam**, mottles appearing at 4.0 m, coarse angular gravel at 5.15 m
	6.0 - 6.45	light brownish grey (10YR 6/2) **clay** with few fine Mn nodules
	7.0 - 9.3	yellowish brown (10YR 5/4) **clay** with common greyish brown (10YR 5/2) mottles transitioning to lamella, coarsens to **clay loam** at 8.0 m
Well 7	1.0 - 2.7	dark yellowish brown (10YR 4/4) **clay loam**
	2.7 - 3.5	strong brown (7.5YR 5/6) **loam** with common coarse sand
	3.5 - 4.0	dark brown (7.5YR 4/4) **gravely loamy sand** with common rounded gravel, clay lens at 3.8 m
	4.0 - 5.0	dark yellowish brown (10YR 4/4) **loam** with common medium gravel
	5.0 - 6.0	strong brown (7.5YR 4/6) **loamy sand** with 2 cm grey (7.5YR 6/1) **clay lens**
	6.0 - 7.0	pale brown (10YR 6/3) **clay**

	Depth	Description
Well 8	0 - 1.00	very dark brown (7.5YR 2.5/2) grading to dark brown (7.5YR 4/3) **clay**, with CaCO3 nodules at 0.13 m
	1.0 - 1.50	dark yellowish brown (10YR 4/4) **silty clay loam** with common CaCO3 nodules
	2 - 2.45	dark yellowish brown (10YR 4/4) **silty loam** with very dark grey (7.5 YR 3/1) inclusions
	3 - 3.45	dark brown (7.5YR 4/4) **loam** with common very dark grey (7.5YR 3/1) inclusions
	4 - 6.3	strong brown (7.5YR 4/6) grading to greyish brown (10YR 5/2) **gravelly sandy loam** with common coarse gravel, and thin brownish grey (10YR 6/2) **clay lenses**
	7 - 7.45	grey (2.5Y 6/1) **silty clay**
	8 - 8.45	light brownish grey (10YR 6/2) **silty clay loam** with common coarse yellowish brown (10YR 5/4) inclusions
	9 - 9.3	yellowish brown (10YR 5/4) **silty clay loam**
Well 9	0 - 0.29	dark brown (7.5YR 3/2) **clay**
	0.29 - 2.45	dark greyish brown (10YR 4/2) **silty clay** with reddish brown (5YR 4/4) mottles at 1.0 m, common angular sand at 2.0 m
	3.00 - 5.00	dark brown (10YR 4/3) grading to pale brown (10YR 6/3) **clay** at 4 m
	5.0 - 7.0	light brownish grey (10YR 6/2) grading to brown (10YR 5/3) **clay**

Appendix 4.3 – X-Ray Diffration Results

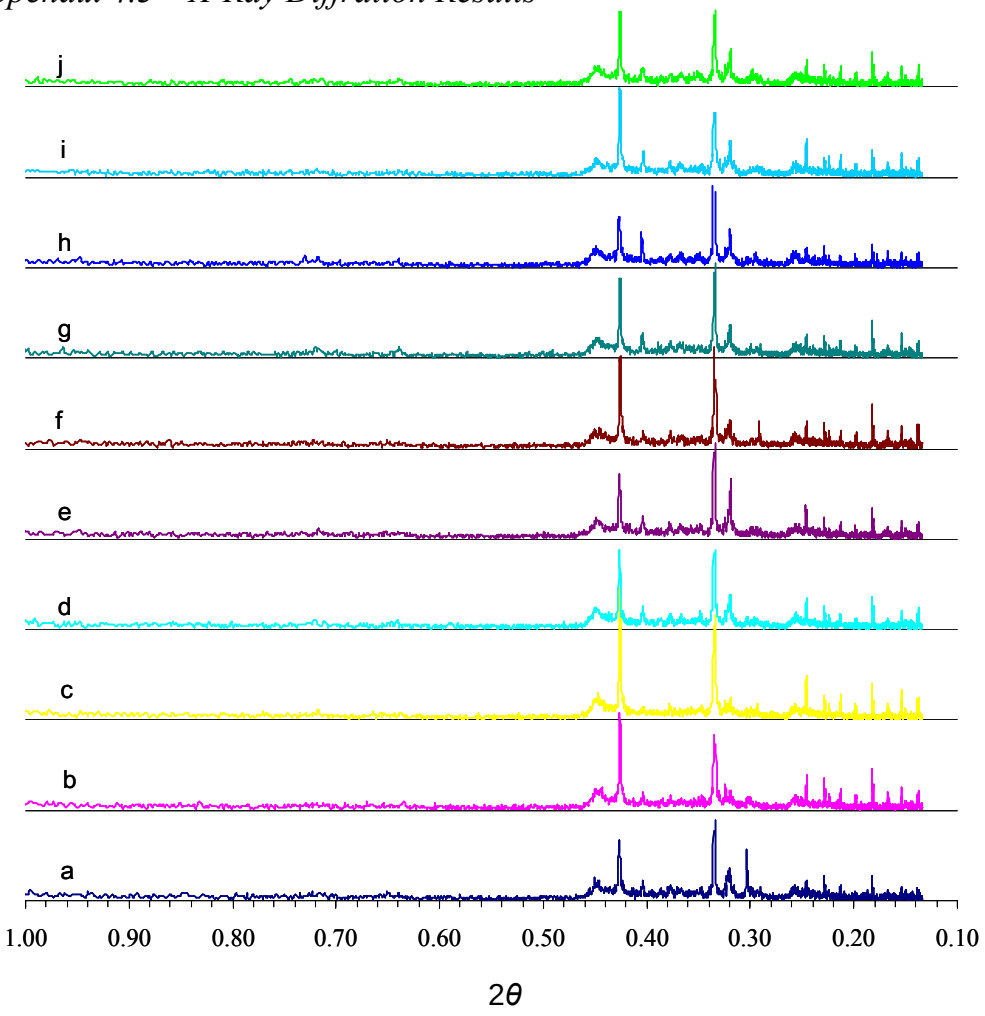

Figure 4.25, X-ray diffraction data for samples located at various depths throughout the paddock. Locations shown in table below.

Trace	Location	Depth
		m
a	AUS 1.2	0.0 – 1.0
b	Well 4	3.0 – 3.5
c		5.0 – 5.5
d		8.0 – 8.3
e	Well 5	3.0 – 3.5
f		5.0 – 5.5
g		8.0 – 8.8
h	AUS 1.2	1.5 – 2.0
i		4.5 – 5.0
j		7.5 – 8.0

Chapter 5

Prediction of continuous Ksat fields from geophysical and soil property data

5 Prediction of continuous K_{sat} fields from geophysical and soil property data

A key issue for simulation modelling is the accuracy of the data to parameterise a groundwater model. Spatially detailed subsoil and regolith information is therefore an important requirement for hydrological and groundwater models. The key to efficiently obtaining this data is to get the maximum information from the fewest number of measurements.

Although direct observation of soil properties gives the best understanding of the local hydrogeology, coring methods are both costly and intrusive. Over the last two decades, there has been a paradigm shift in field of hydrology toward having many relatively uncertain measurements, rather than a few direct observations (Anderson, 1995). This shift recognises the uncertainty in measured soil properties, such as K_{sat}, meaning the number of measurements required to predict the spatial variability of the property is often unobtainable. Recognising this limitation, hydrologic predictions have been improved through the use of stochastic modelling (assuming that the variability in a soil property cannot be measured, but can be predicted from a distribution of likely values and solved through multiple simulations) or the incorporation of ancillary data to improve on a few measured soil properties. Geophysical information is a type of ancillary data set which can be strongly correlated with hydrologic properties and can be a much more efficient way to obtain hydrologic data (Hubbard et al., 1999; de Lima and Niwas, 2000; Endres and Anonymous, 2001; Vervoort and Annen, 2006; Wendroth et al., 2006). This practice is the basis of the field of *hydrogeophysics* (Anderson, 1995).

Electromagnetic induction (EM) is a valuable tool for obtaining ancillary data in semi-arid environments as soil electrical conductivity relates to differences in many different soil properties (Lesch et al., 2005). Like many geophysical instruments, EM requires an inversion algothrim to predict the vertical distribution of EC from multiple measurements (vertical sounding). The choice in the inversion algorithm is somewhat subjective and can dramatically affect EC predictions (Borchers et al., 1997; Hendrickx et al., 2002; Deidda et al., 2003; Schultz and Ruppel, 2005; Vervoort and

Annen, 2006). Unlike seismic, radar, and resistivity methods, which are more commonly used in petroleum and groundwater exploration, the relation between apparent electrical conductivity (as derived from EM measurements) and hydraulic conductivity has received very little attention. Considering the rapid adoption of this technology by agriculturalists to aide in their understanding of soil properties (Corwin and Lesch, 2005c) and the need to improve water use efficiency (Section 2.2.5), it is likely that there will be significant demand for this type of information in the near future.

In order to obtain accurate soil hydrologic predictions from these instruments, there are several aspects which need to be investigated in detail. This chapter aims to explore several hypotheses related to the inversion of electromagnetic induction and the subsequent use of this information to predict the distribution of the soil and regolith hydraulic conductivity:

- Conditioning the inversion of the EC_a profiles using Tikhonov regularisation will improve the prediction of the profiles from the original McNeill inversion model.
    - A 0^{th} order regularisation will outperform the most commonly-used, 2^{nd} order regularisation since this method better retains geologic boundaries.
    - Temporal variation in soil EC_a will significantly affect predicted EC profiles.
- The use of ancillary data to derive scaling factors improves the spatial prediction of saturated conductivity from soil property data.
    - The use of a priori information of the local geology and the relationship between K_{sat} and EC will improve this classification process.
    - A scaling relationship based on modelled EC data will improve predictions based solely on ordinary 3-D kriging of the measured soil property data,

- Regression kriging, which uses the maximum amount of data (measured soil properties and EM data), should provide the maximum amount of support to image the soil hydraulic properties.

Inversion of electromagnetic induction measurements

Electromagnetic induction is commonly used to predict the lateral variation of apparent electrical conductivity (EC_a) and related soil properties. The most commonly derived soil properties include clay content (Williams and Hoey, 1987; Doolittle et al., 1994; James et al., 2003; Triantafilis and Lesch, 2005), salinity (Williams and Baker, 1982; Lesch et al., 1992; Sheets et al., 1994; Lesch et al., 1995b; Triantafilis et al., 2000) and water content (Sheets and Hendrickx, 1995). Because electromagnetic induction instruments measure the bulk electrical conductivity over the effective depth of penetration (Section 2.5.1), predicting electrical conductivity and the related soil properties with depth is not as straight-forward, however.

When operating at low induction numbers (Section 2.5.1), the vertical distribution of electrical conductivity can be derived by taking several readings from the instrument at various heights above the soil surface or by using multiple instruments (Williams and Baker, 1982; Slavich, 1990; Cook and Walker, 1992a; Borchers et al., 1997; McBratney et al., 2000; Hendrickx et al., 2002; Schultz and Ruppel, 2005; Vervoort and Annen, 2006). Subsequently, an inversion algorithm must be used to deconvolute the apparent electrical conductivity measurements (EC_a) in order to predict the electrical conductivity (EC) distribution. In many cases, there are fewer measurements than layers to be predicted. The inverse problems are therefore ill-posed, meaning that many different solutions can describe the observed measurements (Aster et al., 2005).

Several inversion algorithms are useful for predicting the vertical distribution of electrical conductivity from electromagnetic induction instruments. These are classified as linear or non-linear, depending on the assumed relationship between soil EC and the instrument response (Section 2.5.1.1). The benefits of using EM is that the instrument response is "geometrically limited" (McNeill, 1980b), unlike other geophysical instruments such as resistivity and ground-penetrating radar which require non-linear inversion models to predict changes in soil properties with depth

(Lazaro-Mancilla and Gomez-Trevino, 2000; Auken and Christiansen, 2004). Although advances in computer processing have reduced the overall processing time for inverting geophysical data, the linear models require substantially less computation time due to their simpler algorithms, and are based on fewer assumptions (Hendrickx et al., 2002).

5.1.1 McNeill Model

The Geonics "EM series" instruments are calibrated to the soil electrical conductivity based on a linear relationship between the bulk EC_a of the soil and the ratio of the measured primary to secondary magnetic fields (Equation 2.17) (Section 2.5.1, 3.4.1). At low induction numbers, the prediction is weighted to the instrument response curves (Figure 2.13) over the effective penetration depth. McNeill (1980) suggests a model using Equations 2.19 and 2.20, based on these assumptions to predict M uniform layers of conductivity σ_M, and magnetic permeability μ_M with a thickness t_M from M measurements (the "McNeill model"). Each measurement is weighted by the instrument response curve at the measured dipole orientation (Equation 2.21, 2.22) and the amount of air between the instrument and the ground, h. Hendrickx et al. (2002) show this graphically in the following schematic:

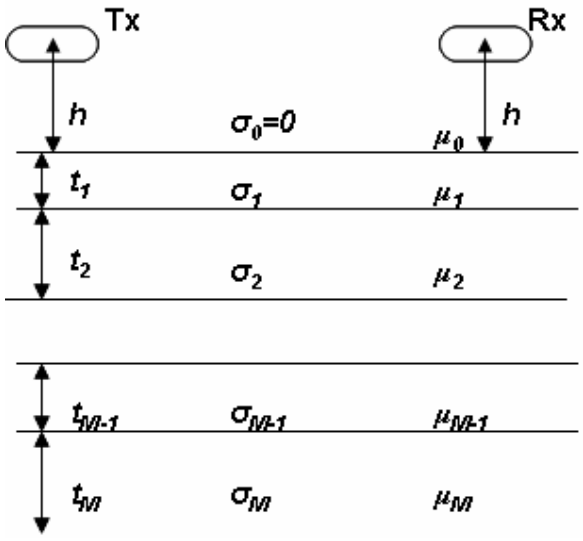

Figure 5.1. General schematic of inversion cross section. From Hendrickx et al (2002)

Combining all possible permutations of predicted layers and measurements produces a *K* matrix of *j* responses by *i* predictions (Equation 2.23). A vector of observations *d* (apparent electrical conductivity, EC_a) is then used to solve for the actual electrical conductivity (EC) of the desired layers by minimising the errors of the non-unique solution to the system of linear equations.

5.1.2 Tikhonov regularisation

Coupled with the complexity and non-uniqueness of the minimisation solution, small measurement errors can lead to unrealistic predictions of EC. This is particularly the case as more layers are added to the problem and the problem becomes under-conditioned (Borchers et al., 1997). Therefore, the minimisation generally requires regularisation of the least squares solution, as explained in Section 2.5.1.1.

For this study, Tikhonov regularisation was used to condition the minimisation, based on an operator of the 0^{th}, 1^{st}, or 2^{nd} derivative of the conductivity function. The dampening of the responses can be thought of as minimising variation in the values, the slope, or the change in slope in the profiles. To date, 2^{nd} order regularisation is most commonly used in soil science due to the smooth nature of observed soil conductivity profiles (Borchers et al., 1997; Hendrickx et al., 2002; Deidda et al., 2003; Vervoort and Annen, 2006). However, if distinct geologic units control the distribution of electrical conductivity, 2^{nd} order regularisation may unnecessarily smooth the EC prediction, effectively removing the distinct boundaries observed in the field (McBratney et al., 2000).

5.1.3 General linear model assumptions

Linear instrument response

The underlying assumption in the linear model is that the instrument is operating under the low induction number principle. This assumption relates the coil separation to the predicted skin depth, which depends on the instrument frequency and soil electrical conductivity (Section 2.5.1). Under these conditions, the response curve is solely based on the instrument frequency and not on the soil conductivity. The predicted depth is therefore based on the instrument response being linearly shifted with the height of the instrument.

When the soil conductivity is sufficiently low (less than 100 mS m^{-1} (McNeill, 1980b)), the instrument depth of penetration is said to be "geometrically limited" because the strongest component of the secondary eddy currents are generated from waves travelling parallel to the ground surface (Figure 2.10). Because electromagnetic waves preferentially flow through conductive media, the instrument response curve should be affected by soil heterogeneity (McNeill, 1980b). In the presence of highly conductive bodies the response is stretched based on the conductivity of the predicted layer and the layers above it. Nonlinear inversion incorporates this using Maxwell's equation, bypassing the linear assumptions (Hendrickx et al., 2002).

Hendrickx and co-workers compared EM 38 EC_a measurements with those from a Rhoades conductivity probe to identify the effects of vertical heterogeneity and high electrical conductivity on the instrument response (Hendrickx et al., 2002). The instrument response was not significantly affected by vertical heterogeneity in less conductive environments, but it diverged considerably from the conductivity probe readings above 500 mS m^{-1}. Because 75% of the EC_a measurements taken in this study were less than 102 mS m^{-1}, with a maximum conductivity of 180 mS m^{-1}, linear inversion methods were considered appropriate.

A homogeneous semi-infinite layer exists below the lowest predicted layer.

The inversion algorithms incorporate a semi-infinite layer of homogeneous conductivity into the bottom layer. This layer has been arbitrarily set to the conductivity of the lowest layer, in accordance with earlier studies (Borchers et al., 1997; Hendrickx et al., 2002). It has been shown that this layer significantly affects the predicted profiles when the conductivity of this layer is set to zero (Hilgendorf, 1997).

The soil magnetic permeability is equal to that of free space.

The EM instrument response is based on the assumption that the magnetic permeability of the soil is equal to that of free space (Equation 2.17). This is a valid assumption in most soils, due to the relatively rare presence of magnetite or native metals which accumulate in specific depositional environments (i.e. black sand).

Lateral homogeneity

In a dipole-dipole configuration, it can be shown that the EM waves mostly travel horizontally. Therefore, the instrument response assumes that the soil under the coils is laterally homogeneous (McNeill, 1980b). Where the coil spacing is sufficiently small relative to the spatial covariance of the measured properties (such as the EM 38 and EM 31) this is not an issue. However, the EM 34 instrument uses coil spacings of 10, 20, and 40 m and may therefore underpredict the lateral variation in EC associated with the palæochannel, which is approximately 30 m wide and laterally-discontinuous.

Temperature and diurnal effects

The EM data used in this model were collected over a week. It has been shown that the effects of temperature and solar activity can shift the conductivity profiles over several hours (Sudduth et al., 2001). In this study the EM 38 was the most sensitive instrument to transient changes which appeared to be related to soil temperature and moisture fluctuations (Section 4.3.1.1.1), however this data was not used in the inversion process because measurements were not taken on all transects inside the paddock. Comparisons were made between Survey 1 and Survey 5 to test the model sensitivity to transient differences in EM data because these surveys contained the most co-located measurements.

5.1.4 Methods

Using the various instrument configurations for the EM 31 and EM 34 described in Section 3.4.1, conductivity layers were predicted at 0.5 m increments to a depth of ten metres. In order to reduce the variability from multiple surveys, only measurements from Survey 1 were used in the inversion process. The resulting dataset consisted of EM 31 and EM 34 measurements across eight transects located inside the paddock at ten metre spacing, totalling 688 measurements (8 measurements at 86 locations).

The McNeill layered earth model predicts homogeneous conductivity layers based on the difference in the geometrically-limited instrument detection depth (Table 3-1). Using this model, eight layers of varying thickness from 0 – 1.5, 1.5 – 2.0, 2.0 to 3.0, 3.0 – 4.5, 4.5 – 5.0, 5.0 – 6.0, 6.0 – 7.5, and 7.5 – 15 m depth were predicted

from the EM 31 and EM 34 measurements. The instrument response curves from the various configurations were combined to construct the *K* matrix (Equation 2.23). The linear system of equations (Equation 2.2.4) was solved using the *optim* function in R (R development core team 2004) as a least squares minimisation problem. The initial guess for the conductivity profile was based on the mean of all conductivity values for the predicted layers. To constrain the prediction to positive EC values, the EC predictions were shifted by the absolute value of the minimum prediction for the profile if negative values occurred. Finally, to generate 20, 0.5 m thick layers from the 8 variably-thick predictions, the values were coerced into a 20 element vector using the smooth.spline function in R (R development core team 2004) using a spar of 0.5. This procedure was constrained by lower and upper bounds of 1 and 500 mS m^{-1}, respectively. This procedure is analogous to that used by Vervoort and Annen (2006).

For the Tikhonov regularisation methods, homogeneous layers of equal thickness at 0.5 m intervals were predicted down to ten metres. The choice in layers is based on the location of soil samples for calibrating the model, in accordance with similar studies (Borchers et al., 1997; Vervoort and Annen, 2006). The inversion process was implemented following code previously described by Borchers et al. (1997) and Vervoort et al. (2006) using the same *K* matrix, but with L derivative operators of 0, 1, and 2 (Equation 5.1). The *optim* procedure in R was again used to solve the minimisation of Equation 2.24. Unlike the McNeill method the Tikhonov regularisation uses a penalty function, based on the derivative operator, to smooth the profile:

$$L_0 = \begin{bmatrix} 1 & 0 & 0 & & \\ 0 & 1 & 0 & & \\ & & \cdots & & \\ & & & \cdots & \\ & & 0 & 0 & 1 \end{bmatrix}$$

$$L_1 = \begin{bmatrix} 1 & -1 & 0 & & & \\ 0 & 1 & -1 & & & \\ & & \cdots & & & \\ & & & \cdots & & \\ & & & 0 & 1 & -1 \end{bmatrix}$$

$$L_2 = \begin{bmatrix} 1 & -2 & 1 & & & & \\ & 1 & -2 & 1 & & & \\ & & & \cdots & & & \\ & & & & \cdots & & \\ & & & & & 1 & -2 & 1 \end{bmatrix} \quad (5.1)$$

The L-curve operator smooths the profile based on the minimisation of the predicted electrical conductivity layers and the derivative operator function, where the two functions are plotted against each other (Figure 5.2). A general cross validation (GCV) function was used to find the point of maximum curvature for the plot. The 0th and 2nd order regularisation methods produced clear minimums in the GCV curve. However, the 1st order regularisation method failed to produce the characteristic L-curve and minimum. For this reason, the point of maximum curvature was found using the maximum of the second derivative of the L-curve (Figure 5.2).

To compare the effectiveness of the inversion processes, a forward model of EC_a was calculated based on the soil properties from the deep cores. This process, which follows from Rhoades et al. (1989a) calculates EC_a based on several soil properties:

$$EC_a = \left[\frac{(\theta_S + \theta_{WS})^2 EC_{WS} EC_S}{\theta_S EC_{WS} + (\theta_{WS}) EC_S} \right] + (\theta_W - \theta_{WS}) EC_{WS} \quad (5.2)$$

Based on the assumptions outlined in Teliatnikov (1998),
θ_S – volumetric fraction of soil solid
θ_W – volumetric water content
θ_{WS} – volumetric water content in small discontinuous pores
θ_{WC} – volumetric water content in large continuous pores
EC_s – electrical conductivity of solid phase
EC_{WS} - electrical conductivity of θ_{WS}

EC_{WC} – electrical conductivity of θ_{WC}
EC_W – electrical conductivity of θ_W

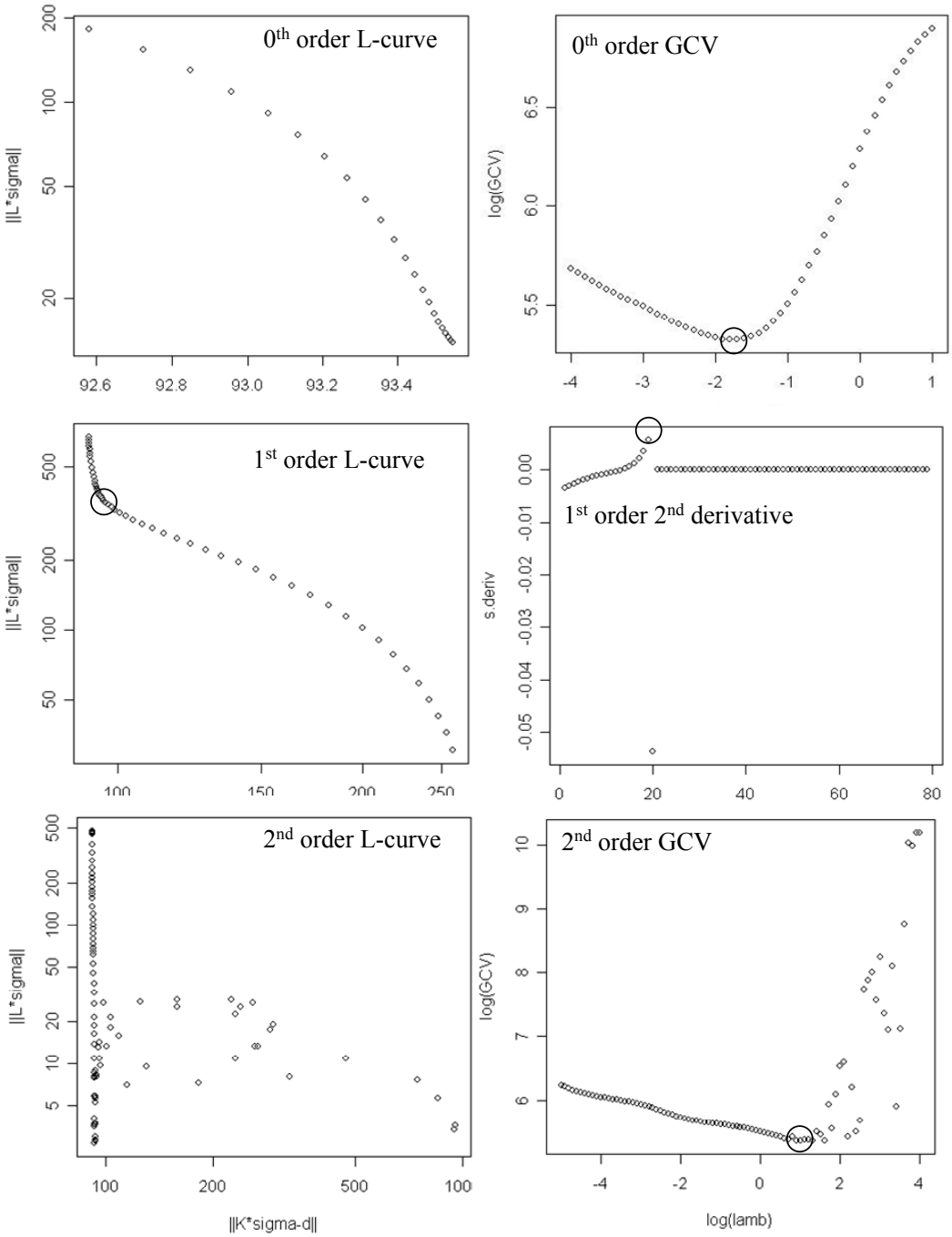

Figure 5.2. Examples of L-curves for the same location using the 0th, 1st and 2nd order Tikhonov methods. Solutions for the minimisation problem for the 0th and 2nd order regularisation are both are circled. In the 1st order curve, the maximum of the second derivative was used to find the solution (circled).

5.1.5 Results

The inverted electrical conductivity predictions, *EC,* from the apparent electrical conductivity measurements, EC_a, differed for each of the four methods. During the model simulation, the McNeill method appeared unstable and often predicted highly oscillating electrical conductivities. These predictions were subsequently constrained by the lower bounds in the smoothing operation. They were then transformed by the addition of the absolute value of the lowest prediction, which resulted in the translation of the profiles by 5.8 to 29 mS m^{-1}. Without this translation, a large portion of predicted values would appear at the estimated lower bound (1 mS m^{-1}).

Comparing the vertical EC trends with the EC_a predictions from the forward model (Figure 5.3) the McNeill method closely resembled the measured EC_a in Well 1, but in other wells did not reflect the trend. Although the McNeill inversion method was not significantly correlated to EC_a over the modelled area (Figure 5.4), it was more strongly correlated with several soil physical properties than the 1st and 2nd order methods, including silt, clay, and coarse sand (Table 5-1).

Table 5-1. Soil properties related to EC predictions from the four inversion methods. Bolded text denotes the best predictor for each property. In general, the most regularised method (Tikh 2) more closely related to the soil properties which vary smoothly in the profile, while the 0th order regularisation method was a better predictor of most of the physical soil properties.

soil		Tikh 0		Tikh 1		Tikh 2		McNeill	
property	units	r^2	RMSE	r^2	RMSE	r^2	RMSE	r^2	RMSE
silt	(g g^{-1})	**0.16**	0.05	0.07	0.05	0.00	0.06	0.13	0.05
clay		**0.36**	0.09	0.13	0.13	0.01	0.11	0.16	0.10
c.sand		0.21	0.12	0.05	0.13	0.00	0.14	**0.26**	0.12
f.sand		**0.06**	0.09	0.06	0.09	0.01	0.10	0.01	0.09
gravel	(%)	**0.12**	4.11	0.05	4.27	0.01	4.36	0.11	4.12
BD	(g cm^{-3})	**0.12**	0.10	0.08	0.10	0.01	0.11	0.03	0.10
pH		0.12	0.43	**0.16**	0.42	0.04	0.44	0.08	0.44
Cl	(ppm)	0.16	80.97	0.00	88.21	**0.23**	77.40	0.14	82.13
EC_a	(mS m^{-1})	**0.36**	36.6	0.16	41.8	0.34	37.0	0.03	44.9
EC_e		0.01	158.6	0.12	149.9	**0.19**	143.6	0.00	159.4

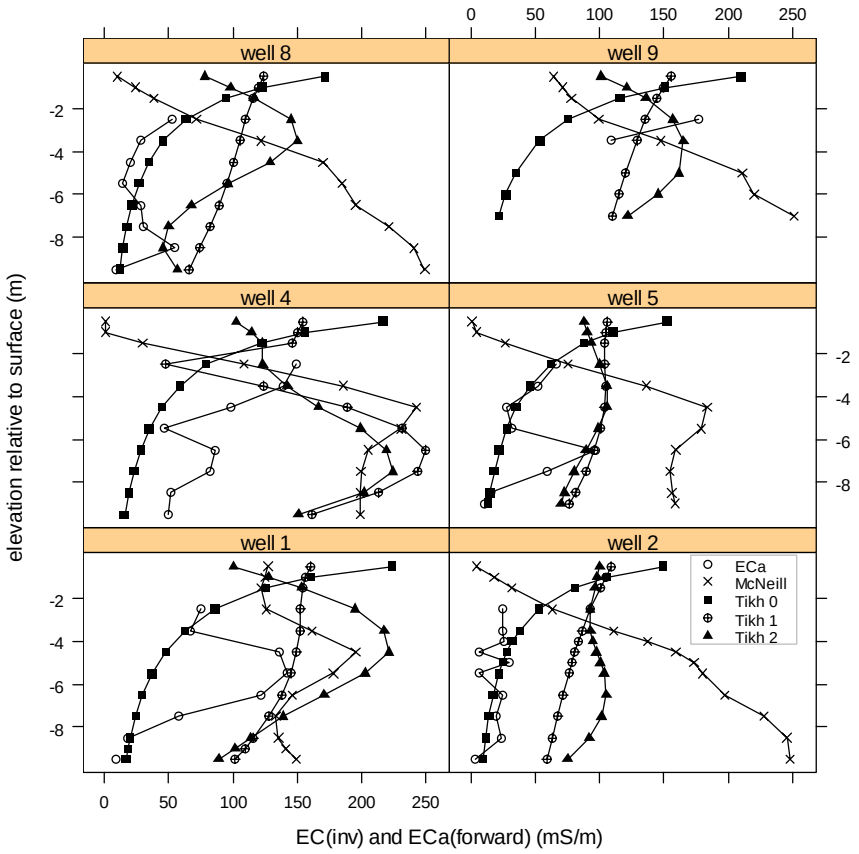

Figure 5.3. Predicted EC profiles for deep cores inside the paddock using the four inversion techniques and the forward model calculation. All techniques predict a significant change in conductivity associated with the palæochannel ($p < 0.001$).

The McNeill method produces vertical slices which are laterally discontinuous below four metres (Figure 5.5). In Transect 4, a localised low occurring in the upper metre of the profile from 40 to 70 metres along the transect reflects the presence of the palæochannel. The McNeill method also predicts a much larger range in EC throughout the profile than the regularised methods, (Figure 5.5). Method-specific transects can be found in Appendix 5.3, to compare differences between transects within each method.

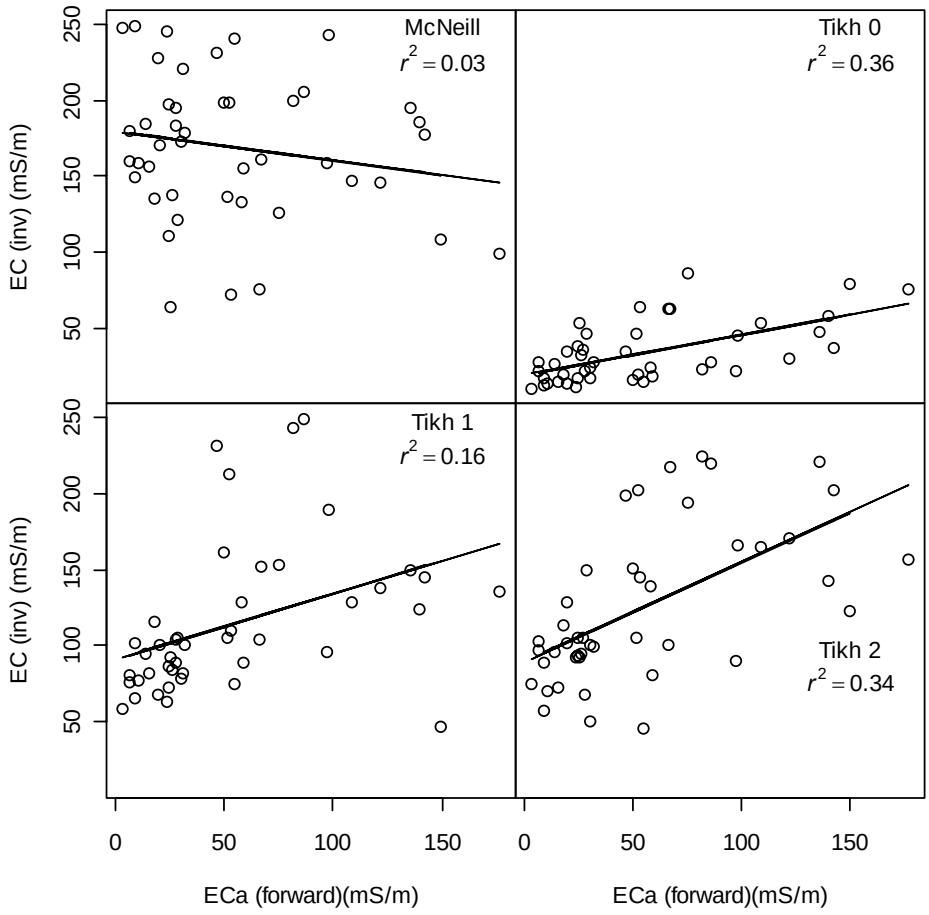

Figure 5.4. Relationships between EC from inverted EM data using the 4 inversion techniques and EC_a from the forward model calculation based on soil properties.

In many cases, the regularised methods predict EC profiles which are similar to those of the modelled EC_a (Figure 5.3). For example, the 2nd order Tikhonov regularisation method provides a close fit to the EC_a data down the profile, nearly matching the EC_e profiles in Well 1 (Figure 5.3). Using all measured points, the 2nd order method is significantly correlated to EC_a (Table 5-1). The method also predicts the presence of the palæochannel, appearing as a low conductivity region from 50 to 60 metres along Transect 4 (Figure 5.5). The channel is also associated with an asymmetrical region of high EC which pinches out towards the palæochannel.

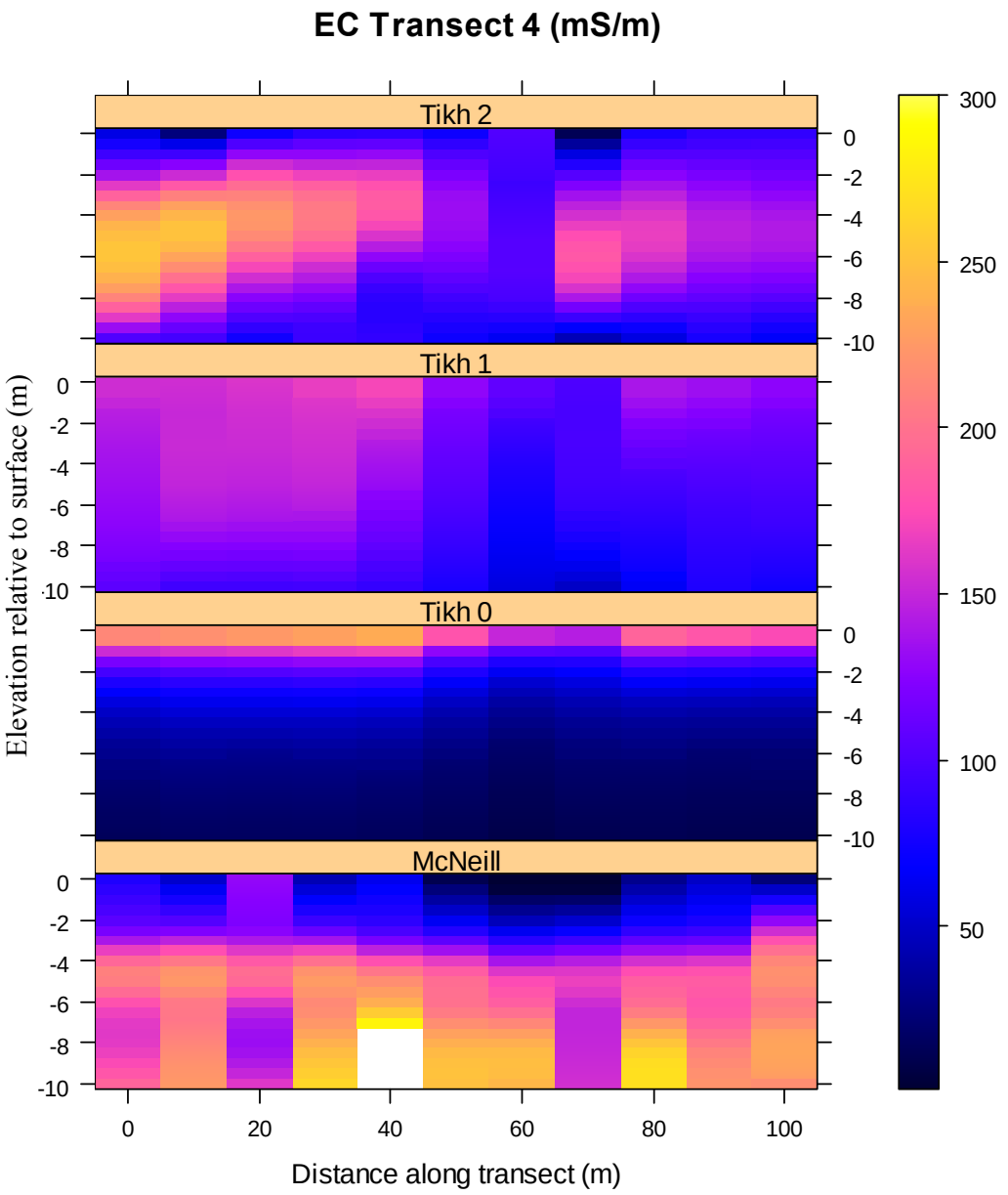

Figure 5.5. Electrical conductivity profiles for Transect 4 from the four inversion techniques. The white areas shown in the McNeill method are due to anomalously high EC predictions, which are truncated by the scale.

While the 2nd order Tikhonov methods produces results which are similar to the measured EC_a, the 1st order results are more strongly correlated with EC and pH than with any other soil property (Table 5-1). The method produces very little curvature down the profile (Figure 5.3), but predicts reasonable EC trends across Transect 4 (Figure 5.5), with low EC associated with the palæochannel and the

surrounding topsoil sediments. Similar to the 2nd order method, the method predicts a smooth lateral variation, but over a smaller range of EC.

Compared to the other regularised methods, the 0th order method appears to predict very little lateral variation in EC with the palæochannel appearing as a less conductive region occurring at 60 to 80 metres along the transect (Figure 5.5). This trend was reflected in all of the profiles with the exception of Transect 8, which did not appear to cross the palæochannel using this subset of the data (Appendix 5.2). EC predictions using this method are most strongly correlated with the EC_a from the measured soil properties (Appendix 5.1) which is reflected in the wells (Figure 5.3). In most cases, the 0th order method is the best predictor of other soil physical properties such as bulk density and soil texture (Table 5-1).

All the regularised methods predict significantly lower EC inside the palæochannel unlike the McNeill method which predicts significantly higher EC inside the channel (Table 5-2). The McNeill predictions also have the largest range and the highest coefficient of variation (75) over the study area, followed by the 0th order Tikhonov method (58).

Table 5-2. EM inversion results for points coinciding with soil sample locations. Methods are compared by column, with different populations denoted with letters (α = 0.05). Means compared inside and outside channel by row and denoted as being significantly less conductive where: * p < 0.05, ** p < 0.01, *** p < 0.001

	Study area				Inside channel		Outside channel	
method	mean	stdev	min	max	mean	stdev	mean	stdev
	mS m^{-1}							
Tikh 0	109.7a	61.2	9.6	248.8	65.3a***	50.2	127.3ab	56.1
Tikh 1	125.0b	33.9	26.4	249.4	97.2b***	18.0	135.9a	32.5
Tikh 2	110.4a	32.0	40.8	224.3	95.3b***	19.1	116.4b	34.1
McNeill	89.3c	67.0	1.0	250.8	113.7b	80.0	79.9c***	58.7

5.1.5.1 Model response to transient effects

The EM data sets from two different surveys affect the inverted predictions differently. Based on the 2nd order Tikhonov inversion, transient effects in the conductivity measurements have little effect on the predicted output. Comparing Survey 1 and Survey 5 (which have the most matched points and an 8.1 mS m^{-1} difference in the mean EC_a), the change in instrument responses result in a linear shift of predicted EC throughout the profile (Figure 5.6). Contrary to this, the McNeill method predicts a significantly different EC profile (Figure 5.6) from the prediction made from EC_a data from Survey 1 (Table 5-3, Appendix 5.3). While the regularised profiles are very similar ($r2 = 0.97$, $p < 0.001$), the McNeill profiles appear highly sensitive to transient changes and predict significantly different profiles from the two surveys ($r2 = 0.001$, $p = 0.21$). This again suggests instability of the inversion, where small fluctuations in conductivity measurements translate to large differences in the predicted electrical conductivity.

Table 5-3. Transient response comparison for the McNeill and 2nd order Tikhonov inversion methods. Comparisons made between all methods using α = 0.05

Inversion method	Survey	Mean	p5	p95
		——— mS m^{-1} ———		
McNeill	1	75.8a	68.4	83.2
	5	140.6b	133.1	148.0
Tikhonov 2	1	112.3c	104.9	120.9
	5	113.5c	106.1	119.7

5.1.6 Discussion

The McNeill layered earth model does not predict the layering observed in the field or (in most transects) the lower conductivity associated with the presence of the palæochannel. This is probably due to instability in the inversion process, and is likely the result of the large number of predicted layers. Similar results were found by Borchers et al. (1997), who suggested that 2nd order regularisation of the conductivity

predictions was needed to stabilise the inversion process. In contrast, Vervoort and Annen (2006) found that the McNeill method adequately predicted the presence of a similar palæochannel structure using the EM 38, and EM 34 instruments, and was a better predictor of most soil properties than 2nd order Tikhonov regularisation. While the use of multiple instruments may have been a large contributing factor to the different findings, it is likely that a large difference could have been due to the physical relationships between EM and the soil property of interest. The study by Borchers et al. (1997) was aimed at identifying vertical changes in soil salinity, while the study by Vervoort et al. looked at changes in the soil texture at depth, which was likely to change more rapidly.

While 2nd order Tikhonov method has been most practical for describing the distribution of dissolved salts in the soil profile (Borchers et al., 1997; Hilgendorf, 1997; Hendrickx et al., 2002), Vervoort and Annen (2006) found that the 2nd order Tikhonov method was not a significant predictor of $EC_{1:5}$, unlike the McNeill method. This is likely related to the differences in the study site. While the previous studies were performed in relatively uniform soils to a maximum depth of three metres, Vervoort and Annan (2006) used multiple instruments to detect geologic layering in a vertically discontinuous setting. The abrupt changes in the geologic properties were likely more clearly reflected in the McNeill model which is constrained by discontinuous layers determined by the instrument's depth of penetration

Considering the smooth nature of Cl and EC_e profiles on the study site (Figure 4.6), the smoother 1st and 2nd order regularisation methods appear to adequately predict these soil properties (Table 5-1). Again, this is likely due to the smoothing of the observed geologic boundaries (McBratney et al., 2000), which have a much sharper transition than the chemical properties which are continuously being transported through the soil profile through leaching and diffusion (Rhoades, 1996).

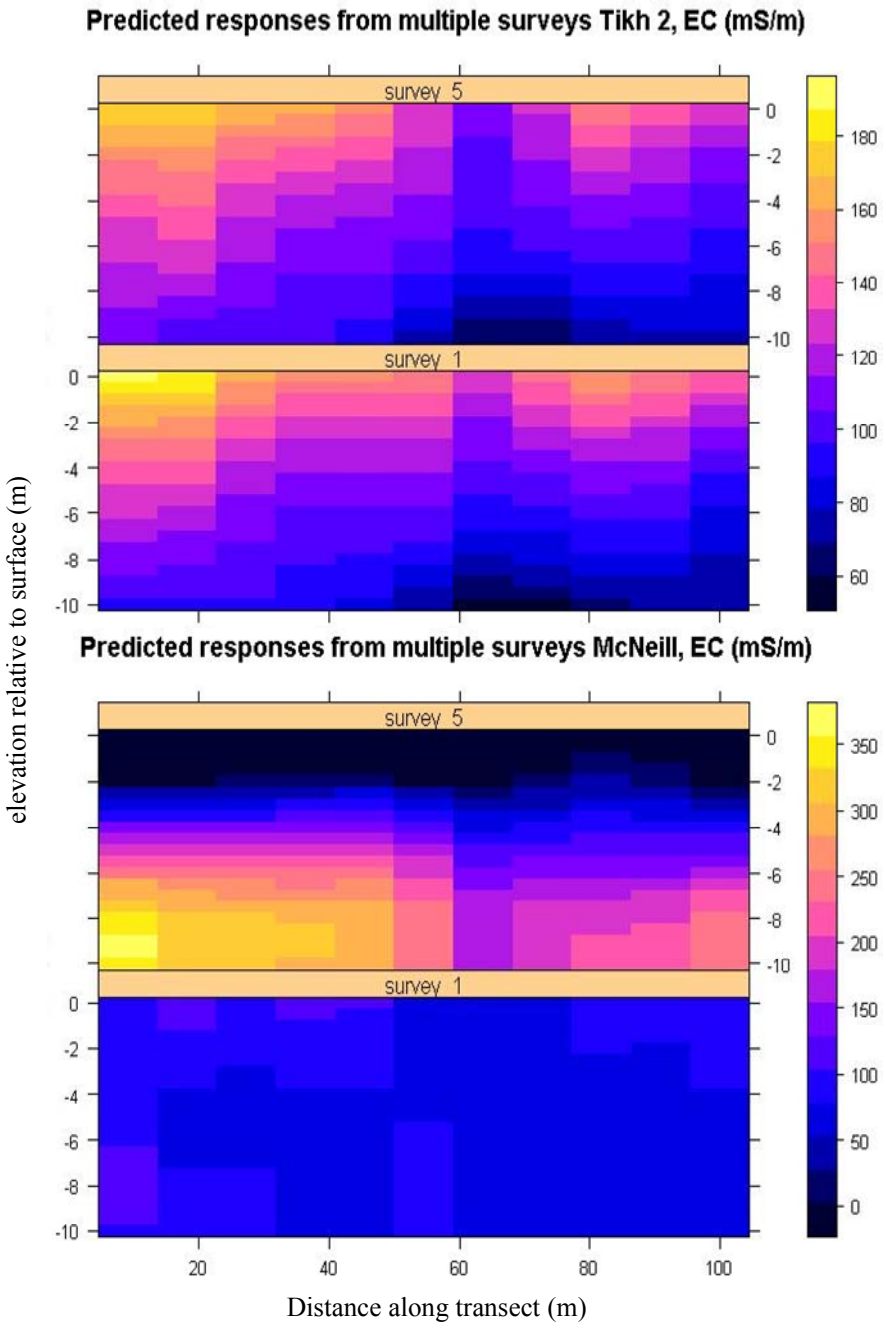

Figure 5.6. Profiles of Transect 5 showing the differences in the predicted electrical conductivity using the regularised (Tikhonov 2nd order) and non-regularised (McNeill) inversion methods from Survey 1 and Survey 5.

Contrary to this, the 0^{th} order regularisation method which appeared smoother (likely due to high predicted EC in the topsoil) (Figure 5.5) is the strongest predictor of EC_a. The method is also significantly correlated with clay content (Figure 5.4), and only weakly correlated with EC_e (Table 5-1). This indicates that it is a better predictor of the soil physical properties, and hence the geologic boundaries. This is similar to the results found by McBratney et al. (2000), where 0^{th} order regularisation outperformed the 1^{st}, 2^{nd}, and 3^{rd} order regularisation orders in predicting soil boundaries.

Unlike the majority of studies which have used synthetic EM data (Gomez-Trevino et al., 2002; Deidda et al., 2003), or data from only one instrument (Borchers et al., 1997; Hilgendorf, 1997; Hendrickx et al., 2002), Vervoort and Annen (2006) used the 2^{nd} order Tikhonov method to regularise EC_a data from multiple instruments, which is a more realistic comparison. It is possible that this combination of instruments are better suited for this environment, or that the large number of measurements made in this study lead to an over-conditioned solution (Hilgendorf, 1997).

This could point to the difficulty with using data from multiple instruments, where the error term in each profile is correlated to depth, nullifying an assumption in the inversion process (Aster et al., 2005). Errors inherent in each of the instruments are due to the instrument electronics) and the geometry of the coil spacing. Compared to the other instruments, the EM 34 has a much coarser resolution and contains more instrument noise, meaning that the measurements are more likely to include larger errors, even though they have the same accuracy (

Table 5-4). The large footprint of the EM 34 means that signal response should be sufficiently dampened due to the averaging affects of the soil EC_a over the much larger volume measured (Table 4-10). The inversion model is therefore highly sensitive to this information, where small changes in the averaged EC_a could be the result of large changes in one or several of the layers predicted using this data (Aster et al., 2005).

Table 5-4. Manufacturer reported precision, accuracy and noise, over the effective range of each of the Geonics instruments. In this case the EM 34 instrument is twice as noisy as the EM 31, and has a much coarser resolution (likely due to the analogue interface).

Instrument	Range	Instrument noise	Precision (full range)	Accuracy (range)
	—— mS m^{-1} ——		——— % ———	
EM 38	1000	0.5	0.1	5 (30 mS m^{-1})
EM 31	1000	0.1	0.1	5 (20 mS m^{-1})
EM 34	1000	0.2	2.0	5 (20 mS m^{-1})

5.2 The prediction of K_{sat} fields

Saturated conductivity (K_{sat}) is one of the most variable and difficult to measure soil properties, and is also the most important predictor of water flow in soil and groundwater (McKenzie and Jacquier, 1997). Generally, three different strategies have been employed to describe the variation of K_{sat} across the field using ancillary data (such as geophysical surveys). The ancillary data has been used to identify hydraulically important features (e.g. aquifers) (Cook et al., 1989b; Rogers et al., 2002), shape the stochastic distribution of K_{sat} (which is assumed to relate to the geophysical measurement) (Hubbard et al., 1999; Kowalsky et al., 2005), or directly estimate K_{sat} through regression analysis (such as regression kriging) (de Lima and Niwas, 2000; Garambois et al., 2002; Vervoort and Annen, 2006). Whereas the stochastic procedures are only computationally expensive, they are (by definition) more uncertain. Regression kriging contains much more information but is therefore, more costly. This study aims to minimise the uncertainty of stochastic prediction and expense of regression kriging by using geophysical data to predict K_{sat} from a limited number of cores based on previously observed relationships between the two properties.

Apparent electrical conductivity measurements made using electromagnetic induction techniques are often correlated with soil physical properties such as clay content (Williams and Hoey, 1987; Doolittle et al., 1994; Triantafilis and Lesch, 2005). Clay content can also be used to predict saturated conductivity, through the use of pedotransfer functions (Schaap and Leij, 1998; Minasny and McBratney, 2000; Schaap et al., 2001). In this study, the 0^{th} and 1^{st} order regularised predictions are significantly and positively correlated to clay content (Appendix 5.1). Therefore,

there should be a physically-based link between saturated hydraulic conductivity and electrical conductivity at a particular scale of measurement at the field site (Section 2.6.3). In the absence of highly conductive pore fluids (i.e. greater than 700 mS m^{-1}), empirical and semi-empirical relationships between hydraulic conductivity and resistivity show a linear positive relationship between the two properties (de Lima and Niwas, 2000; Niwas and de Lima, 2003).

Based on these assumptions, a scaling approach can be developed which uses the geophysical data to shape the distribution of K_{sat} values from a limited number of soil property measurements. This strategy follows a similar approach of using scaling factors to upscale capillary flow predictions in sediments (Miller and Miller, 1956).

If the scaling factors are linked to one reference K value, problems using the linear scaling approach might occur. For example, the K_{sat} of the low EC regions might be underpredicted if the reference K is chosen from the high clay regions, or the K_{sat} of the high EC regions might be overpredicted if the reference K is chosen from the low clay regions. Furthermore, in a multi-modal system (such as this one), the mean of any soil property has little physical significance. For this reason, the particle size clusters were used to define geologic units, which each have a reference K_{sat}.

It is also likely that a physically-defined minimum and maximum K_{sat} value exists, which is related to the sediment properties (and subsequently linked to predicted EC). Therefore, a third scaling factor approach examines the possibility of using a logistic curve to limit the range in predictions (Triantafilis et al., 2000).

5.2.1 Scaling factor assumptions

The scaling factor approach to predict K_{sat} from EC relies on several assumptions. These are primarily based on the physical relationship between the properties, differences in support scale from the methods, and temporal variation in the soil properties.

Relationship between EC and K_{sat}

A clear relationship between clay content and K_{sat} exists at the field site (Figure 5.7). In theoretical and laboratory studies, linear relationships between $\log K_{sat}$ and EC have also been demonstrated (de Lima and Niwas, 2000; Niwas and de Lima, 2003). Laboratory investigations of this relationship show that the linearity of this

relationship is dependant on the pore water quality and quantity (Nadler and Frenkel, 1980; Taylor and Barker, 2002), however a strong correlation between the properties exists under most conditions based on the relationship between Darcy's and Ohm's laws. Matching the EC profiles to the K_{sat} data, a similar relationship is observed (Figure 5.8) with a lower limit occurring at approximately 3.16 cm day^{-1} and an upper limit occurring at 316.2 cm day^{-1}. Considering the relationship between clay content and apparent electrical conductivity, a characteristic "S" curve should describe the relationship between K_{sat} and EC_a (Figure 5.7).

Homogeneous moisture distribution

Because the EM instruments are being used quantitatively to predict saturated conductivity, various assumptions must be made about other contributing factors to the electrical conductivity. This model assumes that there is a relationship between EC_a, clay content, which is linked to CEC, and saturated hydraulic conductivity. However, other factors in this relationship which are not related to saturated hydraulic conductivity include temperature, moisture content, pore fluid EC and magnetic permeability (McNeill, 1980a). Considering the observed water table fluctuations (Figure 4.13), the most influential of these properties on the field site is likely to be volumetric water content. In this study, the electrical conductivity was significantly different at different times of the year (Figure 4.19) which was further compounded by the inversion process (Figure 5.6). This would translate to changes in the predicted hydraulic conductivity, due to the change in the scaling factor. The observed shift in predicted EC between surveys (Table 4-9), resulted in a range of 38.7 mS m^{-1}, over several seasons. Compared to the 150 mS m^{-1} range in EC_a values over the field (using the ground-based measurements), this factor is relatively small, but significant (26% of the observed variation).

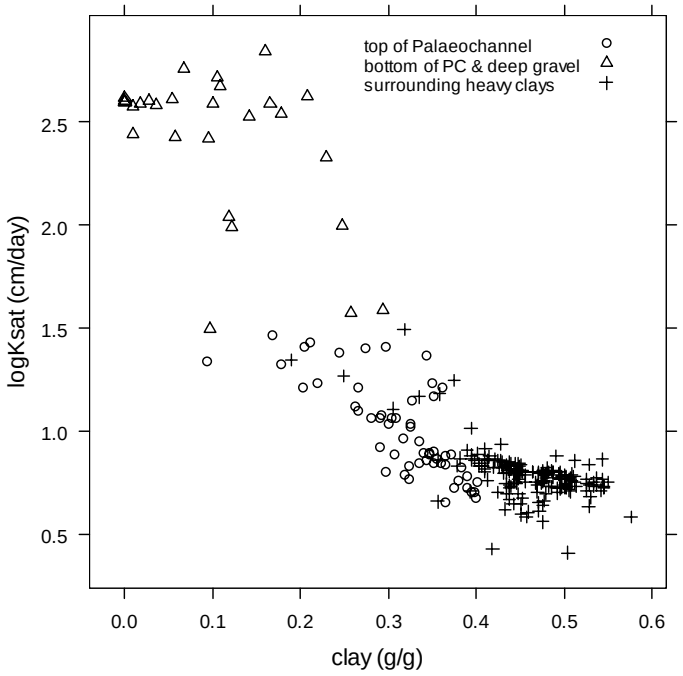

Figure 5.7. Relationship between $logK_{sat}$ as predicted from Neurotheta, and clay content for all soil data. This plot reveals an "S" shape relationship which has a minimum of 3.1 cm day^{-1}, and a maximum of 316.2 cm day^{-1}, where the minimum is defined by the heavy clay sediments and the maximum defined by the coarse sand deposits.

5.2.2 Scaling model

5.2.2.1 Methods

The inverted EC data were used to generate scaling factors in three ways. The first, herein referred to as "scaling without clusters", was based on the assumption that there was an inverse relationship between EC and the scaling factors. The scaling factor multiplier then determined the distribution of the K_{sat} values, following (Miller and Miller, 1956) where:

$$\log(K_{sat(predicted)}) = \lambda \times (\log(K_{ref(ptf-derived)})) \quad (5.3)$$

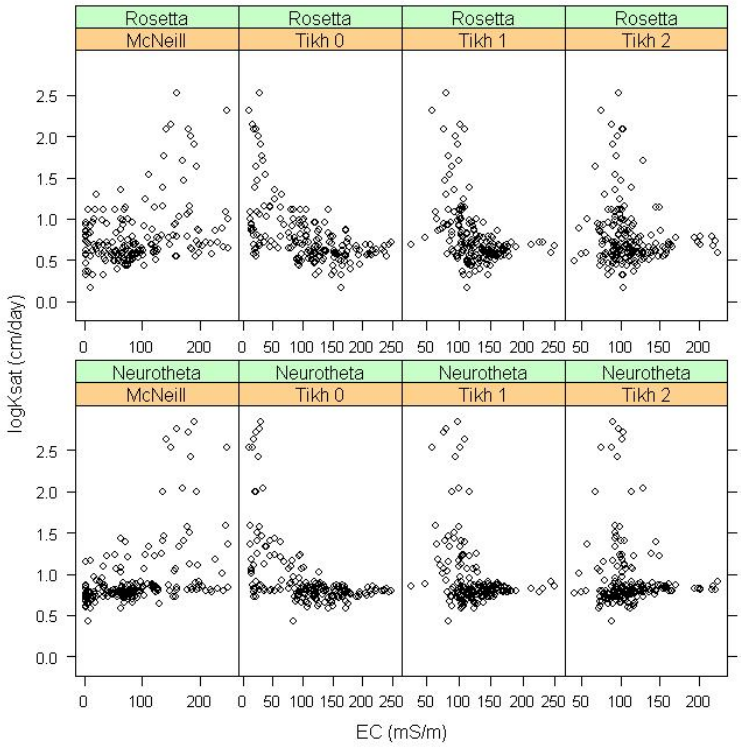

Figure 5.8. Relationship between EC from the inverted EC_a profiles and log K_{sat} from the two pedotransfer function software packages.

In this case, a reference K_{sat} (6.6 cm day^{-1}) was chosen based on the average log(K_{sat}) of all measurements made inside the paddock. This was considered appropriate because samples outside the paddock were disproportionally skewed towards the deep sediments (including the coarse-textured Narrabri Formation below ten metres). Although a log transform was applied to the conductivity values (Figure 4.11) the values were still highly skewed towards the palæochannel deposit. Therefor, it is possible that the reference K_{sat} value may overestimate the field hydraulic conductivity.

The scaling factor λ at any point is based on the distribution of EC measurements. In the linear model, λ is calculated as:

$$\lambda = \frac{1}{\mathrm{EC}} \times \left[mean\left(\frac{1}{EC} \right) \right]^{-1} \tag{5.4}$$

This scaling factor is based on the relationship found in prior studies where $K_{sat} = EC^{-1}$ (de Lima and Niwas, 2000; Niwas and de Lima, 2003) under the

assumption that EC (derived from inverted electromagnetic induction measurements) is inversely related to resistivity (derived from a direct current source). The scaling factor is further divided by the mean of EC^{-1} to produce a distribution with a mean of 1 (assuming that the mean EC^{-1} coincides with the reference K_{sat} value).

Because the distribution of measured $\log(K_{sat})$ (Figure 4.11), and EC_a values (Figure 4.16) were trimodal and highly skewed, it may be inappropriate to define the K_{ref} based on the mean of the K_{sat} predictions. Based on the assumption that three distinct geologic units exist, each with its own distribution of K_{sat} values (Figure 5.7), this relationship produces three distinctly different slopes for the linear model. This procedure therefore mimics the generation of hydrological response units using scaling factor approaches (Becker and Braun, 1999), which has been an effective way to address heterogeneity in complex systems (Teles et al., 2004). The model was fit through the three generated clusters separately, where:

$$\begin{aligned} K_{sat_{Cluster1}} &= \lambda_1 \times K_{ref_1} \\ K_{sat_{Cluster2}} &= \lambda_2 \times K_{ref_2} \\ K_{sat_{Cluster3}} &= \lambda_3 \times K_{ref_3} \end{aligned} \tag{5.5}$$

In this instance, K_{refi} is based on the average $\log(K_{sat})$ within the cluster, which was previously defined from the particle size data (Figure 4.11). The three K_{ref} values used were 6, 10.7, and 12.0 cm day^{-1}. The scaling factors were based on the clustered EC data, where the average EC value for each cluster λ_i is assumed to coincide with $K_{ref(i)}$ for the cluster.

A third scaling factor model was developed based on upper and lower limits in the predicted K_{sat} estimates, defined by the range of EC data. This relationship is physically based on the assumption that the limit as K_{sat} approaches the maximum value corresponds to the electrical conductivity of the least conductive material, in this case coarse sand. The lower K_{sat} limit is conversely bound by the highest electrical conductivity (in this case, the most clay-rich sediments). These limits impose an S-shape curve, with horizontal asymptotes defined by the minimum and maximum EC. It reflects the relationship between K_{sat} and clay (Figure 5.7) and that between EC and clay for the 0^{th} and 1^{st} order Tikhonov profiles (Appendix 5.1). This relationship is shown in Figure 5.8.

The scaling factor λ was based on a logistic function:

$$\lambda = 2 + \frac{2}{1 + e^{-\left[\frac{EC - m}{s}\right]}} \tag{5.6}$$

where:

$m = \text{mean}(EC)$
$s = \text{mean}(EC) - \min(EC)$

The parameters m and s control the mean and slope of the S-curve, respectively, and were empirically fit to the data. Theoretically, s should reflect the range of conductivity values (i.e. max(EC) – min(EC)), however this resulted in an unrealistical steeply-sloping curve which created a highly bimodal distribution with most values occurring at the upper and lower bounds.

The scaling relationships for the four inversion methods and the three scaling factors methods show that the maximum scaling factor for the clusters is less than without clusters and greater than the logistic curve (Figure 5.9). The shape of the curves depends on the distribution of EC values. Where the McNeill and 0^{th} order Tikhonov methods produce steeply-sloping curves, the 1^{st} and 2^{nd} order Tikhonov results are nearly linear. This is due to the skewed EC distribution in the two least regularised methods, compared to normal distributions in the other two methods (Figure 5.10). The scaling factor of 10 (in the case of the non clustered McNeill method) is unrealistic, resulting in a maximum hydraulic conductivity of 2.0×10^{10} cm day^{-1}. In all cases, the prediction ranges were constrained by the three clusters and the logistic function, where the range of the single linear scaling factor is greater than the three linear factors which is greater than the logistic scaling factors.

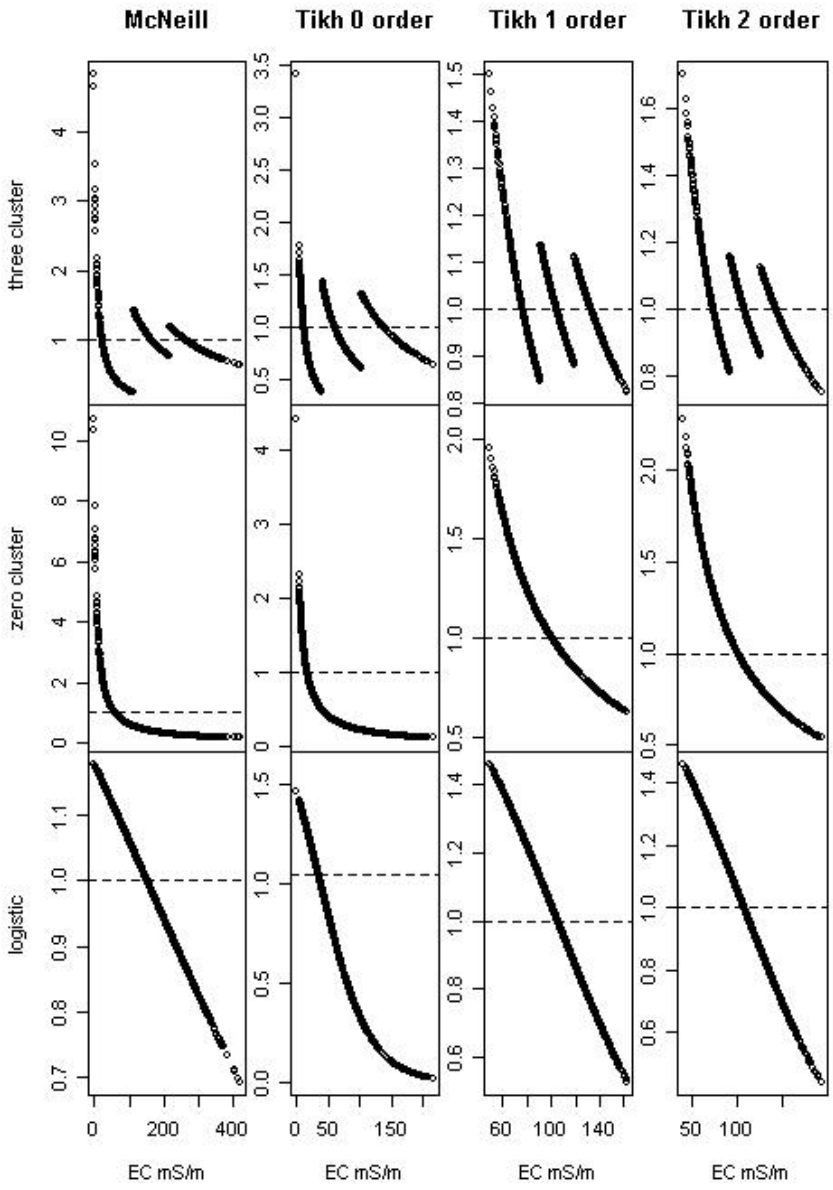

Figure 5.9. Scaling relationships from the four inversion techniques. Dashed line shows the mean of the scaling relationship, which is generally close to 1. The relationship shows the inflation of the scaling factors in the McNeill and Tikhonov 0th order methods, due to the large range of EC predictions in those methods.

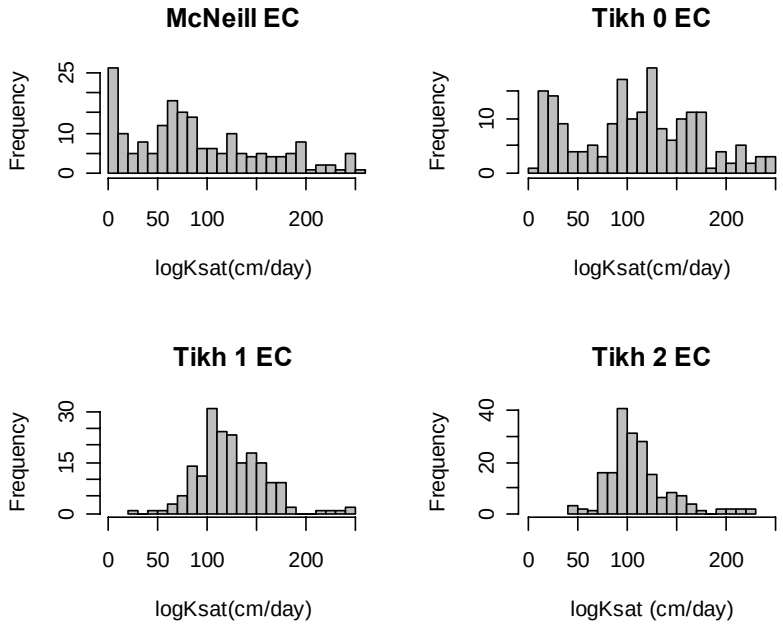

Figure 5.10. EC distribution from the four inversion techniques, using the sampled locations. The large number of prediction at the lower bounds is apparent in the McNeill method. Both the 0^{th} order and McNeill methods produce trimodal distributions similar to those from ptf-derived K_{sat}, while the 1^{st} and 2^{nd} order methods appear normally distributed.

5.2.2.2 Results and discussion

The distribution of predicted K_{sat} is highly influenced by the different scaling factors and inversion methods. Compared to the distribution of measured soil properties, most of the methods fall within the range of measured K_{sat} (Figure 5.11). The non-clustered method consistently predicts the left-skewed distribution from the measured properties, but does not appear to predict the range of K_{sat} values observed in the cores. The clustered method appears to most accurately predict the mean K_{sat} values (Table 5-5), while the logistic approach overpredicts the presence of coarse-textured sediments. The means of the predictions were significantly different from the measured soil properties in 7 of the 12 methods used (Table 5-5). The McNeill K_{sat} values from the clustered and non-clustered methods are several orders of magnitude greater than the measured properties, but show similar trends, while the logistic model did predict values which were similar to the measured soil properties (Figure 5.11).

Table 5-5. Means and 5% confidence limits for the predicted saturated conductivity values from the various methods at sampled locations. Statistical comparisons are based on Dunnett's t-test using the measured properties as the control. Bolded text is not significantly different from the Neurotheta predictions (α = 0.05).

	Method	Mean	p5	p95	Dunnett's t-test
		– log K_{sat} (cm day^{-1}) –			p value
McNeill	Clustered	1.32	1.11	1.53	0.001
	Logistic	**1.01**	**1.00**	**1.02**	**0.998**
	No cluster	1.92	1.50	2.34	0.000
Tikh 0	**Clustered**	**0.87**	**0.84**	**0.91**	**0.995**
	Logistic	0.80	0.71	0.88	0.641
	No cluster	0.46	0.40	0.53	0.000
Tikh 1	**Clustered**	**0.92**	**0.89**	**0.95**	**1.000**
	Logistic	1.22	1.18	1.25	0.048
	No cluster	0.83	0.79	0.87	0.878
Tikh 2	**Clustered**	**0.97**	**0.94**	**0.99**	**1.000**
	Logistic	1.39	1.37	1.42	0.000
	No cluster	**0.95**	**0.91**	**0.99**	**1.000**
Neurotheta		0.94	0.88	1.00	1.000

As would be expected from the inversion results, the McNeill method predicts unrealistic saturated conductivity values which range from 1.4 to 6.0×10^9 cm day^{-1}. The extremely high values correspond to the low EC measurements, where the lower bounds had constrained the prediction to 1 (Figure 5.10). Disregarding the anomalously high K_{sat} values (appearing as white, Figure 5.12), the K_{sat} prediction shows similar trends as the EC predictions (Figure 5.6) where high K_{sat} occurs in the topsoil above the palæochannel, but with little indication of the palæochannel presence in the profile.

The regularised methods all produced reasonable predictions of K_{sat}, which varied mostly in their smoothness, normality and range (Figure 5.12, 5.13, 5.14). The 0^{th} order Tikhonov method has a strong vertical trend throughout the profiles. Because of this, the palæochannel presence does not contrast as greatly as the 1^{st} and 2^{nd} order methods which produce clear contrasts over a smaller range of values (Figure 5.12).

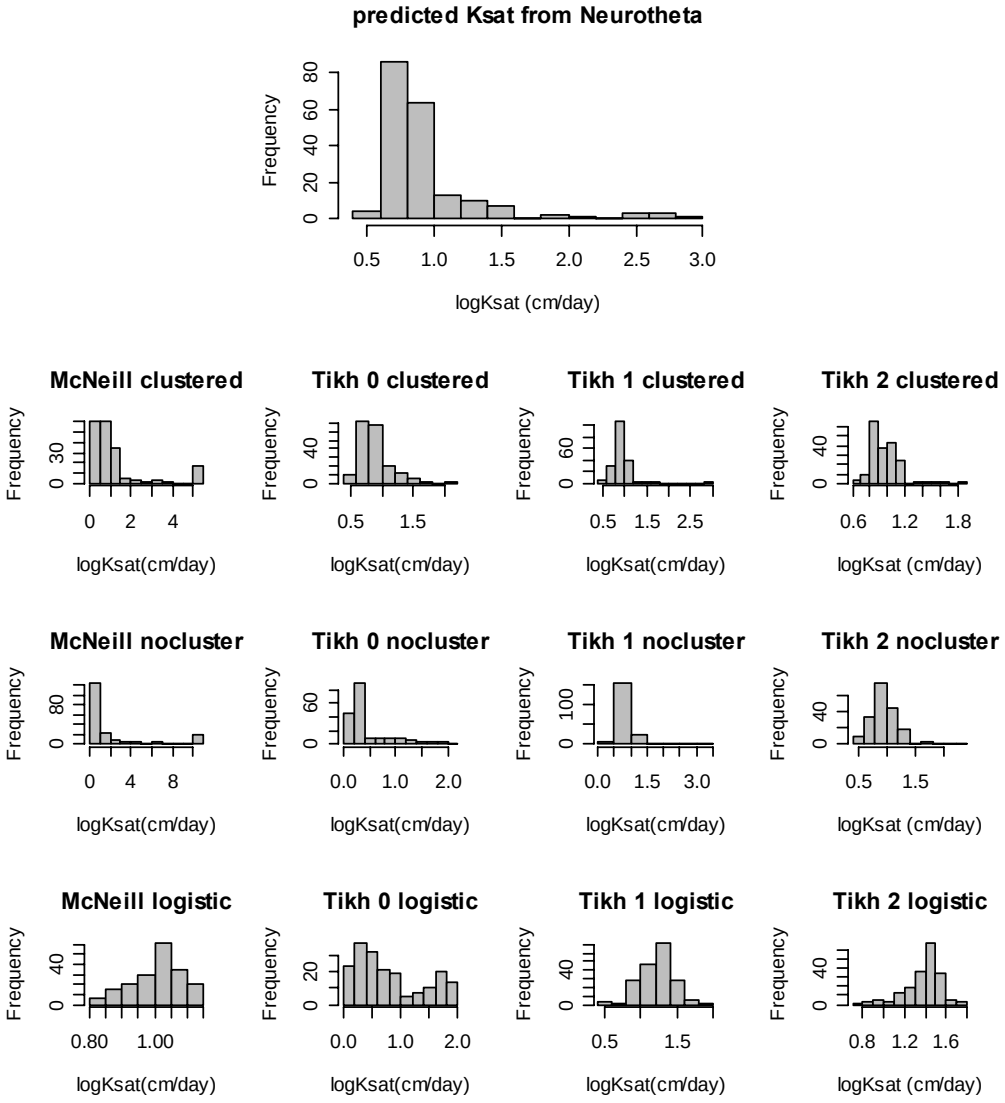

Figure 5.11. Distribution of predicted K_{sat} from points with soil property measurements. In general, most of the methods predict the right-skewed distribution from the ptf-derived soil properties.

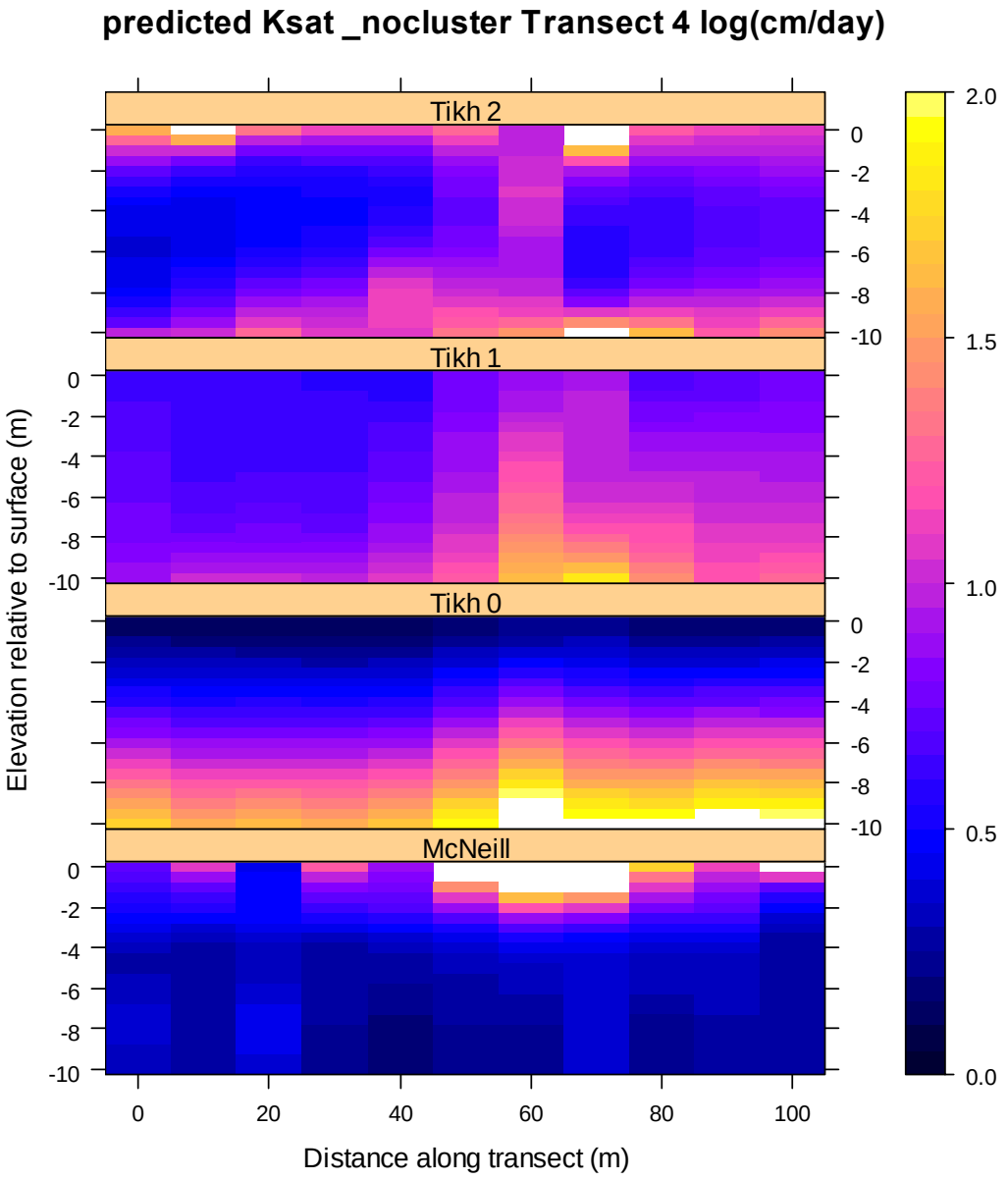

Figure 5.12. Results from the non clustered scaling method for Transect 4. The McNeill scaling method produces unrealistic saturated conductivity values of $10x10^{9}$ cm day^{-1}. Due to this, the scale maximum is set at 2.5 cm day^{-1}, with greater values appearing as white.

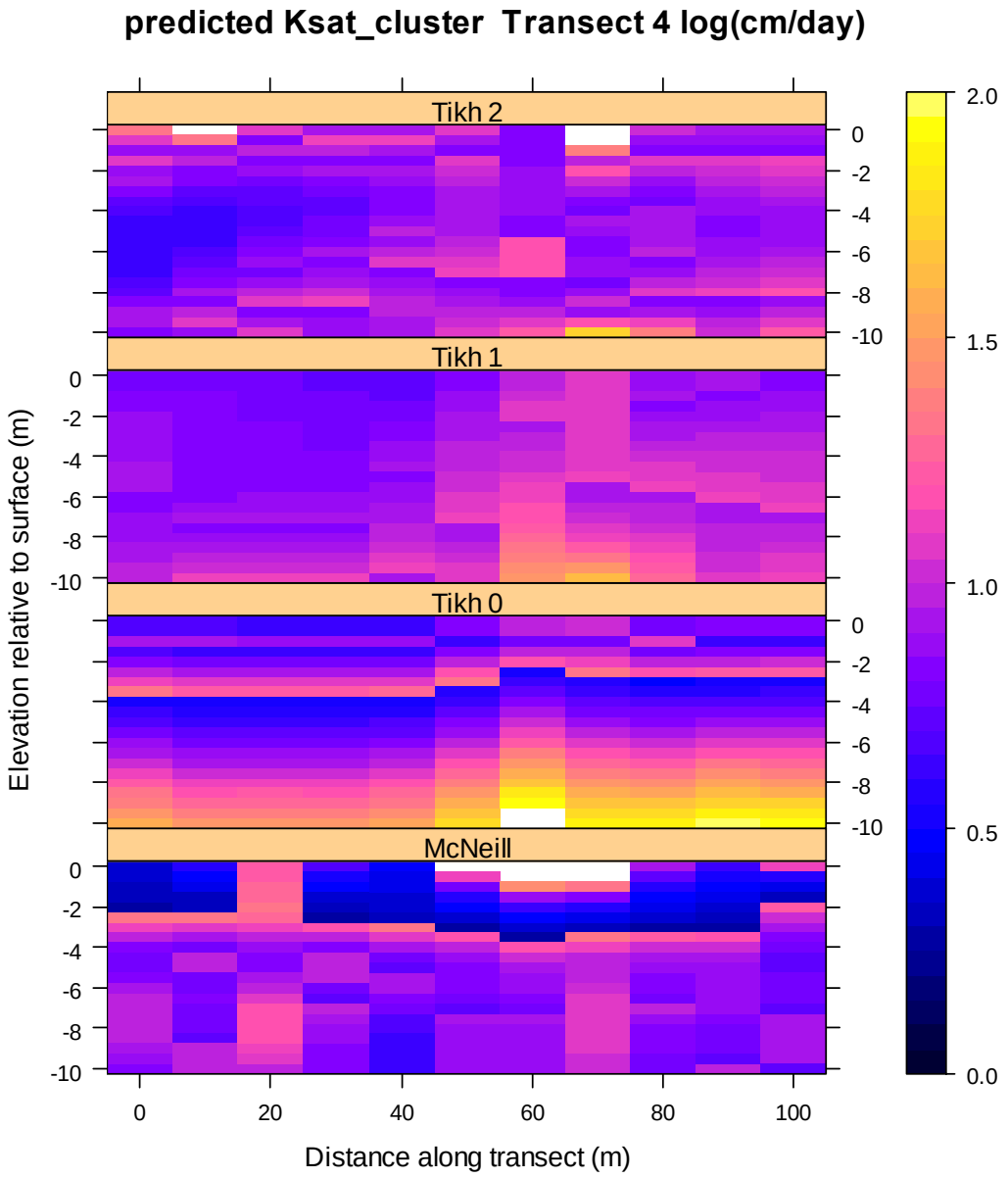

Figure 5.13. Predicted saturated conductivity of Transect 4 using the clustered scaling factors approach. Similar to the other linear scaling approach, the McNeill method produces unrealistic K_{sat} predictions (values above $\log K_{sat} = 2.5$ shown as white).

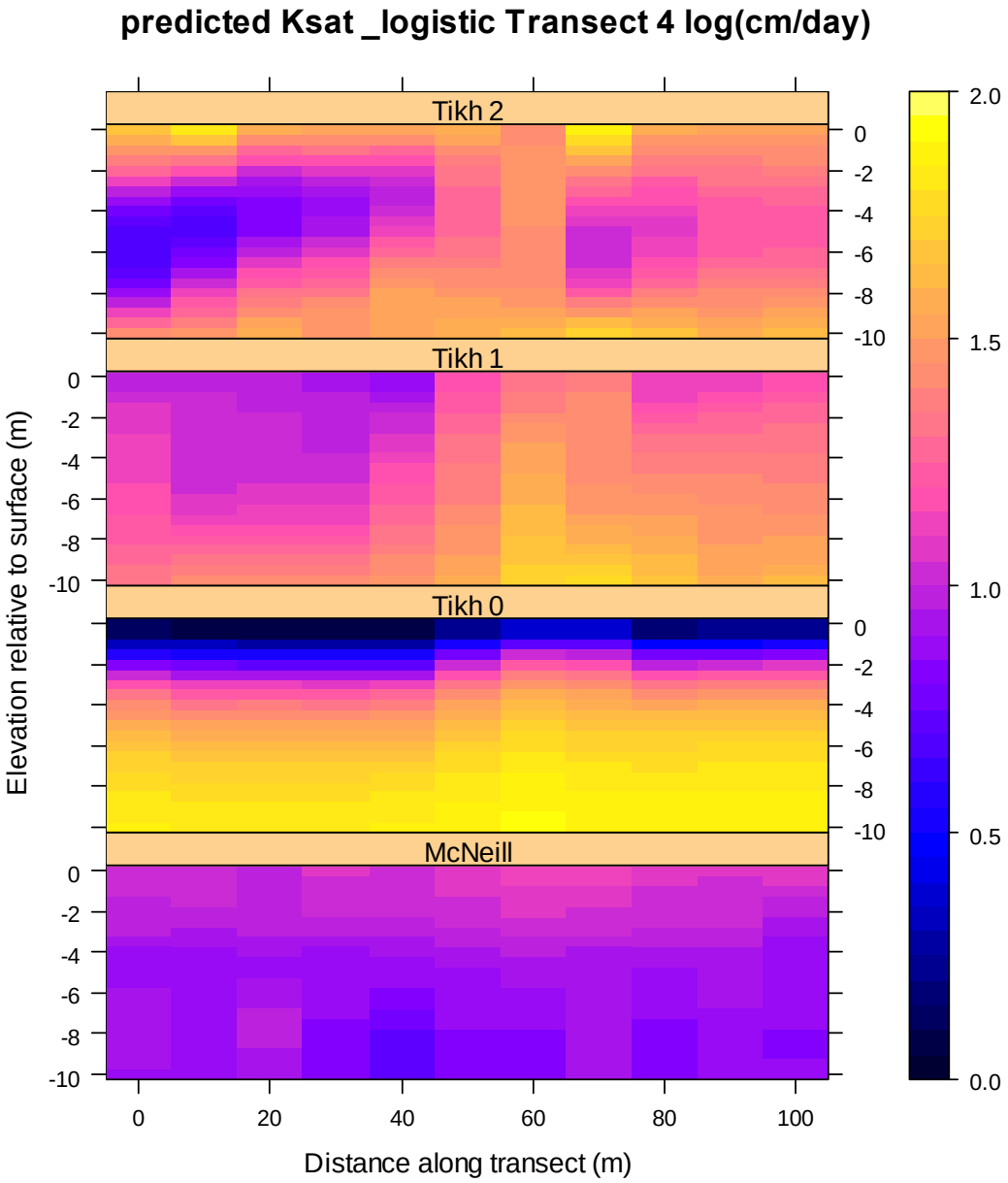

Figure 5.14. K_{at} predictions from various inverstion algorihms using the logistic scaling method.

The addition of geologic clusters imposed distinct boundaries in the K_{sat} fields, particularly in the 0^{th} order method (Figure 5.13). This is because the scaling factor relationships for the clusters lack coherence. Given the strong vertical trend in the data, this creates discontinuities at the cluster boundaries. The same is true for the McNeill method. Although these trends are not as apparent in the 1^{st} and 2^{nd} order methods (Figure 5.13), the clustering method does not improve the relationship between the scaling factors and pedotransfer function-predicted saturated conductivity values. The three regularised profiles all predict the presence of the palæochannel, but appear to underpredict the measured data, with the greatest range occurring in the 0^{th} order Tikhnov method (Table 5-5).

Compared to the other two approaches, the logistic scaling factor method produced very smooth profiles. The palæochannel is apparent in each of the inversion methods, although it appears to costrast the most in the 1^{st} and 2^{nd} order Tikhonov profiles. Interestingly, the McNeill method produced reasonable results using this method. In this case, the palæochannel appears as an area of higher K_{sat} occurring at the observed location along the profile. Given the unrealistic prediction generated by the McNeill inversion method, it appears that the logistic algorithm smoothed the predictions to where the outliers had a much smaller impact on the prediction of the K_{sat} fields across the transect (Figure 5.14).

Several of the predictions from scaling factor methods produced results which were linearly related to the K_{sat} predictions which were generated from measured soil properties (Figure 5.15). Of these, the 0^{th} and 1^{st} order methods give the least biased prediction of K_{sat} values, as indicted by the slopes and intercepts of the predictions (Table 5-6). The 0^{th} order relationship most closely resembles the ptf-derived properties, with the logistic and non-clustered results showing similar relationships. The McNeill method, which produced unrealistic predictions of K_{sat}, generally does not relate to those derived from soil properties (Table 5-6). Under the constrained logistic scaling approach, the model outperformed the 1^{st} and 2^{nd} order predictions using the same technique. Considering the poor relationship with the other measured soil properties, it appears that the data were coerced into the relationship with ptf-derived predications through the limits placed on the scaling relationship. However, it should be noted that the relationship gives a negative slope (Figure 5.15).

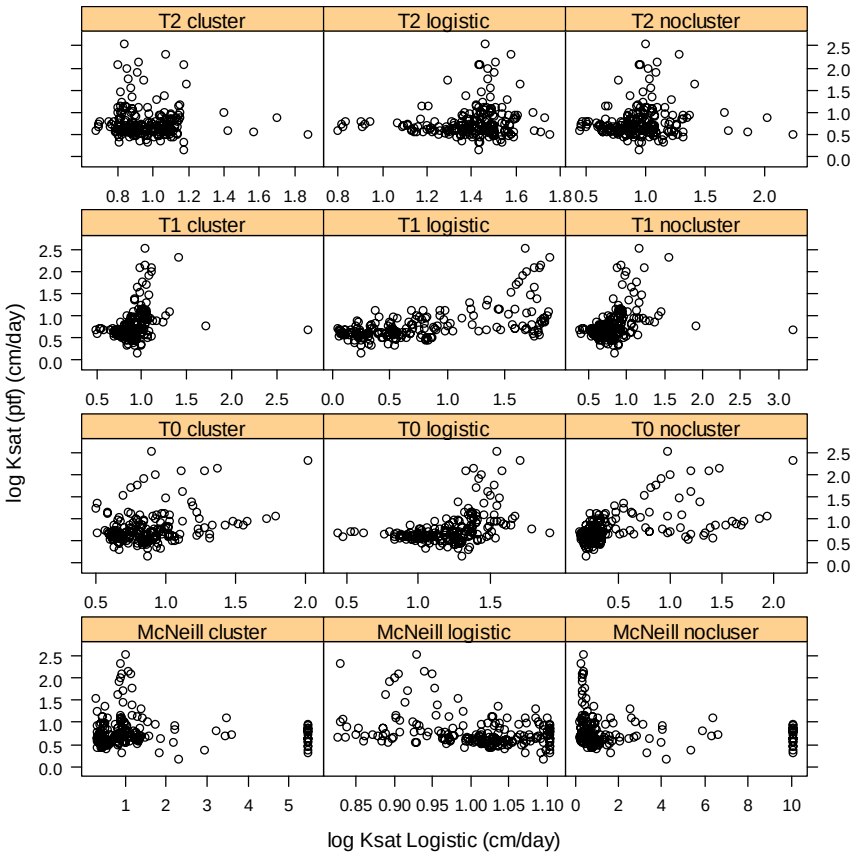

Figure 5.15. Scaling factor method compared with Neurotheta-derived predictions of saturated hydraulic conductivity.

Table 5-6 Regression analysis between the ptf-derived Ksat and predicted Ksat from the scaling approach. Bolded text denotes the best two predictors for each criteria. Slopes and intercepts are all different from 0 (p < 0.001), unless otherwise denoted, where *p > 0.05, **p > 0.01, ***p > 0.005.

Scaling method	Inversion method	r^2	RMSE	Intercept	Slope
cluster	Tikh 0	0.12	0.39	**0.43**	**0.59**
	Tikh 1	0.07	0.40	0.48	0.51
	Tikh 2	0.00	0.41	1.05*	-0.11*
	McNeill	0.02	0.41	1.00*	-0.04**
no cluster	Tikh 0	**0.34**	**0.34**	0.68	0.56
	Tikh 1	0.09	0.39	0.57*	0.45
	Tikh 2	0.01	0.41	0.82	0.12*
	McNeill	0.06	0.40	1.01	0.03
logistic	Tikh 0	**0.34**	**0.33**	0.61	0.41
	Tikh 1	0.12	0.39	**0.23**	**0.59**
	Tikh 2	0.01	0.41	0.59**	0.25
	McNeill	0.20	0.37	3.42	-2.46

5.2.3 Ordinary 3-dimensional kriging

5.2.3.1 Methods

One of the most common methods for determining the spatial outlay of soil properties at unmeasured locations is interpolation, usually using a geostatistical algorithm such as kriging. Ordinary kriging is based on the premise that spatial correlation exists between measured points. The weighting of the interpolation is based on the semivariogram, which is a plot of the change in a soil property versus the distance between measurements. This method can be performed in three dimensions, where the semivariogram incorporates lateral and vertical differences in soil properties.

Three dimensional kriging was performed on all predicted K_{sat} data using the different scaling relationships and the predictions from the pedotransfer functions. This was implemented using the *Random Fields* package in R (R core development team), which fits three dimensional variogram functions using *fitvario* to the experimental variograms generated from the data using the *EmpericalVariogram* functions. The nugget of the spherically-fitted variograms was constrained to 0, and the maximum distance for the calculation of the covariance structure was set to 150 m. This was an empirically-based decision, following from the closeness of fit of the variogram. The range and sill of the predicted variogram was fit using fitvario using standard least squares (Appendix 5.4).

Prior to this, the depth dimension was multiplied by 25 to give a similar range as the x and y coordinates due to the highly anisotropic nature of the observations (ranging from 0 – 250, 0 – 312, and 0 – 10 m in the x, y, and z directions, respectively). This same process could have been performed by specifying an elipsoidal (rather than spherical) search radius for the variogram calculation to incorporate fewer points in the z direction. While the use of an ellipsoidal search radius is more commonly performed, it was difficult to implement this feature in *R* in three dimensions. The distortion of the data set from this process is likely to affect the results further from the measured points.

Several of the inversion and scaling factor methods gave predictions which produced strong vertical trends. These methods had to be identified and detrended using a mathematical transform prior to fitting the semi-variogram. The vertical

trends were first identified by examining the three dimensional variograms, which did not produce a clear sill or range (Appendix 5.4). The 0^{th} order regularisation methods were detrended using a natural logarithm. The other logistic methods produced were only linearly related to depth, and required a simple linear transform. These data were then back transformed following the kriging process.

Three dimensional ordinary kriging was performed on the measured soil properties to describe the spatial relationship of K_{sat} at depth using the same process. This process was used to compare the effectiveness of using the ancillary data as opposed to only using the information gained from the soil samples to predict the presence of the palæochannel.

5.2.3.2 Results and discussion

Although three dimensional ordinary kriging has not been be commonly applied in soil science, the method improves on the more commonly-used ordinary kriging, by incorporating more data into the spatial covariance structure to reduce bias in the estimation of soil properties (Triantafilis et al., 2001a). Where topsoil cores are located, the palæochannel presence is clearly shown. However, below the depth of the topsoil cores, the interpolation provides little support for the presence of the palæochannel (Figure 5.16).

Compared to the ordinary kriging approach, the scaling factors approach predicts the palæochannel to a depth of seven metres, one metre deeper than was observed (Figure 5.17). Above this depth, the palæochannel is apparent, but is not as clearly shown as in the ordinary kriging of the soil properties alone. Furthermore, a strong vertical trend appears in the 0^{th} order predictions. This is most obvious in the surrounding sediments, where much larger K_{sat} values are predicted than would be expected from the measured soil properties. The 0^{th} order method also predicts a significantly lower K_{sat} than was predicted from the soil property measurements. This same trend was apparent in half of the scaling factor methods (Table 5-7).

Due to the poorly-correlated inversion results, the McNeill method generates unrealistic predictions of the K_{sat} distribution. Following the interpolation process, the logistic approach appears to give the best correlation coefficients for the linear regression between the raw values and those predicted using the scaling factor approach (Table 5-7). However, the anomalously high values of mean($\log K_{sat}$) in the

1st order method suggests problems with the data, which are possibly related to the detrending process.

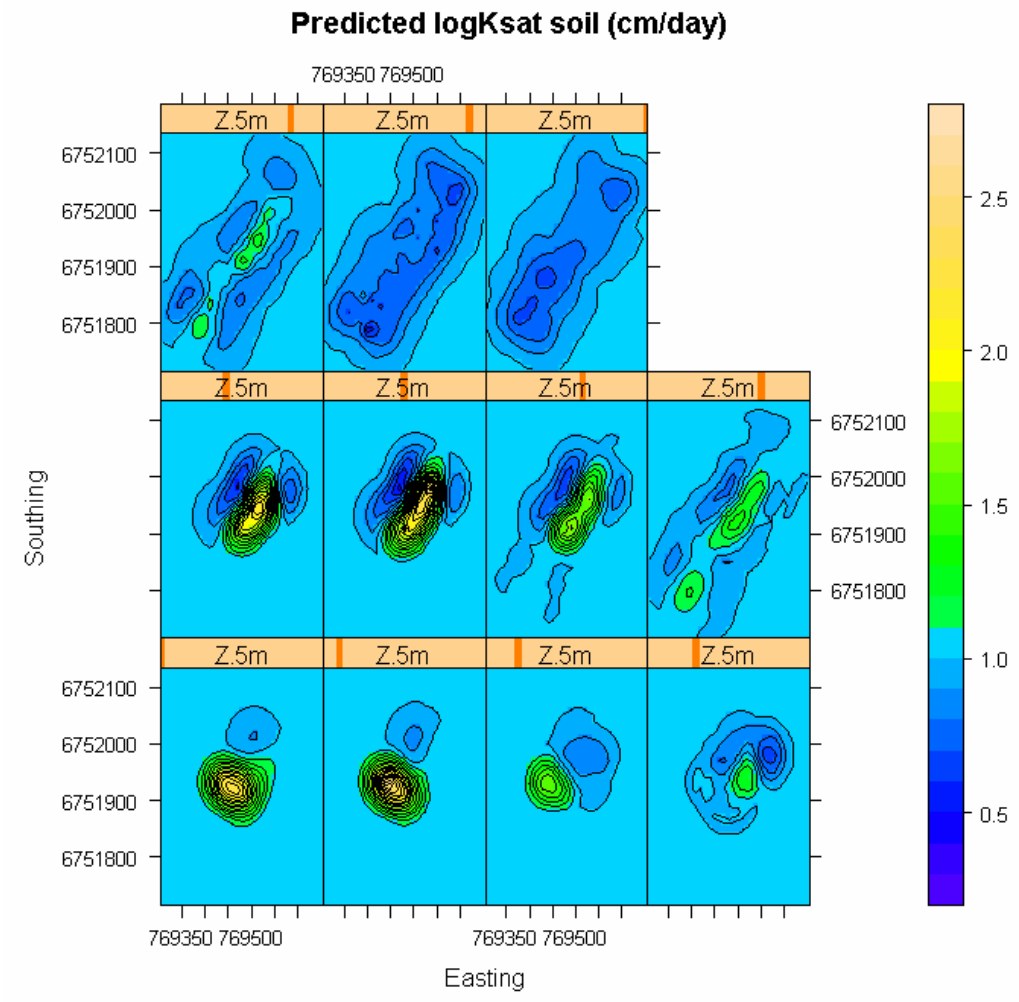

Figure 5.16. X-Y slices of 0.5 m thickness at 1 m increments from 0 (top right) to 10 m (bottom left) below the surface derived from three dimensional ordinary kriging of the measured soil properties. Contour lines represent 0.1 cm day^{-1}.

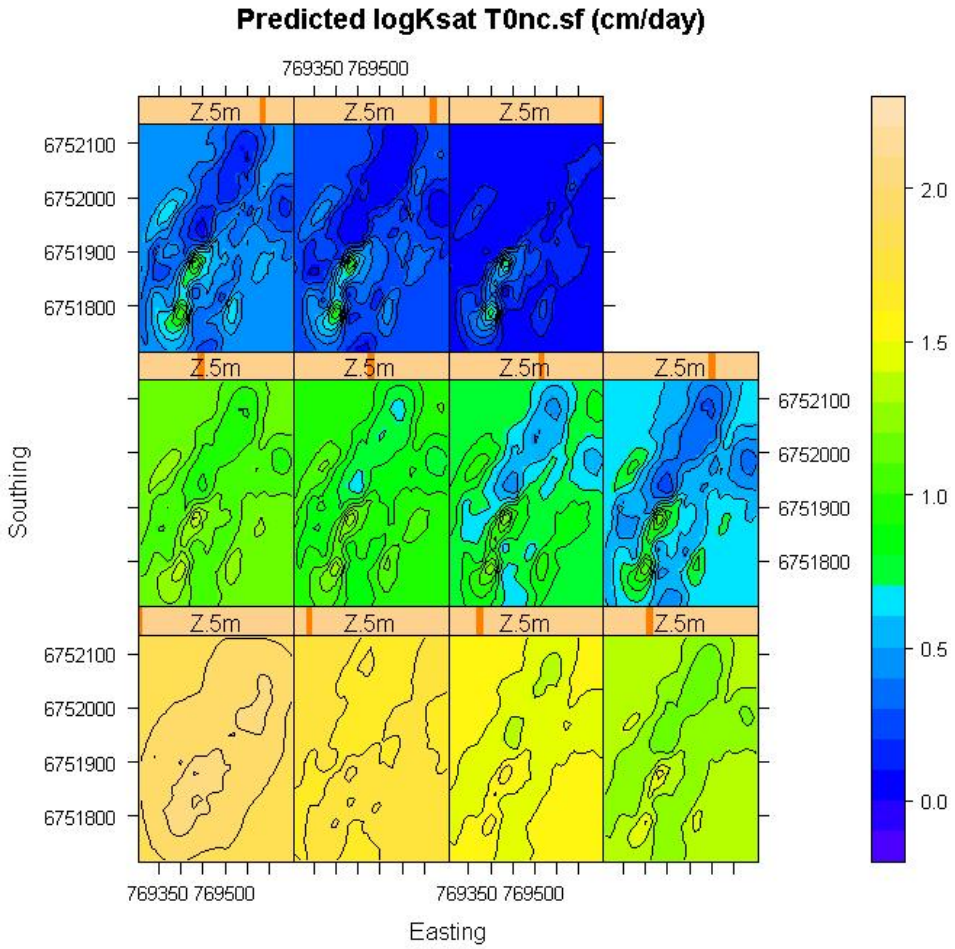

Figure 5.17. Results from X-Y slices at 1 m increments from 0 to 10 m below the surface using ordinary kriging of the scaling factor method for 0th order Tikhonov without clusters. Contour intervals represent 0.1 cm day^{-1}.

Table 5-7. Ordinary kriged soil properties and scaling factor approach compared with measured soil properties. Statistical comparisons are made using Dunnett's t-test, comparing means to control (raw ptf-derived K_{sat}) with * p < 0.05 **p < 0.01, ***p < 0.001 denoting similar to mean. Bolded values denote best predictors from linear regression between kriged properties and raw data.

Scaling method	Inversion method	Mean $logK_{sat}$	Linear regression with ptf-derived $logK_{sat}$			
		cm day^{-1}	r^2	RMSE	Slope	Intercept
cluster	Tikh 0	0.88**	0.08	0.4	**0.43**	0.57
	Tikh 1	1.08*	0.02	0.41	-0.22	1.20
	Tikh 2	1.03*	0.01	0.41	-0.13	1.09
	McNeill	0.73	0.07	0.4	0.14	0.86
no cluster	Tikh 0	0.43	0.30	0.35	**0.52**	0.73
	Tikh 1	1.08*	0.04	0.41	-0.27	1.25
	Tikh 2	1.05*	0.05	0.4	-0.28	1.24
	McNeill	0.45	0.01	0.41	0.07	0.82
logistic	Tikh 0	0.71	**0.35**	**0.33**	0.40	**0.07**
	Tikh 1	4.22	**0.32**	**0.34**	0.17	**0.24**
	Tikh 2	1.39	0.03	0.41	-0.35	1.45
	McNeill	1.02**	0.13	0.39	-1.44	2.43
Ptf-based		0.92***	0.70	0.23	1.05	0

Using the sampled points as a calibration set, the differences between the kriged soil properties and the raw soil properties are minimal, but the r^2 of 0.70 indicates that the kriging process introduced an error in the prediction. This is likely due to the smoothing operations in the algorithm. Compared to the difference in the calibration set of the measured soil properties, the scaling-factors measurements had a much lower correlation with the pedotransfer-derived predictions from the measured soil properties (Table 5-7). However, because of the limited number of deep cores, there was little support for the interpolation process from the soil cores alone, and the palæochannel presence could not be discerned below three metres. In some instances, scaling factors clearly improved the predictions of K_{sat} over the field to the depth of interest, but an improvement in the relationship between the soil properties and the EM data would also improve the predictions.

Compared to the ordinary kriging of measured soil properties the scaling factors approach provides more support for the presence of the palæochannel outside

of the measured points but with a greater uncertainty. The Narrabri Formation appears more laterally continuous than was predicted from the soil properties alone, and appears at 10 m below the surface, 2 m deeper than was observed. The method predicts a much smaller range in the K_{sat} within the palæochannel when compared to the surrounding sediments. The vertical trend is also apparent in the data, where the predicted Ksat monotonically increases with depth (Figure 5.17)

5.2.4 Regression kriging

5.2.4.1 Methods

Regression kriging uses the residuals from a linear regression between the EM data (in this case EC^{-1}) and the soil properties at measured points to predict the variation of the measured soil properties at the unmeasured points (Odeh et al., 1995). This in an iterative process which involves the following steps:

1.) compare K_{sat} with EC data at measured locations to obtain linear model and regression estimates at measured locations (in this case $\log(K_{sat}) = EC^{-1}$) (Figure 5.8),

2.) detrend and interpolate EC data using three dimensional ordinary kriging in the *Random Fields* package (R development core team, 2004)

3.) predict K_{sat} from kriged EC data using the previously defined linear regression,

4.) interpolate regression errors (from step 1) using three dimensional ordinary kriging, using the same method in step 2.

5.) add interpolated K_{sat} estimates (3) to interpolated regression errors (4).

Similar to the ordinary kriging procedure, the anisotropy was taken out of the data, as was the vertical trend in the McNeill and Tikhonov 0^{th} order data.

5.2.4.2 Results and discussion

Because this method uses the maximum amount of information (based on all the soil cores and EM data), the regression krigging approach serves as the “baseline”

to compare the scaling factors approach. Using the 0th order data as the ancillary predictor, the palæochannel is clearly identified and extends throughout the paddock to a depth of six metres, where it abruptly ends (Figure 5.18). This compares favourably to observations made in the field (Table 4.1). Compared to the non-clustered scaling factors approach (Figure 5.17) there is a stronger contrast between the palæochannel sediments and the surrounding soil. The method still has a more realistic vertical trend (which is not as steep as the scaling factors method) and is, interestingly, opposite that of the scaling factors approach (K_{sat} decreasing with depth) (Figure 5.17).

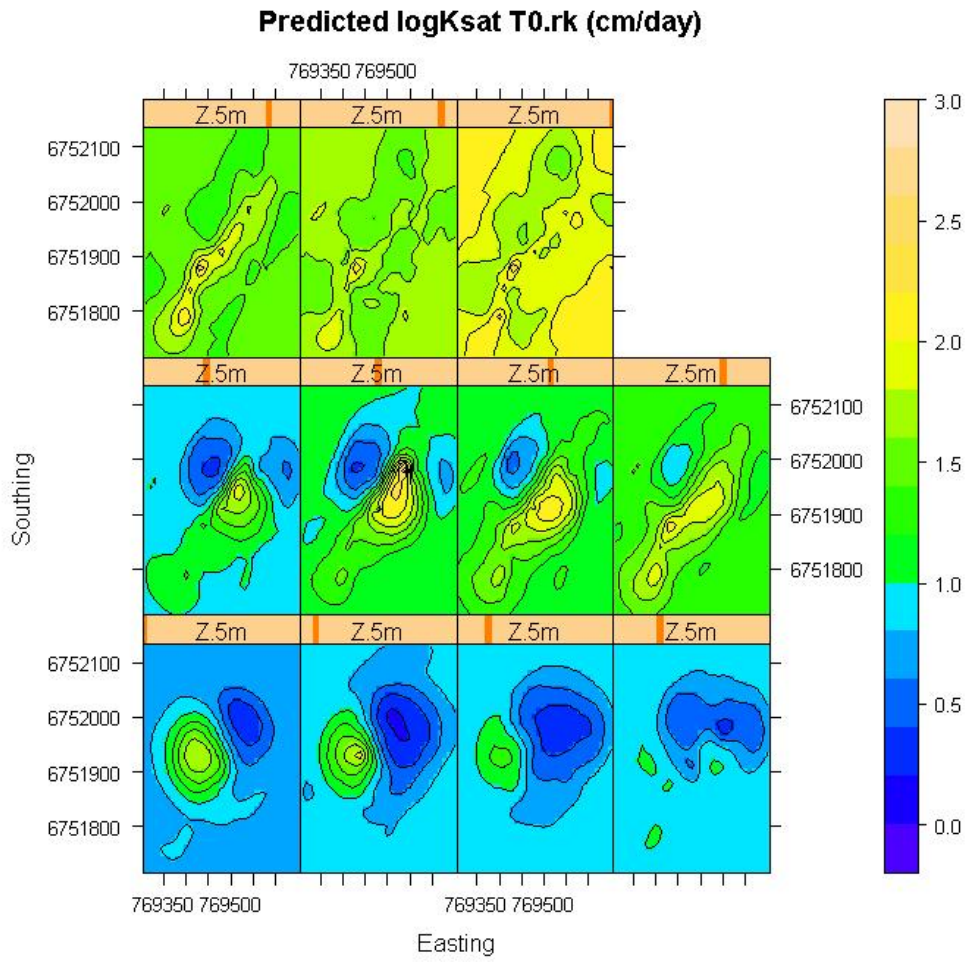

Figure 5.18. Results from the regression kriged soil properties using the 0th order Tikhnoov inversion EC as the ancillary data.

The 0th order Tikhonov method was considered a best case scenario for the regression krigging procedure because of the significant correlation between the measured Ksat and the EC data (Table 5-8). However, the method failed to predict the spatial distribution of the measured soil properties (Table 5-9). This could be due to the spatially-correlated error associated with the use of multiple instruments. One of the assumptions with regression kriging is that the data contain a random error term, which has no spatial dependence (Triantafilis et al., 2001a). Considering the discussion presented earlier (Section 5.1.6), it is likely that the inverted data contains a spatially-dependent error term, which would be most strongly reflected in the 0^{th} order Tikhonov method because it is the least regularised approach.

Table 5-8. Relationship between resistivity (EC-1) and logK_{sat}. Note 1 ohm-m = 1/1000 mS/m. Bold text denotes intercepts and slopes significantly different from 0 ($\alpha = 0.05$).

Inversion method	Linear regression with ptf-derived logK_{sat} (ohm-m)			
	r^2	RMSE	Slope	Intercept
McNeill	0.03	28.7	**12.4**	**234.43**
Tikh 0	0.33	15.2	**25.4**	**-7.06**
Tikh 1	0.08	3.10	**2.24**	**6.58**
Tikh 2	0.01	2.81	0.50	**9.30**

In the absence of a good ancillary predictor of K_{sat} (e.g. the McNeill EC data), the error term is equal to the difference between the mean K_{sat} and the measured K_{sat} value (Odeh et al., 1994). In this scenario, the slope of the regression between the measurement and the predictor approaches zero. Therefore, very little weight is given to the ancillary data, and the regression prediction approaches that of the ordinary kriged prediction. This is exemplified in the McNeill regression kriging approach in Figure 5.19 which is similar to the plot of the ordinary kriged soil properties (Figure 5.16). The McNeill, and the two higher-order Tikhonov methods are strongly correlated to the soil properties when compared to the 0^{th} order Tikhonov which is not significantly correlated with the measured soil properties (Table 5-9).

Table 5-9. Comparisons between regression kriged predictions and measured soil properties. Statistical comparisons are made using Dunnett's t-test, comparing means to control (raw ptf-derived K_{sat}) with * p < 0.05 **p < 0.01, ***p < 0.001 denoting similarity to mean. Bolded values denote best predictors from linear regression between kriged properties and raw data.

Inversion method	Mean $logK_{sat}$	Linear regression with ptf-derived $logK_{sat}$			
	cm day^{-1}	r^2	RMSE	Slope	Intercept
McNeill	0.91*	0.52	0.29	0.76	0.26
Tikh 0	1.53	0.00	0.41	-0.04	1.01
Tikh 1	0.90*	**0.71**	**0.22**	1.06	**0.00**
Tikh 2	0.92*	0.62	0.25	**0.96**	0.07
measured	0.92***	0.70	0.23	1.05	0

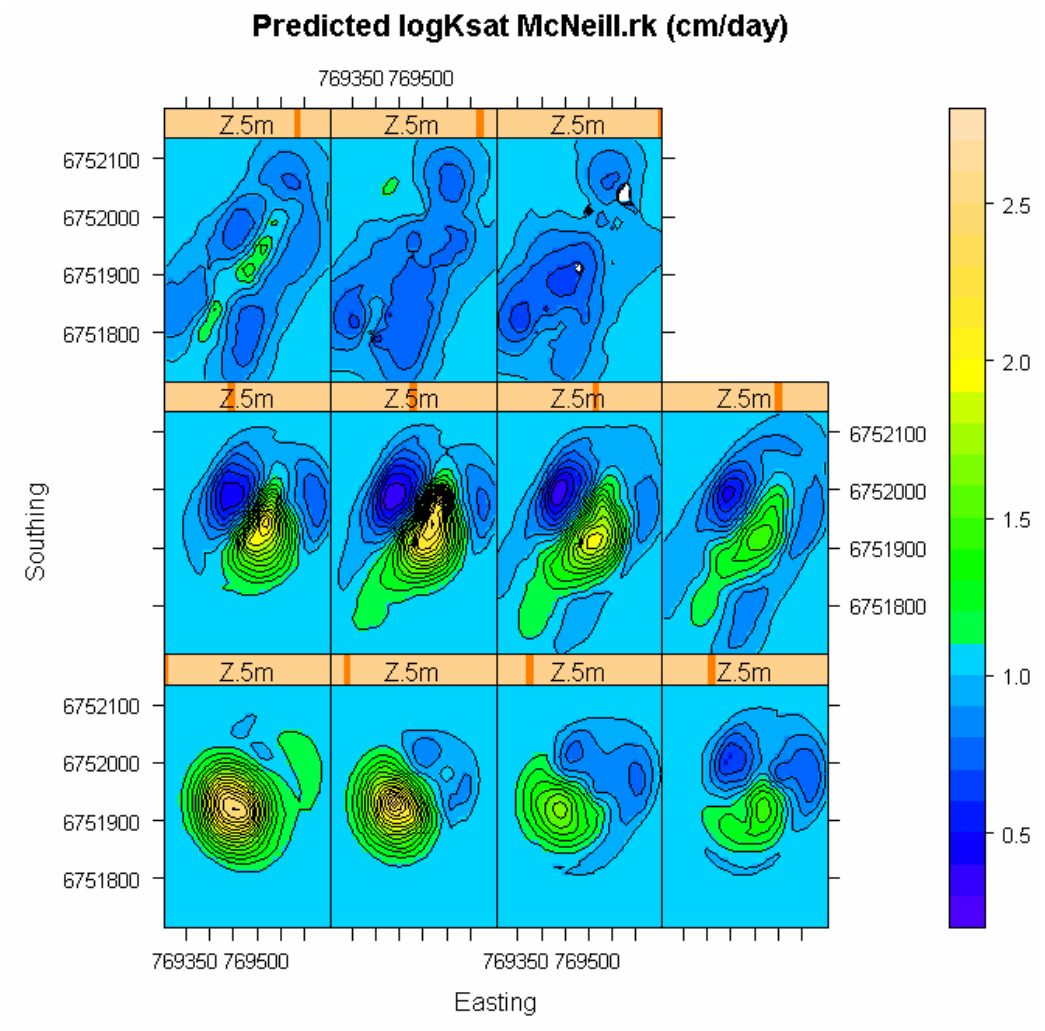

Figure 5.19. Regression kriging of K_{sat} and EC data using the McNeill inversion method. The plot is very similar to the ordinary kriging of soil properties, based on the very low prediction power of the EC data, which were not correlated to the measured soil properties.

The scaling factor approach produced slice plots which were similar to the regression kriging plots, but did not appear to accurately predict the range in K_{sat} values. This is likely due to the smooth nature of the regularisation results (Hendrickx et al., 2002). There are similarities between the regression kriged topsoil K_{sat} distribution (Figure 5.18) and those from the scaling factors approach (Figure 5.17). Both methods compare favourably with the ordinary kriged predictions (Figure 5.16), which had a relatively high resolution of sampled points at this depth.

In all methods where a trend existed between the EC and K_{sat} data, the presence of the palæochannel was predicted (Appendix, Figures A9 – A24). In most cases (including the regression kriging), the sharp vertical contrasts in K_{sat} beneath the palæochannel were not predicted. This is likely due to the smoothing of the EC profiles during the regularisation process, and is considered a significant limitation to this method.

5.3 Conclusion

The predicted electrical conductivity profiles as derived from the apparent electrical conductivity measurements were highly sensitive to the inversion algorithm used. In the case where regularisation was not used, the profiles were erratic and strongly influenced by temporal variations in the electrical conductivity. However, by regularising the profiles, the solutions were much more stable and linearly responded to temporal changes in EC_a measurements. Similar to the results found by Shultz and Ruppel (2005) and Hendrickx et al. (2002), it appears that conditioning of the algorithm is necessary to predict multiple layers from vertical sounding measurements.

The trade-off between profile smoothness and stability is demonstrated in the differences between the 0^{th} and 2^{nd} order Tikhonov methods. While both methods predicted realistic EC profiles, the more pronounced regularisation associated with the 2^{nd} order method resulted in relatively poor predictions of soil physical properties, including clay content and saturated conductivity. The close relationship between the EC_e measurements and the smooth profiles could be explained by the presence of soluble minerals such as carbonates and gypsum identified in the soil cores. These minerals would only affect the surface conduction of the EM wave under saturated conditions, when the ions are liberated (as is the case in laboratory measurements).

In general, the model relating the inverted electrical conductivity to the saturated hydraulic conductivity gave poor predictions of K_{sat}, when compared to the measured values derived from the pedotransfer functions. In comparison with these measured values, the 0^{th} order Tikhonov inversion method coupled with the non clustered or logistic scaling best described the measured data. Although the relationships with the measured K_{sat} values are relatively poor, the EM measurements still provide favourable results when compared to alternative methods such as ordinary kriging, where the small number of measurements did not predict the presence of the palæochannel below three metres. An alternative approach to these two methods would be the use of stochastic prediction which assumes a random distribution of K_{sat}. This method, which has becom common in groundwater modelling would not account for the strong influence that the palæochannel has on the variability of soil properties throughout the site.

The scaling factors approach compared favourably to the regression kriging of the soil properties and the ancillary data. However, it should be noted that, while the regression kriging approach should not be considered a control, it is the best prediction method available with the existing data. The benefit of the scaling factor approach is the minimal number of direct observations needed to describe the variability of the soil. In this approach, the number of direct measurements required on a site would be constrained to the available soil data from nearby locations. These data could be acquired from literature reviews, or through the newly-released online soils database ASRIS (McKenzie, 2007). As long as a reference K_{sat} value can be found (or estimated) and the model assumptions are obeyed (i.e. the soil solution is not highly saline) this method can effectively predict the distribution of K_{sat}. In the case where the salinity of the soil solution is significantly great and is assumed to be laterally homogeneous, a non-linear inversion algorithm would be more appropriate.

Appendix 5.1 - Bivariate plots of EC_e versus EC and clay

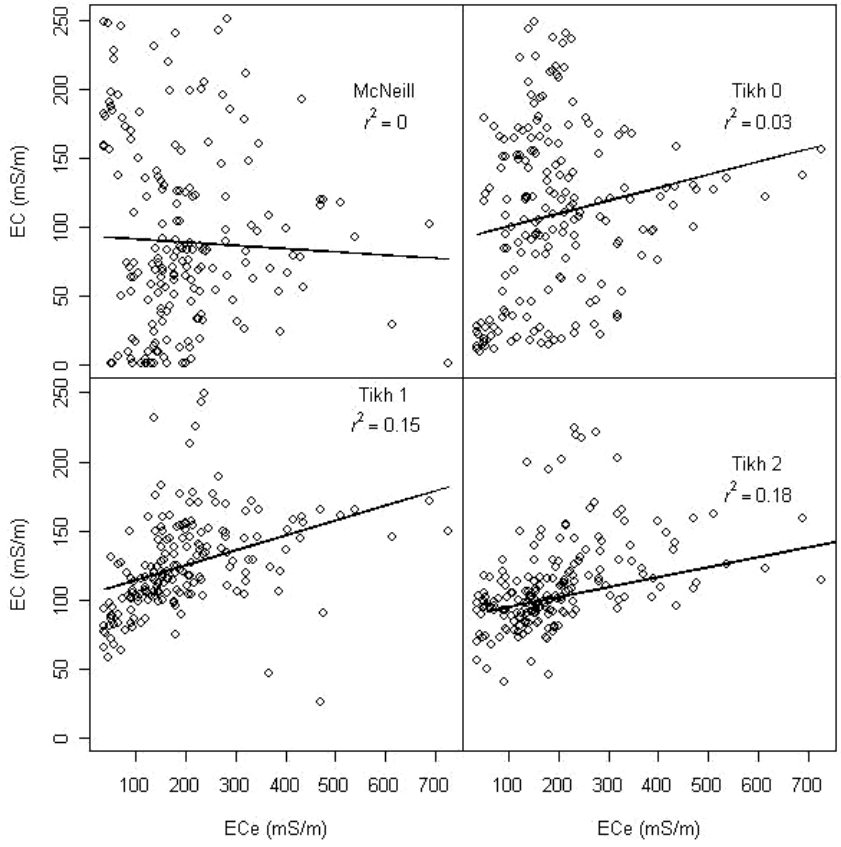

Figure 5.20. Relationship between EC from inverted EM measurements and EC_e from laboratory measurements. The McNeill inversion method did not describe the variation in laboratory-measured EC_e ($p = 0.52$) while the 0th order Tikhonov method only weakly described it ($p = 0.04$). The 1st and 2nd order Tikhonov methods produced similar results, which were significantly correlated to EC_e ($p < 0.001$).

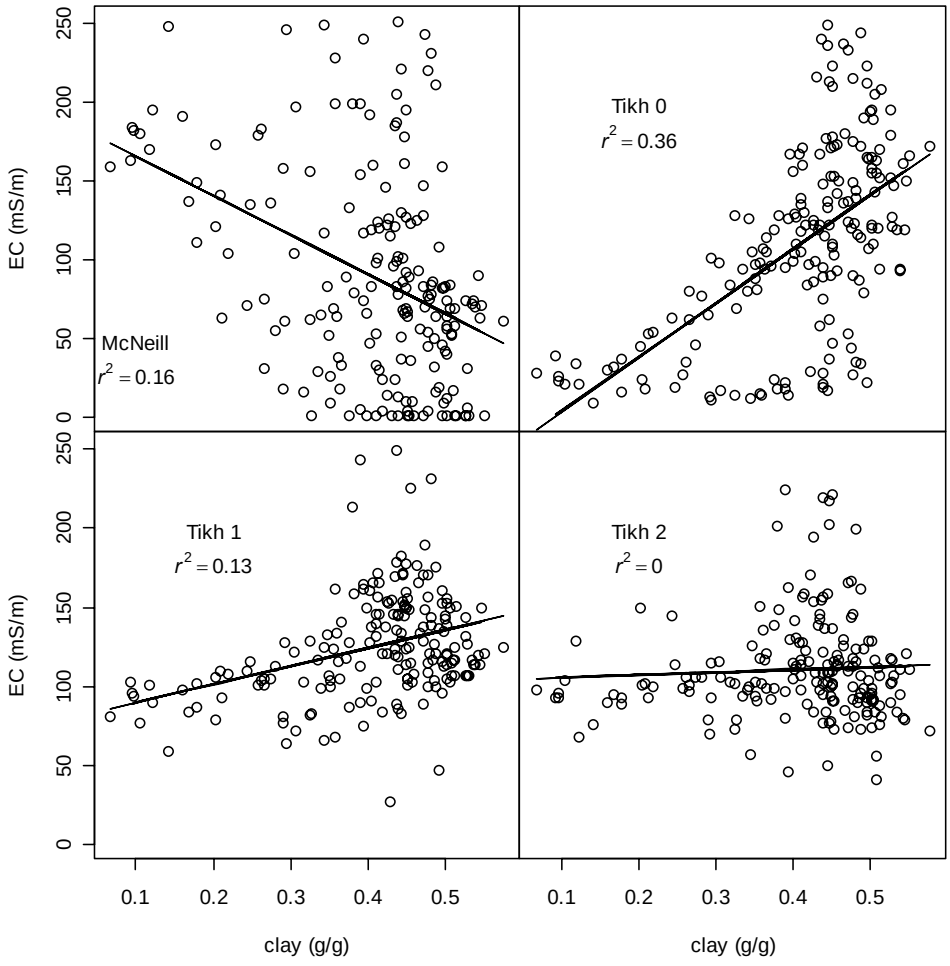

Figure 5.21 Relationship between EC from inverted EM measurements and clay content from laboratory measurements.

Appendix 5.2 – Transect plots of EC

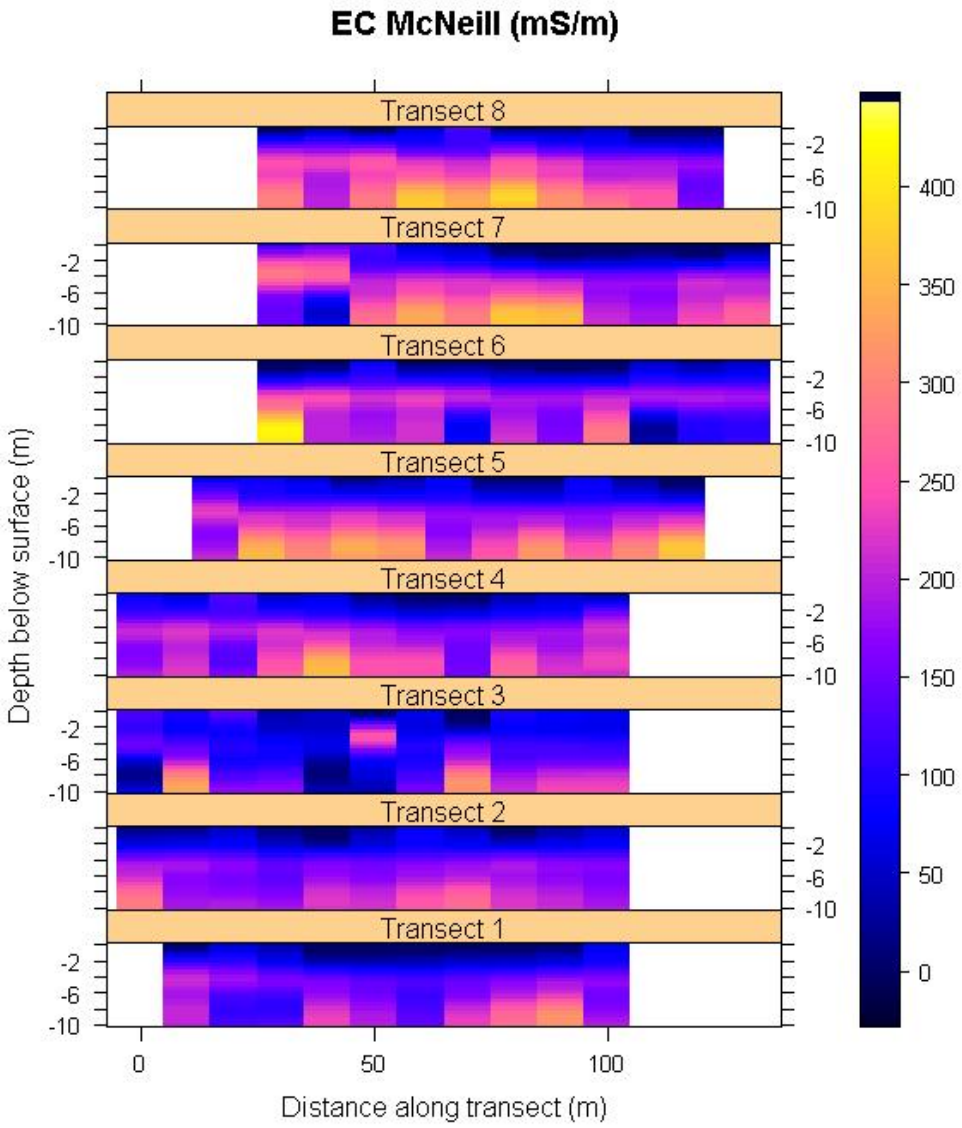

Figure 5.22 EC profiles from the McNeill inversion algorithm for all transects located within the paddock. The presence of the palaeochannel is weakly reflected in the upper two metres of the profiles, which is shown as a localised low in EC.

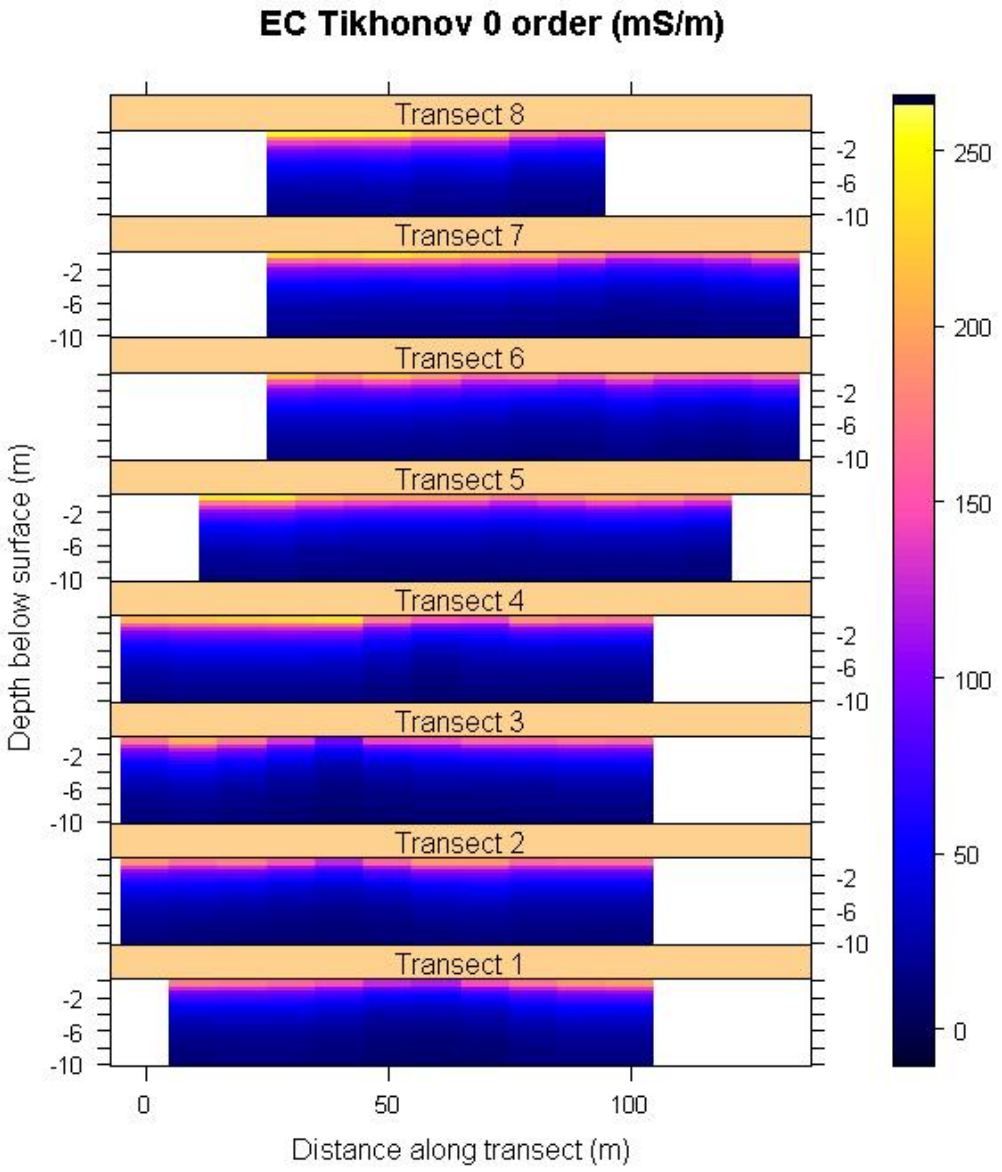

Figure 5.23 EC profiles from 0th order Tikhonov regularisation from all transects located within the paddock. The palæochannel presence is indicated by a region of lower conductivity, occurring at the midpoint of most transects.

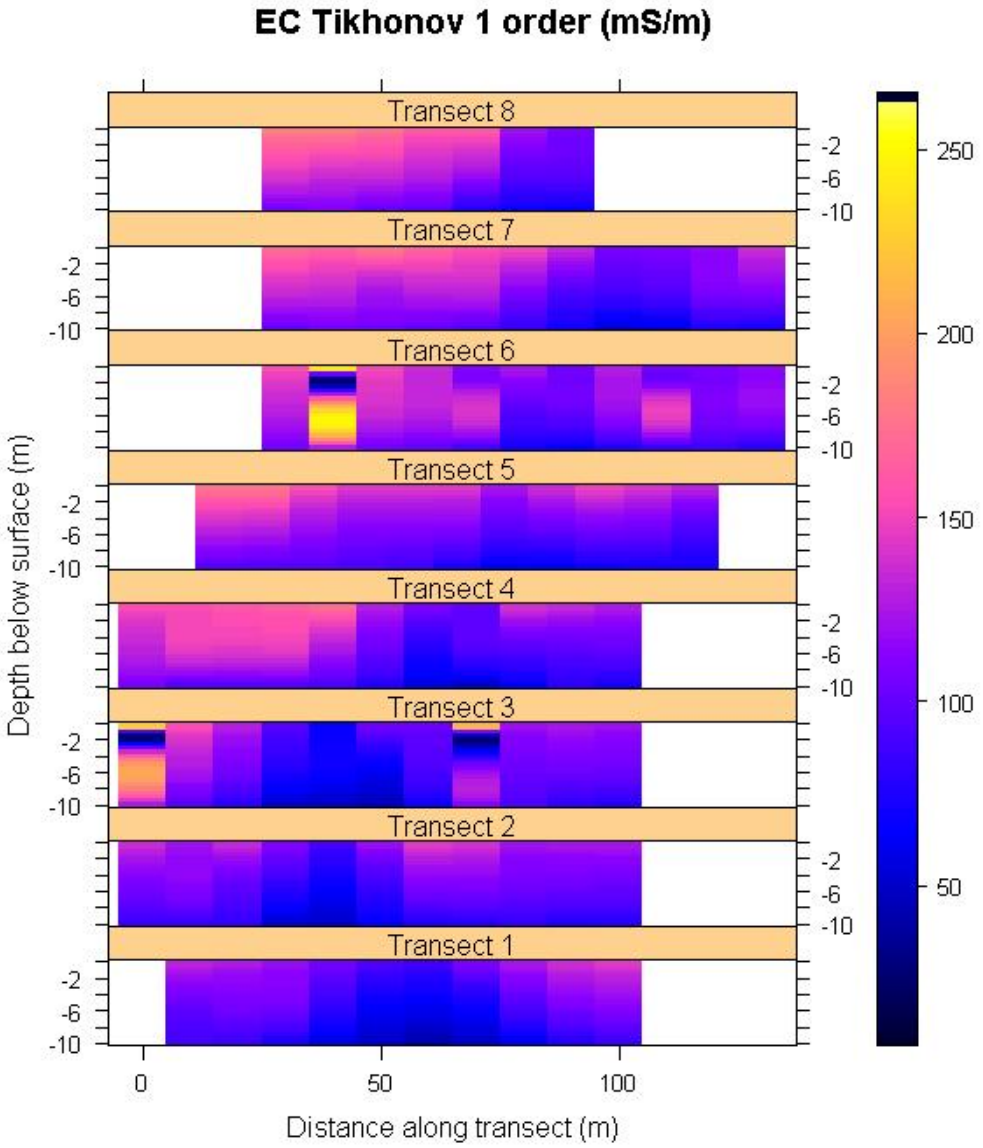

Figure 5.24 EC profiles from the 1st order Tikhonov regularisation method for all transects located inside the paddock. The palæochannel is shown as a region of low conductivity occurring at the midpoint of most of the transects. Several unstable profiles are shown in Transects 3 and 6 which appear as highly oscillating vertical trends.

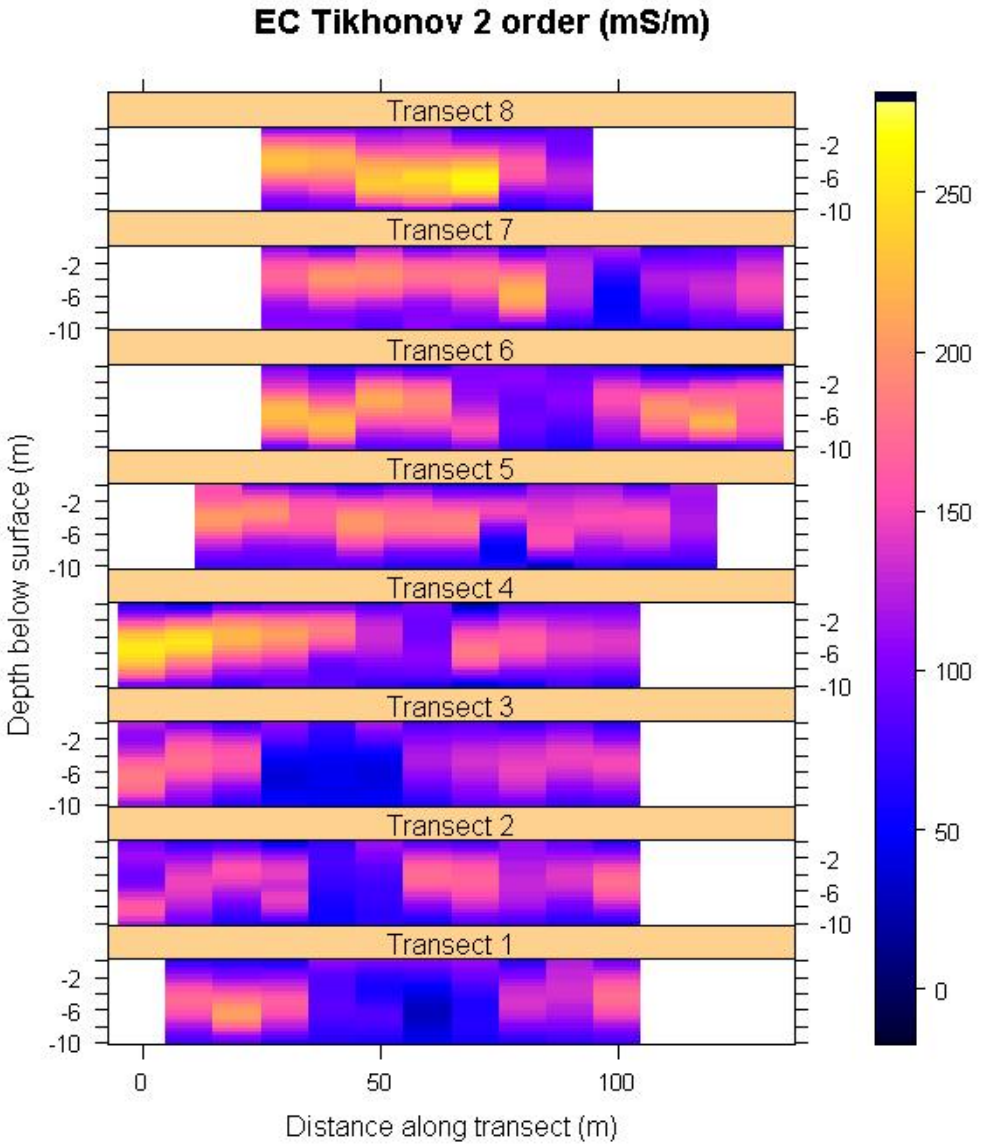

Figure 5.25 EC profiles using the 2nd order Tikhonov regularisation method from all transects inside the paddock. The palæochannel presence is strongly reflected in the low conductivity values occurring half way through most of the transects.

Appendix 5.3 – Transient response bivariate plots

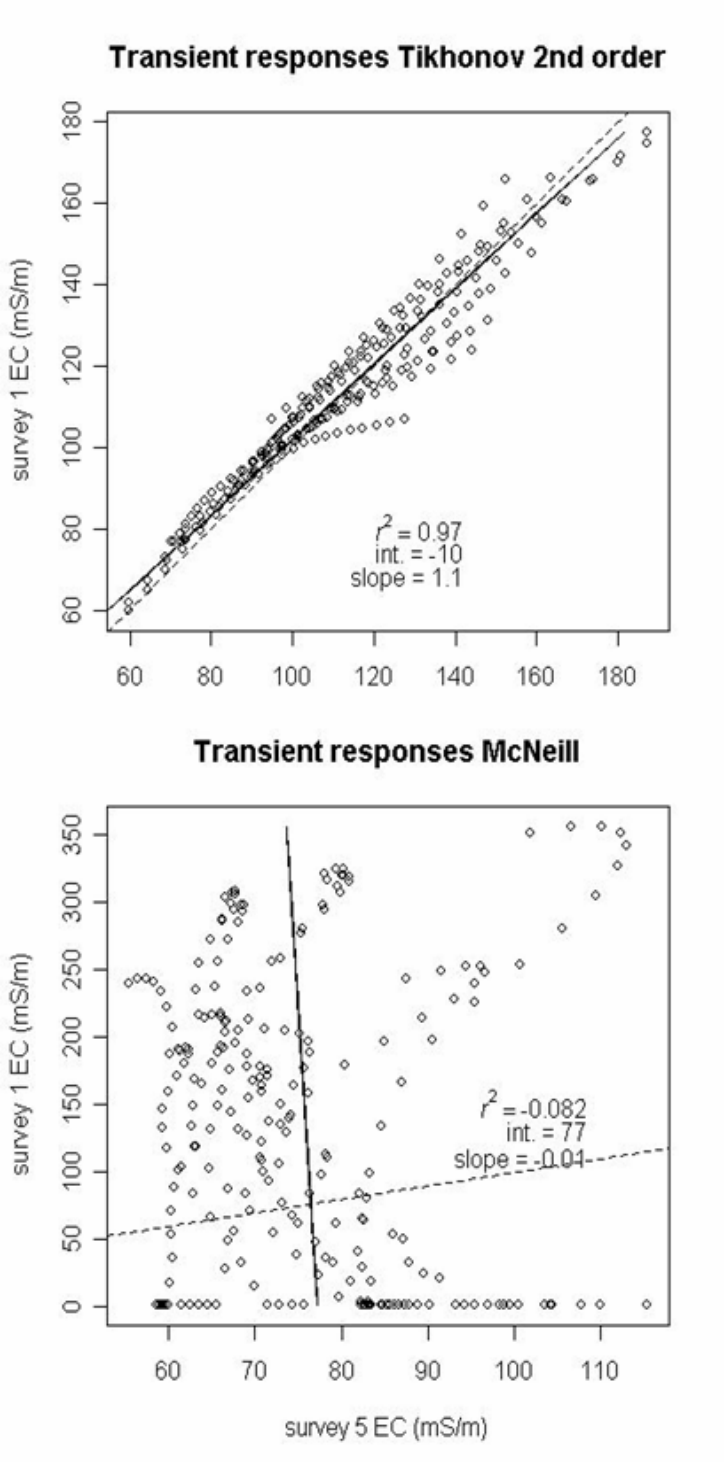

Figure 5.26 Comparison of transient responses from the McNeill and 2nd order Tikhonov regularisation methods from Transect 5. Comparisons are made between Survey 1 and Survey 5, showing the very weak correlation in the unregularised method.

Appendix 5.4 – Semivariograms for 3-D ordinary kriging

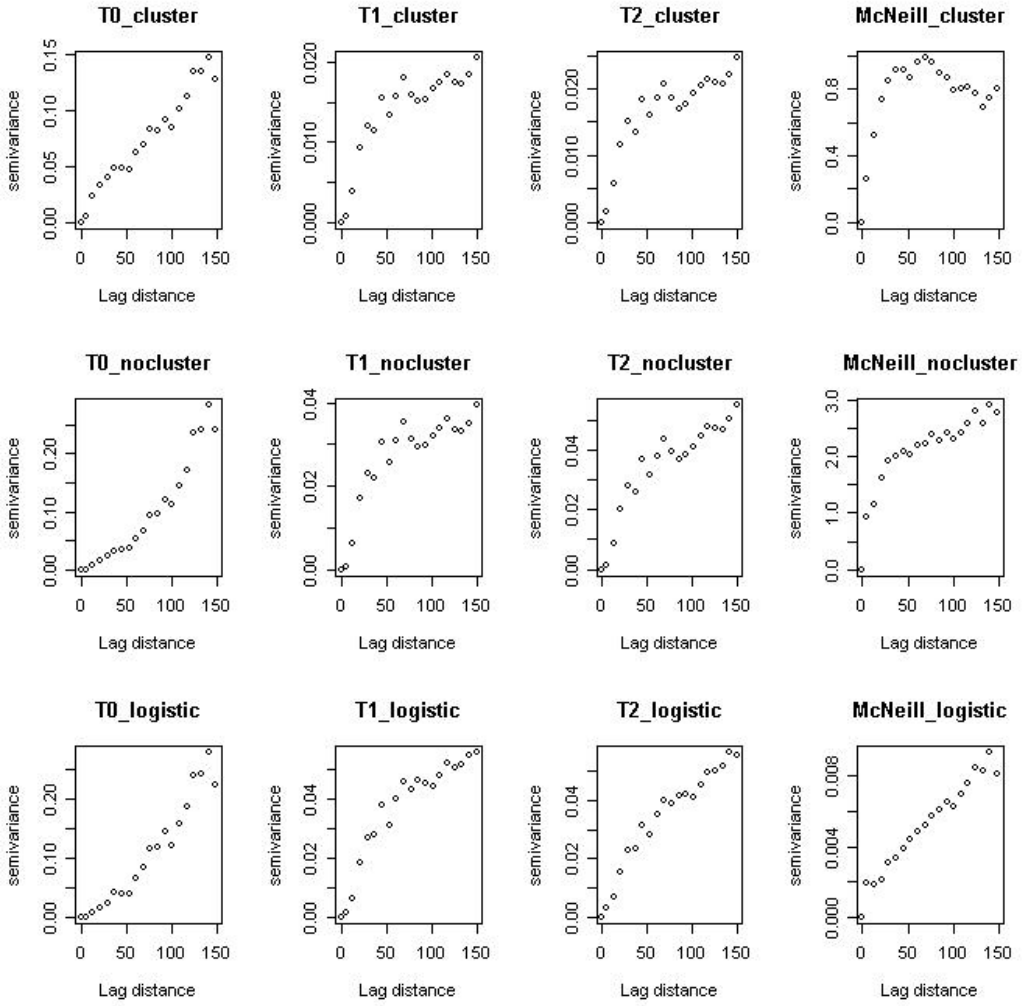

Figure 5.27. Three dimensional semivariograms of all regularisation and scaling factor methods with trend.

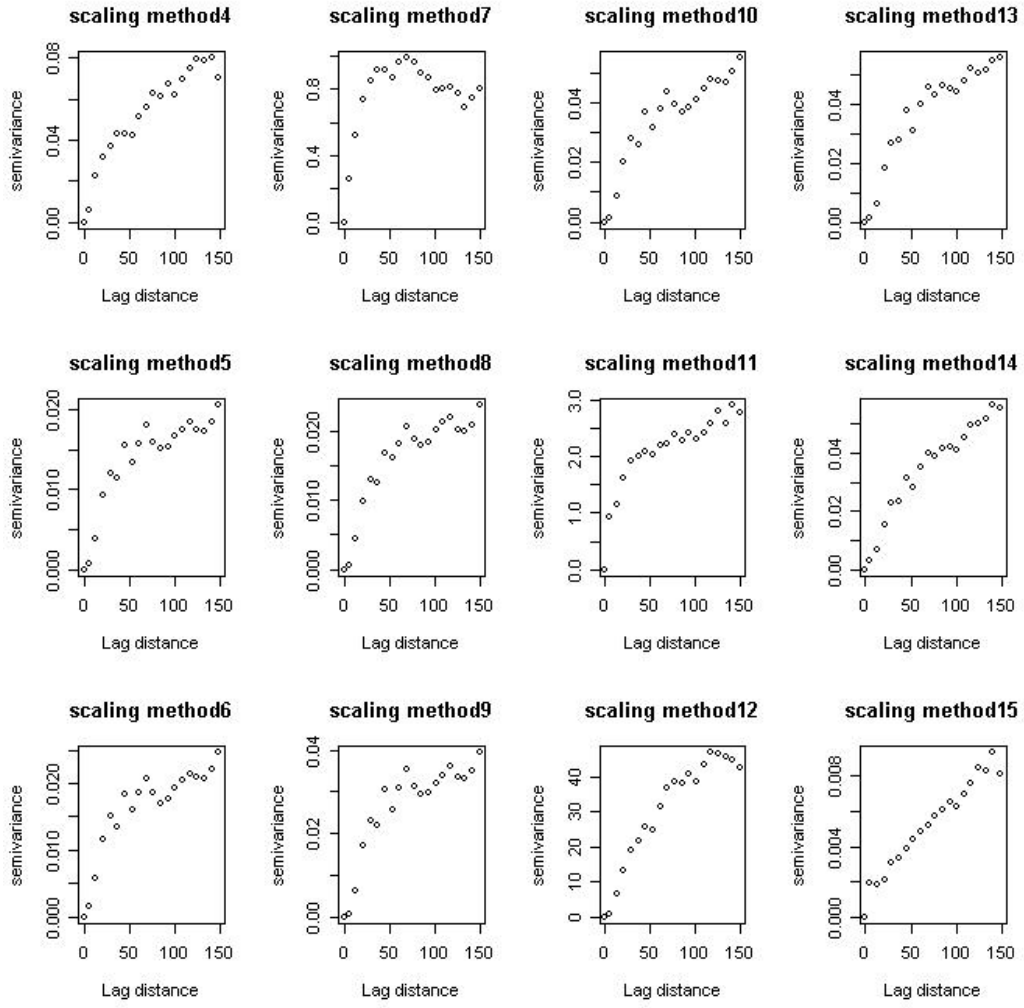

Figure 5.28 Detrended three dimensional semivariograms corresponding to Figure 5.27

Appendix 5.5 – Slice plots for predicted K_{sat} fields

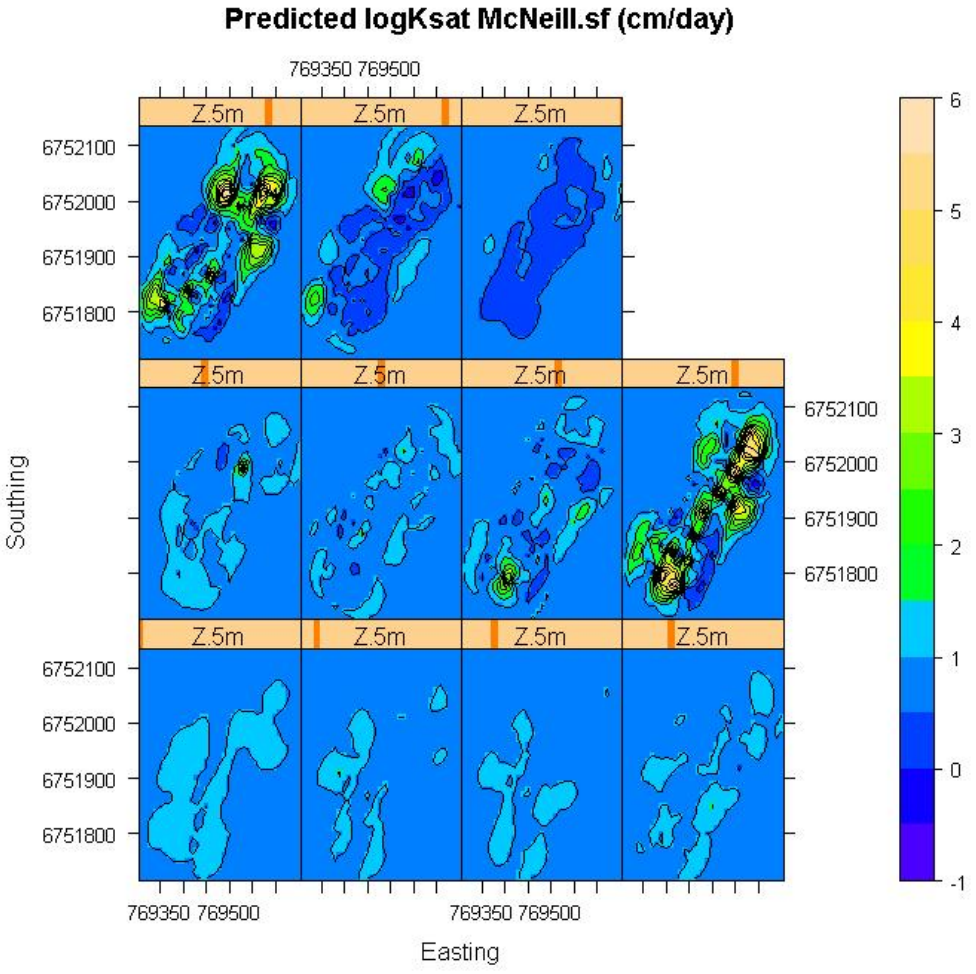

Figure 5.29 Predicted K_{sat} slices from 0 (top right) to 10 m (bottom left) at 1m intervals using the McNeill inversion method with clustered scaling factors.

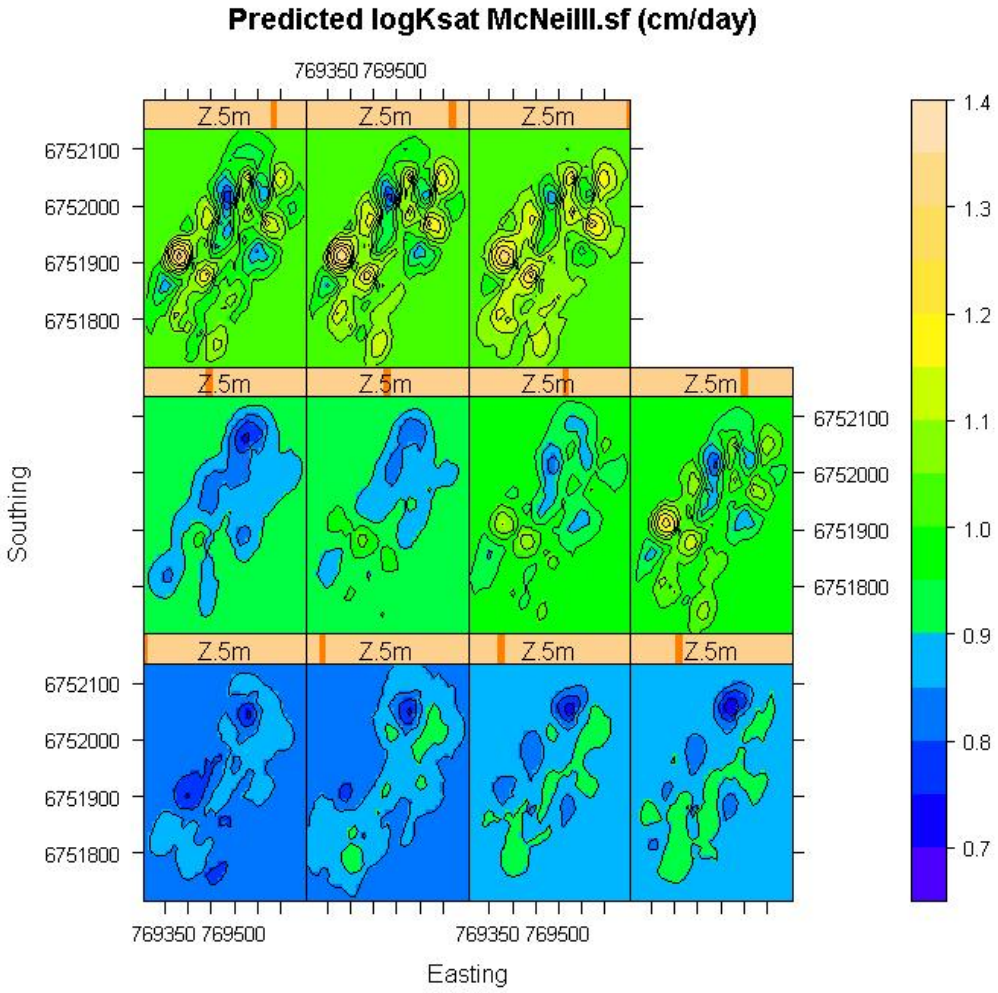

Figure 5.30 Predicted K_{sat} slices from 0 (top right) to 10 m (bottom left) at 1m intervals using the McNeill inversion method with logistic scaling factors

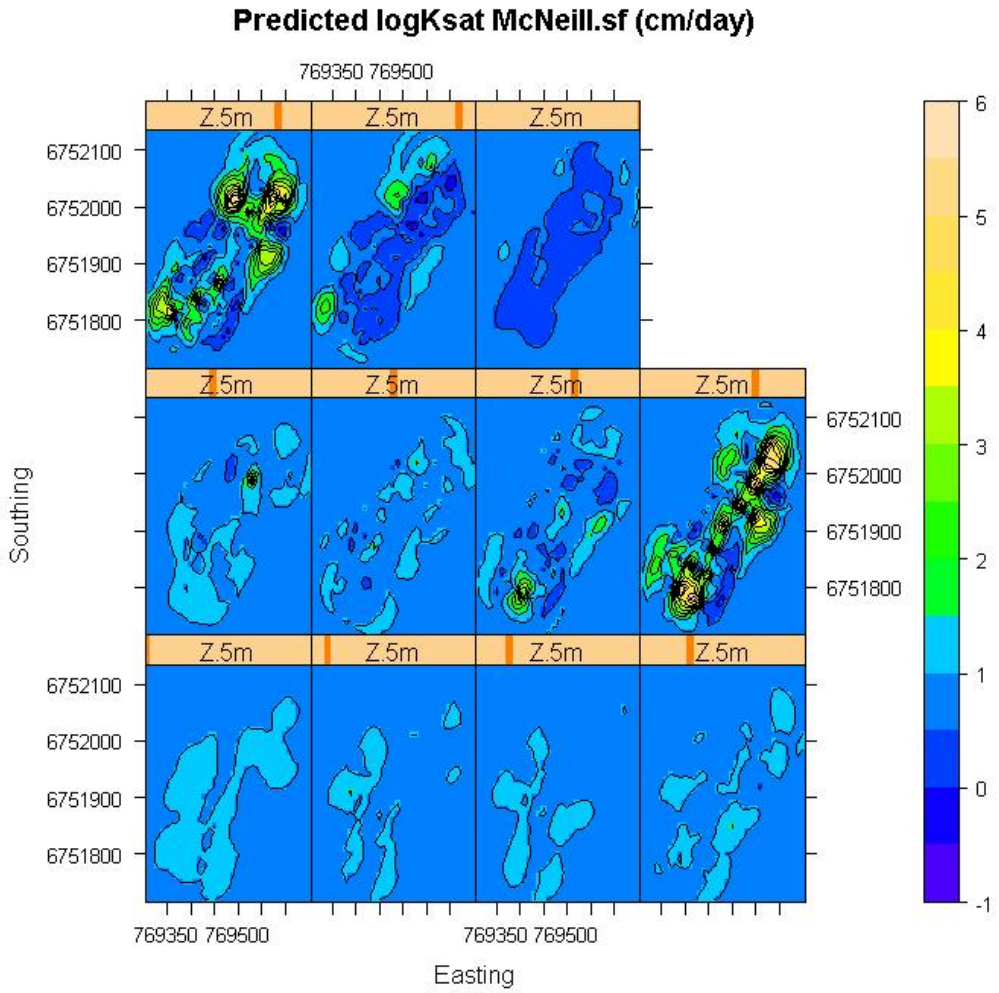

Figure 5.31 Predicted K_{sat} slices from 0 (top right) to 10 m (bottom left) at 1m intervals using the McNeill inversion method with unclustered scaling factors.

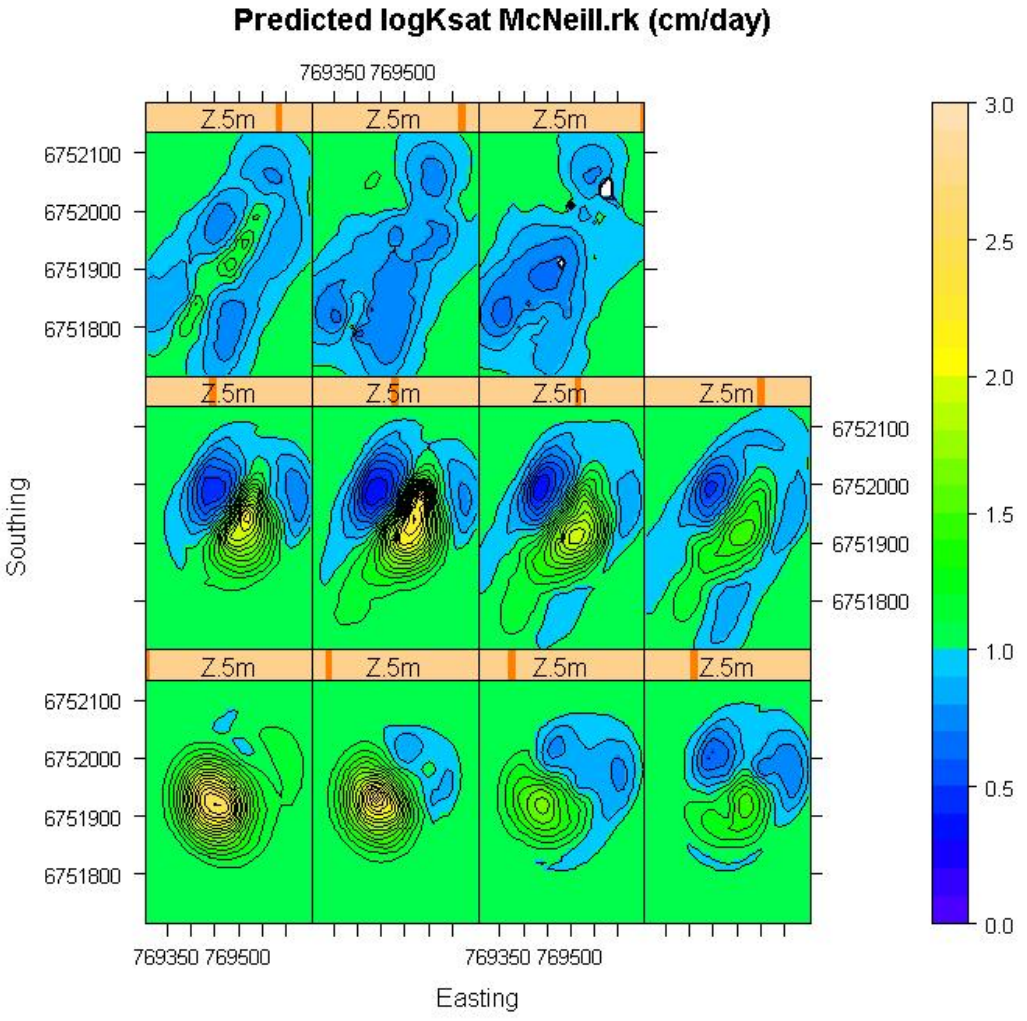

Figure 5.32 Predicted K_{sat} slices from 0 (top right) to 10 m (bottom left) at 1m intervals using McNeill inversion with regression kriging.

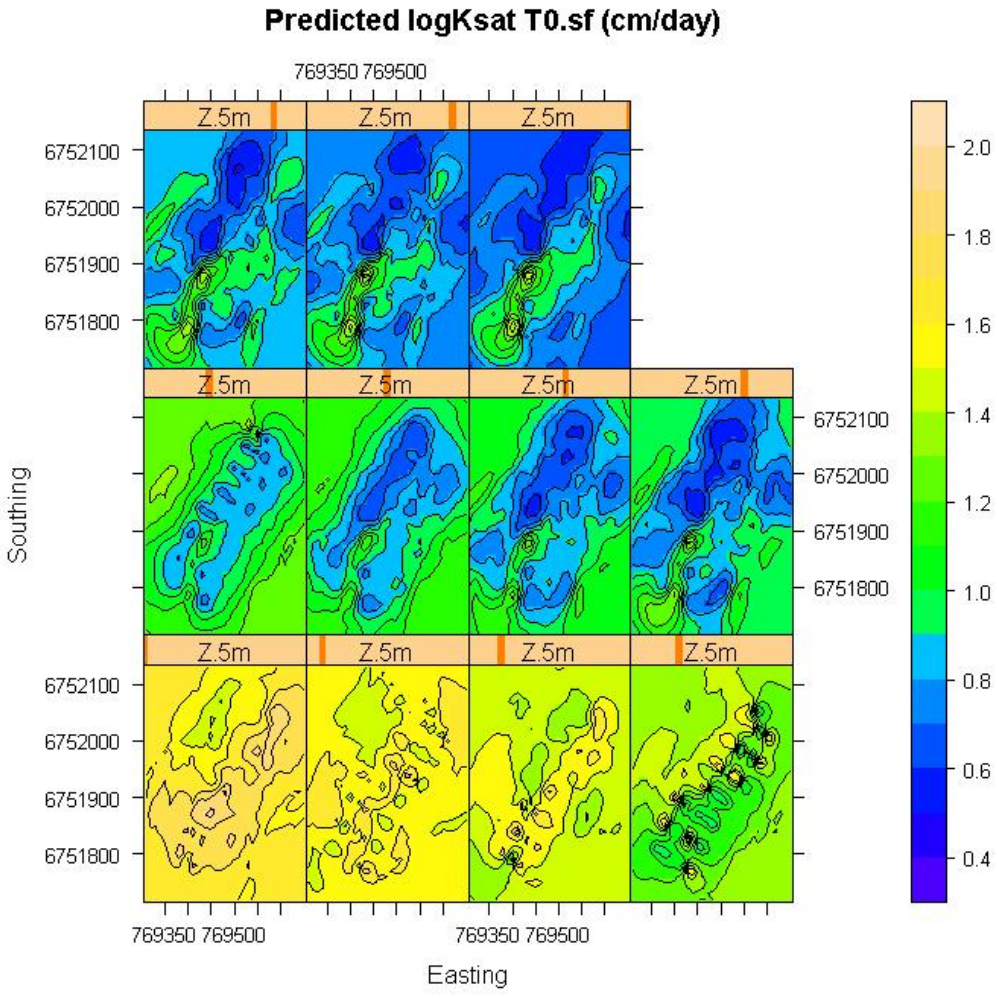

Figure 5.33 Predicted K_{sat} slices from 0 (top right) to 10 m (bottom left) at 1m intervals using 0^{th} order Tikhonov inversion with clustered scaling factors.

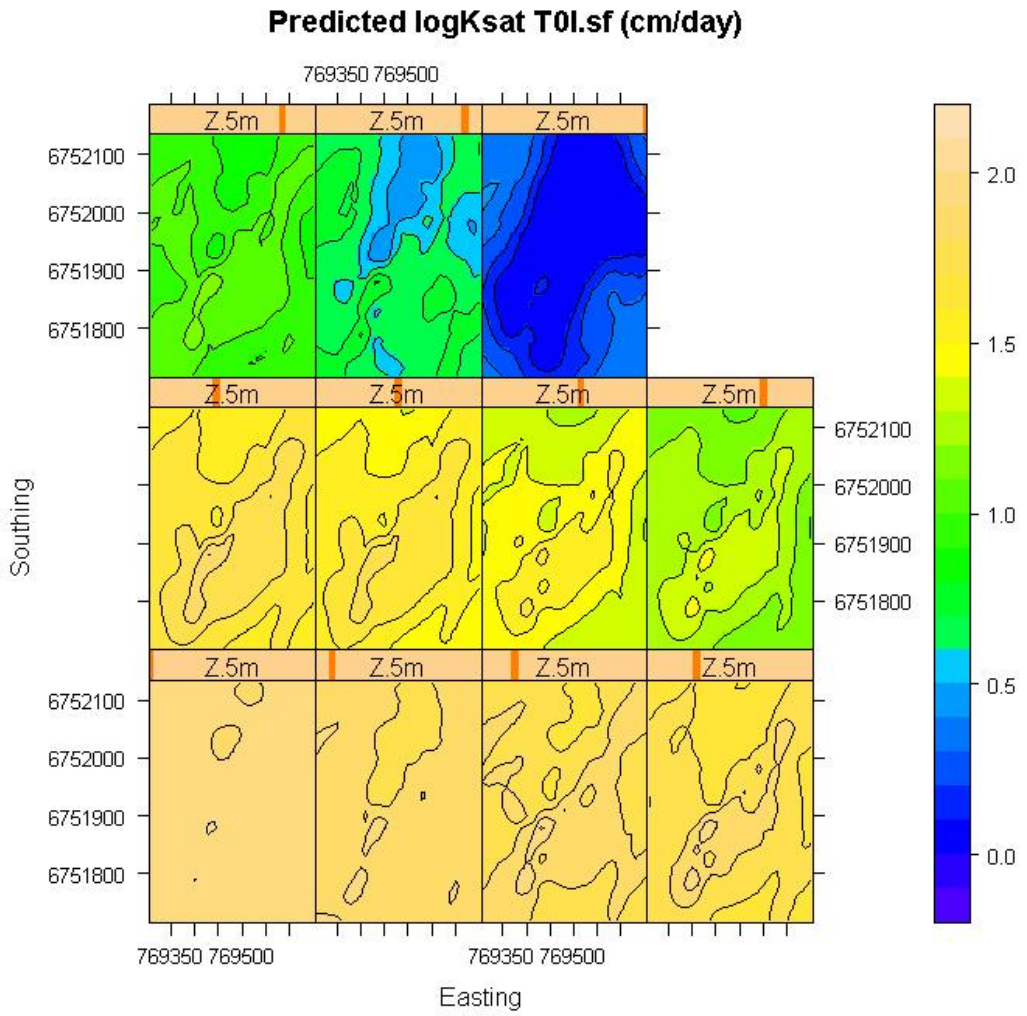

Figure 5.34 Predicted K_{sat} slices from 0 (top right) to 10 m (bottom left) at 1m intervals using 0th order Tikhonov inversion with logicstic scaling factors.

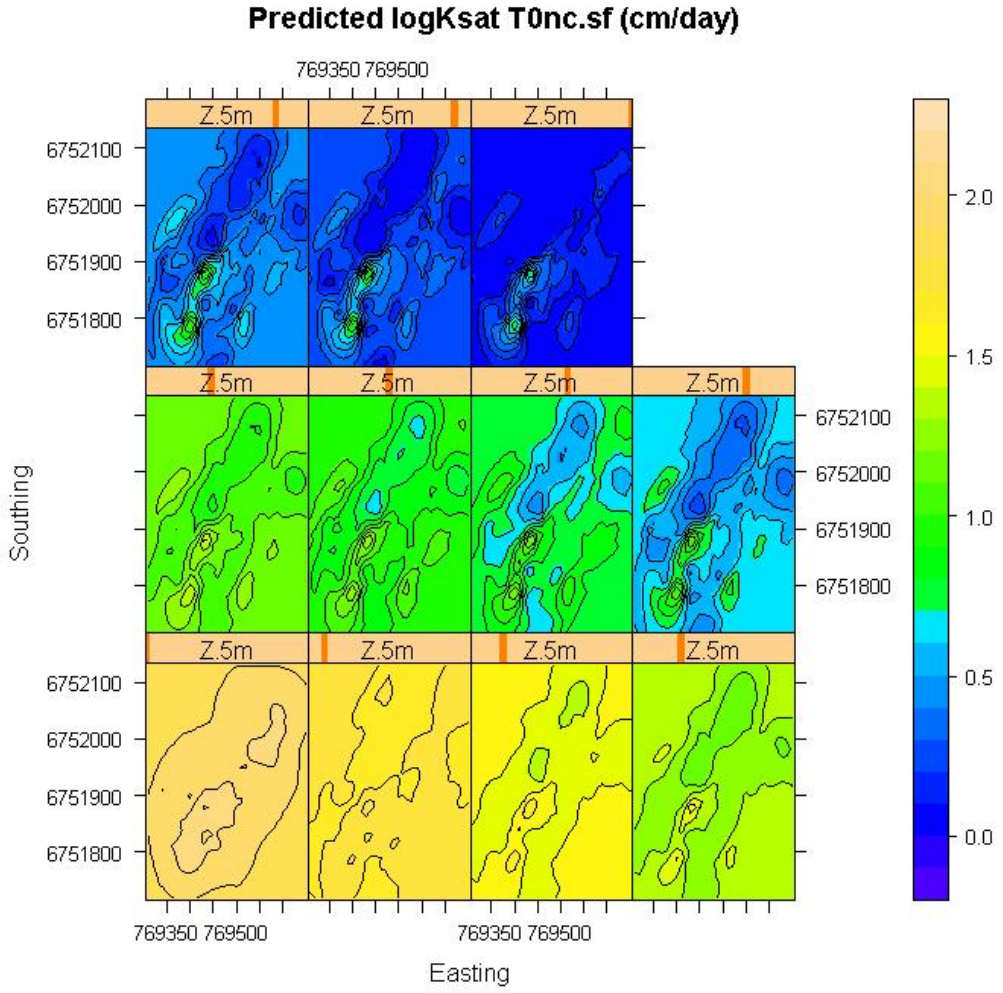

Figure 5.35 Predicted K_{sat} slices from 0 (top right) to 10 m (bottom left) at 1m intervals using 0th order Tikhonov inversion with unclustered scaling factors.

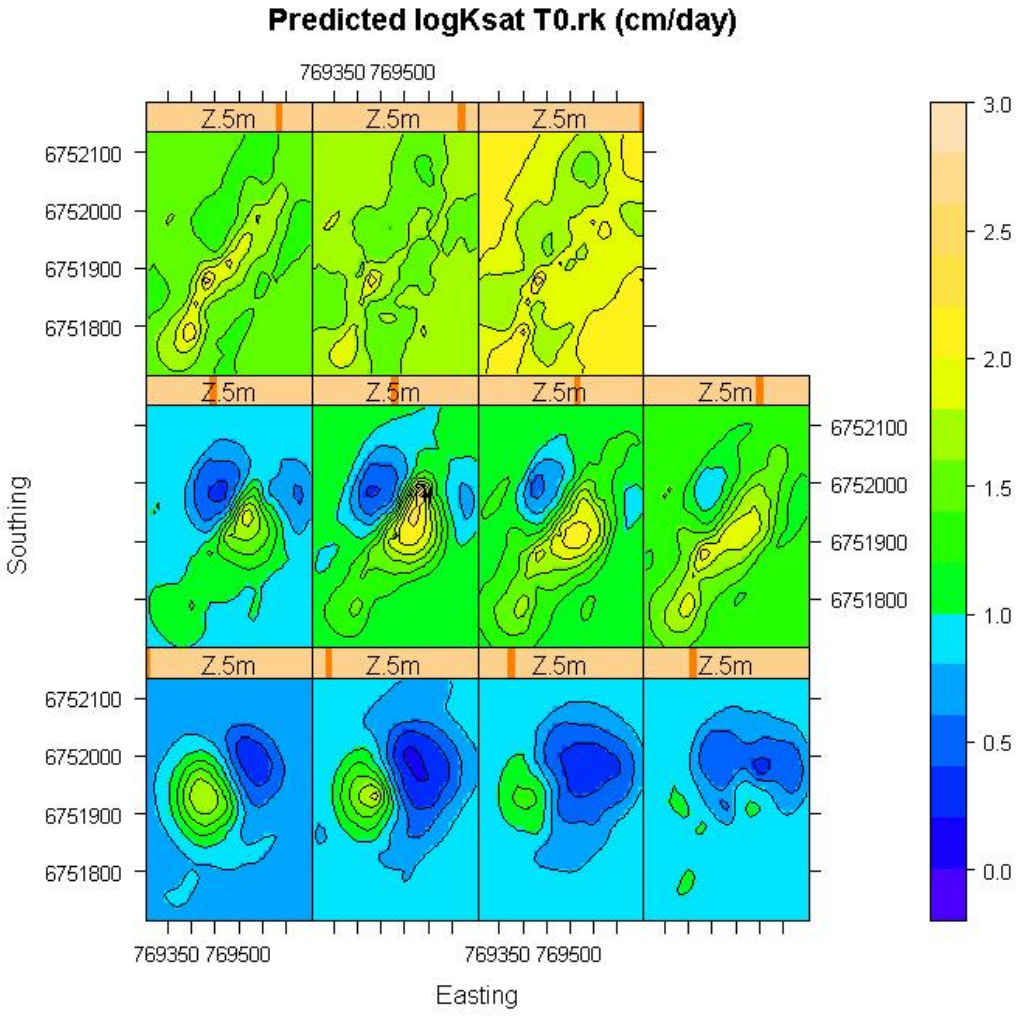

Figure 5.36 Predicted K_{sat} slices from 0 (top right) to 10 m (bottom left) at 1m intervals using 0^{th} order Tikhonov inversion with clustered scaling factors.

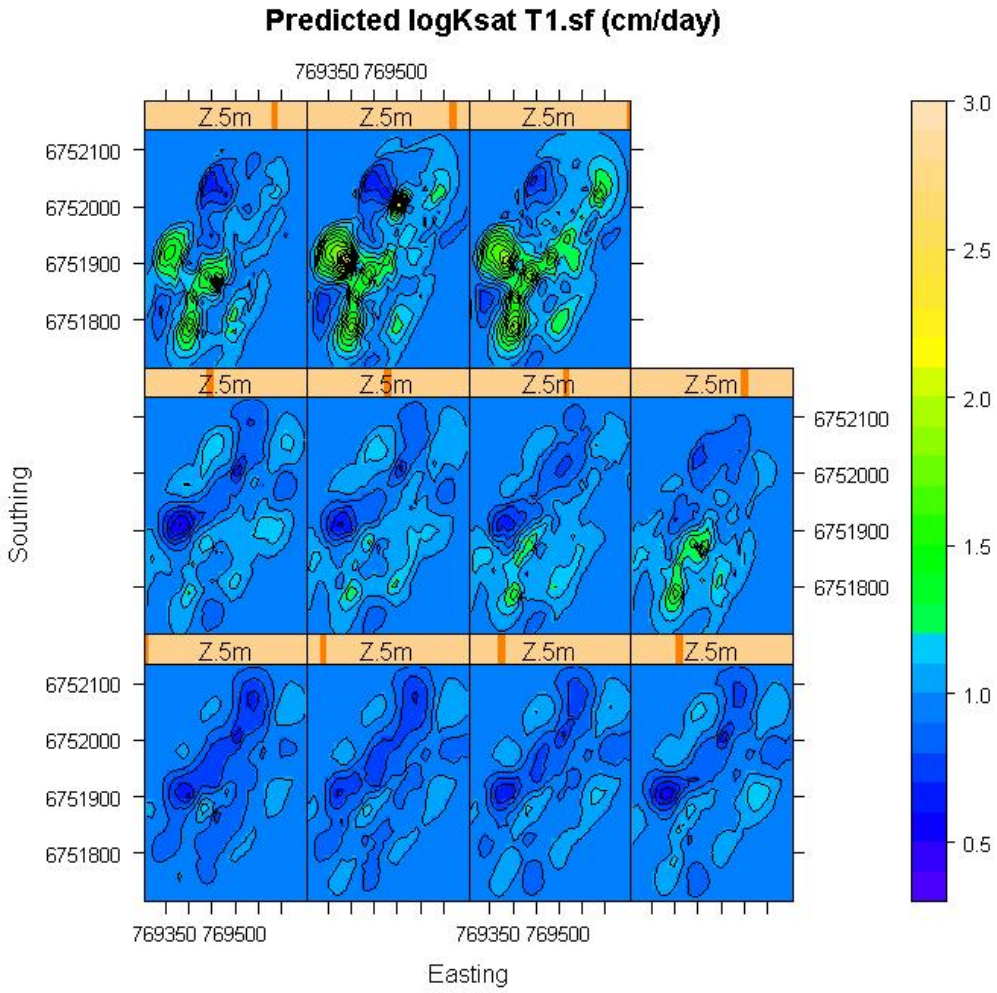

Figure 5.37. Predicted Ksat slices from 0 (top right) to 10 m (bottom left) at 1m intervals using 1st order Tikhonov inversion with clustered scaling factors.

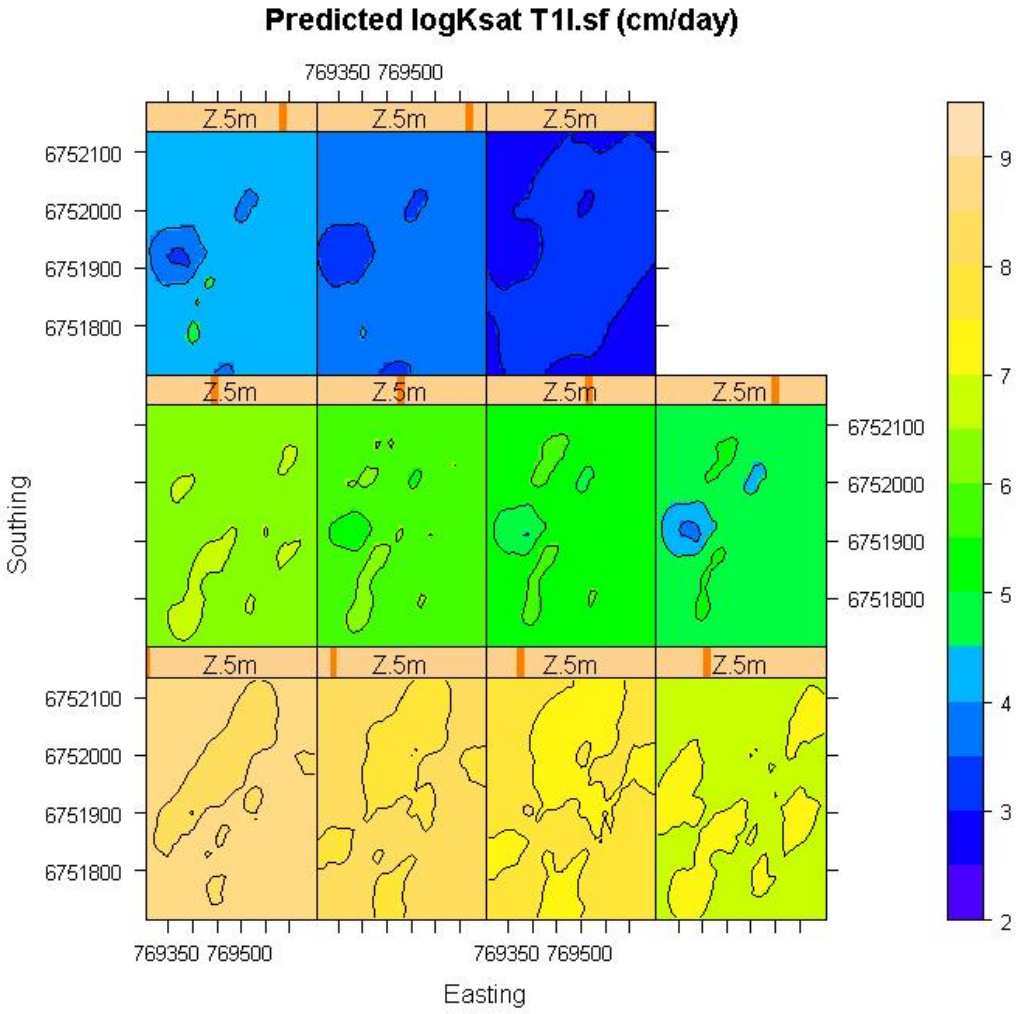

Figure 5.38. Predicted K_{sat} slices from 0 (top right) to 10 m (bottom left) at 1m intervals using 1st order Tikhonov inversion with logistic scaling factors.

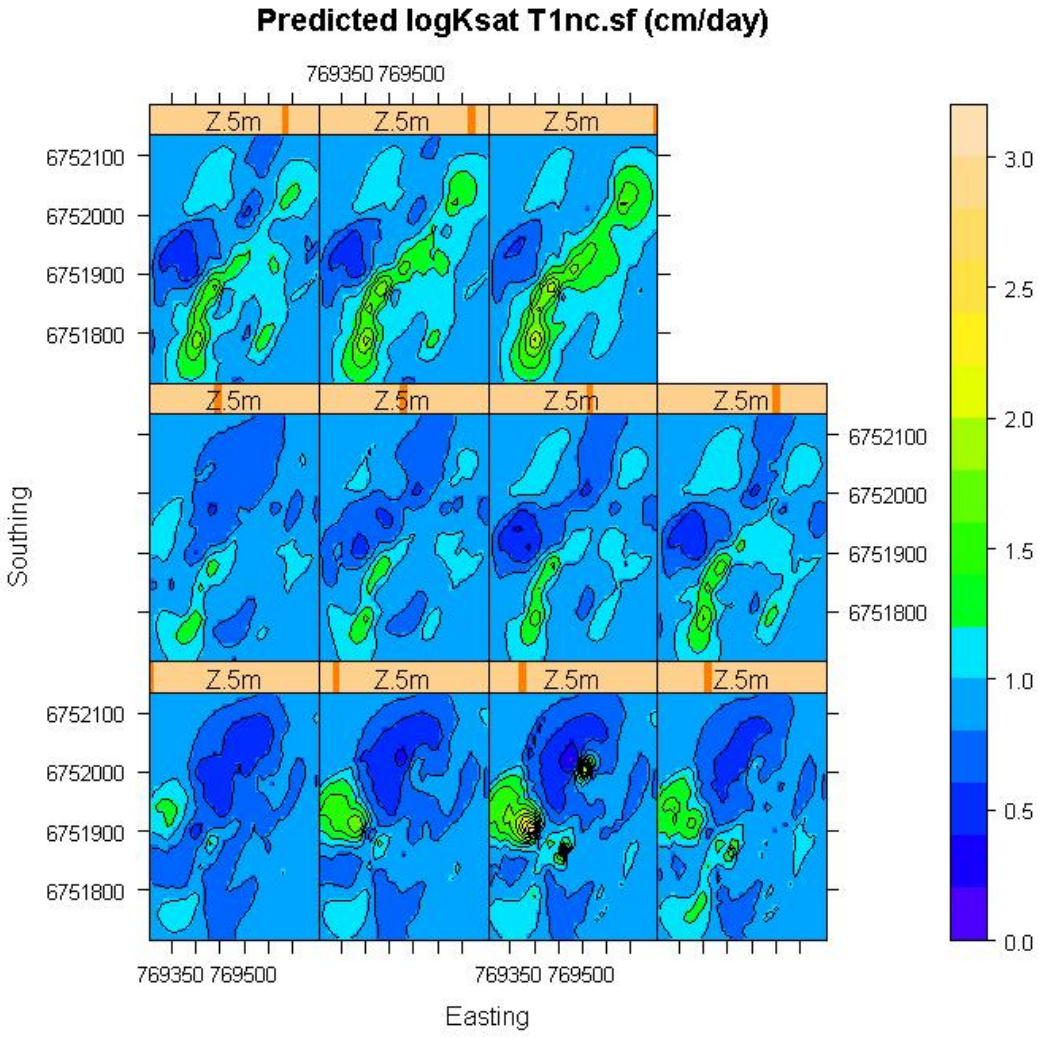

Figure 5.39 Predicted K_{sat} slices from 0 (top right) to 10 m (bottom left) at 1m intervals using 1st order Tikhonov inversion with unclustered scaling factors.

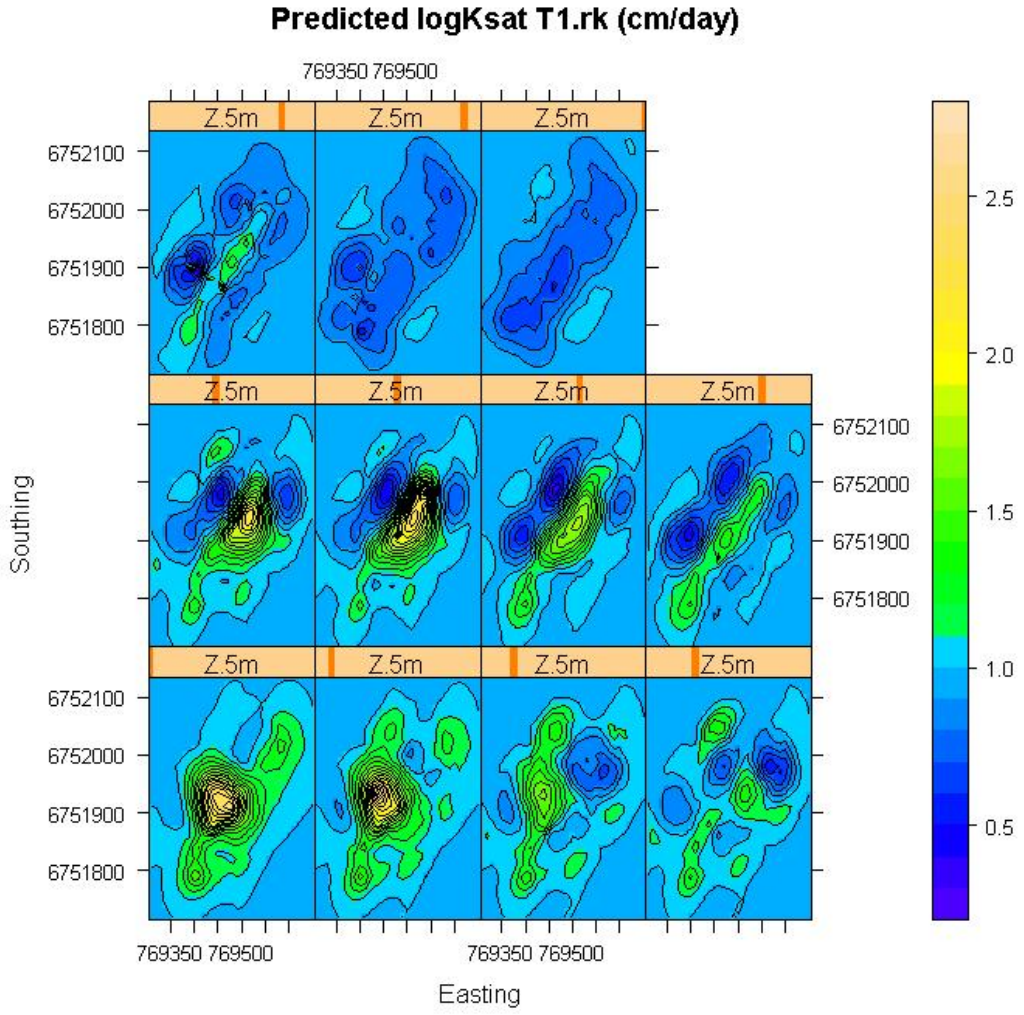

Figure 5.40. Predicted K_{sat} slices from 0 (top right) to 10 m (bottom left) at 1m intervals using 1st order Tikhonov inversion with regression kriging.

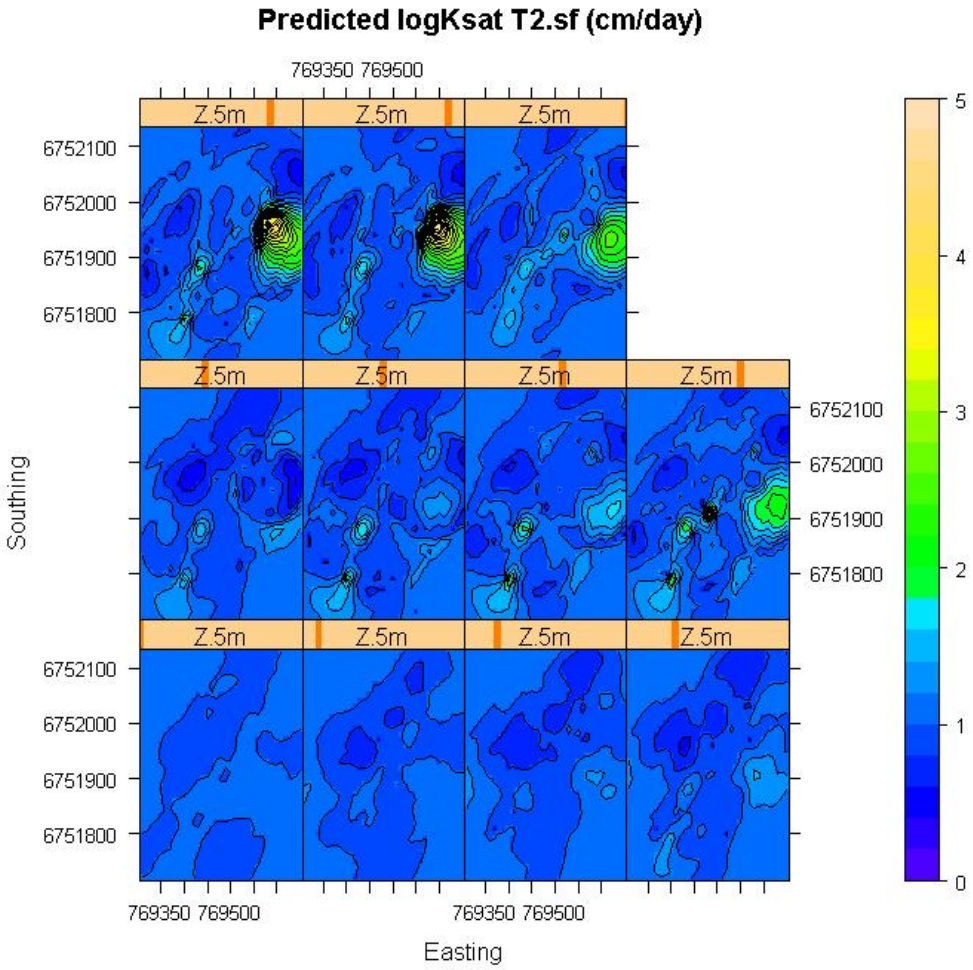

Figure 5.41. Predicted K_{sat} slices from 0 (top right) to 10 m (bottom left) at 1m intervals using 2nd order Tikhonov inversion with clustered scaling factors.

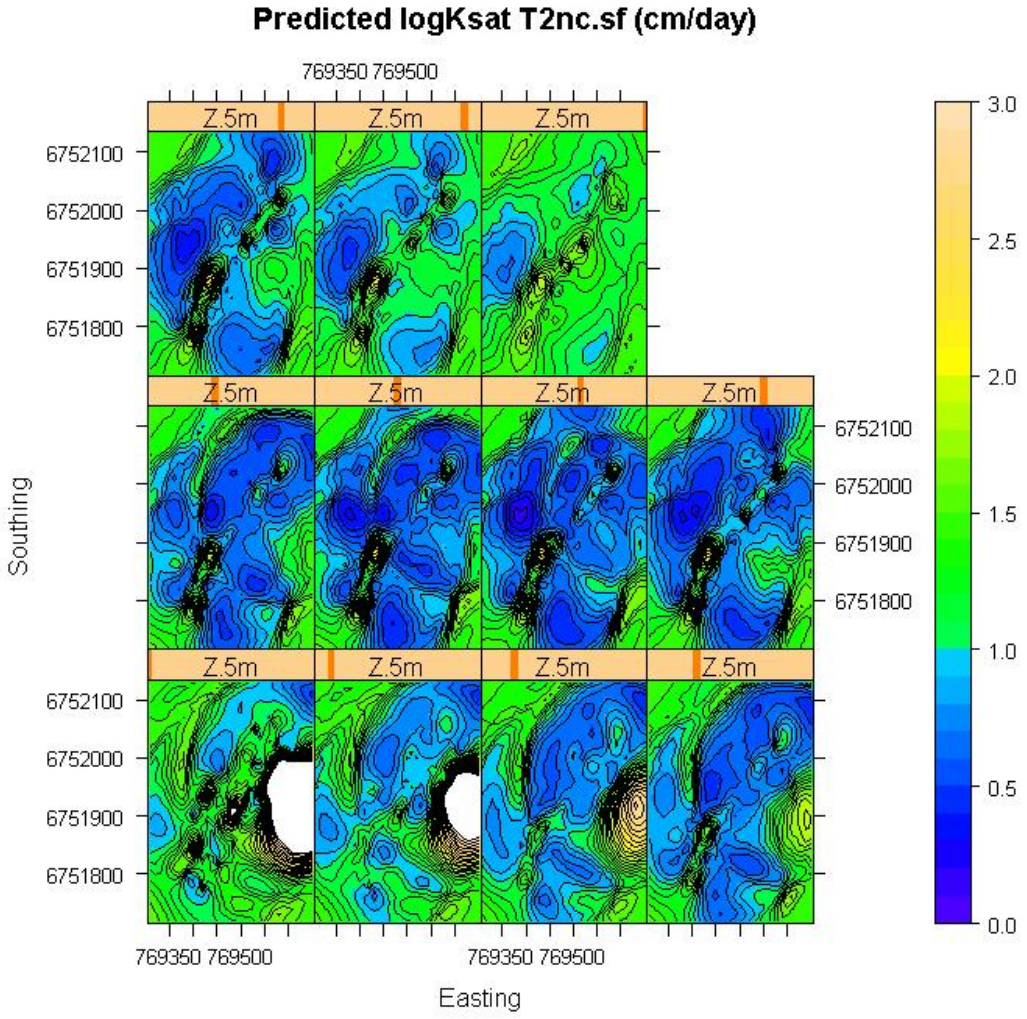

Figure 5.42. Predicted K_{sat} slices from 0 (top right) to 10 m (bottom left) at 1m intervals using 2nd order Tikhonov inversion with nonclustered scaling factors. Results truncated at 3.0 cm day^{-1} due to anomalously high results.

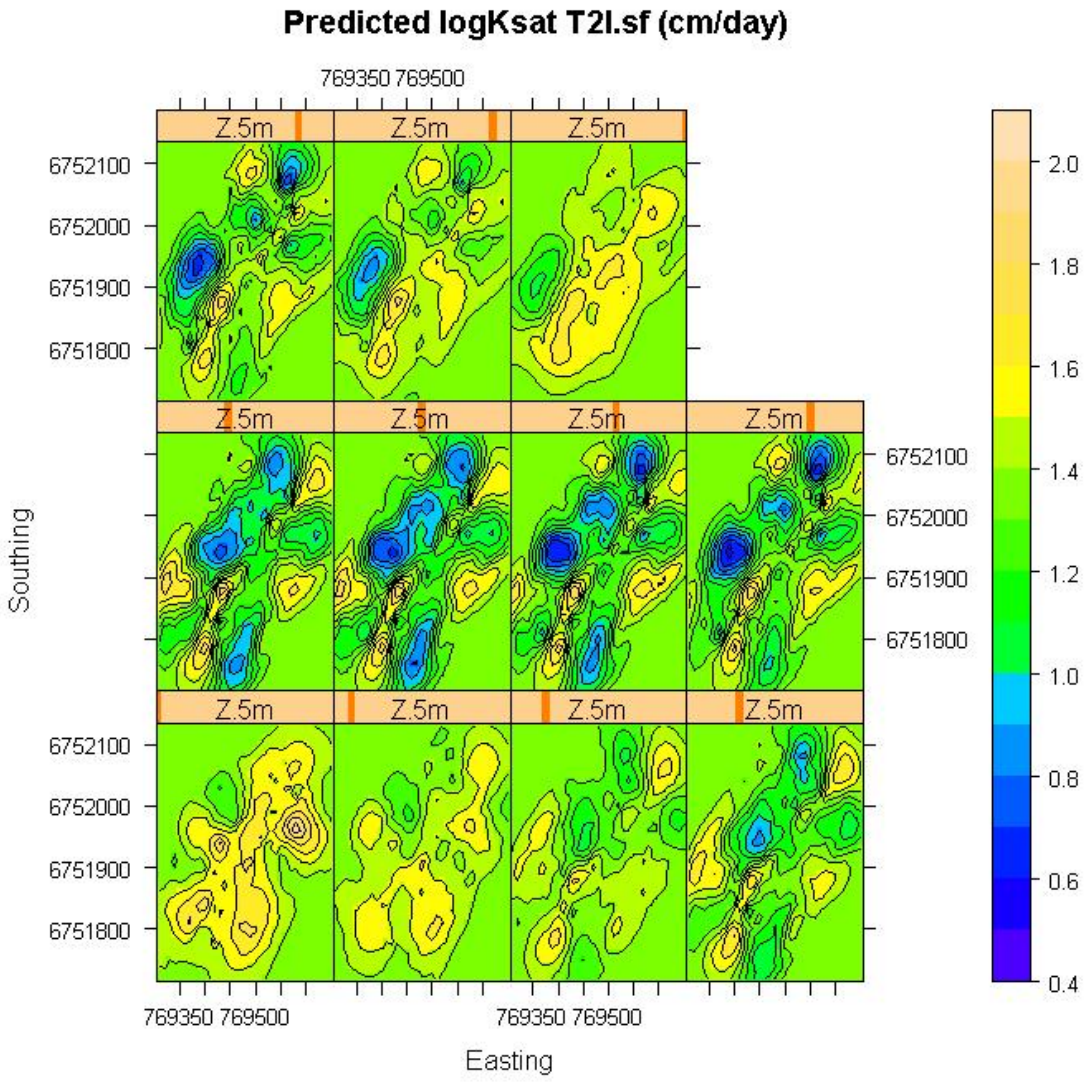

Figure 5.43. Predicted K_{sat} slices from 0 (top right) to 10 m (bottom left) at 1m intervals using 2nd order Tikhonov inversion with logistic scaling factors.

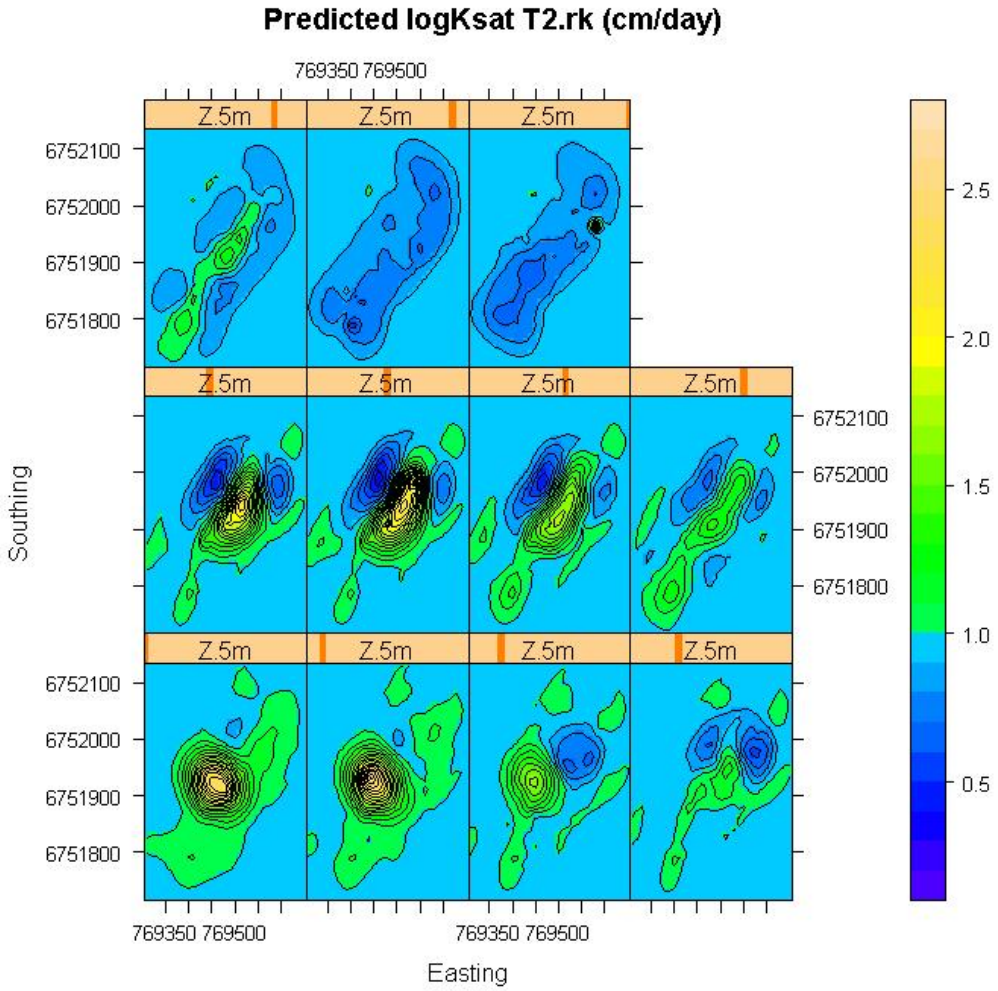

Figure 5.44. Predicted K_{sat} slices from 0 (top right) to 10 m (bottom left) at 1m intervals using 2nd order Tikhonov inversion with logistic scaling factors.

Chapter 6

General discussion and future research

6 General discussion and future research

6.1 Project summary

In 1968, a detailed soil survey by Stannard and Kelly (1968) identified palæochannels and surrounding areas as being inappropriate for surface irrigation, based on the coarser-textured topsoil. In practice, the structures are commonly incorporated into irrigated paddocks, mostly due to their ubiquitous presence and lack of surface expression. Previous studies have used electromagnetic induction to map the aerial extent and predicted the risk of deep drainage based on the cation exchange capacity of the soils above palæochannels (Triantafilis et al., 2003a; 2004). However, there have been limited investigations aimed at understanding the exact hydrological behaviour of the structures.

Palæochannels in other parts of New South Wales have varying characteristics and impacts on the surrounding landscape. In the Murrumbidgee Irrigation District, palæochannels are generally disconnected from present water courses and harbour salinity (Page and Nanson, 1996; Rogers et al., 2002; Timms and Acworth, 2002). Conversely, they are thought to be more strongly connected to present day watercourses in the Namoi Catchment. Here, structures and are generally thought to inhibit groundwater recharge from the river to lower aquifers (Merrick et al., 1987; Williams et al., 1989; Young et al., 2002), but have been shown to contribute to groundwater recharge under certain conditions (Ross et al., 1991; Bish and Ross, 2001). Previous studies have suggested that palæochannels in the Gwydir Catchment Area are similar to those from the Namoi (Stannard and Kelly, 1968; Triantafilis et al., 2003a), based primarily on soil survey information.

This study aimed to investigate hydrological impacts of palæochannels in the Gwydir River Basin. This was exemplified in an agricultural setting where palæochannels are likely to have the largest impact on the environment. The study used traditional geologic and hydrologic methods, coupled with the development of a more rapid and economical means of exploration. By combining existing knowledge of the soil properties with geophysical information, the spatial distribution of the physical properties controlling the hydrological behaviour was predicted.

6.2 General conclusions

Specifically, this study finds that:

- The morphology of the palæochannel is very complex and spatially variable with multiple successions of deposited materials within the structure. A strong aeolian component overlyies the structure and a deposit of heavy clay of variable thickness underlies the structure
- A perched water table forms within the palæochannel coinciding with water levels in a nearby irrigation channel. In this setting, there is a much stronger component of lateral flow within the structure compared to the deep drainage potential from water applied to the surface
- While the EM proved to be an effective tool to delineate the horizontal component of the palæochannel, the vertical dimensions were not as easily determined due to the use of multiple instruments and subjectivity in the inversion algorithms used. The use of ground-penetrating radar in these environments is severely limited due to the high electrical conductivity of the soils
- The use of scaling factors likely improved on traditional soil coring techniques or stochastic simulation to predict hydraulic properties; however, due to limitations in the prediction of the vertical contrasts in soil properties and the use of pedotransfer functions, which carry a relatively high degree of uncertainty, this method stands to be improved before being incorporated into traditional hydrologic investigations.

These topics are discussed in detail in the following subsections, followed by a discussion of how this study can be used to build on our general understanding of these structures, and how we can use techniques similar to those presented to improve our ability to quantify groundwater flow in heterogeneous environments.

6.2.1 Palæochannel characteristics

Similar to the geologic interpretation by Stannard and Kelly 1968, three distinct geologic units were found to exist within the regolith surrounding the palæochannel. These were mainly identified through K means clustering of the soil

physical properties following Odeh et al. (1992), McBratney et al. (1992) and Triantafilis et al. (2003b). The units consisted of:

- a coarse-grained deposit on the bottom of the palæochannel, consisting of poorly-sorted coarse sands and gravels, likely to have been the former stream bedload (Schumm, 1968; Stannard and Kelly, 1977);
- an overlying medium- to fine-grained deposit, comprised of medium to fine sands and kaolinitic clays, which extends from the channel banks on alternating sides of the channel. This feature was likely deposited during the waning stages of the stream, and during overbank conditions, and appears to contain an aeolian component (Stannard and Kelly, 1977; Page and Nanson, 1996); and
- the background soil comprised of mostly smectite-dominated Vertosols (Stannard and Kelly, 1968; Stannard and Kelly, 1977; Triantafilis et al., 2003a).

6.2.2 Deep drainage associated with the palæochannel

Based on previous studies in the region, it was hypothesised that excessive deep drainage was occurring above the palæochannel, due to the coarser-textured topsoil sediments (Triantafilis et al., 2003a; Triantafilis et al., 2004). These statements were based on the salt and leaching fraction model (Shaw and Thorburn, 1985), which empirically relates the soil texture CEC and irrigation water quality to deep drainage potential. It is assumed that if the majority of deep percolation occurred through the soil matrix, this would be reflected in the chloride content (Thorburn et al., 1990; Willis et al., 1997; Weaver et al., 2005), which was not significantly lower inside the palæochannel.

However, predominant matrix flow seems unlikely considering the significant changes in soil textural properties between the background soil, the palæochannel deposit and the overlying soil (Bouma and Wosten, 1979; Thorburn and Rose, 1990). There are several possible explanations for the chloride profiles. The first explanation is that the profiles reflect dramatic changes in soil texture, where breakthrough would only occur during saturated conditions (Bouma, 1981). This theory would require water to accumulate at a depth of approximately two metres (where the soil texture changes above the palæochannel), until it evaporates. This would not be the case

outside the palæochannel where the soil texture is relatively uniform, but a similar curve would result from the flushing of salts below the root zone during irrigation events. Support for this argument comes from the chloride data which shows a maximum concentration at two metres below the surface and sharply decreases below this. Alternatively, as the study site concentrated mainly on the tail drain end of the field, the tail ditch may have affected the chloride distribution due to the evaporation of excess irrigation water (Amali et al., 1997). This is supported by the higher topsoil chloride and EC_e measurements occurring to the west of the palæochannel (nearest the tail ditch) with the highest concentration of dissolved solids found at the end of Transect 8 which is located nearest the junction with the return channel.

Another possible explanation is that infiltration is dominated by bypass flow, meaning that residual chloride is not leached from the profile during infiltration. This process commonly affects deep drainage predictions from chloride mass balance predictions in Vertosols (Bronswijk, 1988; Jarvis and Leeds-Harrison, 1990; Thorburn and Rose, 1990; Willis et al., 1997) (Section 2.4.1). This process would be likely in the background soil under very dry conditions due to the shrink-swell nature of Vertosols (Bronswijk, 1988; Thorburn and Rose, 1990), but could also occur in other areas (Larsson and Jarvis, 1999; Seiler et al., 2002). This would reflect the high spatial variability of chloride as was found on this site.

Ideally, a more direct approach could be used to quantify deep drainage through palæochannels. Unfortunately, this study cannot support any of these arguments due to the malfunctioning tube tensiometers. These instruments have been fixed, but long-term monitoring will be necessary to be able to quantify the drainage events. In the future, the drainage meters will hopefully provide considerable insight in the rate and timing of deep drainage occurring within and around the palæochannel.

6.2.3 Groundwater flow through the palæochannel

Based on the soil variability and water table dynamics along the length of the palæochannel, a two-dimensional conceptual model of palæochannel behaviour can be developed. In particular, observations from the piezometers indicate that water flow is anisotropic, with the horizontal component being far greater than the vertical component. The immediate response to irrigation events, where water appeared to be flowing from the irrigation channel into the paddock via the palæochannel supports

this notion. However, the peaks in the groundwater hydrograph are generally not aligned with the dates of water applied to the soil surface. This is likely explained by the presence of an irrigation canal, which bisects the palæochannel at the north side of the paddock. This channel often carries in excess of two metres of water, which would rapidly flow through the coarse palæochannel sediments and would likely be perched on top of the fine sediments underlying the palæochannel. These observations have been seen in other palæochannel systems which have direct connection to present-day streams (Sophocleous, 1991).

The connection between the palæochannel and the irrigation channel has several environmental and economical implications. The first is that water (and agrochemicals) which percolate into the palæochannel during irrigation events could move offsite (Steinheimer et al., 1998). In the case presented in this study, there is strong possibility that this water will eventually flow into the nearby stream, or possibly drain into the Narrabri Formation where the underlying clay layer thins out. Of economic consequence to the farmer, is the significant loss of water from the irrigation channel into the palæochannel. Considering the dimensions and specific yield of the palæochannel and given the measured one metre rise in groundwater levels associated with the pulse through the irrigation channel, this translates to at least 2.1 Ml per event (defined by the pulse of water through the irrigation channel). It can be seen from the hydrological data that this pulse occurred 13 times over the course of the season due to the use of the irrigation channel to supply water to neighbouring paddocks. Over the course of the observation period (10 months), this translates to a loss of 27.3 Ml water into the palæochannel. This loss is a very conservative estimate based on the piezometer farthest away from the channel, and assumes an instantaneous pulse, which terminates at the piezometer. Given the conservative estimate of the water loss from the channel and the ubiquitous presence of palæochannels in this area, it is likely that the farm is losing many more megalitres per year through the palæochannel structures.

The nested piezometers indicated that there was a direct connection between the palæochannel and the fine sediments below. This was shown by a very short lag in time between the rapid rise in water levels in the palæochannel and the start of a slower rise in levels in the clay sediments beneath. This could also be related to changes in the overburden or barometric pressure (Rasmussen and Crawford, 1997).

Long term monitoring of groundwater levels in the Narrabri Formation is necessary to determine whether the majority of water percolates downwards into the formation, or laterally into the stream. The current groundwater level in the Narrabri Formation is 15 metres below the surface. Considering the high specific yield of the formation, it seems unlikely that the water from a localised source like this could contribute to groundwater rise in the formation. However, a similar process happened over several decades in the Murrumbidgee Irrigation District to the south (Willis and Black, 1996), and some areas of the neighbouring Namoi and Border Rivers Catchment area (Williams et al., 1989).

The quality of the water would depend on whether the irrigation is carrying water to the paddock (which would be similar to the source of the irrigation water) or whether it is carry water from the paddock (which would most likely contain salts and agrochemicals). While the second case would be more environmentally detrimental, the amount of deep drainage occurring through the palæochannel would probably be much less due to the lower hydraulic heads in the canals during the return of tail water to the settling ponds.

6.2.4 EM efficacy in natural vegetation

Similar to the results found by Barrett et al (2002), the efficacy of EM instruments in this semi-arid environment with heavy clays appears to be strongly controlled by the soil moisture content. This was most apparent in the area of natural vegetation, where the instruments were unable to detect the palæochannel, even though it was clearly identified in the soil cores. There are several possible explanations for this.

During the quadbike EM survey, the topsoil moisture content was approximately 0.15 g g^{-1} outside the paddock. Taylor and Barker (2002) showed that a dramatic decrease in electrical conductivity occurs around 0.1 to 0.2 g g^{-1} in sandstones saturated with groundwater ranging from 400 to 1600 μS cm^{-1}. Below this threshold, surface conduction, which is the primary flow pathway for EM waves in highly conductive clays with non-saline soil water, dominates the pathway (McNeill, 1980a). This is because of the minimal difference in the electrical conductivity of the solid fraction. A minimum moisture content threshold exists based on the thickness of the diffuse double layer surrounding the clay particles (Rhoades et al., 1989b). This

threshold would be based primarily on the clay content and mineralogy and would be site specific, but empirical relationships could be determined in the laboratory where the moisture content and solution EC could be strictly controlled (Nadler and Frenkel, 1980; Emerson and Yang, 1997). This complex interplay between saturation percentage, clay content and electrical conductivity highlights a significant weakness in the scaling factors approach due to the assumptions made in models. The model is based on the findings of De Lima and others who assumed a simplified linear approximation of this relationship based on the effective medium theory (de Lima and Sharma, 1990; de Lima, 1995; de Lima and Niwas, 2000; de Lima et al., 2005). While this relationship may have existed inside the paddock, where the moisture content was not limiting surface conduction, it is not likely a valid approximation under drier conditions, where electromagnetic flow paths are controlled by water content, rather than cation exchage capacity.

6.2.5 Ground-penetrating radar results

The lack of reliable results from the GPR system highlights the necessity to explore other rapid, non-invasive methods for mapping highly conductive soils, such as are commonly found in Northern New South Wales. It was hoped that, by using an unshielded bistatic antenna of relatively low frequency and high Q output, the affects of signal attenuation would have been minimised to the point where reflections would not be lost over the less-conductive palæochannel. However, it was found that this was still an ineffective method for mapping the palæochannel sediments in these environmental conditions.

The use of the common-midpoint surveys allowed for the direct calculation of the soil moisture content, which correlated very well with direct measurements. This was possible because of the minimal distance that the signal had to travel. Although this method not new (Huisman et al., 2003), the findings support the use for rapid assessment of topsoil moisture content in this region.

6.2.6 The EM vertical sounding method

In contrast to ground-penetrating radar, the EM instruments were well-suited for imaging the heavy clays in the irrigated paddock. This was due to the strong contrast in physical properties between the palæochannel and the surrounding

sediments. The prediction of soil properties with depth was limited due to the use of multiple instruments and the inversion algorithms explored in this study. According to McNeill (1980), the depth of penetration is limited by the geometric configuration of the coil separation in most environments. While McNeill's statements have been challenged over the years (i.e. Merrick (1997)), the simplicity of this arrangement is attractive when considering the prediction of geologic properties with depth. The alternative, nonlinear inversion models are more complex, and therefore incorporate more physically-based assumptions, making them (seemingly) more subjective. However, this study highlights the strong influence that the choice of inversion algorithm has on EC prediction. This means that each regularised method produced EC estimates which correlated to different soil properties. Similar to this study, Borchers et al. (1997) and Hendrickx et al. (2002) found good correlation between 2^{nd} order regularisation and salinity, whereas McBratney et al. (2000) found 0^{th} order to be the best predictor of soil boundaries. Because there were no depth-constrained apparent conductivity readings at depth (i.e. through the use of a conductivity probe), it is not possible to say which of these methods performed best, however the 0^{th} order method was most strongly correlated to the predicted EC from the forward modelled EC_a predictions. In this sense, the use of down-hole EM would be ideal for comparison (as the conductivity probe would be depth-limited).

The inversion method could have been improved using several methods. For example, downhole EM or predicted EC_a from soil properties could be used to constrain the conductivity predictions, or provide a better initial guess for the inversion algorithm (Auken and Christiansen, 2004). While the inversion would only be constrained at the measurement points (in this case, only 8 points across the paddock), lateral constraints could also be used to help shape the inversion. Several commercially-available non-linear inversion algorithms have this function built into them, and it is likely that this would have resulted in more stable solutions for all of the methods (Schultz and Ruppel, 2005). While these approaches are more common in petroleum and groundwater exploration studies, they require extensive coring, which would undermine the goals of this study..

6.2.7 Scaling factor prediction of K_{sat} fields

The scaling factor approach to predict K_{sat} fields is an attractive idea, based on the amount of information gained from a relatively inexpensive data set. The approximate cost of obtaining the soil physical property information (from sample collection to laboratory analysis) was $48 000, with an additional $11 500 for the EM surveys. This makes the cost of the regression kriging approach (which contains the maximum amount of information and the minimum amount of uncertainty) approach $60 000 to image a 40 ha site (not including the cost of computation). Had the K_{sat} of the cores been measured in the laboratory (rather than using pedotransfer functions) this cost rises to $109 000 (using laboratory prices from 2000 (Minasny and McBratney, 2002a)). The scaling factors approach using a reference K_{sat} from reported literature would reduce this cost to around $10 000 for the 40 ha field (assuming a limited number of vertical soundings).

This cost savings, however, comes at the expense of uncertainty. Although Minasny and McBratney (2002) argue for more relatively uncertain measurements, compared to a limited number of certain ones, estimating the uncertainty in hydrological and geophysical models is difficult and has the potential to induce subjectivity (Binley and Beven, 2003; Pappenberger and Beven, 2006). The uncertainty in this model would best be addressed through Monte Carlo or Latin-hypercube sampling techniques, where a distribution of likely values is sampled several times and the results used to constrain the predictions (Schaap and Leij, 1998; Minasny and McBratney, 2002b; Vervoort et al., 2004). In this case, there would be several distributions, including the K_{ref} value (which could be directly extracted from Neurotheta predictions), the EM data (using the reported values for instrument-specific noise), and the regularisation order of the inversion method. However in a comparable study, the pedotransfer function uncertainty far outweighed differences due to the inversion or interpolation method (Vervoort and Annen, 2006).

There are still some critical issues with this model that need to be addressed, before it can be applied widely. The most obvious is the poor correlation between the modelled saturated conductivity and the measured saturated conductivity, which is likely due to a combination of physically and empirically-derived errors discussed below.

6.2.7.1 Smoothing operations

Smoothing of the data has been introduced at several steps in this model. The first is from the initial generation of EC predictions using the inversion algorithm. In the case of the Tikhonov regularisation, this step is necessary in order to predict a stable solution, but the choice in the smoothing operator is arbitrary. At this field site, the least smoothed 0^{th} order regularisation was most strongly correlated with modelled EC_a as well as the soil physical properties, while the most smoothed 2^{nd} order regularisation was most strongly correlated with soil EC_e. In the McNeill method, a smoothing operator was used to generate layers of equal thickness, which also had significant impacts on the predictions following the inversion of the EC_a data. Smoothing was later introduced in the three dimensional kriging process, which (compared to regression or trend kriging) has been shown to give the most biased estimate (Triantafilis et al., 2001b). This procedure likely had a very large impact on the data, which was reflected in the regression coefficient of 0.70 from the kriged versus non-kriged measured soil properties. This amount of bias would likely have translated to the scaling factor methods, and could possibly explain the poor relationship with soil properties following the kriging procedure.

6.2.7.2 Inversion of data from multiple instruments

Apart from Vervoort and Annen (2006) there has been little research into the use of multiple instruments to derive conductivity profiles. More commonly, synthetic data, data from the EM 38 at various heights, or from the EM 34 at various separation distances has been inverted (Borchers et al., 1997; Hilgendorf, 1997; Gomez-Trevino et al., 2002; Schultz and Ruppel, 2005). This difference is likely to have a large impact on the inversion, due to spatially-correlated errors owing to instrument specific noise and resolution of the deeper penetrating instruments. Considering that the inversion algorithm is most sensitive to errors from these instruments (Aster et al., 2005), the relatively poor correlation with soil properties is not surprising. In addition, the EM signal is sensitive to a range of soil properties (Friedman, 2005), so it partly depends on which property dominates and best describes the variation. In this study, it was assumed that clay content was the strongest predictor of the apparent electrical conductivity (e.g. Triantafilis et al., 2003a; Vervoort and Annen, 2006), but it is possible that in this case another property

(EC_e) dominated the instrument response (e.g. Borchers et al., 1997; Hendrickx et al., 2002).

6.2.7.3 The use of pedotransfer functions to predict regolith properties

The use of pedotransfer functions to predict saturated conductivity has been a widely accepted practice in soil physics, mainly due to the extreme variability in K_{sat}, and the difficulty and expense of measurement (McBratney et al., 2002). The two software packages used in this study rely on relatively robust data sets to train the artificial neural network, relating the particle size and bulk density data to measured saturated conductivity. Although the predictions for topsoil K_{sat} fell well within the range of expected values, those for the deeper sediments were several orders of magnitude larger than measured using in situ methods. This would have translated to a shift in the reference K_{sat} (assumed to be the mean K_{sat}) and this in turn would affect the scaling relationship. It is likely that this discrepancy reflects the training sets used for the programs, which were based on topsoil samples (Schaap et al., 2001; Minasny and McBratney, 2002c). Because of overburden pressure, which in particular would compress the clay-rich sediments, the saturated conductivity would be much lower than would be expected in topsoil sediments (Timms and Acworth, 2002). This would have a cumulative effect down the profile where overburden pressure would increase linearly with depth, and hence more strongly affect the deeper sediments. It would be of interest to see if a depth-dependent correction factor applied to the PTF predictions would match the observed hydraulic conductivity from in situ methods.

6.3 Future research

In this study, the effects of the palæochannel on the surrounding landscape were inferred from the soil properties and geophysical data, but the real proof of their effects is in the measurement of the soil water dynamics. The hydrological data presented in this study shows a snapshot of the dynamic nature of the water table. Long-term monitoring of the hydrological response could further clarify the hydrological processes associated with shallow palæochannels in the Gwydir Basin. The use of the tube tensiometer data in conjunction with the piezometers could help bridge the gap between groundwater recharge and deep drainage estimates (Silburn et al., 2004).

Although this research revealed very dynamic field-scale hydrological behaviour, the ideal application for these methods is to predict the hydraulic properties of hydrogeologic facies on the landscape scale. Given the time-intensive nature of using several EM instruments, the vertical sounding procedure would likely be carried out at a limited number of sites following a recognisance survey to predict the spatial covariation of EC_a (Triantafilis et al., 2004). The mobile EM systems would be a perfect compliment to this sampling regime at the farm scale (Triantafilis et al., 2002; Corwin and Lesch, 2005b), where the lateral variation is first identified using the mobile system, followed by a detailed vertical sounding to identify the structure characteristics. Aerial EM would provide support at the catchment scale, and would likely save on the cost associated with land-based mapping, but would not be appropriate for fine-scale applications (Barbiero et al., 2001; Metternicht and Zinck, 2003).

The scaling factors approach could easily be used to predict the hydrologic properties across the landscape, but only under the outlined assumptions. The largest potential problem would come from salinity-affected soils, where the electrical conductivity of the soil water outweighs that of the surface conduction from the clay minerals (Lesch et al., 1992; Borchers et al., 1997; Sudduth et al., 2005). In these situations, a different relationship exists between saturated conductivity and electrical conductivity, and would therefore require a different linear prediction. According to Archie's Law, it would be inverse negative, rather than inverse positive and would be more sensitive to the soil moisture content (Niwas and de Lima, 2003). Although much of the Gwydir Valley is not likely to include this scenario, some of the productive lands in the Northern Murray-Darling Basin are not (MDBC, 1999). It would therefore be worthwhile to repeat this experiment using existing data from salinity-affected areas, such as the Murrumbidgee or Namoi Irrigation Districts.

The ultimate reason for generating the K_{sat} distribution is to use the parameter as input for a groundwater simulation model. This follows the approach of using ancillary data to estimate a hydrologically-important variables to explain how various irrigation management scenarios would affect the outcome of applied water (Triantafilis et al., 2003a; Triantafilis et al., 2004). However, in this case, a much more detailed picture could be derived from the three dimensional data. Given the groundwater measurements, meteorological conditions, and irrigation scheduling, this

model could be calibrated and used for prediction purposes, once the uncertainty in the data is estimated. Although there were significant differences in some of the prediction techniques, it is still unclear how much these differences will affect the prediction of groundwater. It is also unclear wether or not the high-resolution predictions would actually improve on the model predictions using a single reference K_{sat} for the palæochannel, and another for the surrounding sediments. Therefore, multiple groundwater simulations should be carried out comparing the three prediction methods (three dimensional ordinary kriging of measured soil propeties, scaling factor generation, and regression kriging). Because the kriged soil K_{sat} model does not predict the palæochannel - irrigation channel junction, it is unlikely that the different scenarios will produce similar results.

Ideally, this model could also be built on a stochastic framework, where the range in predictions from the pedotransfer functions could be used to generate the distribution of predictions at a single point. This would replace the single K_{ref} value, but would still be scaled according to the EM data. Thus, the palæochannel structure would be maintained, and the power of stochastic prediction could be used to set confidence limits to the predictions.

References

SAS Institute, Inc. 2003. JMP. Release 5.1. SAS Institute, Inc., Carry, NC, USA.

Aboumatar, H., and G.G. Goble. 1997. SPT dynamic analysis and measurements. Journal of Geotechnical and Geoenvironmental Engineering 123:921-928.

ABS. 2005. Australian farming in brief. Australian Bureau of Statistics.

Ahmed, M.F. 2001. Simulating and assessing salinisation in the lower Namoi valley. M.Sc. Agr. thesis, The University of Sydney, Sydney.

Al-Jamal, M.S., S. Ball, and T.W. Sammis. 2001. Comparison of sprinkler, trickle and furrow irrigation efficiencies for onion production. Agricultural Water Management 46:253-266.

Al-Qinna, M.I., and A.M. Abu-Awwad. 1998. Soil water storage and surface runoff as influenced by irrigation method in arid soils with surface crust. Agricultural Water Management 37:189-203.

Allison, G.B., and M.W. Hughes. 1983. The use of natural tracers as indicators of soil-water movement in a temperate semi-arid region. Journal of Hydrology 60:157-173.

Allison, G.B., G.W. Gee, and S.W. Tyler. 1994. Vadose-zone techniques for estimating groundwater recharge in arid and semiarid regions. Soil Science Society of America Journal 58:6-14.

Allison, G.B., P.G. Cook, S.R. Barnett, G.R. Walker, I.D. Jolly, and M.W. Hughes. 1990. Land clearance and river salinisation in the western Murray Basin, Australia. Journal of Hydrology 119:1-20.

Amali, S., D.E. Rolston, A.E. Fulton, B.R. Hanson, C.J. Phene, and J.D. Oster. 1997. Soil water variability under subsurface drip and furrow irrigation. Irrigation Science 17:151-155.

Anand, R.R., and M. Paine. 2002. Regolith geology of the Yilgarn Craton, Western Australia: implications for exploration. Australian Journal of Earth Sciences 49:3-162.

Anderson, M.P. 1995. Groundwater modeling in the 21st century, p. 79-93, *In* A. I. El-Kadi, ed. Groundwater Models for Resources Analysis and Management. CRC, Boca Raton, Fl.

Armstrong, D.W., and K.A. Narayan. 1998. Groundwater processes and modelling, p. 17, *In* L. Zhang, ed. Basics of recharge and discharge. CSIRO Publishing, Melbourne.

Asmussen, L.E., H.F. Perkins, and H.D. Allison. 1986. Subsurface descriptions by ground-penetrating radar for watershed delineation. Georgia Agricultural Experiment Stations College of Agriculture University of Georgia, Athens, Ga.

Asprion, U., and T. Aigner. 1999. Towards realistic aquifer models: three-dimensional georadar surveys of Quaternary gravel deltas (Singen Basin, SW Germany). Sedimentary Geology 129:281-297.

Aster, R.C., C.H. Thurber, and B. Borchers. 2005. Parameter estimation and inverse problems Elsevier Academic Press, Amsterdam ; Boston.

Auken, E., and A.V. Christiansen. 2004. Layered and laterally constrained 2D inversion of resistivity data. Geophysics 69:752-761.

Ayars, J.E., C.J. Phene, R.B. Hutmacher, K.R. Davis, R.A. Schoneman, S.S. Vail, and R.M. Mead. 1999. Subsurface drip irrigation of row crops: a review of 15 years of research at the Water Management Research Laboratory. Agricultural Water Management 42:1-27.

Bailey, S.D., A.G. Wintle, G.A.T. Duller, and C.S. Bristow. 2001. Sand deposition during the last millennium at Aberffraw, Anglesey, North Wales as determined by OSL dating of quartz. Quaternary Science Reviews 20:701-704.

Banerjee, D., K. Page, and K. Lepper. 2002. Optical dating of palaeochannel deposits in the Riverine Plain, southeastern Australia: Testing the reliability of existing thermoluminescence dates. Radiation Protection Dosimetry 101:327-332.

Barbiero, L., S. Cunnac, L. Mane, C. Laperrousaz, C. Hammecker, and J.L. Maeght. 2001. Salt distribution in the Senegal middle valley: Analysis of a saline structure on planned irrigation schemes from N'Galenka creek. Agricultural Water Management 46:201-213.

Barrett, B., G. Heinson, M. Match, and A. Telfer. 2002. Geophysical methods in saline groundwater studies: locating perched water tables and fresh-water lenses. Exploration Geophysics 33:115-121.

Barth, G.R., M.C. Hill, T.H. Illangasekare, and H. Rajaram. 2001. Predictive modeling of flow and transport in a two-dimensional intermediate-scale, heterogeneous porous medium. Water Resources Research 37:2503-2512.

Batty, J.C., S.N. Hamad, and J. Keller. 1975. Energy inputs to irrigation, pp. 293-307 Journal of the Irrigation and Drainage Division, Proceedings of the American Society of Civil Engineers, Vol. 101.

Baumhardt, R.L., C.W. Wendt, and J.W. Keeling. 1993. Tillage and furrow diking effects on water-balance and yields of sorghum and cotton. Soil Science Society of America Journal 57:1077-1083.

Bear, J., and A. Verruijt. 1987. Modeling groundwater flow and pollution: with computer programs for sample cases D. Reidel Publishing Company, Boston, U.S.A.

Beard, J.S. 2002. Palaeogeography and drainage evolution in the Gibson and Great Victoria Deserts, Western Australia. Journal of the Royal Society of Western Australia 85:17-29.

Becker, A., and P. Braun. 1999. Disaggregation, aggregation and spatial scaling in hydrological modelling. Journal of Hydrology 217:239-252.

Beven, K., and P. Germann. 1982. Macropores and Water-Flow in Soils. Water Resources Research 18:1311-1325.

Binley, A., and K. Beven. 2003. Vadose zone flow model uncertainty as conditioned on geophysical data. Ground Water 41:119-27.

Binley, A., G. Cassiani, R. Middleton, and P. Winship. 2002. Vadose zone flow model parameterisation using cross-borehole radar and resistivity imaging. Journal of Hydrology 267:147-159.

Bird, T.L., T.M. Willis, and G.J. Melville. 1996. Subsoil hydraulic conductivity estimates for the Lower Macquarie Valley. Australian Journal of Soil Research 34:213-228.

Bish, S., and J.B. Ross. 2001. Recharge Assessment for Priority Groundwater Systems within NSW. Department of Land and Water Conservation.

Bishop, T.F.A., and A.B. McBratney. 2001. A comparison of prediction methods for the creation of field-extent soil property maps. Geoderma 103:149-160.

Boll, J., R.P.G. van Rijn, K.W. Weiler, J.A. Ewen, J. Daliparthy, S.J. Herbert, and T.S. Steenhuis. 1996. Using ground-penetrating radar to detect layers in a sandy field soil. Geoderma 70:117-132.

BOM. 2002. Climate averages for Australia [Online]. Available by Australian Bureau of Meteorology, Commonwealth of Australia www.bom.gov.au (verified Januray, 2006).

Bond, W.J., and I.R. Phillips. 1990. Ion-transport during unsteady water-flow in an unsaturated clay soil. Soil Science Society of America Journal 54:636-645.

Bond, W.J., B.N. Gardiner, and D.E. Smiles. 1982. Constant-flux absorption of a tritiated Calcium-Chloride solution by a clay soil with anion exclusion. Soil Science Society of America Journal 46:1133-1137.

Borchers, B., T. Uram, and J.M.H. Hendrickx. 1997. Tikhonov Regularization of electrical conductivity depth profiles in field soils. Soil Science Society of America Journal 61:1004-1009.

Borrell, A., A. Garside, and S. Fukai. 1997. Improving efficiency of water use for irrigated rice in a semi-arid tropical environment. Field Crops Research 52:231-248.

Bottraud, J.C., and J.D. Rhoades. 1985. Effect of exchangeable sodium on soil electrical conductivity-salinity calibrations. Soil Science Society of America Journal 49:1110-1113.

Bouma, J. 1981. Soil morphology and preferential flow along macropores. Agricultural Water Management 3:235-250.

Bouma, J. 1989. Using soil survey data for quantitative land evaluation. Advances in Soil Science 9:177-213.

Bouma, J., and J.H.M. Wosten. 1979. Flow patterns during extended saturated flow in two, undisturbed swelling clay soils with different macrostructures. Soil Science Society of America Journal 43:16-22.

Boydell, B., and A.B. McBratney. 2002. Identifying potential within-field management zones from cotton-yield estimates. Precision Agriculture 3:9-23.

Braaten, R., and G. Gates. 2003. Groundwater-surface water interaction in inland New South Wales: a scoping study, p. 48 7, 215-224 Water Science and Technology. IWA Publishing House, London.

Breiman, L. 1996. Bagging predictors. Machine Learning 24:123-140.

Bronswijk, J.J.B. 1988. Effect of swelling and shrinkage on the calculation of water balance and water transport in clay soils. Agricultural Water Management 14:185-193.

Brus, D.J., M. Knotters, W.A. van Dooremolen, P. van Kernebeek, and R.J.M. van Seeters. 1992. The use of electromagnetic measurements of apparent soil electrical conductivity to predict the boulder clay depth. Geoderma 55:79-93.

Buchter, B., P.O. Aina, A.S. Azari, and D.R. Nielsen. 1991. Soil spatial variability along transects. Soil Technology 4:297-314.

Buckingham, E. 1907. Studies on the movement of soil moisture. Bulletin 38. U.S. Department of Agriculture Bureau of Soils, Government Printing Office, Washington D.C.

Butler, B.E. 1950. A theory of prior streams as a causal factor of soil occurrence in the Riverine Plain of southeastern Australia. Australian Journal of Agricultural Research 1:231-252.

Butnor, J.R., J.A. Doolittle, L. Kress, S. Cohen, and K.H. Johnsen. 2001. Use of ground-penetrating radar to study tree roots in the southeastern United States. Tree Physiology 21:1269-1278.

Calf, G.E. 1978. An investigation of recharge to the Namoi Valley aquifers using environmental isotopes. Australian Journal of Soil Research 16:197-207.

Cameron, D.R., E. Dejong, D.W.L. Read, and M. Oosterveld. 1981. Mapping salinity using resistivity and electromagnetic inductive techniques. Canadian Journal of Soil Science 61:67-78.

Cardimona, S.J., W.P. Clement, and K. Kadinsky-Cade. 1998. Seismic reflection and ground-penetrating radar imaging of a shallow aquifer. Geophysics 63:1310-1317.

Cattle, S.R., G.H. McTainsh, and S. Wagner. 2002. Æolian dust contributions to soil of the Namoi Valley, northern NSW, Australia. CATENA 47:245-264.

Chan, C.Y., and R.J. Knight. 1999. Determining water content and saturation from dielectric measurements in layered materials. Water Resources Research 35:85-93.

Chan, C.Y., and R.J. Knight. 2001. Laboratory measurements of electromagnetic wave velocity in layered sands. Water Resources Research 37:1099-1105.

Charlesworth, P.B. 2005. Irrigation insights No.1 - Soil water monitoring 2nd National Program for Irrigation research and Development. CSIRO Publishing, Melbourne.

Chen, C., and R.J. Wagenet. 1992. Simulation of water and chemicals in macropore soils Part 1. Representation of the equivalent macropore influence and its effect on soilwater flow. Journal of Hydrology 130:105-126.

Chen, X., J. Goeke, and S. Summerside. 1999. Hydraulic properties and uncertainty analysis for an unconfined alluvial aquifer. Ground Water 37:845.

Chiew, F.H.S., T.C. Piechota, J.A. Dracup, and T.A. McMahon. 1998. El Nino/Southern Oscillation and Australian rainfall, streamflow and drought: links and potential for forecasting. Journal of Hydrology 204:138-149.

Clarke, C.J., R.J. George, R.W. Bell, and T.J. Hatton. 2002. Dryland salinity in south-western Australia: its origins, remedies, and future research directions. Australian Journal of Soil Research 40:93-113.

Collins, M.E., and J.A. Doolittle. 1987. Using ground-penetrating radar to study soil microvariability. Soil Science Society of America Journal 51:491-493.

Constable, G.A., and A.S. Hodgson. 1990. A comparison of drip and furrow irrigated cotton on a cracking clay soil: III. Yield and quality of 4 cultivars. Irrigation Science 11:149-153.

Cook, P.G., and G.R. Walker. 1992a. Depth profiles of electrical-conductivity from linear-combinations of electromagnetic induction measurements. Soil Science Society of America Journal 56:1015-1022.

Cook, P.G., and G. Walker. 1992b. Depth profiles of electrical conductivity from linear combinations of electromagnetic induction measurements. Soil Science Society of America Journal 56:1015-1022.

Cook, P.G., G.R. Walker, and I.D. Jolly. 1989a. Spatial variability of groundwater recharge in a semiarid region. Journal of Hydrology 111:195-212.

Cook, P.G., M.W. Hughes, G.R. Walker, and G.B. Allison. 1989b. The calibration of frequency-domain electromagnetic induction meters and their possible use in recharge studies. Journal of Hydrology 107:251-265.

Copty, N., Y. Rubin, and G. Mavko. 1993. Geophysical-hydrological identification of field permeabilities through Bayesian updating. Water Resources Research 29:2813-2825.

Corwin, D.L., and J.D. Rhoades. 1982. An improved technique for determining soil electrical conductivity-depth relations from above-ground electromagnetic measurements. Soil Science Society of America Journal 46:517-520.

Corwin, D.L., and J.D. Rhoades. 1990. Establishing soil electrical-conductivity - depth relations from electromagnetic induction measurements. Communications in Soil Science and Plant Analysis 21:861-901.

Corwin, D.L., and S.M. Lesch. 2005a. Apparent soil electrical conductivity measurements in agriculture. Computers and Electronics in Agriculture.

Corwin, D.L., and S.M. Lesch. 2005b. Characterizing soil spatial variability with apparent soil electrical conductivity Part II. Case study. Computers and Electronics in Agriculture 46:135-152.

Corwin, D.L., and S.M. Lesch. 2005c. Apparent soil electrical conductivity measurements in agriculture. Computers and Electronics in Agriculture 46:11-43.

Crase, L., L. O'Reilly, and B. Dollery. 2000. Water markets as a vehicle for water reform: the case of New South Wales. Australian Journal of Agricultural and Resource Economics 44:299-321.

Crase, L., P. Pagan, and B. Dollery. 2004. Water markets as a vehicle for reforming water resource allocation in the Murray-Darling Basin of Australia. Water Resources Research 40.

CRCD. 2005. Annual Operating Plan 2005 - 2006. Cotton Research and Development Corporation, Narrabri, NSW.

Crestana, S., and C. Manoel Pedro Vaz. 1998. Non-invasive instrumentation opportunities for characterizing soil porous systems. Soil and Tillage Research 47:19-26.

Cuevas, R., A. Viguria, J.P. Vaca, and E. Fereres. 1984. Drip irrigation for cotton. Agricultura, Spain 53:504-505.

Curran, P.J. 1985. Aerial-photography for the assessment of crop condition - a review. Applied Geography 5:347-360.

da Silva, A.P., S. Imhoff, and M. Corsi. 2003. Evaluation of soil compaction in an irrigated short-duration grazing system. Soil and Tillage Research 70:83-90.

Daniells, I., B. Manning, and L. Pearce. 2002. Profile descriptions. District guidelines for managing soils in North-West NSW, p. 118 pp. Profile descriptions. District guidelines for managing soils in North-West NSW.

Darcy, H. 1856. Les Fontaines Publiques de la Ville de Dijon Dalmont, Paris.

Dasberg, S., and D. Or. 1999. Drip Irrigation Springer-Verlag, Berlin.

Davis, J.L., and A.P. Annan. 1986. High-resolution sounding using ground-probing radar. Geoscience Canada 13:205-208.

Davis, J.L., and A.P. Annan. 1989. Ground-penetrating radar for high-resolution mapping of soil and rock stratigraphy. Geophysical Prospecting 37:531-551.

Dawes, W., G. Walker, and M. Stauffacher. 1997. Model building: process and practicality, pp. 317-322, *In* A. D. McDonald and M. McAleer, (eds.) International Conference on Modelling and Simulation, Hobart, Tasmania.

Day, R.W., A.J. Franzsen, and J. Rogers. 1992. Coast-parallel palaeochannels off southern Namibia. Marine Geology 105:299-304.

de Lima, O., A. L. 1995. Water saturation and permeability from resistivity, dielectric, and porosity logs. Geophysics 60:1756-1764.

de Lima, O.A.L., and M.M. Sharma. 1990. A grain conductivity approach to shaly sandstones. Geophysics 55:1347-1356.

de Lima, O.A.L., and S. Niwas. 2000. Estimation of hydraulic parameters of shaly sandstone aquifers from geoelectrical measurements. Journal of Hydrology 235:12-26.

de Lima, O.A.L., M.B. Clennell, G.G. Nery, and S. Niwas. 2005. A volumetric approach for the resistivity response of freshwater shaly sandstones. Geophysics 70:F1-F10.

DeBoer, D.W., and S.T. Chu. 2001. Sprinkler technologies, soil infiltration, and runoff. Journal of Irrigation and Drainage Engineering-Asce 127:234-239.

Deidda, G.P., E. Bonomi, and C. Manzi. 2003. Inversion of electrical conductivity data with Tikhonov regularization approach: some considerations. Annals of Geophysics 46:549-558.

Diamond, D. 2001. Determination of chloride by flow injection analysis colorimetry QuikChem Method 10-117-07-1-H, Milwaukee, WI.

Doble, R., C.J. Simmons, I., and G. Walker. 2004. Spatial modelling of groundwater discharge patterns to predict floodplain salinisation and impacts on vegetation health. Technical Report 01/04. CSIRO Land and Water.

Dobson, M.C., F.T. Ulaby, M.T. Hallikainen, and M.A. Elrayes. 1985. Microwave dielectric behavior of wet soil: 2. Dielectric mixing models. IEEE Transactions on Geoscience and Remote Sensing 23:35-46.

Doolittle, J.A. 1987. Using Ground-penetrating Radar to Increase the Quality and Efficiency of Soil Surveys. Soil Survey Techniques, SSSA Special Publication 20:11-32.

Doolittle, J.A., and M.E. Collins. 1995. Use of soil information to determine application of ground penetrating radar. Journal of Applied Geophysics 33:101-108.

Doolittle, J.A., and M.E. Collins. 1998. A comparison of EM induction and GPR methods in areas of karst. Geoderma 85:83-102.

Doolittle, J.A., K.A. Sudduth, N.R. Kitchen, and S.J. Indorante. 1994. Estimating depths to claypans using electromagnetic induction methods. Journal of Soil and Water Conservation 49:572-575.

Doolittle, J.A., S.J. Indorante, D.K. Potter, S.G. Hefner, and W.M. McCauley. 2002. Comparing three geophysical tools for locating sand blows in alluvial soils of southeastern Missouri. Journal of Soil and Water Conservation 57:175-182.

Dury, G.H. 1976. Discharge prediction, present and former, from channel dimensions. Journal of Hydrology 30:219-245.

Dwivedi, R.S., and K. Sreenivas. 2002. The vegetation and waterlogging dynamics as derived from spaceborne multispectral and multitemporal data. International Journal of Remote Sensing 23:2729-2740.

Emerson, D.W., and Y.P. Yang. 1997. Effects of water salinity and saturation on the electrical resistivity of clays. Preview 19:19-24.

Endres, A.L., and Anonymous. 2001. Connecting aquifer properties to borehole geophysical data; an overview. Abstracts with Programs - Geological Society of America 33:412.

English, P. 1999. Palaeodrainage mapping at Uluru (Ayers Rock) Northern Territory, pp. 43, *In* A. Rowett, (ed.) Exploring ancient landscapes. Primary Industries and Resources South Australia, Adelaide.

Esfandiari, M., and B.L. Maheshwari. 2001. Field evaluation of furrow irrigation models. Journal of Agricultural Engineering Research 79:459-479.

Facchi, A., B. Ortuani, D. Maggi, and C. Gandolfi. 1994. Coupled SVAT-groundwater model for water resources simulation in irrigated alluvial plains. Environmental Modelling & Software 19:1053-1063.

Fensham, R.J., and R.J. Fairfax. 2002. Aerial photography for assessing vegetation change: a review of applications and the relevance of findings for Australian vegetation history. Australian Journal of Botany 50:415-429.

Fergusson, C.L. 1984. The Gundahl Complex of the New-England Fold Belt, eastern Australia: a tectonic melange formed in a Palaeozoic subduction complex. Journal of Structural Geology 6:257.

Fergusson, C.L. 2003. Ordovician-Silurian accretion tectonics of the Lachlan Fold Belt, southeastern Australia. Australian Journal of Earth Sciences 50:475-490.

Fetter, C.W. 2001. Applied hydrogeology. 4th ed. Prentice Hall, Upper Saddle River, N.J.

Fielding, C.R., J.D. Trueman, G.R. Dickens, and M. Page. 2003. Anatomy of the buried Burdekin River channel across the Great Barrier Reef shelf: how does a major river operate on a tropical mixed siliciclastic/carbonate margin during sea level lowstand? Sedimentary Geology 157:291-301.

Foley, J.L., and D.M. Silburn. 2002. Hydraulic properties of rain impact surface seals on three clay soils - influence of raindrop impact frequency and rainfall intensity during steady state. Australian Journal of Soil Research 40:1069-1083.

Foley, J.P., and S.R. Raine. 2001. Centre pivot and lateral move machines in the Australian cotton industry 1000176/1. National Centre for Engineering in Agriculture, USQ, Toowoomba.

Foster, D.A., and D.R. Gray. 2000. Evolution and structure of the Lachlan Fold Belt (Orogen) of Eastern Australia. Annual Review of Earth and Planetary Sciences 28:47-80.

Fried, A.W. 1993. Late Pleistocene river morphological change, southeastern Australia: the conundrum of sinuous channels during the Last Glacial Maximum. Palaeogeography, Palaeoclimatology, Palaeoecology 101:305-316.

Friedman, S.P. 2005. Soil properties influencing apparent electrical conductivity: a review. Computers and Electronics in Agriculture 46:45-70.

Garambois, S., P. Senechal, and H. Perroud. 2002. On the use of combined geophysical methods to assess water content and water conductivity of near-surface formations. Journal of Hydrology 259:32-48.

Gee, G.W., and J.W. Bauder. 1986. Particle size analysis, *In* K. A., ed. Methods of Soil Analysis Part 1. American Society of Agronomy, Soil Science Society of America, Madison, Wisconsin.

Gee, G.W., J.M. Keller, and A.L. Ward. 2005. Measurement and prediction of deep drainage from bare sediments at a semiarid site. Vadose Zone Journal 4:32-40.

Gee, G.W., P.J. Wierenga, B.J. Andraski, M.H. Young, M.J. Fayer, and M.L. Rockhold. 1994. Variations in water-balance and recharge potential at 3 western desert sites. Soil Science Society of America Journal 58:63-72.

Geonics. 1998. EM38 ground conductivity meter operating manual. Geonics Ltd., Mississauga, Ont.

Gish, T.J., W.P. Dulaney, K.J.S. Kung, C.S.T. Daughtry, J.A. Doolittle, and P.T. Miller. 2002. Evaluating use of ground-penetrating radar for identifying subsurface flow pathways. Soil Science Society of America Journal 66:1620-1629.

Glen, R.A. 2000. The geology of New South Wales - a summary. NSW Department of Primary Industries, Minerals Division.

Gloaguen, E., M. Chouteau, D. Marcotte, and R. Chapuis. 2001. Estimation of hydraulic conductivity of an unconfined aquifer using cokriging of GPR and hydrostratigraphic data. Journal of Applied Geophysics 47:135-152.

Godwin, R.J., and P.C.H. Miller. 2003. A review of the technologies for mapping within-field variability. Biosystems Engineering 84:393-407.

Gomez-Trevino, E., F.J. Esparza, and S. Mendez-Delgado. 2002. New theoretical and practical aspects of electromagnetic soundings at low induction numbers. Geophysics 67:1441-1451.

Goodman, D. 1994. Ground-Penetrating Radar Simulation in Engineering and Archaeology. Geophysics 59:224-232.

Goyne, P.J., and G.T. McIntyre. 2003. Stretching water - Queensland's water use efficiency cotton and grains adoption program. Water Science and Technology 48:191-196.

Gray, D.R., D.A. Foster, and M. Bucher. 1997. Recognition and definition of orogenic events in the Lachlan fold belt. Australian Journal of Earth Sciences 44:489-501.

Gray, P.M., and J.W. Guthrie. 1977. The influence of sprinkler irrigation and postharvest residue removal practices on the seedborne population of *Drechslera poae* on *Poa pratensis* 'Merion'. Plant Disease Reporter 61:90-93.

Greacen, E.L., and C.T. Hignett. 1984. Water balance under wheat modelled with limited soil data. Agricultural Water Management 8:291-304.

Greaves, R.J., D.P. Lesmes, J.M. Lee, and M.N. Toksoz. 1996. Velocity variations and water content estimated from multi-offset, ground-penetrating radar. Geophysics 61:683-695.

Greco, R. 2002. Preferential flow in macroporous swelling soil with internal catchment: model development and applications. Journal of Hydrology 269:150-168.

Green, M.D. 1982. A report of a study tour to northern Victoria to examine the use of laser beam technology in land forming for flood irrigation. Western Australian Department of Agriculture, Harvey.

Green, M.D. 1991. Landforming construction techniques. Australian Cottongrower 12(1):52-53.

Green, M.D., and J.P. Middlemas. 1985. Laser levelling land for flood irrigation. Journal of Agriculture Western Australia 26:39-42.

Grimmond, C.S.B., S.A. Isard, and M.J. Belding. 1992. Development and evaluation of continuously weighing mini-lysimeters. Agricultural and Forest Meteorology 62:205-218.

Grote, K., S. Hubbard, and Y. Rubin. 2003. Field-scale estimation of volumetric water content using ground-penetrating radar ground wave techniques. Water Resources Research 39:1-14.

Hallikainen, M.T., F.T. Ulaby, M.C. Dobson, M.A. Elrayes, and L.K. Wu. 1985. Microwave dielectric behavior of wet soil: 1. Empirical-models and experimental-observations. IEEE Transactions on Geoscience and Remote Sensing 23:25-34.

Harrington, G.A., G.R. Walker, A.J. Love, and K.A. Narayan. 1999. A compartmental mixing-cell approach for the quantitative assessment of groundwater dynamics in the Otway Basin, South Australia. Journal of Hydrology 214:49-63.

Healy, R., and A.D. Ronan. 1996. Documentation of computer program VS2DH for simulation of energy transport in variably saturated porous media -- modification of the U.S. Geological Survey's computer program VS2DT. Report U.S. Geological Survey Water-Resources Investigations Report 96-4230.

Hele-Shaw, H.S. 1898. Experiments on the nature of surface resistance of water and streamline motion under certain experimental conditions. Transactions of The Institution of Naval Architects 40:21-46.

Hendrickx, J.M.H., F.M. Phillips, and J.B. Harrison. 2003. Water flow processes in arid and semi-arid vadose zones, *In* I. Simmers, ed. Understanding Water in a Dry Environment. A.A. Balkema Publishers, Lisse, The Netherlands.

Hendrickx, J.M.H., B. Borchers, D.L. Corwin, S.M. Lesch, A.C. Hilgendorf, and J. Schlue. 2002. Inversion of soil conductivity profiles from electromagnetic induction measurements: Theory and experimental verification. Soil Science Society of America Journal 66:673-685.

Heng, L.K., R.E. White, K.R. Helyar, R. Fisher, and D. Chen. 2001. Seasonal differences in the soil water balance under perennial and annual pastures on an acid Sodosol in southeastern Australia. European Journal of Soil Science 52:227-236.

Herczeg, A.L., S.S. Dogramaci, and F.W.J. Leaney. 2001. Origin of dissolved salts in a large, semi-arid groundwater system: Murray Basin, Australia. Marine and Freshwater Research 52:41-52.

Hilgendorf, A.C. 1997. Linear and Nonlinear Models for Inversion of Electrical Conductivity Profiles in Field Soils from EM-38 Measurements. Master of Science in Mathematics with Operations Research and Satistics Option, New Mexico Institute of Mining and Technology, Socorro, New Mexico.

Hill, M.C., R.L. Cooley, and D.W. Pollock. 1998. A controlled experiment in ground water flow model calibration. Ground Water 36:520-535.

Hillel, D. 1998. Environmental Soil Physics. Academic Press, San Diego.

Hills, R.C. 1971. Lateral flow under cylinder infiltrometers: A graphical correction procedure. Journal of Hydrology 13:153-162.

Hodgson, A.S., G.A. Constable, G.R. Duddy, and I.G. Daniells. 1990. A comparison of drip and furrow irrigated cotton on a cracking clay soil: II. Water-use efficiency, waterlogging, root distribution and soil structure. Irrigation Science 11:143-148.

Holbrook, J., and S.A. Schumm. 1999. Geomorphic and sedimentary response of rivers to tectonic deformation: a brief review and critique of a tool for recognizing subtle epeirogenic deformation in modern and ancient settings. Tectonophysics 305:287-306.

Holcombe, R.J., C.J. Stephens, C.R. Fielding, D. Gust, T.A. Little, R. Silwa, J. McPhie, and A. Ewart. 1997. Tectonic Evolution of the Northern New

England Fold Belt: Carboniferous to Early Permian transition from active accretion to extension, p. 66-79, *In* P. M. Ashley and P. G. Flood, eds. Tectonics and Metallogenesis of the New England Orogen: Alan H. Voisey Memorial Volume, Vol. 19.

Holland, K., I. Overton, I.D. Jolly, and G. Walker. 2004. An analytical model to predict regional groundwater discharge patterns on the floodplains of a semi-arid lowland river. Technical Report 6/04. CSIRO Land and Water.

Hou, B., L. Flakes, N. Alley, V. Stamoulis, and A. Rowett. 1999. The application of geological and geophysical technology to the study of Tertiary palaeochannels draining the Gawler Craton, SA., pp. 43, *In* A. Rowett, (ed.) Exploring ancient landscapes. Primary Industries and Resources South Australia Adelaide.

Hubbard, S., E. Majer, J. Geller, J. Peterson, B. Parsons, and Anonymous. 1996. Permeability estimation using geophysical data. Eos, Transactions, American Geophysical Union 77:220.

Hubbard, S.S., and Y. Rubin. 2000. Hydrogeological parameter estimation using geophysical data: a review of selected techniques. Journal of Contaminant Hydrology 45:3-34.

Hubbard, S.S., Y. Rubin, and E. Majer. 1999. Spatial correlation structure estimation using geophysical and hydrogeological data. Water Resources Research 35:1809-1825.

Hubbard, S.S., J.E. Peterson, Jr., E.L. Majer, P.T. Zawislanski, K.H. Williams, J. Roberts, F. Wobber, and R. Knight. 1997. Estimation of permeable pathways and water content using tomographic radar data. Leading Edge 16:1623-1628.

Huckel, A.I. 2001. Estimating clay content and deep drainage at the field scale in the lower Gwydir River Valley. M.Sc. Agr, The University of Sydney, Sydney, Australia.

Huisman, J.A., C. Sperl, W. Bouten, and J.M. Verstraten. 2001. Soil water content measurements at different scales: accuracy of time domain reflectometry and ground-penetrating radar. Journal of Hydrology 245:48-58.

Huisman, J.A., J.J.J.C. Snepvangers, W. Bouten, and G.B.M. Heuvelink. 2002. Mapping spatial variation in surface soil water content: Comparison of ground-penetrating radar and time domain reflectometry. Journal of Hydrology 269:194-207.

Huisman, J.A., S.S. Hubbard, J.D. Redman, and A.P. Annan. 2003. Measuring Soil Water Content with Ground Penetrating Radar: A Review. Vadose Zone J 2:476-491.

Hulugalle, N.R. 2004. Using poor quality water to irrigate cotton, p. 251-258, *In* H. Dugdale, et al., eds. WATERpak - a guide for irrigation management in cotton. Cotton Research and Development Corporation, Narrabri, NSW.

Humphreys, E., E. Edraki, and M. Bethune. 2003. Deep drainage and crop water use for irrigated annual crops and pastures in Australia - A review of determinations in fields and lysimeters 14/03. CSIRO Land and Water, Griffith.

Hutchinson, P.A., and W.J. Bond. 2001. Routine measurement of the soil water potential gradient near saturation using a pair of tube tensiometers. Australian Journal of Soil Research 39:1147-1156.

Hvorslev, M. 1951. Time lag and soil permeability in groundwater observations Waterways Experiment Station, U.S. Army Corps of Engineers, Bulletin 36, Vicksburg, Mississippi.

Ife, D., and K. Skelt. 2004. Murray-Darling Basin Groundwater Status 1990-2000: Summary Report 32/04. Murray-Darling Basin Commission, Canberra.

Iqbal, M.Z., and N.C. Krothe. 1995. Infiltration mechanisms related to agricultural waste transport through the soil mantle to karst aquifers of southern Indiana, USA. Journal of Hydrology 164:171-192.

Isbell, R.F. 1996. The Australian soil classification CSIRO Australia, Collingwood, VIC, Australia.

Jacobsen, O.H., and P. Schjonning. 1993. A laboratory calibration of time domain reflectometry for soil water measurement including effects of bulk density and texture. Journal of Hydrology 151:147-157.

James, I.T., T.W. Waine, R.I. Bradley, J.C. Taylor, and R.J. Godwin. 2003. Determination of soil type boundaries using electromagnetic induction scanning techniques. Biosystems Engineering 86:421-430.

Jarvis, N.J., and P.B. Leeds-Harrison. 1990. Field test of a water balance model of cracking clay soils. Journal of Hydrology 112:203-218.

Johnson, C.B., and K.G. McQueen. 2001. The nature of gold-bearing palaeochannel sediments in the Gidji area north of Kalgoorlie, Western Australia. Quaternary International 82:51-62.

Johnston, C.D. 1987. Distribution of environmental chloride in relation to subsurface hydrology. Journal of Hydrology 94:67-88.

Jones, N.S., P.D. Guion, I.M. Fulton, M.K.G. Whateley, and D.A. Spears. 1995. Sedimentology and its applications within the UK opencast coal mining industry. International Journal of Rock Mechanics and Mining Science & Geomechanics Abstracts 32:330A.

Joshi, B., and C. Maule. 2000. Simple analytical models for interpretation of environmental tracer profiles in the vadose zone. Hydrological Processes 14:1503-1521.

Kale, V.S. 1990. Morphological and hydrological characteristics of some allochthonous river channels, Western Deccan Trap Upland region, India. Geomorphology 3:31-43.

Kennett-Smith, A., P.G. Cook, and G.R. Walker. 1994. Factors affecting groundwater recharge following clearing in the south western Murray Basin. Journal of Hydrology 154:85-105.

Khan, S., L. Best, and B. Wang. 2002. Surface-groundwater interaction model of the Murrumbidgee Irrigation Area (development of the hydrogeological databases). Technical Report 36/02. CSIRO Land and Water, Griffith, NSW.

Khan, S., T. Rana, J. Carroll, B. Wang, and L. Best. 2004. Managing climate, irrigation and ground water interaction using a numerical model: A case study

of the Murrumbidgee Irrigation Area. Technical Report 13/04. CSIRO Land and Water.

Khosla, B.K., R.K. Gupta, and I.P. Abrol. 1979. Salt leaching and the effect of gypsum application in a saline-sodic soil. Agricultural Water Management 2:193-202.

Kim, J.G., C.M. Chon, and J.S. Lee. 2004. Effect of structure and texture on infiltration flow pattern during flood irrigation. Environmental Geology 46:962-969.

King, P.L., A.J.R. White, B.W. Chappell, and C.M. Allen. 1997. Characterization and origin of aluminous A-type granites from the Lachlan Fold Belt, Southeastern Australia. Journal of Petrology 38:371-391.

Kingham, R.A. 1998. Geology of the Murray-Darling Basin - Simplified lithostratigraphic groupings. 1998/21.

Klein, C., and S.H. Cornelius. 1993. Manual of Mineralogy. 21 ed. John Wiley & Sons, Inc., New York.

Knight, A., K. Blott, M. Portelli, and C. Hignett. 2002. Use of tree and shrub belts to control leakage in three dryland cropping environments. Australian Journal of Agricultural Research 53:571-586.

Koekkoek, E.J.W., and H. Booltink. 1999. Neural network models to predict soil water retention. European Journal of Soil Science 50:489-495.

Kowalik, P., J. Loveday, D.S. McIntyre, and C.L. Watson. 1979. Deep percolation during prolonged ponding of a swelling soil, and the effect of gypsum treatment. Agricultural Water Management 2:131-147.

Kowalsky, M.B., S. Finsterle, J. Peterson, S. Hubbard, Y. Rubin, E. Majer, A. Ward, and G. Gee. 2005. Estimation of field-scale soil hydraulic and dielectric parameters through joint inversion of GPR and hydrological data.

Lambot, S., J. Rhebergen, I. van den Bosch, E.C. Slob, and M. Vanclooster. 2004. Measuring the soil water content profile of a sandy soil with an off-ground monostatic ground penetrating radar. Vadose Zone Journal 3:1063-1071.

Larsson, M.H., and N.J. Jarvis. 1999. Evaluation of a dual-porosity model to predict field-scale solute transport in a macroporous soil. Journal of Hydrology 215:153-171.

Lavitt, N. 1999. Integrated Approach to Geology, Hydrogeology and Hydrochemistry in the Lower Mooki River Catchment, The University of New South Wales, Sydney.

Lawrence, P.A., B.J. Radford, G.A. Thomas, D.P. Sinclair, and A.J. Key. 1994. Effect of tillage practices on wheat performance in a semi-arid environment. Soil & Tillage Research 28:347-364.

Lazaro-Mancilla, O., and E. Gomez-Trevino. 2000. Ground penetrating radar inversion in 1-D: an approach for the estimation of electrical conductivity, dielectric permittivity and magnetic permeability. Journal of Applied Geophysics 43:199-213.

Lee, T.-C., K.-F. Huang, M.-L. Hsiao, S.-T. Tang, and S.-T. Young. 2004. Electrical lumped model for arterial vessel beds. Computer Methods and Programs in Biomedicine 73:209-219.

Leitch, E.C. 1975. Plate tectonic interpretation of Paleozoic history of New-England Fold Belt. Geological Society of America Bulletin 86:141-144.

Lesch, S.M., D.J. Strauss, and J.D. Rhoades. 1995a. Spatial prediction of soil-salinity using electromagnetic induction techniques .2. An efficient spatial sampling algorithm suitable for multiple linear-regression model identification and estimation. Water Resources Research 31:387-398.

Lesch, S.M., D.J. Strauss, and J.D. Rhoades. 1995b. Spatial prediction of soil-salinity using electromagnetic induction techniques .1. Statistical prediction models - a comparison of multiple linear-regression and cokriging. Water Resources Research 31:373-386.

Lesch, S.M., D.L. Corwin, and D.A. Robinson. 2005. Apparent soil electrical conductivity mapping as an agricultural management tool in arid zone soils. Computers and Electronics in Agriculture 46:351-378.

Lesch, S.M., J.D. Rhoades, L.J. Lund, and D.L. Corwin. 1992. Mapping soil-salinity using calibrated electromagnetic measurements. Soil Science Society of America Journal 56:540-548.

Letey, J., A. Dinar, C. Woodring, and J.D. Oster. 1990. An economic-analysis of irrigation systems. Irrigation Science 11:37-43.

Levy, G.J., I. Shainberg, and H. Daniel. 2005. Sodic Soils, p. 504-513 Encyclopedia of Soils in the Environment. Elsevier, Oxford.

Lincare, S. 2005. Water use on Australian farms [Online]. Available by ABS.

Maas, E.V., and G.J. Hoffman. 1977. Crop salt tolerance - current assessment. Journal of the Irrigation and Drainage Division 103:115-134.

Macphail, M.K., and M.S. Stone. 2004. Age and palaeoenvironmental constraints on the genesis of the Yandi channel iron deposits, Marillana Formation, Pilbara, northwestern Australia. Australian Journal of Earth Sciences 51:497-520.

Mailhol, J.C., M. Priol, and M. Benali. 1999. A furrow irrigation model to improve irrigation practices in the Gharb valley of Morocco. Agricultural Water Management 42:65-80.

Massmann, J.W., and M.T. Hagley. 1995. A comparison of model and parameter uncertainties in groundwater flow and solute transport predictions, p. 3-24, *In* A. I. El-Kadi, ed. Groundwater Models for Resources Analysis and Management. CRC, Boca Raton.

Mateos, L., H. Gomez, and E. Fereres. 1991a. Drip irrigation of cotton grown in the Marismas of Guadalquivir. Investigacion Agraria, Produccion y Proteccion Vegetales 6:241-253.

Mateos, L., J. Berengena, F. Orgaz, J. Diz, and E. Fereres. 1991b. A comparison between drip and furrow irrigation in cotton at two levels of water supply. Agricultural Water Management 19:313-324.

Mawhinney, W. 2005. Water quality monitoring in the Gwydir Catchment - 2003 - 2004. report. NSW Department of Natural Resources.

McBratney, A.B., R. Webster, and T.M. Burgess. 1981. The design of optimal sampling schemes for local estimation and mapping of regionalized variables - I. Computers & Geosciences 7:331-334.

McBratney, A.B., J.J. De Gruijter, and D.J. Brus. 1992. Spacial prediction and mapping of continuous soil classes. Geoderma 54:39-64.

McBratney, A.B., T.F.A. Bishop, and I.S. Teliatnikov. 2000. Two soil profile reconstruction techniques. Geoderma 97:209-221.

McBratney, A.B., B. Minasny, S.R. Cattle, and R.W. Vervoort. 2002. From pedotransfer functions to soil inference systems. Geoderma 109:41-73.

McBride, J.L., and N. Nicholls. 1983. Seasonal relationships between Australian rainfall and the Southern Oscillation. Monthly Weather Review 111:1998-2004.

McCord, J.T., and M.T. Goodrich. 1994. Benchmark testing and independent verification of the VS2DT computer code. Technical report SAND--91-1526. Sandia National Labs, Albuquerque, NM.

McDonald, M.G., and W.A. Harbaugh. 1988. A modular three-dimensional finite-difference ground-water flow model. US Geological Survey Techniques of Water Resources Investigations, Vol. Book 6, Chapter A1.

McKay, B., I. Lambert, and S. Miyazki. 2000. The Australian Mining Industry, *In* AGS, (ed.). The Australian Bureau of Statistics.

McKenzie, N. 2007. Australian Soil Resource Information System. CSIRO Land and Water.

McKenzie, N., and D. Jacquier. 1997. Improving the field estimation of saturated hydraulic conductivity in soil survey. Australian Journal of Soil Research 35:803-825.

McNeill, J.D. 1980a. Electrical conductivity of soils and rocks. Geonics Limited, Mississauga, ON, Canada.

McNeill, J.D. 1980b. Electromagnetic terrain conductivity measurement at low induction numbers. Geonics Limited, Mississauga, ON, Canada.

McNeill, J.D. 1983. Use of EM31 in-phase information, Mississauga, ON, Canada.

McNeill, J.D. 1985. EM34-3 Measurements at two inter-coil spacings to reduce sensitivity to near-surface materials, Mississauga, ON, Canada.

McNeill, J.D. 1991. Advances in electromagnetic methods for groundwater studies. Geoexploration 27:65-80.

McNeill, J.D. 1996. Why doesn't Geonics Limited build a multi-frequency EM31 or EM38, Mississauga, ON, Canada.

MDBC. 1999. The Salinity Audit of the Murray Darling Basin. Murray-Darling Basin Ministerial Council, Canberra, ACT.

Merrick, N.P. 1997. Exploration Geophysics 28:106-109.

Merrick, N.P., J.B. Ross, and R.M. Williams. 1986. Groundwater in the lower NamoiValley, New South Wales, pp. 393-403, *In* A. W. R. Council., (ed.)

AWRC Conference, Groundwater Systems Under Stress. Australian Government Publishing Service, Brisbane.

Merrick, N.P., J.B. Ross, and R.M. Williams. 1987. Groundwater in the lower Namoi Valley, NSW, pp. 461-471 Australian Water Resources Council Conference Series, vol.13, Brisbane, Qld., Australia.

Metternicht, G.I., and J.A. Zinck. 2003. Remote sensing of soil salinity: potentials and constraints. Remote Sensing of Environment 85:1-20.

Middlemis, H., N.P. Merrick, and J.B. Ross. 2001. Groundwater flow modelling guideline Project No. 125. Murray-Darling Basin Comission.

Miller, E.E., and R.D. Miller. 1956. Physical Theory for Capillary Flow Phenomena. Journal of Applied Physics 27:324-332.

Minasny, B., and A.B. McBratney. 2000. Evaluation and development of hydraulic conductivity pedotransfer functions for Australian soil. Australian Journal of Soil Research 38:905-926.

Minasny, B., and A.B. McBratney. 2002a. The efficiency of various approaches to obtaining estimates of soil hydraulic properties. Geoderma 107:55-70.

Minasny, B., and A.B. McBratney. 2002b. Uncertainty analysis for pedotransfer functions. European Journal of Soil Science 53:417-429.

Minasny, B., and A.B. McBratney. 2002c. The neuro-m method for fitting neural network parametric pedotransfer functions. Soil Science Society of America Journal 66:352-361.

Minasny, B., and A.B. McBratney. 2003. NeuroTheta, pedotransfer function for predicting soil hydraulic properties for Australian soil. Australian Centre for Precision Agriculture, The University of Sydney.

Minasny, B., A.B. McBratney, and K.L. Bristow. 1999. Comparison of different approaches to the development of pedotransfer functions for water-retention curves. Geoderma 93:225-253.

Minasny, B., J.W. Hopmans, T. Harter, S.O. Eching, A. Tuli, and M.A. Denton. 2004. Neural networks prediction of soil hydraulic functions for alluvial soils using multistep outflow data. Soil Science Society of America Journal 68:417-429.

Morgan, K.H. 1993. Development, sedimentation and economic potential of palaeoriver systems of the Yilgarn Craton of Western Australia. Sedimentary Geology 85:637-656.

Nadler, A., and H. Frenkel. 1980. Determination of soil solution electrical conductivity from bulk soil electrical conductivity measurements by the four-electrode method. Soil Sci Soc Am J 44:1216-1221.

Nakashima, Y., H. Zhou, and M. Sato. 2001. Estimation of groundwater level by GPR in an area with multiple ambiguous reflections. Journal of Applied Geophysics 47:241-249.

Nanson, G.C., and R.W. Young. 1981. Downstream reduction of rural channel size with contrasting urban effects in small coastal streams of southeastern Australia. Journal of Hydrology 52:239-255.

Nanson, G.C., T.J. East, and R.G. Roberts. 1993. Quaternary stratigraphy, geochronology and evolution of the Magela Creek Catchment in the monsoon tropics of Northern Australia. Sedimentary Geology 83:277-302.

NHT. 2001. Australian natural resources atlas. National Heritage Trust, Canberra

NHT. 2005. Innovations in irrigation. National Heritage Trust, Canberra.

Niwas, S., and O.A.L. de Lima. 2003. Aquifer parameter estimation from surface resistivity data. Ground Water 41:94-99.

Noon, D.A., G.F. Stickley, and D. Longstaff. 1998. A frequency-independent characterisation of GPR penetration and resolution performance. Journal of Applied Geophysics 40:127-137.

Northcote, K.H. 1979. A Factual Key for the Regognition of Australian Soils. CSIRO, Adelaide.

Nott, J., D. Price, and G. Nanson. 2002. Stream response to Quaternary climate change: evidence from the Shoalhaven River catchment, southeastern highlands, temperate Australia. Quaternary Science Reviews 21:965-974.

NSWDLWC. 2000. NSW Salinity Strategy. New South Wales Department of Land and Water Conservation.

NSWDLWC. 2002. Water quality in the Namoi Catchment H0/10/02. NSW Department of Land and Water Conservation, Sydney, NSW.

O'Connell, M.G., G.J. O'Leary, and D.J. Connor. 2003. Drainage and change in soil water storage below the root-zone under long fallow and continuous cropping sequences in the Victorian Mallee. Australian Journal of Agricultural Research 54:663-675.

Odeh, I.O.A., A.B. McBratney, and D.J. Chittleborough. 1990. Design of optimal sample spacings for mapping soil using fuzzy-k- means and regionalized variable theory. Geoderma 47:93-122.

Odeh, I.O.A., A.B. McBratney, and D.J. Chittleborough. 1992. Soil pattern recognition with fuzzy-c-means: application to classification and soil-landform interrelationships. Soil Science Society of America Journal 56:505-516.

Odeh, I.O.A., A.B. McBratney, and D.J. Chittleborough. 1994. Spatial prediction of soil properties from landform attributes derived from a digital elevation model. Geoderma 63:197-214.

Odeh, I.O.A., A.B. McBratney, and D.J. Chittleborough. 1995. Further results on prediction of soil properties from terrain attributes: heterotopic cokriging and regression-kriging. Geoderma 67:215-226.

Odeh, I.O.A., A.B. McBratney, and B.K. Slater. 1999. Predicting soil properties from ancillary information: non-spatial models compared with geostatistical and combined methods, pp. 1008-1019 Geostatistics 96 - Proceedings of the Fifth International Geostatistics Congress. Kluwer Academic Publishers, Wollongong, Australia.

Olsen, H. 1990. Astronomical forcing of meandering river behaviour: Milankovitch cycles in Devonian of East Greenland. Palaeogeography, Palaeoclimatology, Palaeoecology 79:99-115.

Olsthoorn, T.N. 1999. A comparative review of analytic and finite difference models used at the Amsterdam Water Supply. Journal of Hydrology 226:139-143.

Osman, Y.Z., and M.P. Bruen. 2002. Modelling stream-aquifer seepage in an alluvial aquifer: an improved loosing-stream package for MODFLOW. Journal of Hydrology 264:69-86.

Page, K., G. Nanson, and D. Price. 1996. Chronology of Murrumbidgee River palaeochannels on the Riverine Plain, southeastern Australia. Journal of Quaternary Science 11:311-326.

Page, K.J., and G.C. Nanson. 1996. Stratigraphic architecture resulting from Late Quaternary evolution of the Riverine Plain, south-eastern Australia. Sedimentology 43:927-945.

Page, K.J., G.C. Nanson, and D.M. Price. 1991. Thermoluminescence chronology of late Quaternary deposition on the Riverine Plain of South-Eastern Australia. Australian Geographer 22:14-23.

Page, K.J., A.J. Dare-Edwards, J.W. Owens, P.S. Frazier, J. Kellett, and D.M. Price. 2001. TL chronology and stratigraphy of riverine source bordering sand dunes near Wagga Wagga, New South Wales, Australia. Quaternary International 83-5:187-193.

Paine, J.L., J.S. Rowan, and A. Werritty. 2002. Reconstructing historic floods using sediments from embanked flood plains: a case study of the River Tay in Scotland, p. 211-218, *In* F. J. Dyer, et al., eds. The Structure, Function and Management Implications of Fluvial Sedimentary Systems. IAHS Press, Wallingford.

Pappenberger, F., and K.J. Beven. 2006. Ignorance is bliss: Or seven reasons not to use uncertainty analysis. Water Resources Research 42.

Peck, A.J., and T. Hatton. 2003. Salinity and the discharge of salts from catchments in Australia. Journal of Hydrology 272:191-202.

Pels, S. 1964. The present and ancestral Murray River system. Australian Geographical Studies 2:111-120.

Pels, S. 1970. Radio-carbon datings of ancestral river sediments on the Riverine Plain of South-eastern Australia and their interpretation. Journal and Proceedings of the Royal Society of New South Wales 102:189-195.

Pels, S. 1973. The hydrogeology of the lower Murray irrigation areas, N.S.W. and effects on salinity in the river Murray NSW Water Conservation and Irrigation Commission, Sydney.

Petheram, C., G. Walker, R. Grayson, T. Thierfelder, and L. Zhang. 2002. Towards a framework for predicting impacts of land-use on recharge: 1. A review of recharge studies in Australia. Australian Journal of Soil Research CSIRO Publishing, Collingwood, Australia:2002.

Pinto, N., and E.F. Da Costa. 1999. Fungicides applications through overhead sprinkler irrigation for control of bean rust. Pesquisa Agropecuaria Brasileira 34:317-321.

Pittock, A.B. 1975. Climatic change and patterns of variation in Australia rainfall. Search 6:498-504.

Pons, Y., A. Capillon, and C. Cheverry. 2000. Water movement and stability of profiles in drained, clayey and swelling soils: at saturation, the structural stability determines the profile porosity. European Journal of Agronomy 12:269-279.

Prathapar, S.A., W.S. Meyer, S. Jain, and A. Van Der Lelij. 1994. SWAGSIM: A soil water and groundwater simulation model. Divisional Report. CSIRO Division of Water Resources.

Prescott, J.R., and G.B. Robertson. 1997. Sediment dating by luminescence: A review. Radiation Measurements 27:893-922.

Proffitt, A.P.B., R.J. Jarvis, and S. Bendotti. 1995a. The impact of sheep trampling and stocking rate on the physical-properties of a red duplex soil with 2 initially different structures. Australian Journal of Agricultural Research 46:733-747.

Proffitt, A.P.B., S. Bendotti, and D. McGarry. 1995b. A comparison between continuous and controlled grazing on a red duplex soil .1. Effects on soil physical characteristics. Soil & Tillage Research 35:199-210.

Prothero, D.R., and F.L. Schwab. 1996. Sedimentary geology : an introduction to sedimentary rocks and stratigraphy W.H. Freeman, New York.

Punthakey, J.F., N.M. Someratne, S.A. Prathapar, N.P. Merrick, S. Lawson, and R.M. Williams. 1994. Regional groundwater modelling of the Lower Murrumbidgee River Basin: Model development and calibration, Leeton, NSW.

Raine, S.R., J.P. Foley, and C.R. Henkel. 2000. Drip irrigation in the Australian cotton industry: a scoping study Publication 179757/1. USQ, Toowoomba.

Rasmussen, T.C., and L.A. Crawford. 1997. Identifying and removing barometric pressure effects in confined and unconfined aquifers. Ground Water 35:502-511.

RCRC. 2006. Rice growing regions in Australia. The Cooperative Research Centre for Sustainable Rice Production.

Reppert, P.M., F.D. Morgan, and M.N. Toksoz. 2000. Dielectric constant determination using ground-penetrating radar reflection coefficients. Journal of Applied Geophysics 43:189-197.

Rhoades, J.D. 1993. Electrical conductivity methods for measuring and mapping soil salinity. Advances in Agronomy 43:201-251.

Rhoades, J.D. 1996. Salinity: electrical conductivity and total dissolved solids, p. 417-435, *In* D. L. Sparks, et al., eds. Methods of soil analysis. Part 3 - chemical methods. Soil Science Society of America Inc., Madison, USA.

Rhoades, J.D., and D.L. Corwin. 1981. Determining soil electrical-conductivity depth relations using an inductive electromagnetic soil conductivity meter. Soil Science Society of America Journal 45:255-260.

Rhoades, J.D., P.A.C. Raats, and R.J. Prather. 1976. Effects of liquid-phase electrical-conductivity, water-content, and surface conductivity on bulk soil electrical-conductivity. Soil Science Society of America Journal 40:651-655.

Rhoades, J.D., B.L. Waggoner, P.J. Shouse, and W.J. Alves. 1989a. Determining soil salinity from soil and soil-paste electrical conductivities: sensitivity analysis of models. Soil Science Society of America Journal 53:1368-1374.

Rhoades, J.D., N.A. Manteghi, P.J. Shouse, and W.J. Alves. 1989b. Soil electrical conductivity and soil salinity: new formulations and calibrations. Soil Science Society of America Journal 53:433-439.

Ringrose-Voase, A.J., R.R. Young, Z. Paydar, N.I. Huth, A.L. Benrnardi, H.P. Cresswell, B.A. Keating, M. Stauffacher, R.G. Banks, J.F. Holland, R.M. Johnston, T.W. Green, L.J. Gregory, I. Daniells, R. Farquharson, R.J. Drinkwater, S. Heidenreich, and S.G. Donaldson. 2003. Deep drainage under different land uses in the Liverpool Plains catchment Report 3, Agricultural Resource Management Report Series. NSW Agriculture.

Ritter, A., F. Hupet, R. Munoz-Carpena, S. Lambot, and M. Vanclooster. 2003. Using inverse methods for estimating soil hydraulic properties from field data as an alternative to direct methods. Agricultural Water Management 59:77-96.

Roberts, R.G., M.A. Smith, and R. Jones. 1990. Thermoluminescence dating of a 50,000 year old human occupation site in northern Australia. Nature 345:153-156.

Robertson, A.I., P. Bacon, and G. Heagney. 2001. The responses of floodplain primary production to flood frequency and timing. Journal of Applied Ecology 38:126-136.

Robertson, G.B., J.R. Prescott, and J.T. Hutton. 1991. Bleaching of the thermoluminescence of feldspars by sunlight. Nuclear Tracks and Radiation Measurements 18:101-107.

Rogers, M.P., C. E.W., and S. Khan. 2002. Aquifer identification and characterisation for salinity control by shallow groundwater pumping. Technical Report 16/02. CSIRO Land and Water, Griffith, NSW.

Rose, C.W., P.W.A. Dayananda, D.R. Nielsen, and J.M. Biggar. 1979. Long-term solute dynamics and hydrology in irrigated slowly permeable soils. Irrigation Science 1:77-87.

Ross, H.S., A.J.P. Williamson, and Irrigation Association of Australia. 1990. Irrigation for profit: Water Force Queensland Irrigation Association of Australia, Brisbane.

Ross, J.B., S. Bish, and T. Mount. 1991. Impact of Floodplain Management Schemes on Groundwater Recharge, Lower Namoi Valley TS91.046. Department of Water Resources Technical Services Division.

Rubin, Y., G. Mavko, and J. Harris. 1992. Mapping permeability in heterogeneous aquifers using hydrologic and seismic data. Water Resources Research 28:1809-1816.

Rucker, D.F., and T.P.A. Ferre. 2004. Parameter estimation for soil hydraulic properties using zero-offset borehole radar: analytical method. Soil Science Society of America Journal 68:1560-1567.

Saarenketo, T. 1998. Electrical properties of water in clay and silty soils. Journal of Applied Geophysics 40:73-88.

Salama, R.B. 1997. Geomorphology, geology and palaeohydrology of the broad alluvial valleys of the Salt River System, Western Australia. Australian Journal of Earth Sciences 44:751-765.

Salama, R.B., and G.E. Hawkes. 1993. Surficial geology and stratigraphy of the Wallatin Creek area: a Western Australian model of Cainozoic sedimentary deposition on the Yilgarn Craton. Trends in Ecology & Evolution 8.

Salama, R.B., D. Laslett, and P. Farrington. 1993a. Predictive modeling of management options for the control of dryland salinity in a 1st-order catchment in the wheat-belt of Western-Australia. Journal of Hydrology 145:19-40.

Salama, R.B., C.J. Otto, and R.W. Fitzpatrick. 1999. Contributions of groundwater conditions to soil and water salinization. Hydrogeology Journal 7:46-64.

Salama, R.B., P. Farrington, G.A. Bartle, and G.D. Watson. 1993b. The role of geological structures and relict channels in the development of dryland salinity in the wheatbelt of Western Australia. Australian Journal of Earth Sciences 40:45-56.

Salama, R.B., I. Tapley, T. Ishii, and G. Hawkes. 1994a. Identification of areas of recharge and discharge using Landsat-TM satellite imagery and aerial photography mapping techniques. Journal of Hydrology 162:119-141.

Salama, R.B., G. Bartle, P. Farrington, and V. Wilson. 1994b. Basin geomorphological controls on the mechanism of recharge and discharge and its effect on salt storage and mobilization-comparative study using geophysical surveys. Journal of Hydrology 155:1-26.

Sarma, P.B.S., N.H. Rao, and K.V.P. Rao. 1980. Calculation of water balance in the crop root zone by computer. Journal of Hydrology 45:123-131.

Scanlon, B., R. Healy, and P. Cook. 2002. Choosing appropriate techniques for quantifying groundwater recharge. Hydrogeology Journal 10:18-39.

Scanlon, B.R. 1994. Water and Heat Fluxes in Desert Soils .1. Field Studies. Water Resources Research 30:709-719.

Scanlon, B.R. 2000. Uncertainties in estimating water fluxes and residence times using environmental tracers in an arid unsaturated zone. Water Resources Research 36:395-409.

Schaap, M.G., and F.J. Leij. 1998. Using neural networks to predict soil water retention and soil hydraulic conductivity. Soil and Tillage Research 47:37-42.

Schaap, M.G., F.J. Leij, and M.T.v. Genuchten. 1998. Neural network analysis for hierarchical prediction of soil hydraulic properties. Soil Science Society of America Journal 62:847-855.

Schaap, M.G., F.J. Leij, and M.T. van Genuchten. 2001. ROSETTA: a computer program for estimating soil hydraulic parameters with hierarchical pedotransfer functions. Journal of Hydrology 251:163-176.

Schultz, G., and C. Ruppel. 2005. Inversion of inductive electromagnetic data in highly conductive terrains. Geophysics 70:G16-G28.

Schumm, S.A. 1968. River adjustment to altered hydrologic regimen, Murrumbidgee River and palaeochannels, Australia. Professional paper 598. United States Geologic Survey, Washington, U.S.

Schumm, S.A. 1985. Patterns of alluvial rivers. Annual Review of Earth and Planetary Sciences 13:5-27.

Schumm, S.A., and H.R. Khan. 1972. Experimental study of channel patterns. Geological Society of America Bulletin 83:1755-&.

Schwartz, R.C., S.R. Evett, and P.W. Unger. 2003. Soil hydraulic properties of cropland compared with reestablished and native grassland. Geoderma 116:47-60.

Seiler, K.-P., S. von Loewenstern, and S. Schneider. 2002. Matrix and bypass-flow in quaternary and tertiary sediments of agricultural areas in south Germany. Geoderma 105:299-306.

Severino, G., A. Santini, and A. Sommella. 2003. Determining the soil hydraulic conductivity by means of a field scale internal drainage. Journal of Hydrology 273:234-248.

Shaw, R.J., and P.J. Thorburn. 1985. Prediction of leaching fraction from soil properties, irrigation water and rainfall. Irrigation Science 6:73-83.

Sheets, K.R., and J.M.H. Hendrickx. 1995. Noninvasive soil water content measurement using electromagnetic induction. Water Resources Research 31:2401-2409.

Sheets, K.R., J.P. Taylor, and J.M.H. Hendrickx. 1994. Rapid salinity mapping by electromagnetic induction for determining riparian restoration potential. Restoration Ecology 2:242-246.

Shei, T.-c., T.H. Brikowski, and Anonymous. 2006. Resistivity surveys and internal facies, Hays, Kansas. Abstracts with Programs - Geological Society of America 38:7.

Silburn, D.M., and J. Montgomery. 2001. Deep drainage under irrigated cotton in Australia: a review. Cotton Research and Development Corporation, Narrabri, NSW.

Silburn, D.M., R.W. Vervoort, and N. Schick. 2004. Deep Drainage - So What? Report on Northern Murray-Darling Water Balance Workshop 2. Narrabri, 19-20 November 2003.

Silliman, S.E., L.F. Konikow, and C.I. Voss. 1987. Laboratory investigation of longitudinal dispersion in anisotropic porous-media. Water Resources Research 23:2145-2151.

Simpson, H.J., and A.L. Herczeg. 1994. Delivery of marine chloride in precipitation and removal by rivers in the Murray-Darling Basin, Australia. Journal of Hydrology 154:323-350.

Simpson, H.J., M.A. Cane, A.L. Herczeg, S.E. Zebiak, and J.H. Simpson. 1993. Annual river discharge in southeastern Australia related to El Nino-Southern Oscillation forecasts of sea surface temperatures. Water Resources Research 29:3671-3680.

Slavich, P.G. 1990. Determining ECa-depth profiles from electromagnetic induction measurements. Australian Journal of Soil Research 28:443-452.

Slavich, P.G., and J. Yang. 1990. Estimation of field scale leaching rates from chloride mass balance and electromagnetic induction measurements. Irrigation Science 11:7-14.

Slavich, P.G., and G.H. Petterson. 1993a. Anion exclusion effects on estimates of soil chloride and deep-percolation. Australian Journal of Soil Research 31:455-463.

Slavich, P.G., and G.H. Petterson. 1993b. Estimating the electrical conductivity of saturated paste extracts from 1:5 soil, water suspensions and texture. Australian Journal of Soil Research 31:73-81.

Smedema, L.K. 1984. Furrow irrigation design for vertisols. Agricultural Water Management 9:211-218.

Smiles, D.E., and B.N. Gardiner. 1982. Hydrodynamic dispersion during unsteady, unsaturated water-flow in a clay soil. Soil Science Society of America Journal 46:9-14.

Smith, A., and B.L. Maheshwari. 2002. Options for alternative irrigation water supplies in the Murray-Darling Basin, Australia: a case study of the Shepparton Irrigation Region. Agricultural Water Management 56:41-55.

Smith, D.I. 1998. Water in Australia: resources and management. Oxford University Press, Melbourne.

Smith, R.J., S.R. Raine, and J. Minkevich. 2005. Irrigation application efficiency and deep drainage potential under surface irrigated cotton. Agricultural Water Management 71:117-130.

Sophocleous, M., and C.A. Perry. 1984. Experimental studies in natural groundwater recharge dynamics: Assessment of recent advances in instrumentation. Journal of Hydrology 70:369-382.

Sophocleous, M., and S.P. Perkins. 2000. Methodology and application of combined watershed and ground-water models in Kansas. Journal of Hydrology 236:185-201.

Sophocleous, M.A. 1991. Stream-floodwave propagation through the Great Bend alluvial aquifer, Kansas - Field-measurements and numerical simulations. Journal of Hydrology 124:207-228.

Spies, B.R. 1989. Depth of investigation in electromagnetic sounding methods. Geophysics 54:872-888.

Stannard, M.E., and I.D. Kelly. 1968. Irrigation potential of the Lower Gwydir Valley Water Conservation and Irrigation Commission, Sydney.

Stannard, M.E., and I.D. Kelly. 1977. The irrigation potential of the Lower Namoi Valley. Water Resources Commission, Sydney.

Steinheimer, T.R., K.D. Scoggin, and L.A. Kramer. 1998. Agricultural Chemical Movement through a Field-Size Watershed in Iowa: Subsurface Hydrology and Distribution of Nitrate in Groundwater. Environ. Sci. Technol. 32:1039-1047.

Sternberg, S.P.K. 2004. Dispersion measurements in highly heterogeneous laboratory scale porous media. Transport in Porous Media 54:107-124.

Stewart, C.M., A.B. McBratney, and J.H. Skerritt. 2002. Site-Specific durum wheat quality and its relationship to soil properties in a single field in Northern New South Wales. Precision Agriculture 3:155-168.

Stroh, J.C., S. Archer, J.A. Doolittle, and L. Wilding. 2001. Detection of edaphic discontinuities with ground-penetrating radar and electromagnetic induction. Landscape Ecology 16:377-390.

Suarez, D.L. 1989. Impact of agricultural practices on groundwater salinity. Agriculture, Ecosystems & Environment 26:215-227.

Subrahmanyam, K., and P. Yadaiah. 2000. The impact of paleo-channel on groundwater contamination, Andhra Pradesh, India. Environmental Geology 40:169-183.

Sudduth, K.A., S.T. Drummond, and N.R. Kitchen. 2001. Accuracy issues in electromagnetic induction sensing of soil electrical conductivity for precision agriculture. Computers and Electronics in Agriculture 31:239-264.

Sudduth, K.A., N.R. Kitchen, W.J. Wiebold, W.D. Batchelor, G.A. Bollero, D.G. Bullock, D.E. Clay, H.L. Palm, F.J. Pierce, R.T. Schuler, and K.D. Thelen. 2005. Relating apparent electrical conductivity to soil properties across the north-central USA. Computers and Electronics in Agriculture 46:263-283.

Tabbagh, A., M. Dabas, A. Hesse, and C. Panissod. 2000. Soil resistivity: a non-invasive tool to map soil structure horizonation. Geoderma 97:393-404.

Talsma, T. 1981. Transport of salts in catchments and soils. Agricultural Water Management 4:103-113.

Talsma, T., and A. Van Der Lelij. 1976. Water balance estimates of evaporation from ponded rice fields in a semi-arid region. Agricultural Water Management 1:89-97.

Taylor, J.C., G.A. Wood, R. Earl, and R.J. Godwin. 2003. Soil factors and their influence on within-field crop variability, Part II: Spatial analysis and determination of management zones. Biosystems Engineering 84:441-453.

Taylor, M.P., and P.A. Brewer. 2001. A study of Holocene floodplain particle size characteristics with special reference to palaeochannel infills from the upper Severn basin, Wales, UK. Geological Journal 36:143-157.

Taylor, S., and R. Barker. 2002. Resistivity of partially saturated Triassic Sandstone. Geophysical Prospecting 50:603-613.

Teles, V., F. Delay, and G. de Marsily. 2004. Comparison of genesis and geostatistical methods for characterizing the heterogeneity of alluvial media: Groundwater flow and transport simulations. Journal of Hydrology 294:103-121.

Teliatnikov, I.S. 1998. Considerations on determining the soil electrical conductivity profile using a non-invasive electromagnetic induction sensor - (EM 38), The University of Sydney, Sydney.

Thorburn, P.J., and C.W. Rose. 1990. Interpretation of solute profile dynamics in irrigated soils III: a simple model of bypass flow in soils. Irrigation Science 11:219-225.

Thorburn, P.J., C.W. Rose, R.J. Shaw, and D.F. Yule. 1990. Interpretation of solute profile dynamics in irrigated soils I: Mass balance approaches. Irrigation Science 11:199-207.

Timms, W., and R.I. Acworth. 2002. Origin, lithology and weathering characteristics of Upper Tertiary - Quaternary clay aquitard units on the Lower Murrumbidgee alluvial fan. Australian Journal of Earth Sciences 49:525-537.

Timms, W., R.I. Acworth, and D. Berhane. 2001. Shallow groundwater dynamics in smectite dominated clay on the Liverpool Plains of New South Wales. Australian Journal of Soil Research 39:203-218.

Tolmie, P.E., D.M. Silburn, and A.J.W. Biggs. 2004. Estimating deep drainage in the Queensland Murray-Darling basin using soil chloride QNRM03020, Toowoomba, Qld.

Tooth, S. 2000. Process, form and change in dryland rivers: a review of recent research. Earth-Science Reviews 51:67-107.

Topp, G.C., J.L. Davis, and A.P. Annan. 1980. Electromagnetic determination of soil water content: measurements in coaxial transmission lines. Water Resources Research 16:574-582.

Triantafilis, J., and S.M. Lesch. 2005. Mapping clay content variation using electromagnetic induction techniques. Computers and Electronics in Agriculture 46:203-237.

Triantafilis, J., G.M. Laslett, and A.B. McBratney. 2000. Calibrating an electromagnetic induction instrument to measure salinity in soil under irrigated cotton. Soil Science Society of America Journal 64:1009-1017.

Triantafilis, J., I.O.A. Odeh, and A.B. McBratney. 2001a. Five geostatistical models to predict soil salinity from electromagnetic induction data across irrigated cotton. Soil Science Society of America Journal 65:869-878.

Triantafilis, J., A.I. Huckel, and I.O.A. Odeh. 2001b. Comparison of statistical prediction methods for estimating field-scale clay content using different combinations of ancillary variables. Soil Science 166:415-427.

Triantafilis, J., W.T. Ward, and A.B. McBratney. 2001c. Land suitability assessment in the Namoi valley of Australia, using a continuous model. Australian Journal of Soil Research 39:273-290.

Triantafilis, J., M.F. Ahmed, and I.O.A. Odeh. 2002. Application of a mobile electromagnetic sensing system (MESS) to assess cause and management of soil salinization in an irrigated cotton-growing field. Soil Use and Management 18:330-339.

Triantafilis, J., A.I. Huckel, and I.O.A. Odeh. 2003a. Field-scale assessment of deep drainage risk. Irrigation Science 21:183-192.

Triantafilis, J., W.T. Ward, I.O.A. Odeh, and A.B. McBratney. 2001d. Creation and interpolation of continuous soil layer classes in the lower Namoi Valley. Soil Science Society of America Journal 65:403-413.

Triantafilis, J., I.O.A. Odeh, B. Minasny, and A.B. McBratney. 2003b. Elucidation of physiographic and hydrogeological features of the lower Namoi valley using fuzzy k-means classification of EM34 data. Environmental Modelling & Software 18:667-680.

Triantafilis, J., I.O.A. Odeh, A.L. Jarman, M.G. Short, and E. Kokkoris. 2004. Estimating and mapping deep drainage risk at the district level in the lower

Gwydir and Macquarie valleys, Australia. Australian Journal of Experimental Agriculture 44:893-912.

Troisi, S., C. Fallico, S. Straface, and E. Migliari. 2000. Application of kriging with external drift to estimate hydraulic conductivity from electrical-resistivity data in unconsolidated deposits near Montalto Uffugo, Italy. Hydrogeology Journal 8:356-367.

van Grinsven, J.J.M., H.W.G. Booltink, C. Dirksen, N.v. Breemen, N. Bongers, and N. Waringa. 1988. Automated in situ measurement of unsaturated soil water flux. Soil Science Society of America Journal 52:1215-1218.

van Overmeeren, R.A. 1994. Georadar for hydrogeology. First Break 12:401-408.

van Overmeeren, R.A. 1998. Radar facies of unconsolidated sediments in The Netherlands: A radar stratigraphy interpretation method for hydrogeology. Journal of Applied Geophysics 40:1-18.

van Schilfgaarde, J. 1994. Irrigation -- a blessing or a curse. Agricultural Water Management 25:203-219.

Vandenberghe, J., and R.A. van Overmeeren. 1999. Ground penetrating radar images of selected fluvial deposits in the Netherlands. Sedimentary Geology 128:245-270.

Vervoort, R.W., and S.R. Cattle. 2003. Linking hydraulic conductivity and tortuosity parameters to pore space geometry and pore-size distribution. Journal of Hydrology 272:36-49.

Vervoort, R.W., and Y.L. Annen. 2006. Palaeochannels in Northern New South Wales: inversion of electromagnetic induction data to infer hydrologically relevant stratigraphy 44:35-45.

Vervoort, R.W., D.E. Radcliffe, and L.T. West. 1999. Soil structure development and preferential solute flow. Water Resources Research 35:913-928.

Vervoort, R.W., S.R. Cattle, and B. Minasny. 2003. The hydrology of Vertosols used for cotton production: I. Hydraulic, structural and fundamental soil properties. Australian Journal of Soil Research 41:1255-1272.

Vervoort, R.W., C. Glendenning, and I.O.A. Odeh. 2004. Developing a deep drainage risk map for the Border Rivers area SuperSoil 2004: 3rd Australian New Zealand Soils Conference. Published on CDROM, The University of Sydney, Australia.

Vieira Junior, P.A., D. Dourado Neto, O. Smiderle, L.A. Jorge, and S.M. Cicero. 2000. Irrigation methods effect on yield and seed quality of corn. Revista Brasileira de Sementes 22:231-238.

Vieira, R.F., and D.R. Sumner. 1999. Application of fungicides to foliage through overhead sprinkler irrigation - a review. Pesticide Science 55:412-422.

Walker, G., L. Zhang, T. Ellis, T. Hatton, and C. Petheram. 2002. Estimating impacts of changed land use on recharge: review of modelling and other approaches appropriate for management of dryland salinity. Hydrogeology Journal 10:68-90.

Walker, G.R., and L. Zhang. 2002. Plot scale models and their application to recharge studies CSIRO Publishing, Collingwood, VIC.

Walker, W.R., and G.V. Skogerboe. 1987. Surface irrigation: theory and practice Prentice-Hall, Englewood Cliffs, N.J.

Wang, H., and Q. Xie. 2000. Palaeorunoff estimations achieved from palaeoclimatic information for the southwest part of the North China Plain: an attempt to apply a climatological approach to palaeohydrology. Journal of Environmental Sciences 12:330-336.

Ward, S.H., and G.W. Hohmann. 1987. Electromagnetic theory for geophysical applications, p. 131-311, *In* M. N. Nabighian, ed. Investigations in Geophysics, Vol. 3. Society of Exploration Geophysicists, Tulsa, Ok.

Ward, W.T., G.H. McTainsh, D. McGarry, and K.J. Smith. 1999. The soil of the Agricultural Research Station at 'Myall Vale' near Narrabri, NSW with data analysis by fuzzy k-means. Technical Report 21/99. CSIRO Land and Water

Weaver, T.B., N.R. Hulugalle, and H. Ghadiri. 2005. Comparing deep drainage estimated with transient and steady state assumptions in irrigated vertisols. Irrigation Science 23:183-191.

Wendroth, O., S. Koszinski, and E. Pena-Yewtukhiv. 2006. Spatial Association among Soil Hydraulic Properties, Soil Texture, and Geoelectrical Resistivity. Vadose Zone J 5:341-355.

Whelan, B.M., and A.B. McBratney. 2001. The "null hypothesis" of precision agriculture management. Precision Agriculture 2:265-279.

White, M.E. 2000. Running down: water in a changing land Kangaroo Press, East Roseville, N.S.W.

Whittig, L.D., and W.R. Allardice. 1986. X-ray diffraction techniques, p. 331-362, *In* A. Klute, ed. Methods of soil analysis. Part 1. Physical and mineralogical methods. ASA/CSSA/SSSA, Madison, WI.

Wichelns, D. 1999. An economic model of waterlogging and salinization in arid regions. Ecological Economics 30:475-491.

Wild, M.R., A.J. Koppi, D.C. McKenzie, and A.B. McBratney. 1992. The effect of tillage and gypsum application on the macropore structure of an Australian Vertisol used for irrigated cotton. Soil & Tillage Research 22:55-71.

Wilks, S.S. 1932. Certain generalizations in the analysis of variance. Biometrika 24:471-494.

Williams, B.G., and G.C. Baker. 1982. An electromagnetic induction technique for reconnaissance surveys of soil-salinity hazards. Australian Journal of Soil Research 20:107-118.

Williams, B.G., and D. Hoey. 1987. The use of electromagnetic induction to detect the spatial variability of the salt and clay contents of soils. Australian Journal of Soil Research 25:21-27.

Williams, R.M., N.P. Merrick, and J.B. Ross. 1989. Natural and induced recharge in the Lower Namoi Valley, New South Wales, p. vii, 323 p., *In* M. L. Sharma, ed. Groundwater recharge : proceedings of the Symposium on Groundwater Recharge, Mandurah, 6-9 July 1987. A.A. Balkema, Rotterdam.

Willis, T.M., and A.S. Black. 1996. Irrigation increases groundwater recharge in the Macquarie Valley. Australian Journal of Soil Research 34:837-847.

Willis, T.M., A.S. Black, and W.S. Meyer. 1997. Estimates of deep percolation beneath cotton in the Macquarie Valley. Irrigation Science 17:141-150.

Winter, T.C. 1999. Relation of streams, lakes, and wetlands to groundwater flow systems. Hydrogeology Journal 7:28-45.

Wood, J.M., R.G. Thomas, and J. Visser. 1988. Fluvial processes and vertebrate taphonomy: the upper cretaceous Judith River formation, South-Central dinosaur Provincial Park, Alberta, Canada. Palaeogeography, Palaeoclimatology, Palaeoecology 66:127-143.

Wosten, J.H.M., Y.A. Pachepsky, and W.J. Rawls. 2001. Pedotransfer functions: bridging the gap between available basic soil data and missing soil hydraulic characteristics. Journal of Hydrology 251:123-150.

Wray, R.A.L., D.M. Price, and R.W. Young. 2001. Thermoluminescence dating of alluvial sequences in coastal valleys of Southern New South Wales: problems and potential. Australian Geographer 32:201-220.

Yasuda, H., R. Berndtsson, H. Persson, A. Bahri, and K. Takuma. 2001. Characterizing preferential transport during flood irrigation of a heavy clay soil using the dye Vitasyn Blau. Geoderma 100:49-66.

Yoder, R.E., R.S. Freeland, J.T. Ammons, and L.L. Leonard. 2001. Mapping agricultural fields with GPR and EMI to identify offsite movement of agrochemicals. Journal of Applied Geophysics 47:251-259.

Young, R.W., A.R.M. Young, D.M. Price, and R.A.L. Wray. 2002. Geomorphology of the Namoi alluvial plain, northwestern New South Wales. Australian Journal of Earth Sciences 49:509-523.

Youngs, E.G. 1977. The unsteady groundwater mound below an irrigation ditch or leaky canal. Journal of Hydrology 34:307-314.

Zhang, L., M. Stauffacher, G.R. Walker, and P. Dyce. 1997. Recharge estimation in the Liverpool Plains (NSW) for input to groundwater models. Technical Report.